Influence of KF post deposition treatment on the polycrystalline Cu(In,Ga)Se2/CdS heterojunction formation for photovoltaic application

Thomas Lepetit

UNIVERSITÉ DE NANTES

Influence of KF post deposition treatment on the polycrystalline $Cu(In,Ga)Se_2$/CdS hetero-junction formation for photovoltaic application

Thomas LEPETIT

IMN
INSTITUT DES MATÉRIAUX JEAN ROUXEL

l'université nantes angers le mans
PÔLE DE RECHERCHE ET D'ENSEIGNEMENT SUPÉRIEUR

UNIVERSITÉ DE NANTES

Thèse de Doctorat

Thomas LEPETIT

Mémoire présenté en vue de l'obtention du
grade de Docteur de l'Université de Nantes
sous le label de L'Université Nantes Angers Le Mans

École doctorale : *Molécules, Matière et Matériaux en Pays de Loire*

Discipline : *Science des matériaux*
Spécialité : *Composant pour l'électronique*
Unité de recherche : *UMR 6502*

Soutenue le *13 novembre 2015*

Influence of KF post deposition treatment on the polycrystalline Cu(In,Ga)Se_2/CdS heterojunction formation for photovoltaic application

JURY

Rapporteurs :	**Pere ROCA i CABARROCAS**, Directeur de recherche CNRS, Ecole Polytechnique **Olivier BRIOT**, Directeur de recherche CNRS, Laboratoire Charles Coulomb
Examinateurs :	**Ayodhya TIWARI**, Professeur, ETH Zürich **Philippe PAREIGE**, Professeur, Université de Rouen **Guy OUVRARD**, Professeur, Université de Nantes **Nicolas BARREAU**, Maître de conférences HDR, Université de Nantes **Ludovic ARZEL**, Maître de conférences, Université de Nantes **Sylvie HAREL**, Maître de conférences, Université de Nantes
Invité(s) :	**John KESSLER**, Professeur, Université de Nantes **Pawel ZABIEROWSKI**, Assistant professor, Warsaw University of Technology
Directeur de Thèse :	**Nicolas BARREAU**, Maître de conférences HDR, Université de Nantes

Acknowledgements

The work presented in this manuscript has been realized at the Institut des Matériaux Jean Rouxel (IMN), on the campus of the Université de Nantes. I would like to thank my director Nicolas Barreau and my co-supervisors Ludovic Arzel and Sylvie Harel who have trusted me from the beginning and accepted me as a PhD student. You allowed me to perform my researches in very good conditions, gave me the opportunity to present my work in prestigious conferences, you supported my ideas and let me work independently on this thesis which turned-out to be one of the greatest professional experience I ever had. I have really appreciated the scientific and non-scientific fruitful discussions we had all along these three years. I am also grateful to you for sharing your experience on teaching. I would like to specially thank you Nicolas for your availability. You have shared without any restraint your great scientific and technical skills and you have introduced me to your scientific network. Although your schedule was really busy, you always took the time to answer my questions and debate the experimental results. We have imagined so many models to interpret the results before we were convinced of their viability! I also thank all my colleagues from the IMN for the time we spent together. Edouard Leonard, Mathieu Tomassini, Christopher Laurensic, Thomas Painchaud, Pablo Reyes, Tomek Drobiazg, it was a pleasure to share the office with you! Eric Gautron I enjoyed the week at Lyon. Tomek thank you for showing me Warsaw city.

I would like to personally thank Guy Ouvrard for the time we have spent at the synchrotron facilities. You have answered my naive questions about chemistry and you have spent so much time to help me to interpret the absorption measurements. The same acknowledgements go for Pawel Zabierowski. The very interesting discussions we have had about the electrical models –and the metastabilities- have been really helpful to me and this thesis. Thank you also John Kessler for the multiple scientific debates we have had and for reviewing the English in my manuscript. I wish you the best with your company B-plan.

I am really grateful to my family and in particular to my parents who always support me, whatever I do. You have given me the opportunity to study physics in the best conditions and you are at the origin of my scientific curiosity, since you have always tried to answer my questions when I was a child. Thank you also sister to be so kind with me. You have accepted to help me with English even if you are not really interested in physics! Thank you Maman, Papa and Soeurette for your technical support during the writing of this manuscript! My acknowledgements go also to Clairie for the time she was by my side. You listened carefully to all my doubts and supported me when I had to travel. Finally you are also doing a PhD so I wish you the best. I also thank all my friends who understood me and did not tempt me to go out when I was writing this manuscript. Thank you Poune & Bini for your support at the end of the thesis!

Finally I would like to thank my committee members Pere Roca I Cabarrocas, Olivier Briot, Ayodhya Tiwari, Philippe Pareige, Guy Ouvrard and John Kessler for reviewing this manuscript. Thank you Pere Roca I Cabarrocas and Olivier Briot for being the referees of this work.

Abstract

Among photovoltaic technologies, Mo/Cu(In,Ga)Se_2 (CIGS)/CdS/ZnO/ZnO:Al solar cell is the only thin film based structure demonstrating record energy conversion efficiency of 21.7 %. This outstanding level of performance for such polycrystalline and hetero-junction based devices has been made possible by the use of a so-called potassium fluoride post deposition treatment (KF-PDT) after the absorber synthesis. Such treatment indeed improves all photovoltaic parameters of the solar cell (*i.e.* V_{oc}, FF, J_{sc}). Nevertheless, this paradigm appears closely dependent to specific CIGS-surface characteristics which, if not fully satisfied, can yield hindered device performance. In the present work, CIGS absorbers leading to either beneficial or detrimental impact of KF-PDT have been firstly finely investigated. From this study it appeared conclusive that the presence of an ordered vacancy compound (OVC) on top of the CIGS is requested to avoid –detrimental- Cu_xSe segregation and to take advantage of the KF-PDT. It is herein proposed that this superficial Cu-poor chalcopyrite results in a new phase that turns during the chemical bath deposition of CdS into a ~5 nm-thick $CdIn_2S_4$ layer. This mechanism can in particular explain the much more homogeneous CBD-growth of the buffer layer. Moreover, it is shown that cubic $CdIn_2S_4$ material, which has n^+-type conductivity, forms a defect-free interface with the CIGS. The final part of this work aims at discussing the impact of KF-PDT on the electro-optical properties of CIGS/CdS solar cell, based on the modifications it implies on both hetero-junction and grain boundary characteristics.

Keywords

Solar cell, Cu(In,Ga)Se_2, CdS, hetero-junction, thin film, alkali, co-evaporation

Contents

Acknowledgements ..... **i**

Abstract ..... **ii**

Contents ..... **iii**

List of Figures ..... **vii**

List of Tables ..... **xiii**

General introduction **1**

Chapter 1 Theoretical and practical aspects of Cu(In,Ga)Se_2-based thin film solar cell 4

1.1 Basics of the solar cell 4

1.1.1 Standard device structure 4

1.1.2 Operating solar cell 5

1.1.3 Transport 7

1.2 CIGS material 10

1.2.1 Structural properties 10

1.2.2 Opto-electrical properties 11

1.2.3 Doping/defects 11

1.3 CIGS growth 13

1.3.1 Deposition techniques 13

1.3.2 Co-evaporation processes 13

1.3.3 Case of the 3-stage process 13

1.4 High efficiency CIGS/CdS hetero-junctions 15

1.4.1 Role of the chemical bath deposited CdS buffer layer 15

1.4.2 Avoiding interface recombinations 16

1.4.3 Grain boundaries 17

Chapter 2 Alkali in Cu(In,Ga)Se_2-based thin film solar cell: state-of-the-art and issues addressed in this thesis 19

2.1 On sodium 19

2.1.1 Background 19

2.1.2 Na-induced changes during the CIGS growth 20

2.1.3 Increase of the free holes density 23
2.1.4 Origin of the photovoltaic parameters enhancement 24
2.2 On potassium 25
2.2.1 Background 25
2.2.2 Electrical performance enhancement 26
2.2.3 Reported material and and related models 26
2.2.4 Electronic effects 28
2.3 Processing the alkali supply in our laboratory 29
2.3.1 Choice of the method 29
2.3.2 Supplying K – PDT baseline 30
2.3.3 Supplying Na – Optimization of the molybdenum 30
2.4 Issues addressed in this thesis 31
2.4.1 Effect of KF-PDT on electrical performance 31
2.4.2 Distribution of alkali 33
2.4.3 Adressing the hetero-junction formation issues after KF-PDT 34
Chapter 3 Material changes induced by the KF-PDT at the surface of the absorber 37
3.1 Chemical and compositional changes 37
3.1.1 Comparison of the CIGS surface chemistry in the case of beneficial and detrimental effect of the KF-PDT 38
3.1.2 Alkali interactions 42
3.1.3 Effect of rincing the K-treated layer 45
3.1.4 Summary on XPS results 47
3.2 Structural investigations 48
3.2.1 Structural differences in the references 48
3.2.2 Structural effects induced by the KF-PDT 49
3.2.3 Summary on the structural investigations 50
3.3 K-containing chalcogenide 51
3.3.1 State of the art 51
3.3.2 XAS study of K in KF-treated CIGS 53
3.3.3 Discussion 54
3.4 Reaction mechanisms involved during the KF-PDT at the surface of the absorber 54
3.4.1 Case#1 – beneficial effect 54
3.4.2 Case#2 – Detrimental effect 55
3.4.3 Discussion 55
Chapter 4 Material changes induced by the KF-PDT at CIGS interfaces 57

PART I – CIGS/CdS hetero-interface **58**
4.1 CIGS/CdS interface region in complete devices 58
4.1.1 CdSe segregation 58
4.1.2 Interface layer 60
4.1.3 CdS thickness 61
4.1.4 Micro-structural analysis 62
4.2 Comparative study of the chemical bath deposition 64
4.2.1 Cadmium partial electrolyte treatment 64
4.2.2 Modified CdS growth 68
4.2.3 Structural properties of the CdS 74
4.3 CdS grown on indium selenide 75
4.3.1 Literature review 75
4.3.2 Properties of the (CBD)CdS grown on indium selenide 77
4.3.3 Summary 82
4.4 Hetero-junction formation 83
4.4.1 Reaction with the top surface material 83
4.4.2 Model of the buffer layer growth 83
4.4.3 Discussion 84
PART II – CIGS/CIGS homo-interfaces **86**
4.5 K-induced material changes at the grain boundaries in the near CIGS/CdS interface region 86
4.6 K-induced material changes at grain boundaries deep in the absorber 88
4.7 Summary of the chapter 90
Chapter 5 Impact of the material changes induced by the KF-PDT on the opto-electrical performance of the related devices **91**
5.1 Electronic transport 92
5.1.1 Increased open-circuit voltage 92
5.1.2 n+p hetero-junction 97
5.1.3 Improved collection without Ga grading 99
5.1.4 Summary 100
5.2 Discussion of the models 100
5.2.1 (1) Beneficial and detrimental effect 101
5.2.2 (2) CdS chemical bath deposition duration 103
5.3 Learning from the KF-PDT 106
Summary and perspectives **109**

Résumé en Français **112**
A – Technical details - XPS **118**
B – Additional informations – TEM **120**
C – Synthesis method – (CBD)CdS **121**
References **122**

List of Figures

Figure 1.1 – Standard solar cell scanning electron micrograph of a polished cross section obtained by focused ion beam technique (left) with associated scheme (right) 5

Figure 1.2 – AM1.5 incident light spectrum with compounds responsibles of the absorption in the atmosphere 5

Figure 1.3 – Current density – voltage (blue) and power – voltage (red) typical characteristics of solar cell 6

Figure 1.4 – (a) Generation profile in a standard CIGS-based solar cell structure containing ZnO bilayer and CdS/CIGS hetero-junction, After [16]; (b) External quantum efficiency 7

Figure 1.5 – (a) Effect of lowering J_0 or R_s and increasing A or R_{sh} on the J(V) characteristic compare to the ideal case; (b) corresponding values for these parameters in the simulated curves 8

Figure 1.6 - One-dimensional (1D) energy band diagram of a complete solar cell structure in case of non graded CIGS absorber with no copper depleted surface layer, in dark and at 0V bias. 8

Figure 1.7 – Multiple-diodes model 9

Figure 1.8 - (a) Chalcopyrite structure [4], (b) Ternary phase diagram of the Cu-In-Se system [27], (c) Quasi-binary phase diagram of CuInSe2 established by Differential Thermal Analysis (DTA) and microscopic phase analysis.[25] 10

Figure 1.9 - Ga content x from Secondary Ion Mass Spectroscopy measurement and variation of the band gap across an absorber grown on SLG/Mo substrate 15

Figure 1.10 - Band diagrams of CIGS grain boundary (a) freshly etched, (b) after surface oxidation and (c) after surface sulfurization. The straight arrow pointing to the right in (a) refers to the photogenerated electrons, as do the curved arrows in (b) and (c). In (a) it is straight at the GB, because of the recombination due to the surface states. The width of the upwards curving arrows in the middle of (b) and (c) indicate smaller (b) compared to stronger current (c). The dashed up-and down-wards curved lines at the grain boundary (b) show the strong p-type, n-type and weak p-type band bending of a clean (deepest down-ward ones, purple), oxidized (up @ Ec and down @ Ev; red) and partially oxidized (sum of oxidized and clean) surface (intermediate; blue). After [73]. 18

Figure 2.1 - Scanning electron micrographs cross-sections of SLG/Mo/CIGS (containing Na) and SLG/SiN/Mo/CIGS (Na-free) structures 20

Figure 2.2 – (a) Ga grading in-depth SIMS profile of CIGS absorbers grown with different Cu excesses (b) Na depth profile of the top layer of CIGS absorbers grown with different Cu excesses at high temperature determined by SIMS. After [113] 22

Figure 2.3 - Scanning electron micrograph of absorber treated with KF (a) as-deposited (b) rinced with water. After [134] 27

Figure 2.4 - SEM microgrph of CIGS surface treated with KF (up) or not (down) before (left) and after (right) HCl etching. After [134]..... 28

Figure 2.5 – ^{23}Na and ^{39}K SIMS profiles in complete solar cell grown on Mo layers sputtered with DC-powers of 1.5 and 4.6 W/cm^2..... 30

Figure 2.6 – Voc (left) and FF (right) statistical results of solar cells grown on the 3 types of Mo and subjected to KF-PDT (red) or not (black) Each box gives statistical results on 28 cells. The box has lines at the lower quartile, median and upper quartile values. Lines extending from each end of the box show the extent of the rest of the data..... 31

Figure 2.7 – JV characteristic (left) and EQE (right) of solar cells with absorber treated with KF (red) or not (black) that illustrate the beneficial effect of KF-PDT 32

Figure 2.8 - JV characteristics (left) and EQEs (right) of solar cells with absorber treated with KF (red) or not (black) that illustrate the detrimental effect of KF-PDT 32

Figure 2.9 – ^{23}Na (triangle symbols) and ^{39}K (no symbols) SIMS profiles in solar cells with peeled off SLG/Mo with absorber treated with KF (red) or not (black).. 33

Figure 3.1 – Ga $2p_{3/2}$ XPS spectra of untreated (black) and KF-treated (red) absorbers from (a_1) Run#1 and (a_2) Run#2 38

Figure 3.2 – In $3d_{5/2}$ XPS spectra of untreated (black) and KF-treated (red) absorbers from (a_1) Run#1 and (a_2) Run#2 39

Figure 3.3 – Cu $2p_{3/2}$ XPS spectra of untreated (black) and KF-treated (red) absorbers from (a_1) Run#1 and (a_2) Run#2 39

Figure 3.4 – Se 3d XPS spectra of untreated (black) and KF-treated (red) absorbers from (a_1) Run#1 and (a_2) Run#2 40

Figure 3.5 - Effect of KF-PDT on the valence band of absorbers from (a1) Run#1 grown in Na-free conditions and (a2) Run#2, subjected to KF-PDT (red lines) or not (black lines). Valence band normalized in intensity at 3eV is given in inset for case#1. (b) A zoom on the valence band edge (VBE) maximum is also given in that case. Black square and red triangle symbols corresponds to the experimental data of CIGS#1(SiN) and CIGS#1(SiN,K), respectively. Lines corresponding to the fit of experimental data in the BE range [0.7 - 1.4 eV] for the reference absorber and [0.9 - 1.3 eV] (line1) or [1.3 and 2eV] (line2) for the KF-treated absorber are also plotted to extract the energy of the VBE maximum in both samples. 41

Figure 3.6 - Effect of the KF-PDT on the Na 1s XPS spectra in absorber from (a1) Run#1 and (a2) Run#2 subjected to KF-PDT (red) or not (black) 43

Figure 3.7 – (a) K 2p XPS peaks and Se LMM auger transition lines and (b) O 1s XPS peaks in absorbers from Run#1 (grown in presence of Na or not) and from Run#2 subjected to KF-PDT (red) or not (black). 44

Figure 3.8 - Effect of rincing the KF-treated absorbers from Run#2 in diluted amonia on (a) Ga $2p_{3/2}$, (b) Cu $2p_{3/2}$, (c) In $3d_{5/2}$, (d) Se 3d, (e) O 1s, (f) K 2p, (g) F1s and (h) valence band XPS spectra..... 46

Figure 3.9 -- Effect of KF-PDT on RAMAN spectra of CIGS#1 and CIGS#2..... 49

Figure 3.10 - GIXRD patterns of absorbers treated with KF (red) or not (black)50

Figure 3.11 – (a) Ball-and-stick plot with 50% probability thermal ellipsoids emphasizing the adamantane-like structure and polyhedral plot of the $[In_4S_{10}]$ unit in KInS2; (b) (a) Polyhedral representation of the layers of vertex-linked $[In_4S_{10}]$ units in $KInS_2$. Each layer is rotated 90° relative to neighboring layers. The edges of the large $[In_4S_{10}]$ units in one layer nestle into the channels of the layers. After [163].. 51

Figure 3.12 - Views along the channels of potassium atoms showing the interlayer connections in KInS2. (a) Ball-and-stick plot with 50% probability ellipsoids and with the 6 shorter interatomic distances noted; (b) polyhedral plot. 52

Figure 3.13 – X-ray absorption at the K-edge of the potassium in CIGS#1(K). 53

Figure 3.14 - Model of the chemical modification induced by the KF-PDT in absorbers from Run#1 (beneficial effect) and Run#2 (detrimental effect). Scheme of near-surface absorber are given (a) prior (b) during and (c) after the rincing step of the KF-PDT 56

Figure 4.1 – Low magnification HAADF micrographs of the near CIGS/CdS interface regions in Cell#1(K) and Cell#1 59

Figure 4.2 – EDS mapping of the near CIGS/CdS interface region in Cell#1(K)59

Figure 4.3 – TEM micrograph of the absorber/buffer interface in Cell#1(K). 3 red circles indicate the EDS probe size and the investigated zones. Table on the right gives the corresponding EDS atomic percentage quantifications excluding Cu or not.60

Figure 4.4 – TEM micrographs centered in the CdS region in Cell#1 and Cell#1(K) with the corresponding EDS mapping of the oxygen. Boxes represent the area of the mapping that has been considered to extract the profile of O in these samples given on the right. 61

Figure 4.5 - TEM images of the CdS layer in both investigated cells 61

Figure 4.6 – TEM images of the CIGS/CdS interface in Cell#1(K) (left) and Cell#1 (right) 62

Figure 4.7 – HAADF (upper) and TEM (lower) micrographs of the CIGS/CdS interafce in Cell#1(K) 63

Figure 4.8 - Effect of the Cd PE on the photoemission lines corresponding to the valence band of absorbers from Run#1 grown in Na-free conditions and (a1) not subjected to KF-PDT (a2) subjected to KF-PDT. Valence band normalized at 3eV is given in inset. (b) A zoom on the valence band edge (VBE) maximum is also given for absorbers subjected to KF-PDT. Symbols corresponds to the experimental data. Dashed -lines corresponding to the fit of experimental data in the BE range [2 - 1 eV] for CIGS#1(SiN,K) and [2.3 - 1.5 eV] for CIGS#1(SiN,K,PE) are also plotted to extract the energy of the VBE maximum in both samples. 65

Figure 4.9 - Effect of the Cd PE treatment on the (a) K2p, (b) O1s and (c) Se3d XPS spectra of absorbers from Run#1 grown in Na-free conditions and subjected or not to a KF-PDT..... 66

Figure 4.10 – Profile of the Cd atomic concentration in reference and KF-treated absorbers from Run#1 grown in Na-free conditions and subjected to a Cd PE. The Ar+ ion etching was performed at 0.5keV energy. The etching speed has been calculated through the complete erosion of a 2 μm thick CIGS layer. Dashed lines correspond the fit of experimental data (excluding first point) following an exponential decay. A criterion of 1% atomic has been chosen to define the penetration depth of the Cd into the absorber..... 67

Figure 4.11 - Plane view SEM micrographs of absorbers treated (right) or not (left) with KF and dipped into the chemical bath for 0, 1, 3.5 and 7 min (from upper to bottom)..... 69

Figure 4.12 –Effect of dipping 1, 3.5 and 7 minutes in the chemical bath the untreated (left, subscript 1) and the KF-treated absorbers (right, subscript 2) on their (a) XPS spectra in the [0-21 eV] BE range and (b) O1s XPS spectra..... 70

Figure 4.13 - Effect of dipping 1, 3.5 and 7 minutes in the chemical bath the untreated (left, subscript 1) and the KF-treated absorbers (right, subscript 2) on their (a) K 2p and (b) Se3s and S2s XPS spectra..... 71

Figure 4.14 - Effect of dipping 1, 3.5 and 7 minutes in the chemical bath the untreated (1) and the KF-treated absorbers (2) on their $In3d_{5/2}$ XPS spectra..... 72

Figure 4.15 - Schematic plane view model of the CdS growth on untreated and KF-treated absorbers..... 73

Figure 4.16 - Raman diffusion spectra of CIGS#1(K)/CdS (red) and CIGS#1/CdS (black) samples. Raman spectra normalized at the maximum intensity of the A1 mode are given in inset..... 74

Figure 4.17 - Layer type ZnIn2S4 (IIIa) structure of the $CdIn_2S_{4-x}Se_x$ compounds, after [169]..... 76

Figure 4.18 - SEM micrographs of the BufferA ((CBD)CdS on SLG substrates) and the BufferB ((CBD)CdS on SLG/In_xSe_y) cross-sections. A micrograph recorded at lower magnification for the BufferB is given in inset..... 77

Figure 4.19 - XRD patterns (Bragg-Brentano configuration) of the BufferA and the BufferB. Positions of the relevant lines of the $CdIn_2S_4$ are dispayed in red..... 78

Figure 4.20 - XRD patterns (Bragg-Brentano configuration) of the BufferA' and the BufferB'. Positions of the relevant lines of the $CdIn_2S_4$ are dispayed in red. Zooms on the angular position of peaks related to the CdS are given in inset..... 79

Figure 4.21 - Raman spectra of the BufferA and the BufferB..... 80

Figure 4.22 - Absorption coefficient versus photon energy in the BufferA and the BufferB..... 81

Figure 4.23 - I-V measurments of buffer layers grown on SLG and SLG/In_xSe_y substrates. Tables on the right give the corresponding resistivity and conductivity extratacted from these curves considering the geometry of samples given in inset 82

Figure 4.24 – Model of the buffer layer growth in the chemical bath onto untreated or KF-treated absorbers 84

Figure 4.25 - EDS mapping of different elements in the vicinity of a GB close to the absorber surface in CIGS#1(K) 87

Figure 4.26 – Segregation of K in Cell#1(K), profiles at the interface and at a GB extracted from EDS mapping. 88

Figure 4.27 – Segregation of K in Cell#1(K), profiles at the interface and at a GB extracted from EDS mapping. 89

Figure 4.28 - Model of the hetero-junction in KF-treated (red, right) and untreated (black, left) devices 90

Figure 5.1 – Material model of the effect of the KF-PDT on the hetero-junction formation, built from the investigations shown in chapter 4 and 5. (a) Suggested absorbers prior the KF-PDT, leading to a beneficial or detrimental effect of the treatment. (b) New compounds formed at the surface of the absorber in both beneficial and detrimental effect of the treatment (studied in chapter 4). (c) Effect of the (CBD)CdS on the formation of the junction with untreated and treated absorbers, in case of a beneficial effect of the KF-PDT (studied in chapter 5). 91

Figure 5.2 - Evolution of the Voc with the temperature in Cell#1 and Cell#1(K) after white light soaking 94

Figure 5.3 -- Drive-level capacitance measurements in Cell#1 (black) and Cell#1(K) (red) after white light soaking 95

Figure 5.4 - Ga grading profiles (calculated from SIMS measurements) in absorbers from Cell#1 (black) and Cell#1(K) (red) 96

Figure 5.5 – Suggested electronic band diagrams of a standard solar cell (untreated with KF) and that of a device treated with KF, in dark, in a light-soaked state and at 0 V bias. No grading of the absorbers is considered 98

Figure 5.6 – J(V) curves and EQE of cells from Run#3 (no grading), treated (Cell#3(K)) or not (Cell#3) 100

Figure 5.7 -- J(V) and EQE of KF-treated absorbers with various Cu content (y) and Ga content (x) at the surface 103

Figure 5.8 -- Voc (left) and FF (right) statistical results of solar cells with an absorber subjected to KF-PDT (red, magenta or blue) or not (black) and dipped into the CdS chemical bath for 3 (blue), 5 (magenta) and 7 minutes (red and black). Each box gives statistical results on 18 cells. The box has lines at the lower quartile, median and upper quartile values. Lines extending from each end of the box show the extent of the rest of the data 105

Figure 5.9 -- J(V) curves (left) and EQE measurements of solar cells with an absorber subjected to KF-PDT (red, magenta or blue) or not (black) and dipped into the CdS chemical bath for 3 (blue), 5 (magenta) and 7 minutes (red and black).....105

Figure 5.10 -- Growth model of thin (CBD)CdS on untreated absorber, assuming the formation of the $CdIn_2(S,Se,OH)_4$ interface layer 107

List of Tables

Table 1.1 - Collaborations 3

Table 1.1 - Relative concentration of Cu, In/Ga (elements III) and Se in the α- and β-phase 10

Table 1.2 - Most important (in the framwork of this thesis) intrinsic and extrinsic defects in CIGS absorbers 12

Table 2.1 - Details for the "SampleType" entry in sample labels 35

Table 2.2 - Details for the "#Run" entry in sample labels 35

Table 2.3 - Details for the "specificities" entry in sample label 35

Table 2.4 - Summary of the issues adressed in this thesis, with corresponding samples used in each chapter 36

Table 3.1 - Quantification of chemical effects of the KF-PDT in K-treated investigated samples 47

Table 3.2 – Summary of XPS experimental findings in investigated samples .. 48

Table 3.3 – Summary of structural experimental findings in investigated samples 50

Table 3.4 - Summary of the most important experimental findings in investigated samples 56

Table 4.1 - SEM and XPS principal results from the comparative study of the CdS growth on untretaed and KF-treated absorbers 74

Table 5.1 - Effective hole concentration and width of the SCR in Cell#1 and Cell#1(K) after light soaking 95

Table 5.2 -- Correlation of the evolution of the photovoltaic parameters (due to the KF-PDT) with the presence of an OVC prior the treatment and the new compounds formed during the treatment 102

Table 5.3 – Binding energies, suggested associated compound and FWHM of fitted XPS contributions 119

General introduction

Photovoltaics - The world is moving towards a crucial climate change meeting in Paris in December 2015 (COP21), with the goal of setting the world on a sustainable path. According to the International Energy Agency (IEA), energy production and use is responsible for two-thirds of greenhouse-gas (GHG) emissions, and electricity amounts to about 20% of the total energy consumption.

Photovoltaic (PV) systems have a very low energy pay-back time, entail no GHG emissions during operation and do not emit other pollutants (such as oxides of sulphur and nitrogen); additionally, they consume no or little water. As local air pollution and extensive use of fresh water for cooling of thermal power plants are becoming serious concerns in hot or dry regions, these benefits of PV become increasingly important. Moreover solar energy is widely available throughout the world and can contribute to reduced dependence on energy imports. As it entails no fuel price risk or constraints, it also improves security of energy supply.

Total PV systems installed capacity at the end of 2014 globally amounted to 177 GW. They are mostly grid-connected and produce at least 200 billion kWh, which represent about 1% of the electricity demand of the planet. With declining prices in the last few years, PV appeared now in energy policies in numerous countries and plans for PV development have increased rapidly all over the world. In some countries, the transition from the current financially supported market to a more competitive PV market slowed the development of this technology in the last few years. However, according to the IEA roadmap, PV's share of global electricity should reach 16% by 2050, corresponding to 4 600 GW of installed PV capacity that would avoid the emission of up to 4 gigatonnes (Gt) of carbon dioxide (CO2) annually. In order to achieve the vision in this roadmap, the total PV capacity installed each year needs to rise from 38.4 GW (in 2014) to 124 GW per year on average, with a peak of 200 GW per year between 2025 and 2040.

The roadmap mentioned above assumes that the costs of electricity from PV in different parts of the world will converge as markets develop, with an average cost reduction of 25% by 2020, 45% by 2030, and 65% by 2050. Although a part of the cost reduction has to come from the capital (purely economic), Zheng and Kammen [1] assume that the main cost reduction will come from technological innovations.

Nowadays PV is dominated by crystalline-silicon (c-Si) technology, which provides both the highest conversion efficiencies (commercial modules now exceed 21%) and the lowest prices (down to USD $0.72/W_p$ but with lower efficiency). However, the drastic cost reduction mentioned above implies a reduction of the material use and an important increase of the conversion efficiency. The latter could be fulfilled by developing low-cost tandem solar cells that would convert a larger part of the solar spectrum. This would imply to combine different technologies, such as $Cu(In,Ga)Se_2$-based (CIGS) thin film solar cell, as the wide-band gap upper solar cell cannot be made of crystalline silicon since its energy band gap is not tunable.

$CuInSe_2$ technology - PV based on $CuInSe_2$ (CIS) absorber is already commercially available [2]. At laboratory scale this technology now overcomes the performance of its polycrystalline silicon counterpart [3]. It is very promising as it appears to be the ideal combination of low cost, high efficiency and low consumption of material since it can be grown as thin films (few micrometers in modules). Finally the possible tunning of the optical band gap by substituting indium by gallium and selenium (Se) by sulfur in this alloy could enable the synthesis of wide-band gap solar cells which, as previously mentioned, could be used as upper cell in tandem device.

This material has been firstly used for photovoltaic applications in 70's in Bell laboratory (see Ref [4] and references therein) and the first CIS-based thin film solar cell was reported in 1976 by Kazmerski *et al.* [5]. Since then, the -mostly empirical- development of this technology never stopped, leading very recently to a new certified world record conversion efficiency of 21.7% [3]. Reaching such very high efficiency was made possible by the use of a surface post-deposition treatment (PDT) based on the co-evaporation of KF under Se flow after the completion of the CIGS film. Unveiling the material effects induced by such treatment and correlating them to the electrical improvements are the purpose of this work.

Although this material has been widely studied in the past 40 years, there are still open questions that limit the development of the related solar cell technology:

(i) Why performance of device based on polycrystalline CIGS absorber overcome those based on monocrystalline one?

(ii) Why is it not possible to grow high efficiency devices in superstrate configuration?

(iii) Why open-circuit voltage of wide band gap CIGS solar cell is limited?

(iv) Why best solar cells contain a toxic CdS buffer layer deposited by chemical bath deposition?

The purpose of this work is not to answer these questions but some of them will be discussed in the framework of the KF-PDT. We hope it will contribute to unlock the remaining technological barriers mentioned above.

About this thesis - This manuscript intends to summarize three years of research at the Institut des matériaux Jean Rouxel (IMN) and at the Université de Nantes. For the sake of clarity we do not show all the results obtained in the framework of this PhD thesis and specially focus on the experimental findings that help to address the issues related to the understanding of the role of the KF-PDT detailed in chapter 3. In particular we do not report our contribution on the relation between the tolerance on CdS thickness and CIGS growth properties presented at the Material Research Society spring meeting at San Francisco in 2013 [6]. The results of a more fundamental X-ray Absorption Spectroscopy study on the environment of potassium, cadmium and sulfur in CIGS will be published later.

This manuscript is based on the analysis of only 3 absorbers. They were chosen because they are representative of the hundreds of synthesized samples requested to answer the issues.

This work results from national and international collaborations summarized in Table 1.1. I spent one month at Warsaw University of technology, two weeks at Universidad de Valladolid and one week at CLYM in Lyon. As mentioned above, all the results from these collaborations are not included in this manuscript but the fruitful discussions participated to the global understanding of the subject.

Table 1.1 - Collaborations

Technique	University / Laboratory
Capacitance, voltage dependent photo-luminescence (PL(V)), temperature dependent current-voltage measurement (J(V,T))	Warsaw university of technology, Poland
Time resolved Photo-Luminescence, grazing incidence X-Ray Diffraction	Université de Montpellier, France / Laboratoire Charles Coulomb (LCC)
Electron Beam Induced Current	Universidad de Valladolid, Spain / GdS optron laboratory
Transmission Electron Microscope	Institut National des Sciences Appliquées de Lyon, France / Centre Lyonnais de Microscopie (CLYM)
Atomic Probe Tomography	Université de Rouen, France / Groupe de physique des matériaux (GPM)
Kelvin Probe Force Microscopy	International Iberian Laboratory (INL), Braga, Portugal

The manuscript is organized as follow:

- In chapter 1 we provide general information about the CIGS solar cell technology. We detail the technical and theoretical aspects used in the following chapters.
- In chapter 2 we summarize the state-of-the-art concerning the roles and effects of alkali (Na, K) in CIGS and we detail the issues addressed in this thesis.
- In chapter 3 and 4 we report and model the material changes induced by the KF-PDT during both the treatment itself and the subsequent chemical bath deposition of the CdS.
- In chapter 5 we propose an electrical model based on the material assessment performed in previous chapter and we answer the issues.

Chapter 1
Theoretical and practical aspects of $Cu(In,Ga)Se_2$-based thin film solar cell

1.1 Basics of the solar cell

1.1.1 Standard device structure

The $Cu(In,Ga)Se_2$-based (CIGS) thin film solar cell (TFSC) is a stack of polycrystalline thin films. In the standard configuration (i.e. the substrate configuration) various substrates such as stainless steel [7], polyimide [8] or glass [3] can be used, all leading to high efficiencies [9]. The stack is grown layer per layer and is composed of four parts, as represented on the scanning electron micrograph in Figure 1-1, these parts are:

1. The metallic back contact. This is the negative electrode that collects the photogenerated holes. In our laboratory we use DC-sputtered molybdenum because of the good thermal expansion coefficient matching with Soda-Lime Glass (SLG) substrate, robustness towards the selenium environment and the ohmic contact provided by the formation of $MoSe_2$ layer between Mo and CIGS layer [10]–[12].

2. The pn junction, constituted of p- and n-type semiconductors. It creates a built-in electric field that separates the electron-hole pairs photogenerated by the incident light. The CIGS material is the p-type semiconductor. It is generally lower doped than the n-type semiconductor. Hence, the space charge region extends mostly in the CIGS layer. A major part of the electron-hole pairs are photogenerated in this material. It is thus called the ‘‘absorber''. There are several successful methods to grow the CIGS layers [13], in our laboratory we use the co-evaporation method. The n-type semiconductor is often called the ‘‘buffer'' layer and it is much thinner (30-100nm) than the aborber. Several alternative material such as In_2S_3, ZnS or $Zn_{1-x}Mg_xO$ have been studied [2] but in this manuscript we focus on the standard Chemical Bath Deposition (CBD) of CdS, that leads to the best performance at laboratory scale.

3. The Transparent Conductive Oxide (TCO) layer. Generally called the ‘‘window'' layer as its energy band gap is high enough to be almost transparent to the photons in the convertible energy range (400-1300nm). TCO is used to help to the lateral collection of electrons by the front grid contacts. We use the standard RF-sputtered ZnO/ZnO:Al bilayer in our laboratory. Other TCOs such as Indium Tin Oxide (ITO) can be used.

4. The metallic front "grid" contact. This is the positive electrode that collects the photogenerated electrons. In our laboratory we use a Ni/Al/Ni stack deposited using an electron beam evaporator. Ni is used to avoid the oxidation of the aluminium by the ZnO. Our grid design is optimized to cover 2% of the total solar cell area, these cells being 5 x 10 mm².

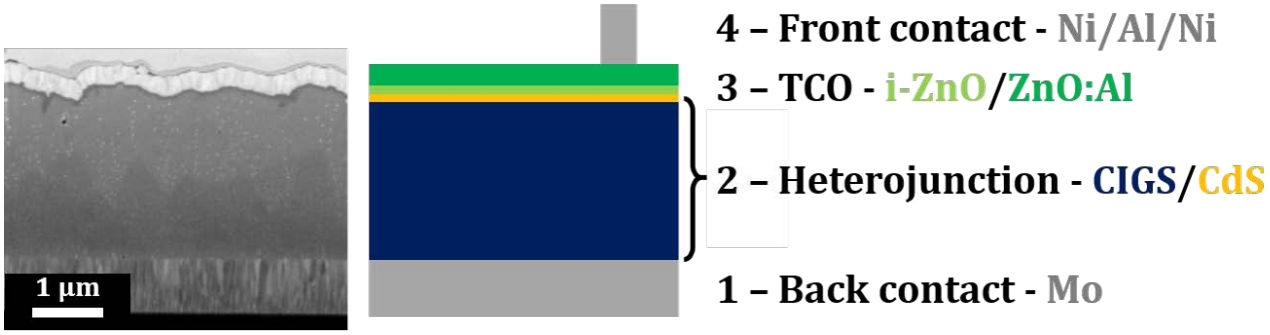

Figure 1-1 – Standard solar cell scanning electron micrograph of a polished cross section obtained by focused ion beam technique (left) with associated scheme (right)

1.1.2 Operating solar cell

Solar resources - Figure 1-2 shows the global AM1.5 incident spectral irradiance density, which is approximately that of a black-body radiating at about 6,000 K, interspersed with absorption lines mostly coming from the water vapor absorption within our atmosphere. It represents the power density carried by the amount of photons at a given wavelength that will reach the earth surface. The solar cell will convert these photons into electron-hole pairs. For example, without any optical losses and a complete collection of photogenerated carriers, a device based on an absorber with a band gap energy of Eg=1.15eV should lead to a short-cicuit current J_{sc} (see next section) of about 41.7 mA/cm² [14].

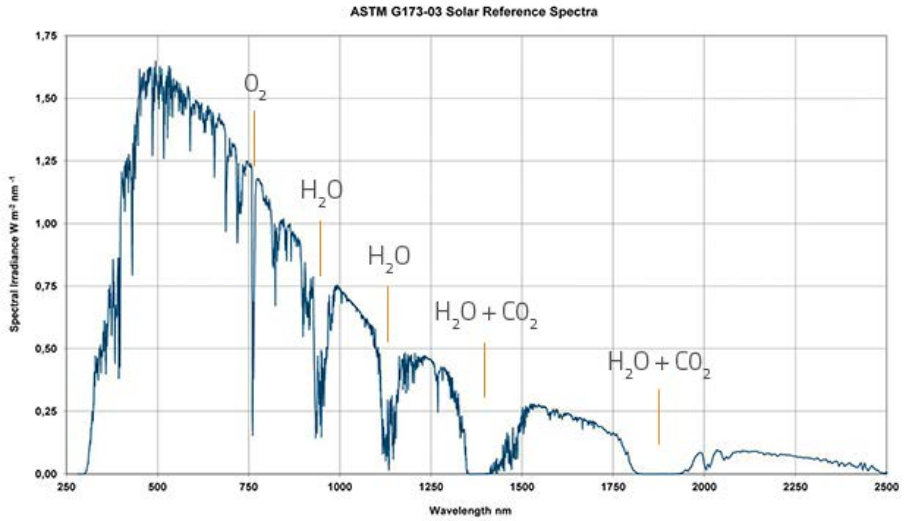

Figure 1-2 – AM1.5 incident light spectrum with compounds responsibles of the absorption in the atmosphere

Outpout power – Typically the buit-in voltage induced by the pn junction helps to collect electron-hole pairs photogenerated by the photovoltaic effect. Figure 1-3 shows the typical power density vs. voltage characteristic for CIGS-based solar cell grown in our laboratory. Convention for the current density and voltage directions are given in the inset. The load must be adapted so that the solar cell can deliver its maximal power density $P_{max} = |V_{max}.J_{max}|$, typically about 20 mW/cm² for best cells. Three output photovoltaic parameters can be defined to calculate the photovoltaic conversion efficiency, that is the

delivered maximal power density relative to the standard 100mW/cm^2 AM1.5 incident power P_{inc} ($\eta=P_{max}/P_{inc}$). These parameters are the open-circuit voltage (V_{oc}), the Fill Factor (FF) and the short-circuit current density (J_{sc}). At V_{oc} no current flows the device (J=0). J_{sc} is the current density at zero bias. Ideally the J_{sc} is equal to the photogenerated current J_L. The FF measures how "square" the J(V) characteristic is. It is represented by the ratio between red and blue area in Figure 1-3. Finally we have:

$$V_{oc} = V(J=0);\quad J_{sc} = J(V=0);\quad FF = \frac{|V_{max}.J_{max}|}{|V_{oc}.J_{sc}|};\quad \eta = \frac{|P_{max}|}{P_{inc}} = \frac{V_{oc}.J_{sc}.FF}{P_{inc}} \qquad (1.1)$$

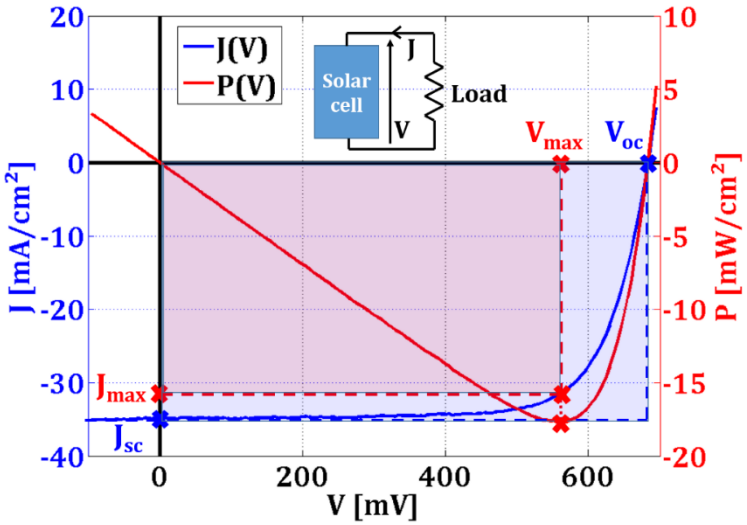

Figure 1-3 – Current density – voltage (blue) and power – voltage (red) typical characteristics of solar cell

Generation - The CIGS material has a direct band gap [15] and thus a strong absorption coefficient; only a few micrometers are needed to absorb almost all of the photons in the visible and near-visible energy range (250-1300 nm). Figure 1-4-a depicts the generation profile in a standard structure as that shown here above, as described by J. Malmström in his PhD thesis [16]. This profile is very useful since the probability for an electron-hole pair to contribute to the output current depends on the location at which it was generated. In Figure 1-4-a, one can see that most of the electron-hole pairs are photogenerated in the first 500 nm of the absorber. Figure 1-4-b shows a simulated external quantum efficiency (EQE) from the PhD thesis of M. Gloecker [17]. EQE represents the proportion of photogenerated carriers that contribute to the output current. J_L can be calculated from the EQE measurement:

$$J_L = q\int_{\lambda} \Phi(\lambda).EQE(\lambda)d\lambda \qquad (1.2)$$

where q is the elementary charge and $\Phi(\lambda)$ the AM1.5 flux density per unit wavelength [cm^{-2}nm^{-1}s^{-1}].

One can see that some losses (EQE<1) are optical (reflexions and non absorption of the photon with associated energy below the band gap) whereas others are electronic. These electronic losses include most of the electron-hole pairs generated outside the absorber. In fact these carriers do not (or poorly) participate to the output current since no effective electric field is present to collect them (window) or due to the presence of a high density of defects (CdS). The red area illustrates the proportion of the carriers photogenerated in the CIGS but not collected because they recombined before reaching the electrodes. Analyses of these recombination processes will follow, but firstly, we need to define the electronic band diagram.

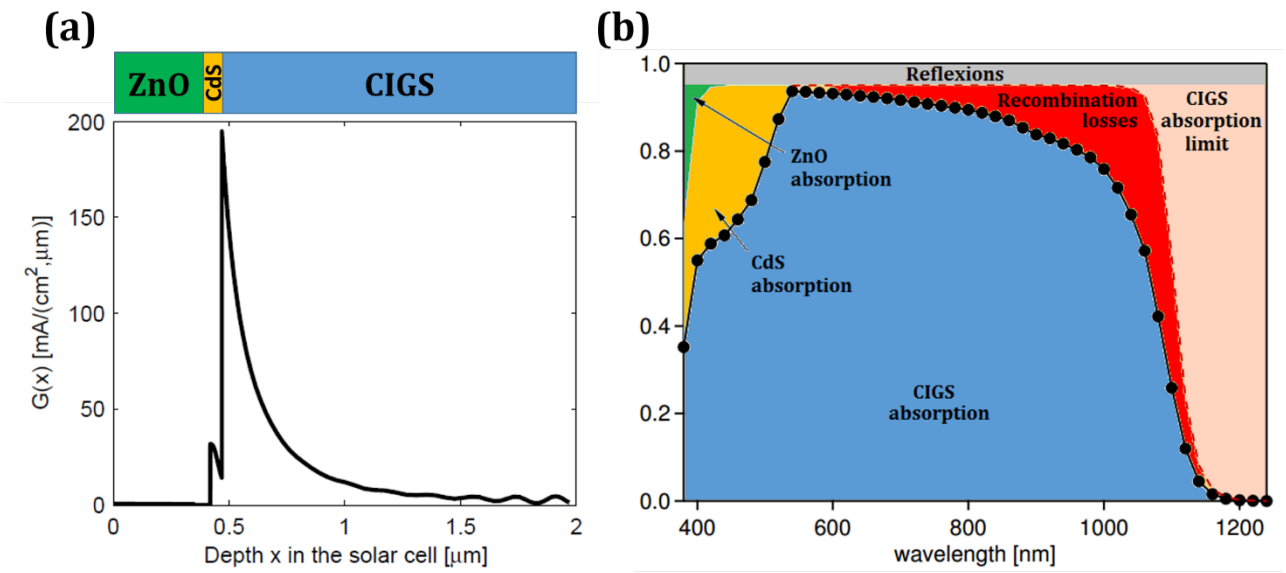

Figure 1-4 – (a) Generation profile in a standard CIGS-based solar cell structure containing ZnO bilayer and CdS/CIGS hetero-junction, After [16]; (b) External quantum efficiency

1.1.3 Transport

One-diode model - Ideally, a solar cell J-V curve represents that of a pn junction diode (recombination current density J_R) shifted by the photogenerated current $J_L \approx J_{sc}$. Parasitic losses can be included into ohmic series (R_s) and shunting (R_{sh}) losses and an ideality factor (A) higher than one in the diode equation current [18]. Finally the current density can be written as:

$$J(V) = J_R + \frac{V - R_s.J}{R_{sh}} - J_L \tag{1.3}$$

$$J_R = J_0\left(e^{\frac{q(V-R_S.J)}{AkT}} - 1\right) \tag{1.4}$$

With J_0 the saturation current density and k the Boltzman constant. Here we assume J_L independent of the applied voltage. Typical values in our solar cells are $J_0=5.10^{-10}$ mA/cm², A=1.5, R_s=1 Ω and R_{sh}=500 Ω. J_0 is a thermally activated quantity and may be written as:

$$J_0 = J_{00}\, e^{\frac{-E_a}{AkT}} \tag{1.5}$$

Where E_a is the activation energy of the saturation current density and J_{00} is a prefactor weakly temperature dependent. Its value and expression depends on the specific recombination mechanism that dominates J_0. Combining (1.3) and (1.4) and assuming $R_{sh}>>V_{oc}/J_L$ we obtain a general expression for the V_{oc}:

$$V_{oc} = \frac{E_a}{q} - \frac{AkT}{q}\ln\left(\frac{J_{00}}{J_L}\right) \tag{1.6}$$

Figure 1-5 illustrates the effect of varying these parameters on the J(V) characteristic; the lower J_0 the higher V_{oc}. The FF decreases as A or R_s increase or as R_{sh} decreases.

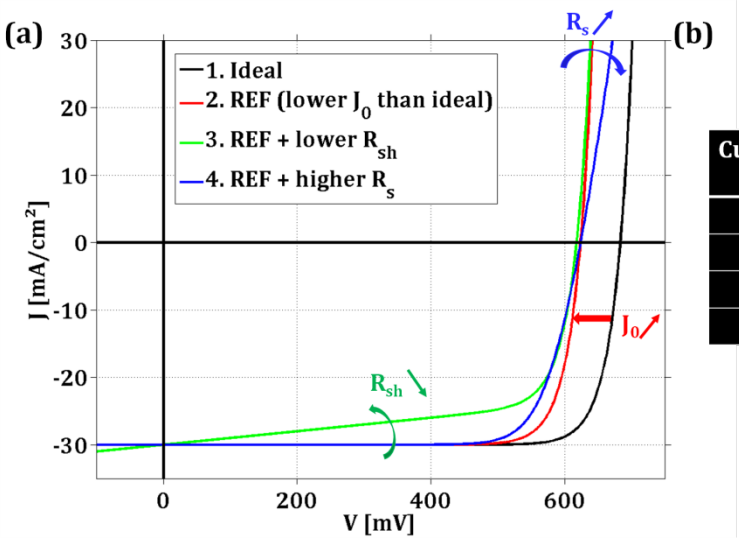

Curve	J_0 [mA/cm²]	R_{sh} [Ω]	R_s [Ω]	A [no unit]
1	1.10^{-10}	∞	0	1
2	$\mathbf{1.10^{-9}}$	∞	0	1
3	$\mathbf{1.10^{-9}}$	**100**	0	1
4	$\mathbf{1.10^{-9}}$	∞	**1**	1

Figure 1-5 – (a) Effect of lowering J_0 or R_s and increasing A or R_{sh} on the J(V) characteristic compare to the ideal case; (b) corresponding values for these parameters in the simulated curves

Band diagram - In contrast to a homo-junction, the use of different materials for p and n semiconductors will have an impact on the electronic band structure of the device. If the electron affinities[1] are different, energy band discontinuities will be induced. The discontinuity at the CIGS/CdS interface has been widely debated (see section 1.4.1). The presence of a "spike", resulting from that the conduction-band minimum in the CdS is at higher energy than the conduction band minimum of the CIGS, would reduce the recombinations of the electron-hole pairs at this interface and could explain why the use of CdS as buffer layer material leads to high efficiencies.

Figure 1-6 shows the one-dimensional (1D) energy band diagram of a device structure in the case of an ideal CIGS absorber, in the dark and at 0V bias. By "ideal" we here mean a CIGS layer without compositional gradients, neither in Ga/In (see section 2.3.2) nor in Cu in the close surface area (see section 2.4.2). One can notice the conduction band discontinuities at the CIGS/CdS and CdS/ZnO interfaces. ZnO:Al is a degenerated semi-conductor and has its Fermi energy level above E_c.

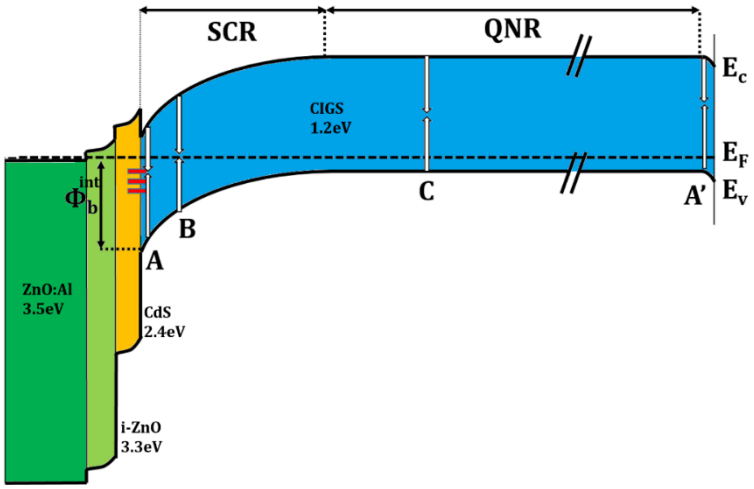

Figure 1-6 - One-dimensional (1D) energy band diagram of a complete solar cell structure in case of non graded CIGS absorber with no copper depleted surface layer, in dark and at 0V bias.

[1] Electron affinitiy is defined as the energy obtained by moving an electron from the vacuum just outside the semiconductor to the bottom of the conduction band just inside the semiconductor,

Recombinations - A part of the photogenerated charge carriers will not participate to the output current as they will recombine before reaching the metallic contacts, i.e. a free electron can be captured by a hole by different recombination pathways described by white arrows in Figure 1-6. These recombination pathways in the absorber can take place either at interfaces, in the Space Charge Region (SCR) or in the Quasi-Neutral Region (QNR), and denoted as (A/A'), (B) and (C) in Figure 1-6.

The different pathways obey the Shockley–Read–Hall (SRH) type recombination [19] and can also be described as diode currents. They are effectively connected in parallel so the V_{oc} will be controlled by the single dominant mechanism with the highest current. The activation energy for recombination at the back contact, in the QNR and in the SCR is equal to the energy band gap E_g whereas in case of recombination at the CIGS/CdS interface it equals Φ_b^{int} (see Figure 1-6). The SRH recombination is greatest through deep trap states in the space charge region where a similar amount of free electrons and holes are available, i.e. p≈n. In this particular case we obtain A=2. In the other recombination pathways A should always be equal to one. In practice, the recombination often may not fit the textbook cases due to, for example, recombination through defect bands rather than discrete states or by tunneling or multistep processes.

In some cases (including metastabilities) there is no dominant mechanism and the one-diode model fails to describe the device [20]. In these cases, more complex multiple-diodes models, as described in Figure 1-7, can be used.

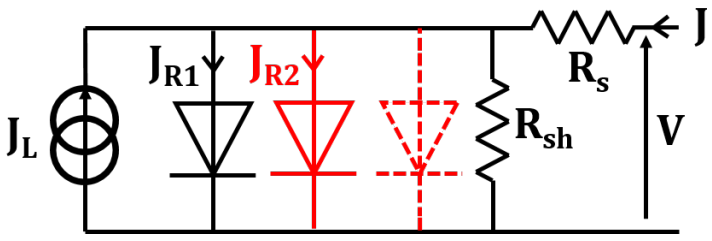

Figure 1-7 – Multiple-diodes model

The linear extrapolation of experimental $V_{oc}(T)$ curves to T=0 K yields the activation energy of the dominant recombination pathway, i.e. $E_a=E_g$ in the bulk or $E_a=\Phi_b^{int}$ at interfaces. Further analyses of the temperature dependence of the ideality factor and the saturation current density J_0 can supply valuable additional informations about the recombination mechanisms. A comprehensive understanding of these advanced analysis can be found in ref [21].

Bulk recombinations, especially in the SCR where p≈n, dominate in high efficiency CIGS-based solar cells. Recombinations at the CIGS/CdS interface are reduced by the presence of a thin layer called Ordered Vacancy Compound (OVC), (see section 1.2.1 and 1.4.2) that has a larger band gap. The barrier Φ_b^{int} is thus increased. The quasi-ohmic contact (instead of Schottky contact) due to the presence of $MoSe_2$ reduces the recombination velocity at the Mo/CIGS interface. However recombinations at this interface have been reported when the absorber is thinned or when a lower amount of $MoSe_2$ is formed [10]–[12]. Finally interface recombinations are reported for absorber layers with high Ga content[22], [23] or high Cu content [24] (see next section).

1.2 CIGS material

1.2.1 Structural properties

CIGS is a solid solution of $CuInSe_2$ (CIS) and $CuGaSe_2$ (CGS), both being semiconductors that belong to the I-III-VI_2 material family. CIS and CGS have the same crystal structure, that of the tetragonal chalcopyrite lattice, shown in Figure 1-8-a. This structure can be deduced from the cubic sphalerite (zincblende) structure by doubling the unit cell [25], [26]. All of the atoms are in tetrahedral sites. Ga is randomly added in the structure by isovalent substitution of indium atoms. We define as x=[Ga]/([In]+[Ga]) and y=[Cu]/([In]+[Ga]) the gallium and copper content with respect to the group III elements concentration (i.e. In and Ga).

Figure 1-8c shows the pseudobinary phase diagram of $CuInSe_2$ for Cu content ranging from 15 to 30%. The diagram is given as a function of temperature. It is extracted from the pseudobinary tie line between Cu_2Se and In_2Se_3 [25] in the ternary phase diagram of the Cu-In-Se system, shown in Figure 1-8b. Four different phases exist in the temperature range used during thin film deposition: the α-phase ($CuInSe_2$), the β-phase ($CuIn_3Se_5$), the δ-phase (the high-temperature sphalerite phase) and Cu_2Se. The β-phase is actually a defect chalcopyrite phase that will be debated in section 1.4.2.

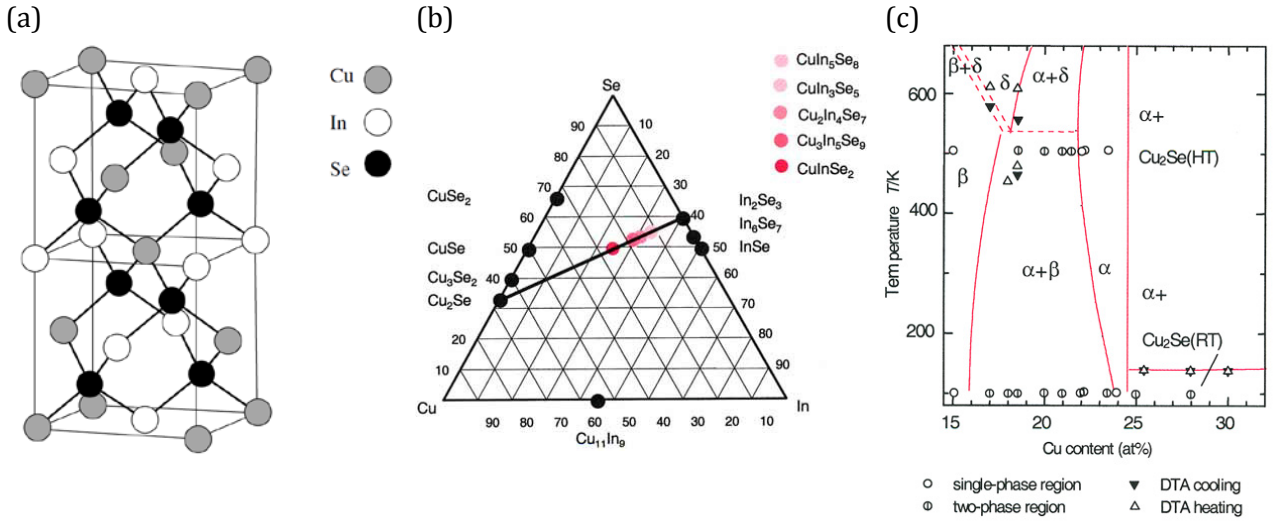

Figure 1-8 - (a) Chalcopyrite structure [4], (b) Ternary phase diagram of the Cu-In-Se system [27], (c) Quasi-binary phase diagram of CuInSe2 established by Differential Thermal Analysis (DTA) and microscopic phase analysis.[25]

One can see that the existence range of the single-phase $CuInSe_2$ does not extend to y=1 (i.e. Cu content = 25%). CIGS films grown for solar cell application have to be copper poor (y~0.9 corresponding to 22-24 at% of Cu) but even for this Cu content the α- and β-phases coexist at room temperature. However it has been shown that In substitution by Ga [28], and the presence of sodium [29], can widen the domain where single-phase $Cu(In,Ga)Se_2$ exists (see "Structural changes" in section 2.1.2).

Table 2.1 highlights that the lower Cu content in the β-phase results in higer contents of both the group III elements, but also of the Se.

Table 1.1 - Relative concentration of Cu, In/Ga (elements III) and Se in the α- and β-phase

Material	[Cu] [%]	[III] [%]	[Se] [%]
$Cu(In,Ga)Se_2$	25.0	25.0	50.0
$Cu(In,Ga)_3Se_5$	11.1	33.3	55.6

1.2.2 Opto-electrical properties

CIGS is a semiconductor and has a direct band gap. It is thus suitable for thin film solar cell as it has a very high absorption coefficient (10^5 cm^{-1}); almost the entire solar spectrum is absorbed within 2µm. The optical band gap E_g^{CIGS} can be tuned by increasing the Ga content from x=0 (pure CIS, E_g^{CIS} = 1.04eV) to x=1 (pure CGS, E_g^{CGS}=1.65eV), following the equation:

$$E_g^{CIGS}(x) = (1-x)\, E_g^{CIS} + x\, E_g^{CGS} - bx(1-x) \quad (1.7)$$

In this equation b refers to the "bowing coefficient", varying from 0.11 to 0.26 in literature. According to Wei *et al.* [28], the theoretical calculated value is 0.21. By using a first-principles band structure method these authors have theoretically found that increasing x in CIGS slightly decreases the energy level of the valence band maximum while the level of the conduction band minimum increases significantly. It means that the Ga content x impacts mostly the conduction band minimum. Other theoretical calculations [30] show that the Cu content y impacts mostly the valence band maximum while the conduction band minimum does not change.

1.2.3 Doping/defects

Unlike in semiconductors such as Si or GaAs, where external impurities are used for doping the materials, the p-type character of CIGS largely results from intrinsic defects. The net hole concentration, that directly influences the built-in voltage (and thus V_{oc}) and the width of the SCR (and thus the collection of the carriers), results from the difference in concentration of acceptor and donor defects in these compensated semiconductors. Best devices are based on Cu-poor absorbers. The CIGS surface and bulk defect physics is based on a high tolerance for off stoichiometry and related low defect formation energies, which is probably the key to a profound understanding of the device performance of these solar cells [15], [30]–[32]. A large amount of intrinsic defects can exist in CIGS. If we consider vacancies, antisites and interstitial sites for all of the constituent atoms of CIGS we find 20 intrinsic defects. Intermixing of elements at the CIGS/CdS interface [33]–[37] complicates the picture with additional extrinsic defects. Interpretations of experimental electronic transitions of these defects have animated the scientific community for years. A comprehensive theoretical work has been performed [28], [30] and compared with experimental data. An interesting result from these calculations is that the defect formation energies depend of the Fermi level position and can be influenced by an applied voltage or a local band-bending.

In this section we will focus on the most important point defects in the CIGS within the framework of this thesis. In particular we will not debate the vacancy complexes at the origin of light and bias metastabilities [20], [38]. For more details one can refer to the rather recent and exhaustive review of doping, point defects and metastabilities in chalcopyrite [15].

Intrinsic defects – According to calculations In_{Cu}, Cu_{In}, V_{Se}, and V_{Cu} should be the most abundant defects (in this order). In_{Cu} and V_{Se} are donor defects (corresponding energy E_T close to that of the conduction band E_C), Cu_{In} is a recombination center (see the following paragraph) whereas V_{Cu} is an acceptor defect (E_T close to the valence band E_V). The shallowest donor defect is interstitial Cu_i, and is important because Cu is known to be highly mobile in CIGS (see for example ref[39]).

The exceptionally low formation energy of the shallow acceptor V_{Cu} is responsible for the intrinsic p-type doping in CIGS, in the range of 10^{14} to 10^{16} cm^{-3}. It easily forms together with the donor In_{Cu} a very stable neutral complex $\{2V_{Cu}^{-} + In_{Cu}^{2+}\}$ which explains the electrically benign character of a large defect density present in non-stoichiometric CIGS and why this material is highly compensated. The pairing induces a very shallow level close to the conduction band, which is consequently not acting as an effective recombination center. Furthermore Zhang *et al.* interpret the existence of ordered compounds $CuIn_5Se_8$, $CuIn_3Se_5$, $Cu_2In_4Se_7$, and $Cu_3In_5Se_9$ as a repeat of a single unit of the $\{2V_{Cu}^{-} + In_{Cu}^{2+}\}$ complex for each n=4, 5, 7, and 9 units, respectively, of CIS.

Extrinsic defects – Cadmium doping at the surface of the CIGS due to Cd in-diffusion is the most debated extrinsic defect in the community because it is thought to be responsible of the surface type inversion of the CIGS. In fact calculations show that Cd_{Cu} is a donor whereas Cd_{In} is an acceptor. Persson *et al.* [40] explain that the position of the Fermi level influences the formation energy of these defects. Therefore in CIS the surface can be doped n-type through the formation of Cd_{Cu} but it is not possible in CGS as the Fermi level position is pinned due to the very low formation energy of V_{Cu} in this compound. According to these authors this could be a reason why CGS cannot be n-type.

Recombination centers – A defect is considered as a recombination center if the probability to re-emit a trapped electron towards the conduction band is lower than the probability to emit it towards the valence band. Their energy is often located around the middle of the band gap. These defects highly limit the photovoltaic parameters. Moreover they can assist SRH recombinations. Interface recombinations through deep acceptor traps have been reported [41], and are enhanced by increasing the Ga content in this region [42], [43]. In fact Heath *et al.* [44] experimentally show the response from a band of defects centered around 0.8 eV from E_V in CIGS. The defect bandwidth, and its position relative to the valence band, remain constant with increasing the Ga content. Therefore this defect band may act as an important recombination center, contributing to the decrease in device efficiency with increasing Ga content.

Conclusion – The highly compensated doping of the absorber has been shown to be the result of the low formation energy of the acceptor V_{Cu}, the donor In_{Cu} and the resulting neutral complex $\{2V_{Cu}^{-} + In_{Cu}^{2+}\}$. Cd_{Cu} can possibly help to invert the surface type of low Ga content absorbers. A defect with energy around 0.8 eV above E_V is evidenced in CIGS independently of the Ga content and thus becomes a recombination center in wide band gap devices. Table 1.2 summarizes the most important defects in the framework of this thesis.

Table 1.2 - Most important (in the framwork of this thesis) intrinsic and extrinsic defects in CIGS absorbers

Defect	Energy (in CIS) [eV]	Type
V_{Cu}	E_V + 0.03	Shallow acceptor
In_{Cu}	E_C - 0.25	Compensating donor
V_{Se}	? (exp E_c - 0.07)	Compensating donor
Cu_i	E_C - 0.20	Compensating donor
Cu_{In}	E_V + 0.29	Recombination center in CIS
?	E_V + 0.8	Recombination center in high Ga content absorber
Cd_{Cu}	E_C - 0.10	Extrinsic compensating donor

1.3 CIGS growth

1.3.1 Deposition techniques

CIGS thin films can be deposited using solution-based techniques such as inks [45] or electrodeposition [46], [47]. These low-cost techniques are promising but still lead to low photovoltaic conversion efficiencies. To date, best efficiencies are achieved using vaccum-based techniques and CIGS modules are already commercially available [2] based on two major CIGS deposition techniques: co-evaporation and sputtering/selenization. A recent review of these techniques can be found in Ref[13]. Modules using absorbers deposited by selenization/sulfurization of Cu, In and Ga metallic precursor stack layer deposited by physical vapor deposition are already industrially implemented at the giga-watt scale [48]. In our laboratory we use the co-evaporation of Cu, In, Ga and Se that leads to the best efficiencies at laboratory scale [3].

1.3.2 Co-evaporation processes

This technique consists in the simultaneous heating of sources containing elemental Cu, In, Ga and Se under high vaccum (between 10^{-7} and 10^{-6} mbar). The evaporated elements can travel directly (sufficient mean free path) to a heated substrate where they condensate back to their solid state, diffuse, react and crystallize to form the thin film.

Many processes have been developed since the first CIS thin film has been co-evaporated in 1976 [5]. Basically, processes involve one, two or three steps [49] in which the substrate temperature and/or the fluxes are changed. One can notice that all of the deposition processes are performed under excess Se atmosphere in order to minimize the creation of Se vacancies V_{Se}, highly detrimental for the device performance.

In this thesis, two absorber growth processes are used to address the issues (see section 2.4.3). CIGS#1 and #2 investigated in chapter 3 and 4 are grown following the so-called 3-stage process detailed in the next section. CIGS#3 refers to an absorber grown following the simplest deposition process (one step process). This consists in simultaneously co-evaporating all of the elements under excess Se at rather high substrate temperature (typically 550°C). In this "one step" process the composition of the film does not vary during the deposition. The metal fluxes are adjusted in order to obtain the composition adapted for photovoltaic application (x~0.3 and y~0.9). Photovoltaic parameters (V_{oc}, FF, J_{sc}) of devices based on absorbers grown following this "one step" process are rather low. However, studying this kind of material is easier since this process does not induce any composition profile grading as in the case of the 3-stage process.

1.3.3 Case of the 3-stage process

This co-evaporation process has been firstly proposed by the National Renewable Energy Laboratory (NREL) [50] and leads to the best photovoltaic conversion efficiency at the laboratory scale[3]. During the first stage an $(In,Ga)_2Se_3$ precursor layer is deposited. Substrate temperature during this step is generally lower (350-400°C) than that of the second and third ones (500-600°C) in order to limit the roughness of the precursor [51]. This stage is followed by the evaporation of copper (under Se excess). The chalcopyrite is formed until the films turns Cu rich (y>1) and Cu_2Se phase segregates at the surface. During the last stage, In and Ga are evaporated again until the film is Cu poor (y~0.9) again.

End-point detection (EPD) method – The emissivity of the Cu_2Se phase being different than that of the CIGS, the power delivered to the substrate heater (lamps) necessary to keep constant the substrate temperature varies as a result of the change in the radiative behavior of the film surface. This output signal has been shown reactive enough to monitor the Cu content of the film [52].

Ga grading – A graded Ga content as a function of film depth is a result of the sequential process. Lundberg *et al.* [53] showed that In and Ga have different diffusion coefficient in CIGS, this difference being enhanced by the presence of Na (see section 2.1.2). This results in a double grading structure firstly evidenced by Gabor *et al.* [54]. An example of such grading profile from absorbers grown in our laboratory is given Figure 1-8; experimental details of how this profil has been obtained can be found in Ref [55]. This figure illustrates that the absorber can be separate into two parts (front/rear) by the "notch" position where the Ga content (and the band gap) is the lowest.

This double grading structure has been highly debated in the scientific community. Although inconsistent results have been reported concerning the effect of the front part of the grading [56], [57], many studies confirm the beneficial effect of the Ga grading in the rear part of the absorber [8], [54], [58], [59], especially when the thickness of the CIGS is reduced [59], [60].

Such a Ga grading is associated with a band gap grading within the absorber and thus establish "quasi-electric"[2] fields, denoted as ξ in Figure 1-9. If the gradings in the front and rear part of the absorber are approximated as straight lines, these "quasi-electric" fields can be written as:

$$\xi = \left|\vec{\xi}\right| = \left|-\overrightarrow{grad(V)}\right| \approx \frac{\Delta E_g}{qd} \tag{1.8}$$

The electrons photogenerated outside of the space charge region deep in the absorber (long wavelength photons) are better collected due to the additional "quasi-electric" field in the rear part of the absorber ξ_R (sometimes denoted as a Back Surface Field (BSF)), leading to an improved J_{sc}. According to Lundberg *et al.*, the BSF passivates the back contact as it will also reject the minority electrons from this interface and thus reduce the recombinations. This could then explain why the gain in V_{oc} and FF is higher in devices based on thinner absorber [59], more recombinations taking place at the back contact when the CIGS thickness is reduced.

As mentioned above the interpretation of the effect of the Ga grading in the front part of the absorber is not straight-forward. Qualitatively increasing the Ga content in the vicinity of the electrical junction will increase the band gap and help to separates charges, thus reducing recombinations. However the additional "quasi-electric" field ξ_F in this region tends to reduce the built-in electric field of the junction, which will have most likely a detrimental effect on the device performance. Although simulations predict an increase of the V_{oc}, Lundberg *et al.* could not conclude to any additional gain in performance due to an increased Ga content in this region.

[2] "Quasi-electric" fields are not the same for electrons and holes, contrary to the case of real electric fields. In this particular case the Ga grading mostly impacts the conduction band. The corresponding "quasi-electric" field will apply to electrons.

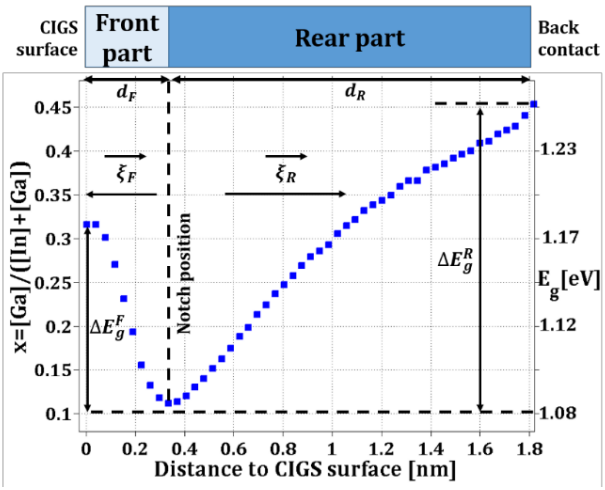

Figure 1-9 - Ga content x from Secondary Ion Mass Spectroscopy measurement and variation of the band gap across an absorber grown on SLG/Mo substrate

Recrystallization – Multi-stage processes are characterized by a step during which the composition of the films become Cu rich (y>1). During this step, the size of CIGS grains is significantly increased. As far as the 3-stage process is concerned this transition from small to large grains, called the recrystallization phenomenon, occurs when the films turn Cu-rich at the end of the second stage [61], [62]. Klenk *et al.* [63] proposed a model explaining such large grain growth based on an enhanced transport of group III elements through the liquid secondary Cu_xSe phase, which segregates when the film is Cu-rich. This model has been further supported by Niki *et al.* [64]. However Lundberg *et al.* found that the grain boundary diffusion was not significantly higher than the diffusion inside the grains, also for Cu-rich layers [53].

Barreau *et al.* [51] have suggested another model based on the grain boundary migration theory [65]. In their model these authors assume that the Cu-rich step decrease the energetic barrier for grain boundaries migration, allowing the increase of the grain size. They do not exclude the presence of the secondary Cu_xSe phase but it is not a necessary condition to explain the phenomenon.

1.4 High efficiency CIGS/CdS hetero-junctions

1.4.1 Role of the chemical bath deposited CdS buffer layer

Although (CBD)CdS layers lead to the best energy conversion efficiency, Cd is toxic and chemical bath deposition remains an issue for industrial scale-up. Moreover, this material has a rather low energy band gap of about 2.4eV. A significant part of the solar spectrum is absorbed in this layer. Unfortunately, corresponding photogenerated carriers are not collected, yielding lowered J_{sc}. Many other materials such as In_2S_3 or ZnS have been tried in order to replace the CdS buffer layer but lead to lower V_{oc} and FF [66]. For decades the role of the (CBD)CdS layer has been widely debated. Interpretations of the beneficial effects of (CBD)CdS are manifold. First a better coverage of the layer deposited by the bath compared to that deposited by physical vapor deposition (PVD) could help protecting the CIGS surface from sputtering damage during the deposition of the subsequent ZnO layer. As already mentioned in section 1.1.3 an adapted band structure configuration at the CIGS/CdS interface could also explain why the V_{oc} is not limited by interface recombinations. The presence of a conduction band offset has been widely studied but the results are inconsistent. XPS and UPS measurements of the valence band

alignment indicate a positive ΔEc between 0.2 and 0.7 eV on (PVD) CdS [67]–[69] whereas indirect measurements using surface voltage technique give ΔEc=-0.1 eV for a junction formed by CBD [70]. CIGS films could also be subjected to chemical etching of the surface during CdS deposition. In particular, native oxides are removed by the ammonia. Thus, the CBD process could clean the CIGS surface and enable a pseudo-epitaxial growth of the CdS buffer layer (especially for low Ga content) [71]. The interface between CIGS and CdS is characterized by intermixing of the chemical species [72]. Direct evidence of Cd in-diffusion and Cu depletion in the close-to-interface region of CIGS suggests the formation of the positively charged Cd_{Cu} defect [34]–[36]. The latter could create a p→n type inversion of the absorber surface and the formation of a homo-junction in the CIGS. Furthermore intermixing of S and Se has been observed and a model of S-induced surface defect passivation has been proposed [73].

1.4.2 Avoiding interface recombinations

Several models have been proposed in order to explain why high efficiency devices are generally not dominated by interface recombinations. Among them a buried homo-junction in the absorber involving a n-type layer at the surface of the absorber has been debated for more than 15 years [68], [29], [74]–[76].

OVC – Although Ordered Vacancy Compound (OVC) can correspond to various compounds in literature, in the framework of this PhD thesis the OVC will refer to the β-phase defect chalcopyrite ($Cu(In,Ga)_3Se_5$, see section 1.2). The OVC has been shown to be n-type [68] and to have a low carrier concentration [77]. The presence of a thin OVC layer at the surface of the absorber would then burry the junction inside the absorber. The p-n homo-junction between the p-type bulk chalcopyrite and the n-type surface defect chalcopyrite would reduce the interface recombinations since the perfect matching of the lattice between the two hetero-junction partners. Local defect relaxation under illumination, as well as Cu-electromigration due to a positively charged surface of this layer have been proposed to explain metastabilities such as the light-induced increase of the V_{oc} [29]. The extension in depth of the Cu depleted region is still subject of an ongoing debate. Recently this issue has been reviewed by Mönig *et al.* [76], underlying the lack of consensus about the thickness of this layer or even its existence. These authors suggest that it is limited to a very thin surface layer, giving rise to the first-principle calculated model of surface reconstruction [32], [78]. Finally n-type OVC layer seems not to exist for high Ga content material [79].

Cd doping – In addition to this OVC layer the beneficial type inversion at the surface of the absorber has been proposed to originate from positively charged Cd_{Cu} compensating donor defects [80], [34]–[36]. These defects would result from the Cd diffusion into the absorber grains during the (CBD)CdS deposition[3]. Hiepko *et al.* have shown by means of Atom Probe Tomography (APT) that Cd can diffuse into the CIGS bulk material [36]. However their extrapolated Cd diffusivity at 60°C (temperature of interest; CBD) is much smaller (D_{Cd} (60°C) ≈ 10^{-19} cm^2s^{-1}) than that reported for the diffusion along GBs at 60°C (3.6 10^{-12} cm^2s^{-1}) [81]. Cd-into-grain diffusion of ~10 nm is considered by Nakada *et al.* [82].

[3] Traditionaly, devices are air-annealed after the synthesis completion in order to improve the electrical performance. One could then suggest that the Cd in-diffusion could also happen during this air-annealing treatment (200°C, two minutes) and not during the CBD, explaining the beneficial effect of such air-annealing treatment.

1.4.3 Grain boundaries

The interest in Grain Boundaries (GBs) is strengthened by the observation that polycrystalline CIGS solar cells outperform their crystalline counter part (CIGS monocrystal). In this section we will only focus on GB properties that are thought to be useful for the understanding of the work presented in this manuscript. For a more general and exhaustive study of the GBs one will refer to the review proposed by Rau *et al.* on this subject [83].

It is surprising that GBs are not detrimental for solar cell efficiencies as these surfaces are likely to exhibit a high density of structural defects that could act as recombination centers. GBs in high efficiency devices have then to be passivated. Basically three models have been proposed to explain the electrically benign or even beneficial behavior of the GBs:

(i) *Intrinsic passivation* – Yan *et al.* [84] propose that the GBs in CIS do not create electrical deep levels in the band gap due to the large atomic relaxation in GB regions. Their assumptions are supported by first-principles calculations and scanning Kelvin probe microscopy measurements in CIGS films.

(ii) *Extrinsic passivation* – A model based on the neutralization of the positively charged V_{Se} defect by oxygen has been proposed by Cahen and Noufi [85], explaining the beneficial effect of air-annealing post treatments. Kronik *et al.* further contributed to this model by explaining the beneficial effect of Na in CIGS film via its catalytic effect on oxygenation at GBs [86]. Li *et al.* [73] have recently proposed a model of passivation of GBs via the sulfurization of these surfaces via the diffusion and occupation of selenium vacancies by S during the (CBD)CdS deposition.

(iii) *Cu-depletion* – The composition of GBs has been shown to be Cu-poor for low Ga content and Cu-rich for high Ga content [87]. Cu depletion is known to lower the valence band E_v. Therefore the composition of the GBs results in a local lowering of E_v in the vicinity of the GB region that repels holes and thus reduces the recombinations [88].

The models explaining the electrically benign behavior of GBs through the nature of intrinsic defects, oxygenation, sulfurization or composition at the GBs can all be modelized through local band-bending (BB) in the vicinity of GBs. We will discuss the schematic representation of the local BB at a GB proposed by Li *et al.* (see Figure 1-10) to describe the oxidation and sulfurization processes in the framework of models mentioned above. Figure 1-10-a can give an idea of a standard GB; p-type band-bending results from intrinsic positively charged donor defects (such as In_{Cu} or V_{Se}) and the lowering of E_v results from the Cu depletion. Figure 1-10-b illustrates the type inversion of the BB due to the oxidation. In this case the beneficial effect comes from the repeling of the electrons from the GB region. A more general trend is the reduction of the p-type BB through the passivation of donor defects, leading in the case of acceptor states creation (such as O_{Se}) to the inversion of the BB. Figure 1-10-c shows the effect of sulfurization. According to these authors p-type BB results from the neutralization of O_{Se} acceptor states by S. The lowering of E_v is due to the Cu depletion. One could also suggest that the sulfurized surface (substitution of Se by S) of the absorber $Cu(In,Ga)(Se,S)_2$ (CIGSS) can also contribute to this lowering of E_v [24].

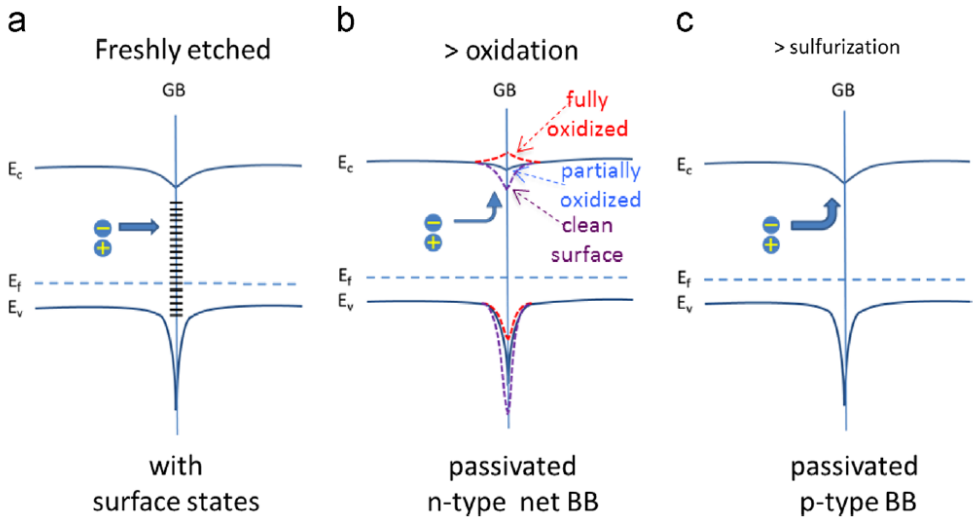

Figure 1-10 - Band diagrams of CIGS grain boundary (a) freshly etched, (b) after surface oxidation and (c) after surface sulfurization. The straight arrow pointing to the right in (a) refers to the photogenerated electrons, as do the curved arrows in (b) and (c). In (a) it is straight at the GB, because of the recombination due to the surface states. The width of the upwards curving arrows in the middle of (b) and (c) indicate smaller (b) compared to stronger current (c). The dashed up-and down-wards curved lines at the grain boundary (b) show the strong p-type, n-type and weak p-type band bending of a clean (deepest down-ward ones, purple), oxidized (up @ Ec and down @ Ev; red) and partially oxidized (sum of oxidized and clean) surface (intermediate; blue). After [73].

In case (a) and (b), the BB of E_v repels holes and thus reduces the recombinations. In the mean time electrons accumulate at the GB due to the BB of E_c. These regions become routes for minority carrier flow due to the low recombination rates in this region. This could explain why polycrystalline CIGS-based device performance overcomes that of devices based on monocrystalline CIGS.

Chapter 2
Alkali in Cu(In,Ga)Se_2-based thin film solar cell: state-of-the-art and issues addressed in this thesis

The purpose of this chapter is to position the work of this thesis within the state-of-the-art related to alkali in CIGS-based TFSC. We discuss the material and electronic changes induced by the presence of such species in the devices reported in literature. Then we explain how we supply alkali in our laboratory and define the issues of this thesis based on the fact that similar KF-PDT performed on *a priori* similar absorbers can lead to completely different electrical performance in related device.

2.1 On sodium

2.1.1 Background

Incorporation of sodium (Na) into the absorber represents one of the major breakthroughs that has allowed the CIGS-based thin film solar cell technology to reach very high efficiencies (see the photovoltaic conversion efficiency increase in 90's in ref [9]). The outstanding role played by Na in CIGS films is a question that has been debated for two decades and that is still not fully understood.

Supply - Hedström *et al.* reported the beneficial effect of Na on the electrical performance of the CIGS-based solar cell when they replaced the expensive borosilicate glass used at that time as substrate by the low-cost soda-lime glass (SLG), containing alkali compounds [89]. Many studies have been done to show [90], [91] and understand [92], [93] how Na diffuses from the glass substrate into the absorber through the molybdenum (Mo) layer. More recently, efforts have been made in order to optimize [94], [55] the Mo layer in order to let diffuse the proper amount of Na into the CIGS films. Mo layers containing a controlled Na amount have been proposed [95], [96]. There exists other approaches to supply Na to the CIGS films, consisting in evaporating NaF, or another Na-containing compound, before [97] or after [98] the CIGS growth. The latter supply method implies a subsequent annealing step after the evaporation of NaF in order to let diffuse Na into the absorber. This method is called the post deposition treatment (PDT).

Effects of Na incorporation – The presence of Na in CIGS film has been reported to lead to higher efficiencies for the complete device by increased the uniformity of short-circuit current density (J_{sc}) [99], higher open-circuit voltage (V_{oc}) [89], [90], [98]–[103] and higher Fill Factors (FF) [89], [99], [104]. Two main phenomenological effects have been found to result from Na incorporation, one related to the crystal growth of the CIGS and one related to it's electronic properties. These two effects are likely to be

inter-dependent and could explain such electrical improvement (see section 2.1.4). If Na is present during the CIGS film growth, the micro-structural properties of the final absorber are modified. These effects will be further discussed in section 2.1.2. Na-containing films have also more favourable electronic properties, especially increased free holes concentration, independently of the supply method [97], [103]. Substantial efforts have been invested to model the impact of Na on defects in CIGS and explain this increase of the free holes density. The debate is to determine whether Na has a direct (creation of shallow acceptor defect) or indirect (removal of compensating donor defect) effect and if this effect is located within the bulk material or at surfaces (including the Grain Boundaries (GBs)). This specific issue will be reviewed in section 2.1.3.

Distribution - The amount of Na required to obtain high efficiencies is rather small, typically in the order of 0.1at% [100]. Two diffusion pathways have recently been quantified [105] : a fast one alongside GBs and a slower one into the volume of CIGS grains, in good agreement with the fact that activation energies are generally lower for a diffusion along the GBs than that in the bulk [65]. Atomic Probe Tomography measurements have revealed [106], [107] that Na mainly segregates at the grain boundaries of the films but it is also detected within the CIGS grains at very low concentrations (50ppm). It is important to notice that in these studies Na was supplied by diffusion through the Mo layer during the CIGS growth and not added afterwards by PDT. Within the grains, Na is expected to segregate at crystalline defects; point defects (cation antisites) or higher dimension defects (dislocations, voids) [31], [106]. Finally Heske *et al.* have reported the presence of Na at the CIGS/CdS interface [72] and have highlighted the "self-limitation" nature of its content at the hetero-junction [108].

2.1.2 Na-induced changes during the CIGS growth

Grain size - When available during the CIGS growth (by diffusion or intentionnaly added with a precursor before the absorber deposition), Na strongly impacts the morphology of the film. However, inconsistent results concern the impact of Na on the size of the CIGS grain as both increased [104], or reduced grain size [109] are reported in presence of Na. Hence the grain size depends on the amount of Na available during the growth and the specific deposition process used [49]. In our laboratory, Na-free absorbers grown following the 3-stage process exhibit larger grains and a reduced grain boundaries density compared to that grown in presence of Na; Figure 2-1 gives scanning electron micrographs of two CIGS layers grown following the standard 3-stage co-evaporation process (see section 1.3) in presence of Na (SLG/Mo as substrate) or in Na-free conditions (SLG/SiN/Mo as substrate).

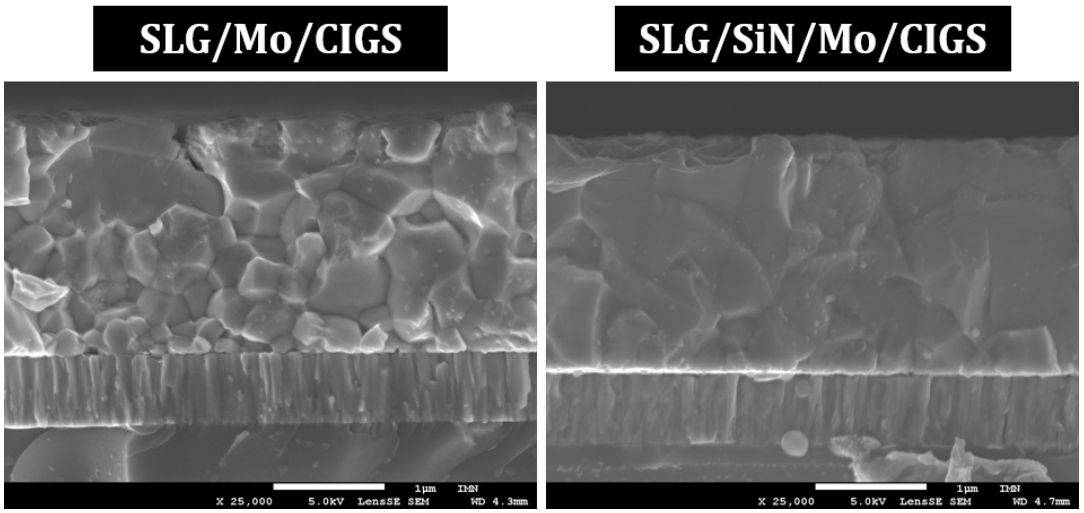

Figure 2-1 - Scanning electron micrographs cross-sections of SLG/Mo/CIGS (containing Na) and SLG/SiN/Mo/CIGS (Na-free) structures

Structural changes - A strong prefered *[112]*-orientation of the films has been reported due to the presence of Na during the growth [89], [97], [110], [51]. Na is also known to inhibit the formation of the OVC [29], [111], [112]. Recently Seyrling *et al.* [113] have shown that the presence of this OVC phase could be related to the amount of Na in the vicinity of the CIGS surface. In case of high amounts of Na at the CIGS surface, Raman scattering measurements did not reveal any OVC and the authors identified by SEM a thin layer with very small grains that may be attributed to a sodium-containing compound forming on the surface.

Theoretical work has been performed by Wei *et al.*. [31] on the formation of secondary phases in $CuInSe_2$ in presence of Na. They predict that Na easily substitutes Cu and that in sufficient amounts could form $NaInSe_2$. According to these authors $NaInSe_2$ exists under chalcopyrite structure (space group $I\bar{4}\bar{2}d$) but is more stable in a $CrNaS_2$–like structure (space group $R\bar{3}m$, see [114]). Being a layered structure with *c* axis along the *[111]* direction ($[112]_{tetra}$ in the tetragonal lattice), if such a phase is formed during the CIGS growth it could alter the film morphology of $CuInSe_2$, rendering it a preferred $(112)_{tetra}$ orientation. They also conclude that this phase separation of Na (and also O) secondary phases on the surfaces and grain boundaries purifies $CuInSe_2$, so it becomes more stoichiometric. This could then explain the inhibition of the formation of the OVC in presence of Na.

Compositional changes - Sodium affects also the diffusion of In and Ga during the CIGS growth. In sodium free films a higher diffusion coefficient of these species has been reported [53] compared to that in films with sodium. Rodriguez *et al.* proposed that Ga diffuses through V_{Cu} in CIGS [115]. As we will see in the following Na could tend to occupy these vacancies, and hinder the Ga diffusion. The presence of Na results in a higher [Ga]/([In]+[Ga]) grading in samples coevaporated following the 3-stage process (see section 1.3.).

Role during recrystallization –Couzinie-Devy *et al.* [116] investigated the composition of the CIGS grain in the vicinity of the GB before and after the recrystallization by means of Atom-Probe Tomography (APT). They show that the Na content within the grain is almost a decade lower after the Cu-poor to Cu-rich transition than it was prior. They also demonstrated that during the recrystallization the amount of Na inside the grain is below the detection limit of APT. Considering the possible sites occupied by Na in the grains they concluded that the recrystallization also minimizes the crystalline defect density in the bulk of CIGS.

Based on these results these authors [117] propose a new explanation of the preferred *[112]*-orientation of the final film in presence of Na mentioned above. Based on the model of grain boundaries migration (GBM) proposed by Barreau *et al.* [51] the grains of lower energy grow through the consumption of their higher energy neighbours during the recrystallization. The free-surface energy of the grain representing an important part of the total energy system they reconsidered the relative stability of the (112) and (220) surfaces when the film is Cu rich. By a first-principle electrostatic approach they show that the (112) surface can only be stabilized by the presence of Na-Se bonds. In Na-free samples grains with *[112]*-orientation are then likely to be consumed by those with the hence more stable (220). They calculated that only 6.5% of Na–Se relative to Cu–Se bonds (due to the presence of Cu_xSe) on top of the CIGS grain surface is sufficient to stabilize the (112) surface, hence to favour the growth of *[112]*-oriented grains at the expense of the *[220]*. Heske *et al.* [118] already suggested that the presence of Na species solely located on the CIGS surface and probably within the GBs reduce the surface dipole.

The model of GBM predicts also that impurities such as Na, because of their influence on the point defect concentration, can either hinder or enhance GB migration. This could explain why the grain size in the presence of Na is different to the Na-free case.

Recently, Seyrling *et al.* investigated the effect of the copper excess in the 3-stage co-evaporation process on Ga grading [119]. They use the end-point detection (see section 1.3) to define the time during which the film is over-stoichiometric and under-stoichiometric during the 2nd step of the growth and they estimate the Cu excess through the ratio of these durations. They show that the higher excess of copper the smoother Ga grading, as shown on Figure 2-2-a. This is understandable as a higher copper excess means a longer time during which the grains are almost Na-free and a longer enhanced In/Ga interdiffusion. In another study they relied this effect on the distribution of Na in the film. Figure 2-2-b gives the Na depth profile of the top layer of the CIGS absorbers grown with two different Cu excesses at high substrate temperatures, as determined by SIMS [113]. A higher Na amount is found in the absorber with the maximum Cu excess. One could assume that more Na diffused from SLG through the Mo during the longer deposition of the absorber with the high copper excess or that more Na was expulsed from the grain to the GBs. However a lower Na amount (-50%) is found in the vicinity of the surface of this absorber compared to that of the absorber with lower Cu excess. Although Heske *et al.* have shown that the Na amount is "self limited" at the CIGS surface [108] the Na amount at the surface of both absorbers should at least be the same. The fact that in the absorber with the higher Cu excess the Na amount is higher deep in the absorber and lower at the surface (with respect to the absorber with the lower Cu excess) means that the Na could not diffuse to the surface. A lower GB density is found in the absorber with the higher Cu excess (higher grain size due to the recrystallization). One could then assume that Na is located in the bulk, or at least bonded to it at the GBs (probably Na-Se bond, as related in the GBM). This lower amount of Na at the surface is extremely important because it allows the formation of the OVC.

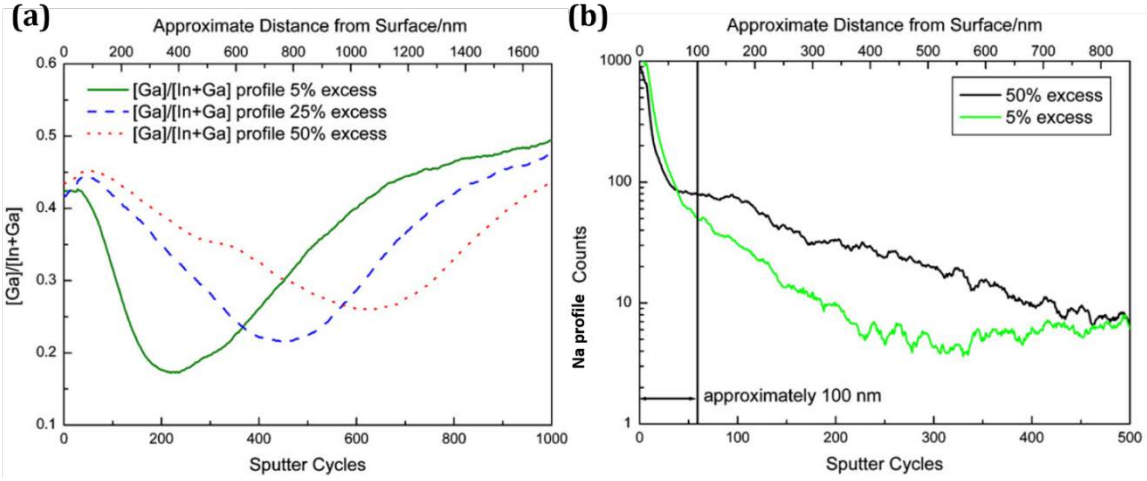

Figure 2-2 – (a) Ga grading in-depth SIMS profile of CIGS absorbers grown with different Cu excesses (b) Na depth profile of the top layer of CIGS absorbers grown with different Cu excesses at high temperature determined by SIMS. After [113]

Partial conclusion – It has been shown that the presence of Na during the growth affects the micro-structural properties of the CIGS film: prefered orientation, grain size, GB density, density of crystalline defects, Ga grading, Ga content at the surface, presence of the OVC. All of these changes are inter-connected and highly process-specific. When Na comes from the SLG, its diffusion is thermally activated through the Mo and varying the parameters of the CIGS deposition process (e.g. substrate temperature, duration of the deposition) will affect the amount of Na which diffuses (with effects on CIGS properties).

2.1.3 Increase of the free holes density

Higher p-type conductivity of the films has been reported in presence of Na [89], [91], [92], whatever the incorporation method [97], and leads to a strong increase of the V_{oc}. The explanations for the Na-induced increase of the p-type conductivity are also manifold. Mainly four types of explanations have been proposed:

(i) The first one is based on a *Na-modified growth* of the CIGS, supported by the impact of Na on the final morphology of the CIGS film [109]. During film growth, the incorporation of Na leads to the formation of sodium selenide compounds. This slows down the growth of CIGS and could simultaneously facilitate the incorporation of Se into the film [120]. The latter implies a decrease of negatively charged, thus compensating donor defect, V_{Se} and could explain the gain in p-type conductivity. Heske *et al.* [118] have suggested another mechanism for such Se incorporation. They identified a "metallic" Na specie that reduces the native oxide SeO_2 and release the elemental Se^0.

(ii) The second explanation is based on *Na-related defect* formation or redistribution [121]. Na could replace In or Ga in the CIGS lattice [122] to form the extrinsic defect $Na_{(In/Ga)}$ that could act as an acceptor. Na could also occupy Cu sites and prevent the formation of the deep double donor In_{Cu}. The incorporation of Na into the CIGS lattice is supported by X-ray diffraction measurements that indicate an increased volume of the unit cell [97]. Both defects would improve the p-type conductivity. Theoretical work performed by Wei *et al.* [31] predicts that Na_{In} (with In on its nominally site) can exist in very low concentrations and is a shallow acceptor. However Na will firstly replace In_{Cu} (more energetically favorable) and then replace V_{Cu} before creating such a defect.

(iii) The third explanation is based on a *Na-enhanced oxygenation* and passivation of grain boundaries that would diminish the positive charge at the grain boundaries and then increases the conductivity of the film. Firstly proposed by Cahen *et al.* [85] and further promoted by Kronik *et al.* [86] at free surfaces (including GBs) this model is based on the chemisorption of oxygen in the presence of Na. The latter only catalyzes the dissociation of O_2 into atomic oxygen that substitutes detrimental Se vacancies. Wei *et al.* have confirmed that O can effectively remove the compensating donor V_{Se} but suggested that O atoms in $CuInSe_2$ form Cu_2O and In_2O_3 compounds that will segregate at the surfaces and GBs.

(iv) The last explanation is based on the *Na-related electrical activity of GB*. Virtuani *et al.* have shown that the high resistivity of Na-free $Cu(In,Ga)Se_2$ results from electrostatic barriers at the grain boundaries and is not a bulk property [123]. Rau *et al.* have also reported significantly lower energy barriers at grain boundaries in Na containing absorbers. Recently, Urbaniak *et al.* [103] proposed a model based on the electrical activity of the GBs. In p-type CIGS, the high density of donor defects located at GBs can create potential barriers for holes. The resulting band bending in the vicinity of the GB decreases the effective holes density in this region. In their model the Na passivates these donor defects and decreases the potential barrier, resulting in an increase of free holes density.

2.1.4 Origin of the photovoltaic parameters enhancement

Open-circuit voltage and fill factor - Although Keyes *et al.* [101] claim that the actual increase in V_{oc} due to Na incorporation is higher than it would be expected simply based on the increase in carrier concentration, the origin of the beneficial effect of Na is mainly attributed in the scientific community to the higher effective acceptor concentration [90], [91], [102], [120], [124]. In post-deposition treatment (PDT) experiments, in which Na is supplied after the completion of the CIGS film, the effects of Na on CIGS growth are excluded, and most of the Na is expected to reside at the GBs. Based on all of these experimental observations and theoretical calculations one could suggest that Na increases acceptor levels through the passivation of compensating donor defects at free surfaces and at the GBs, either via direct substitution of In_{Cu} or via the release of atomic oxygen and the subsequent substitution of V_{Se}. Urbaniak *et al.* argue that if Na replaces In_{Cu} after the completion of the film (Na-PDT) the In has to go somewhere in the lattice and form another defect such as In_i or In_{Se} that are not acceptor defects and have a rather high formation energy so they conclude that Na replacing In_{Cu} cannot explain the increase of the free holes density. However if the substitution $Na_{In_{Cu}}$ takes place at the GBs, one could suggest that the available In and Na could segregate as $NaInSe_2$.

Additional gain on V_{oc} and FF can be explained by an improved hetero-junction. As mentioned above, Heske *et al.* [118] have shown that the presence of Na at the CIGS surface reduces the surface dipole and thus induces a band bending (lowering of the valence band edge maximum with respect to the Fermi energy level). Hence, such band bending helps to invert the semi-conductor type at the surface, resulting in a burried homo-junction (see section 1.4.1).

These authors assume that similar band bending could occur at the GBs. Therefore it would help to repulse holes and thus reduce recombinations through these defective surfaces. However as pointed out by Urbaniak *et al.* these electrostatic barriers can limit the hole transport from grain to grain. Fortunately electrostatic barriers at GBs are lowered by the presence of Na [83], [123]. A competition seem to happen at the GBs. The presence of Na probably diminishes the grains surface dipoles and thus increases the band bending at the GBs. This assumption is corroborated by the fact that the effective diffusion length can be dimisnished if the amount of Na within the film is too high. However, for appropriate amounts of Na this effect seems to be neutralized (or overpassed) by the reduction of positive charges through the passivation of compensating donors at these GBs.

Short-circuit current – Increased J_{sc} in Na-containing CIGS-based devices results from a longer effective diffusion length for minority carriers and/or a stronger Ga grading in absorbers grown following the 3-stage process. Lower minimum band gap allows the absorption of photon with lower energy (higher wavelength) and the stronger gradient in the rear part of the absorber (see section 1.3.3) induces a stronger pseudo-electric field which helps to collect the carriers photogenerated deep in the absorber.

2.2 On potassium

2.2.1 Background

The effect of the incorporation of other group Ia elements (alkali) on the properties of the CIGS absorber has been studied by Contreras *et al.* [97] when the beneficial effect of Na was reported. These authors compared the properties of absorbers grown on polycrystalline alumina substrates coated with thin NaF, KF and CsF precursor layers. They established that K increases the unit cell size of the chalcopyrite and increases the free holes density, but to a lesser degree than does Na. Cs, on the other hand, was found not to produce such effects, and in some instances to decrease the conductivity. These authors assumed that alkali enhance the conductivity by occupying the Cu sites, resulting in a passivation of In_{Cu} donor defect. They concluded that the efficiency of this occupation of Cu sites depends on the ionic radii, which would explain why K is less efficient to increase the conductivity and Cs not at all. Bodegård *et al.* studied the effect of the smallest alkaline element; they grew CIGS on top of LiF precursors but the associated solar cell performance was decreased compared to the reference [125]. All efforts of the scientific community were then focused on Na during more than a decade.

Recently, Wuerz *et al.* have reported a higher efficiency for a device based on an absorber grown on enameled steel sheet compared to that based on absorber grown on standard soda-lime glass (SLG) [7]. They attributed this increased performance to a higher doping and stronger elemental grading profiles due to the higher amount of K that diffused from the enamel into the CIGS layer as compared to the reference samples grown on glass substrate. However the true renewal of interest for potassium arised when Chirilă *et al.* claimed a new photovoltaic conversion world record efficiency for a solar cell based on a CIGS absorber treated with KF and grown on a flexible substrate [126].

These achievements on flexible substrates have opened new perpectives for devices based on glass substrates. Both industrial and academic laboratories improved their champion cell efficiencies, which has led to a new world record PV conversion efficiency for devices based on CIGS absorbers [3], [9].

The EMPA group introduced the potassium fluoride post-deposition treatment (KF-PDT) as a subsequent treatment to a NaF-PDT because they grow the CIGS on alkali-free polyimide foil (PI) substrates. Their CIGS growth process consists in four steps as follow:

(i) Co-evaporation of CIGS (substrate temperature 370-400°C as they use PI substrates)

(ii) NaF-PDT – Evaporation of NaF (30 nm, 1.3 nm/min) on cooled absorber (room temperature)

(iii) Annealing at CIGS growth temperature for 20 min

(iv) KF-PDT – Evaporation of KF (15 nm, 1 nm/min) in the presence of Se at a substrate temperature of about 350°C and cooling.

As in the case of NaF, KF-PDT can be performed at room temperature. The ZSW group (holding the world record efficiency) evaporates 25 nm of KF at 40°C and then anneals the film for 12.5 min at 350°C [127].

2.2.2 Electrical performance enhancement

Higher V_{oc} and FF [3], [126]–[129], as well as J_{sc} [3], [126] have been reported in devices based on absorbers with intentionnaly incorporated K. However in some cases the J_{sc} slightly deteriorates and the FF highly decreases after KF-PDT [130]. Considering the case where KF-PDT is purely beneficial, one can conclude that some of the improvements are (i) directly due to the incorporation of K while others are (ii) induced by a modified growth of the CdS layer due to the modification of the CIGS surface by the KF-PDT:

(i) Laemmle *et al.* have studied the effects of KF-PDT on alkali-free absorber [127]. They show a strong enhancement of the related device efficiency by 43% rel. compared to the reference caused by an increase in the V_{oc} and FF. They attributed these improvements to the passivation of grain boundaries and donor-like defects, as previously demonstrated for Na. In another study [129], these authors report the effect of KF-precursor layers on CIGS growth. They identified smaller grains in the presence of K and found an additional improvement of the J_{sc} due to a K-induced very strong Ga grading. In conclusion the potassium seems at first sight to act similarly as Na, whether it is present during the growth or added by PDT. However, Laemmle *et al.* also reports a strong Cu depletion and In enrichment, associated with a high concentration of K, in the near surface region of the absorber (see next section).

(ii) Chirilă *et al.* report [126] a thinning of the chemical bath deposited (CBD)CdS layer without the losses on Voc and FF that very thin buffer layers usually imply [131]. They explain that the modification of the CIGS surface induced by the KF-PDT allows a reduction of the deposition time in the chemical bath and thus a reduction of the thickness of the CdS. Carriers photogenerated in this low-band gap material (2.4eV) being not collected (see section 1.4.1), such thinning of the layer results in an improved Jsc in the short-wavelength region (400-520nm). Jackson *et al.* [3] also used a very thin CdS buffer layer in order to obtain their record 21.7% efficiency device.

Jackson *et al.* have published a review of the composition of their champion cells [128]. Usually wide-gap chalcopyrite solar-cells exhibit poor V_{oc} [43] due to a high recombination rate at the interface (see section 1.2.3). In this review these authors highlight a shift in viable average Ga content for high efficiency solar cells by the use of KF-PDT that overcomes the V_{oc} limitation towards higher Ga content. In the paper relating the 21.7% efficiency, Jackson *et al.* explain that the KF-PDT allows the growth of absorbers with a significantly stronger Ga grading than that of non-treated ones, resulting in an additional gain on J_{sc} in the infrared (IR) region due to a lower minimum optical band gap. Such strong gradient in the space charge region should induce structural defects and thus recombinations [132]. Hence the autors assume a passivation of these defects by the PDT.

2.2.3 Reported material and and related models

Modified surface – The effect of NaF and KF-PDT on CIGS surface chemistry and morphology has been studied [126]. Chirilă *et al.* claim no clear difference in the surface morphology due to the different PDT treatments; SEM measurements show slighty smoother surfaces but no change in surface roughness is found by atomic force microscopy after KF-PDT. The authors therefore exclude the influence of surface roughness on the modified junction formation. Bare CIGS surfaces (rinced with ammonia to remove any NaF or KF residual from the surface) as well as CIGS/CdS interfaces were investigated by X-ray

Photoelectron Spectroscopy. In and Se peaks appear unchanged by both PDT. After NaF-PDT, Na is found at the outermost surface and a slight Cu and Ga depletion is detected. Decreased Ga content after NaF treatment was already reported by Eid *et al.* [133]. However KF-PDT induces a much stronger Cu and Ga depletion, K is detected in the first few nanometers below the CIGS surface and 20nm need to be etched to retrieve standard CIGS. These changes are not altered by the CdS deposition. As mentioned above Laemmle *et al.* [129] also report a strong Cu depletion, In and K enrichment in the near surface region of the absorber grown on KF-precursor. In this paper they suggest the formation of a $KInSe_2$ phase, but no additional lines were observed by X-ray diffraction. Altough neither structural [129], nor morphological [126] changes have been reported, the presence of a clear top layer containing mostly K, In and Se is clearly identified.

In another study, the EMPA group studied the effect of rincing with water and HCl the CIGS surface treated with KF [134]. In this paper they clearly show morphological changes at the surface of treated absorbers. They identify "self-assembled alkali condensates" with a size and distribution dependent of of the substrate temperature and the amount of KF and NaF evaporated during the treatment. These condensates are dissolved in water, as shown in Figure 2-3.

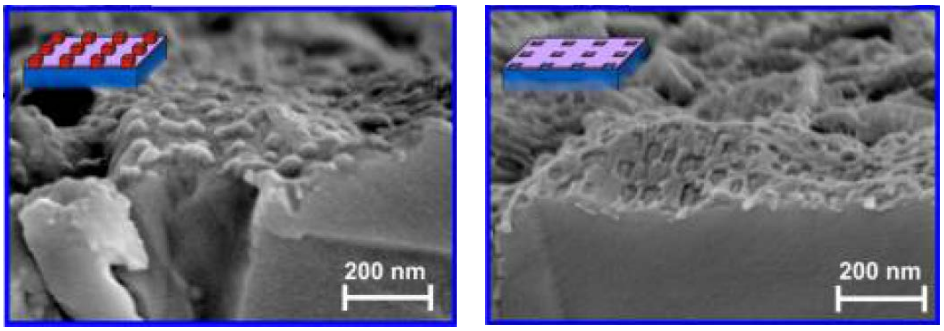

Figure 2-3 - Scanning electron micrograph of absorber treated with KF (a) as-deposited (b) rinced with water. After [134]

These authors analysed the water used to remove the condensates by Inductively Coupled Plasma Mass Spectrometry (ICP-MS) and identified mostly Na, K but also Ga. Due to the technique limitations they could not measure oxygen but they assumed that the Ga found in the rincing water is likely from a soluble Ga oxide catalyzed by K, as explain in Ref [135]. They also showed that the residual top layer could be completely removed by HCl etching. K, In, Se and some Ga was found in the HCl rincing solution by ICP-MS, but no Cu nor Na. Considering the rough surface morphology of K-treated CIGS surfaces after rincing with HCl, and the fact that CIGS is not etched by HCl, they conclude that (i) the top layer is not CIGS and (ii) a reaction occurs between the top layer and the underlying CIGS material.

In the same paper ([134]) the authors suggest that these findings can be used as a technique (called SALT for "self-assembled alkali template") to nanopattern polycrystalline thin film surfaces. Applied to solar cells it leads to localized point contact junctions already used in Si-based technology. They demonstrate a 18.9% efficiency device based on this concept and assure that further improvements can be achieve by minimizing the CdS absorption (growth only in holes) or by the use of nanopatterned functional layer with specific properties (passivated hetero-junction).

However, they also point out that no nanohole openings in the surface-treated layer were found in their previous study [126]; the mechanism involved in the efficiency enhancement due to KF-PDT should therefore not be explained by localized point contact junctions.

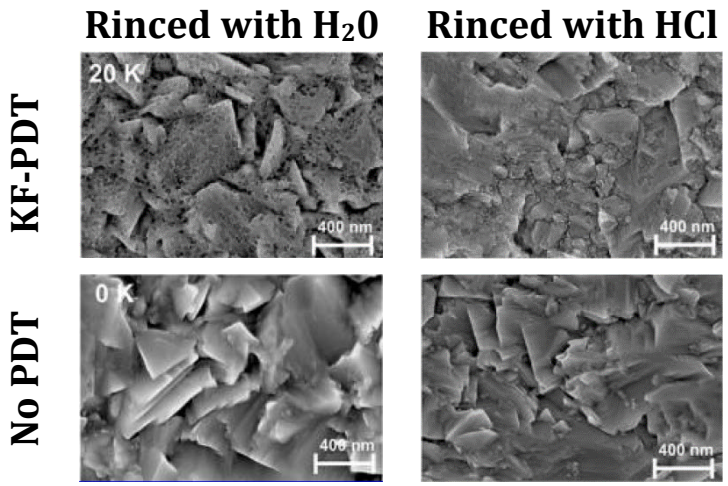

Figure 2-4 - SEM micrograph of CIGS surface treated with KF (up) or not (down) before (left) and after (right) HCl etching. After [134]

Na/K exchange – SIMS measurements have revealed a significant amount of K incorporated into the absorber by PDT [126], [127], not only at the surface, but also within the whole absorber. These measurements also highlight a lowering of the Na content with respect to the K increase. Chirilă *et al.* suggested an ion exchange mechanism (see [126] and references therein) in order to explain this phenomenon.

Minimum K amount – Chirilă *et al.* have reported a minimum duration of 15 min (with an evaporation rate of 1 nm/min) for the KF-PDT in order to be able to thin the CdS layer without lowering the efficiencies.

Cd in-diffusion - Chirilă *et al..* have also shown that the presence of K enhances the Cd diffusion into the CIGS layer during the CdS chemical bath deposition (CBD). Due to the Cu depletion mentioned above, they propose that the improved junction results from increased density of positively charged Cd_{Cu} defects close to the CIGS surface. This model is corroborated by luminescence measurements showing that these defects are likely to act as compensating donors in the CIGS structure [80], which is expected to strengthen the surface n-type inversion and thereby shifts the pn junction into the absorber.

2.2.4 Electronic effects

Diode quality – Jackson *et al.* have analysed the current-voltage (JV) curves of their champion KF-treated solar cells by diode analysis according to the one-diode model (see section 1.1.3). They report a better diode quality compared to the non K-treated cells by a lowering of the ideality factor A and the saturation current density J_0.

Pianezzi *et al.* investigated the effect of different PDT and different CdS thicknesses on the electronic properties of the related solar cells [136]. They show that KF-PDT reduces interface recombinations, which is shown in this paper to dominate in devices without this treatment and thin CdS layers. They assume a strong inversion of the CIGS surface due a high concentration of Cd_{Cu} at the interface (see previous section) that shifts the Fermi level position closer to the conduction band and passivate acceptor states which acted as recombination centers (occupied states due to higher Fermi level energy).

Pianezzi *et al.* confirm that Na is more effective to increase the holes concentration. Ion exchange mechanisms are assumed to explain why K lowers the Na concentration and thus renders the hole concentration independent of the presence of a NaF-PDT during the device preparation.

A strong roll-over of the JV characteristics above Voc is highlighted at low temperatures for samples treated with KF. Considering the improvement of the junction quality due to KF-PDT and the recent correlation between Na concentration and the formation of the $MoSe_2$ phase and thus the height of an electronic barrier at the back contact [11], [12], these authors conclude that this blocking current is related to a secondary diode at the back contact due to a lowering of Na amount at this interface by K.

K-induced defects – Pianezzi *et al.* [137] have also investigated the formation of defects in CIGS due to the incorporation of K by PDT during the growth of the absorber by the 3-stage process at low temperature (~400°C). The presence of K during the 3rd stage leads to the formation of a deep defect level approximately 280 meV below the conduction band that lowers the minority carrier lifetime and the long wavelength photogenerated carrier collection. They could not attribute the observed defect to any of the possible point defects in CIGS. However in Ref [136] these authors show that incorporating K during the growth (at higher temperature than the typical PDT) does not lower the Na content within the absorber. In that case they assume that K could be incorporated in lattice sites that do not prevent further addition of Na by PDT, suggesting that incorporation of Na or K at grain boundaries or into lattice sites have different activation energies for both alkali elements.

Band gap widening – Pistor *et al.* [130] have investigated the surface composition of absorbers subjected to KF-PDT by XPS using synchrotron radiation (high resolution). One should notice that they broke the vaccum before applying the KF-PDT on the CIGS surface. They confirmed the strong Cu depletion at the very near surface region and determined a lowering of the valence band edge maximum of 0.37eV. They attribute this shift to an enlargement of the band gap due to the Cu depletion that they attribute to the signature of an enhanced OVC phase that would lead to an improved junction.

2.3 Processing the alkali supply in our laboratory

2.3.1 Choice of the method

KF-PDT was introduced as a subsequent treatment to NaF-PDT. As reported by Pianezzi *et al.* [138] the amount of Na available at the CIGS surface when KF is supplied is very important. Na can be provided by spontaneous diffusion from the soda-lime glass (SLG) substrate into the absorber through the molybdenum (Mo) back contact layer or added using Na-containing precursors. In this case the precursors can be supplied before, during or after the CIGS growth. The compositional grading induced throughout the absorber by the presence of alkali during the CIGS growth [139] is highly beneficial for photovoltaic parameters. To date, best results are achieved with Na supplied by diffusion through the Mo [3]. Therefore we excluded the supply of the Na by PDT. In this work we will then use DC-sputtered Mo back contacts on SLG substrates to control the amount of Na available during the growth and at the CIGS surface; this specific issue will be debated in section 2.3.3. The K will be provided by PDT as its presence during the CIGS growth leads to the formation of the defect mentioned in section 2.2.4.

2.3.2 Supplying K – PDT baseline

KF-PDT is performed on highly efficient absorbers co-evaporated on SLG/Mo substrates (see next section) following the previously defined 3-stage process (see section 1.3.3). The KF-PDT consists in the evaporation of 15 nm of KF (99.99%) at 0.1 Å/s on the CIGS surface heated at 350°C. The rather high substrate temperature imposes a Se flux during the KF evaporation in order to avoid the creation of Se vacancies at the CIGS surface, detrimental for photovoltaic performance. In order to let K diffuse into the absorber, the substrates were maintained at this temperature for 5 minutes and then slowly cooled down to room temperature.

Although the performance of solar cells grown in our laboratory are reliable, run-to-run variations can occur and reference samples with non-treated absorbers are necessary in order to estimate the real impact of the KF-PDT. These samples are obtained by opening the co-evaporation chamber and saving reference absorbers before supplying the KF. This opening of the co-evaporation chamber oxygenates the CIGS surface before the KF supply, which could impact the chemical processes involved during the KF-PDT. However, as similar performance is obtained supplying the KF directly after the CIGS growth, air exposure seems not to be an issue. Subsequent CdS, ZnO and ZnO:Al layers were grown simultaneously on reference and KF-treated absorbers to complete the devices.

2.3.3 Supplying Na – Optimization of the molybdenum

The amount of Na at the surface of the CIGS layer is critical for the KF-PDT [138]. A part of this PhD thesis has been dedicated to the adaptation of the DC-sputtering conditions of the Mo back contact layer in order to control the Na content available during the CIGS growth and provided by diffusion from the SLG substrates through the Mo. The influence of the partial pressure was studied by M. Tomassini in our laboratory during his PhD thesis [140]. To combine a low resistivity and good adhesion of the Mo layer the argon pressure was 0.27 Pa during the deposition and we varied the DC-power from 1.5 W/cm^2 up to 4.6 W/cm^2. The results have been published in Ref[55]. Figure 2-5 shows the Na and K Secondary Ion Mass Spectroscopy (SIMS) profiles for a complete solar cell grown on Mo layers sputtered with DC-power of 1.5 and 4.6 W/cm^2 and labelled Mo$^{1.5}$ and Mo$^{4.6}$ respectively. Analyses were performed using a Cameca IMS7f. The impact energy was 3 keV and the primary Cs^+ ions beam (55 nA, 5 kV) was rastered (200µm x 200µm) on the samples. As a result alkali segregate mostly at interfaces and their amount is higher in CIGS grown on Mo sputtered with the lowest DC-power.

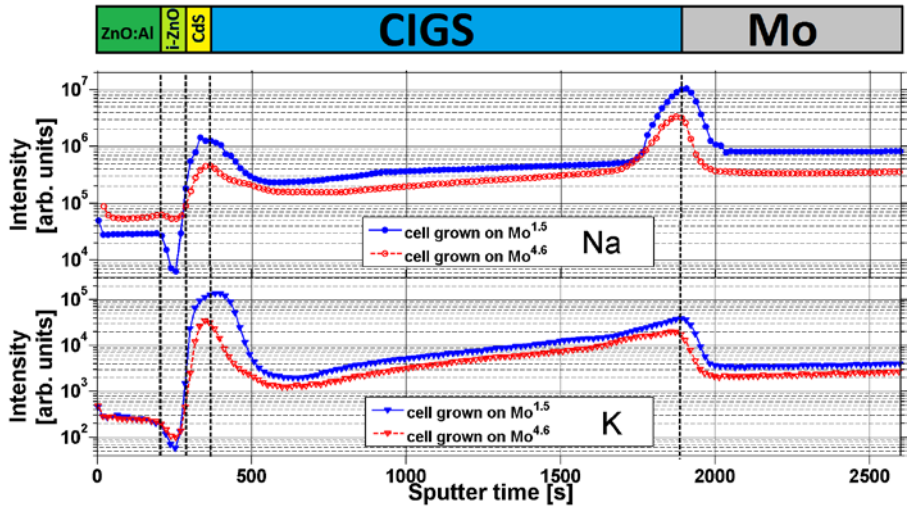

Figure 2-5 – ^{23}Na and ^{39}K SIMS profiles in complete solar cell grown on Mo layers sputtered with DC-powers of 1.5 and 4.6 W/cm^2

Standard KF-PDT has been applied simultaneously on 3 absorbers grown on Mo layers sputtered with 1.5, 3 and 4.6W/cm^2 DC-power and labeled Mo$^{1.5}$, Mo^3 and Mo$^{4.6}$ respectively. To finish the solar cells we then deposited the buffer and window layer in the same conditions on these 3 absorbers and on a non-treated absorber grown on Mo^3 to serve as reference. Figure 2-6 shows the statistics on V_{oc} and FF of this set of samples. Although the gain in V_{oc} is similar (+20/25mV) on all the 3 types of Mo, we observe a decrease of the FF as the DC-power used for the Mo sputtering increases. This result is consistent with the work of Pianezzi *et al.* since Mo$^{1.5}$ is the most ''permeable'' to alkaline species and will provide the highest segregation of Na at the CIGS surface, as shown on Figure 2-5.

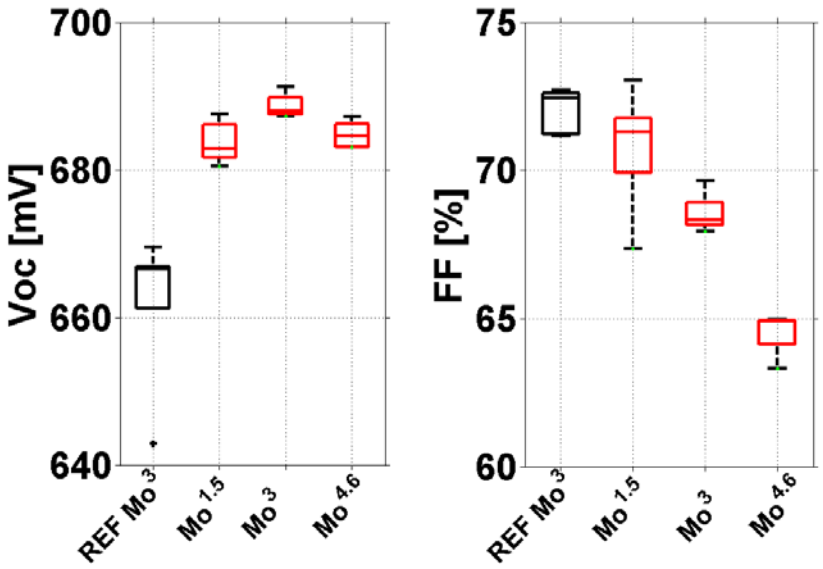

Figure 2-6 – Voc (left) and FF (right) statistical results of solar cells grown on the 3 types of Mo and subjected to KF-PDT (red) or not (black) Each box gives statistical results on 28 cells. The box has lines at the lower quartile, median and upper quartile values. Lines extending from each end of the box show the extent of the rest of the data

One can notice that even for cells with absorbers grown on Mo$^{1.5}$ the FF after KF-PDT can be lower (or higher) than that of the reference. A this stage this can mean that the amount of Na at the CIGS surface is still not enough or, as we will see in the next section, that it is inherent to the KF-PDT process itself and due to another hidden parameter. In the following chapters we will exclusively use SLG/Mo$^{1.5}$ as back contact, except for Na-free condition experiments in which a SiN diffusion barrier will be used. The back contact in this particular case will be SLG/SiN/Mo$^{1.5}$.

2.4 Issues addressed in this thesis

2.4.1 Effect of KF-PDT on electrical performance

KF-PDT can either improve or deteriorate the photovoltaic performance of the solar cell. Figure 2-7 and Figure 2-8 show the current density-voltage (JV) curves and External Quantum Efficiency (EQE) of K-treated and reference representative solar cells when this treatment is beneficial and detrimental, respectively. Photovoltaic parameters are given in inset. In both cases the absorber is grown following our co-evaporation baseline which leads to around 17% energy conversion efficiency without anti-reflective coating if it remains untreated. The same KF-PDT was performed on these two absorbers. All other layers were grown simultaneously.

When KF-PDT is beneficial ((Run#1, Figure 2-7) the main impact is the increase of the V_{oc}. In that case, V_{oc} increases by 5 %abs whereas FF and J_{sc} remain similar to that of the reference. The EQE is very similar; only fluctuations at long wavelengths differ. These fluctuations are inherent to the polycristalline nature of the layers. Indeed photons in this wavelength region are absorbed deep in the absorber region, where the Ga content is rather high and the grain size small. Variations from cell to cell are often encountered in this region.

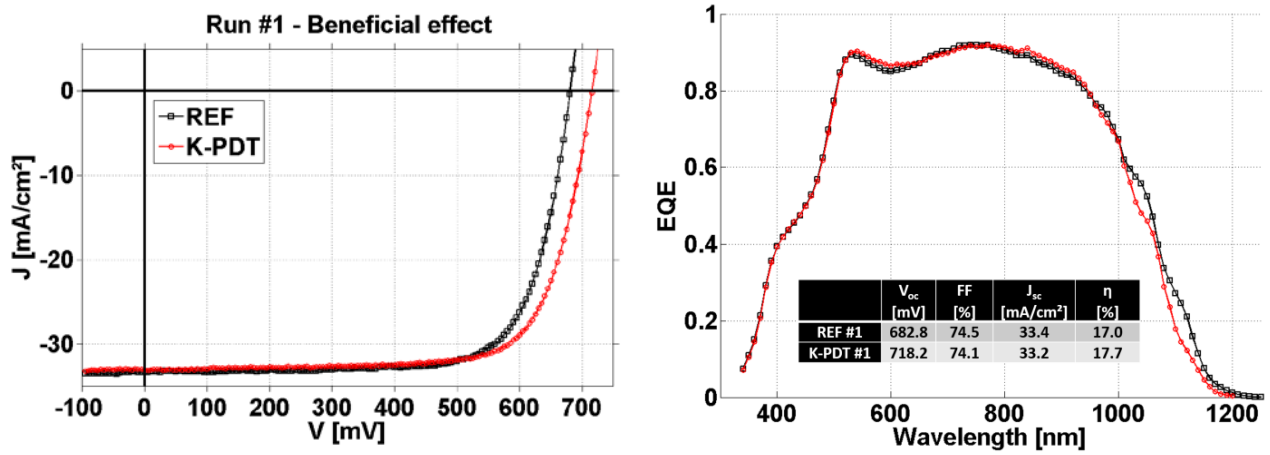

Figure 2-7 – JV characteristic (left) and EQE (right) of solar cells with absorber treated with KF (red) or not (black) that illustrate the beneficial effect of KF-PDT

When KF-PDT is detrimental (Run#2, Figure 2-8) all the parameters are lowered and the efficiency falls down to 5%. The EQE is lowered on the whole wavelength region, suggesting that recombinations do not depend on the location where electron-hole pair has been created. One can then assume that recombinations occur at an interface, most probably the CIGS/CdS interface.

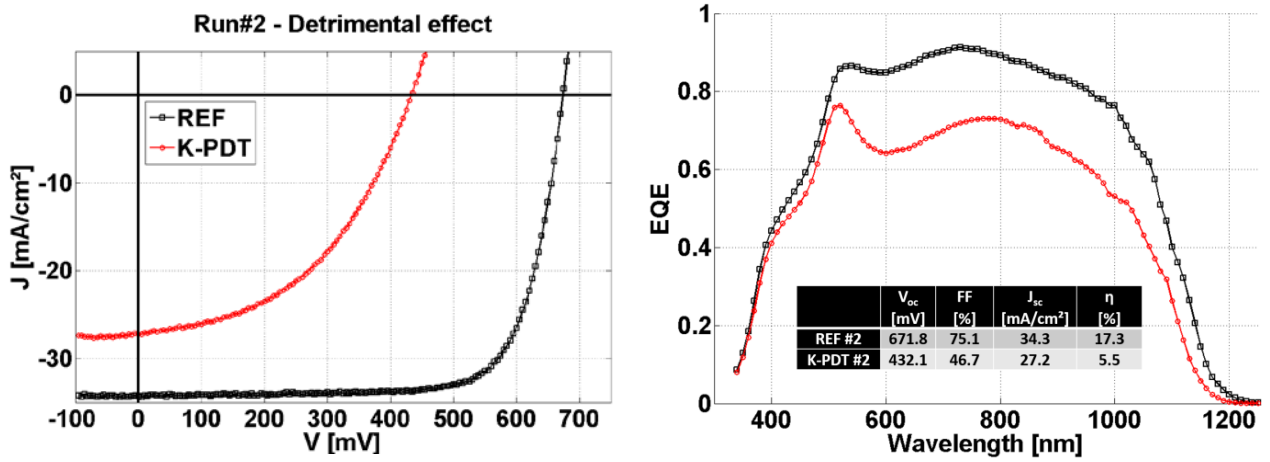

Figure 2-8 - JV characteristics (left) and EQEs (right) of solar cells with absorber treated with KF (red) or not (black) that illustrate the detrimental effect of KF-PDT

2.4.2 Distribution of alkali

The origin of the beneficial or detrimental effect of the KF-PDT can be related to a direct or indirect effect of the presence of the potassium in the device. In fact K could induce microstructural/chemical changes or induce the creation/passivation of electrical defects where it is located (direct effects) or influence the growth (and the material and electrical properties) of the subsequent layers. In both cases it is important to know where the potassium supplied during the PDT is located within the structure at the end of the device fabrication. This issue has been adressed with the help of SIMS. Depth profiles were performed on complete solar cell structures from Run#1. Two kinds of cells were investigated, namely Cell#1 and Cell#1(K). Cell#1 consists of co-evaporated CIGS without any post-deposition treatment, whereas the absorber of Cell#1(K) was treated with KF.

Figure 2-9 shows the ^{23}Na and ^{39}K SIMS profiles in these samples. In order to prevent K implantation (from the CIGS surface where KF was evaporated) during SIMS profiling and thereby enable the evaluation of the actual amount of K that diffused into the CIGS during KF-PDT, we have peeled the CIGS/CdS/ZnO/ZnO:Al stacks off of the SLG/Mo and performed the SIMS analyses from the rear of the absorber towards the window. This lift-off approach has already been used in [141], [142]. The Na and K atoms detected in Cell#1 result from the spontaneous diffusion of alkaline species from the SLG substrate during the absorber growth. Although alkali are found along the whole structure, these species segregate mostly at interfaces, especially the Mo/CIGS interface for Na and the CIGS/CdS interface for K. As expected, the amount of K is much more important in Cell#1(K). A higher amount of K is found at the CIGS surface where the KF has been supplied, but K is also found in the whole CIGS layer. This suggests that even at the rather low temperature of the treatment (350°C), K has diffused through the CIGS layer down to the Mo back contact. This increase of the K amount in Cell#1(K) is accompanied with a lowering of the amount of Na compared to what it was in the reference. Moreover, it seems that the line shapes of K SIMS profile after the PDT are similar to the ones of Na in the reference sample (and the Na profile in Cell#1(K) is similar to the K profile in Cell#1). One can then suggest that K diffuses through the grain boundaries (GBs) of CIGS and replaces Na that is mostly located at the GBs [106]. A model based on the ion exchange mechanism has already been reported by Chirilă *et al.* to explain these features.

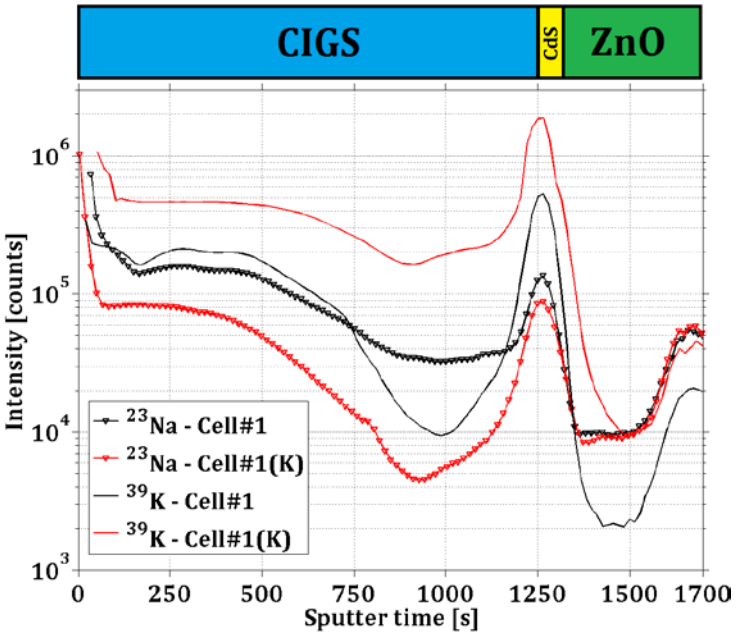

Figure 2-9 – ^{23}Na (triangle symbols) and ^{39}K (no symbols) SIMS profiles in solar cells with peeled off SLG/Mo with absorber treated with KF (red) or not (black).

The last difference between the alkali SIMS profiles of both samples concerns the presence of a shoulder in the K profile in Cell#1(K) at the CdS/ZnO interface. This suggests that K diffuses during the CdS chemical bath deposition and can possibly affect the CdS growth.

2.4.3 Adressing the hetero-junction formation issues after KF-PDT

Objectives - Reproducibility of the device results is crucial for industrial implementation. Considering the complexity and the number of steps involved during the preparation of the solar cell, the process has to show large tolerance to variations. Although small deviations on photovoltaic parameters from run to run can happen, good reproducibility of the performance is usually obtained in CIGS-based solar cells. KF-PDT seems to reduce this tolerance as interface problems can appear in devices based on absorbers that normally (if untreated) lead to very high efficiencies. This completly hinders the beneficial impact of this treatment and the first question that arises is:

(1) What are the absorber properties that make the KF-PDT beneficial or detrimental for the device efficiency?

Once this question is answered, another challenge will be to identify the mechanism underlying the improved junction quality when KF-PDT is beneficial. One objective of this thesis will be to test the validity of the models that have been already proposed. These models involve a stronger inverted CIGS surface corroborated by experimental evidences of reduced interfacial recombinations and based on (i) a higher density of Cd_{Cu} donor defects in the absorber near-surface region or (ii) an extended OVC (in the bulk) with increased band gap.

The purpose of this thesis is to build *(I) a comprehensive growth model for the hetero-junction formation* after the KF-PDT. This model should also be able to address the following question:

(2) Why can we reduce the CdS chemical bath deposition duration without lowering the photovoltaic parameters and why a minimum amount of KF has to be evaporated to do so?

Question (1) has been partially answered in the frame of the proposed model (i) considering that the main role of the chemical bath deposition is the diffusion of Cd into the CIGS layer. Hence, enhanced diffusion in the K-modified Cu depleted near surface region of the absorber allows the reduction of the dipping duration. However, the existing models (i) and (ii) do not take into account the fact that the K-induced top layer is not CIGS and remains after the CdS deposition. Thus, the existing models only partially explain the effect of the KF-PDT. Based on our investigations, we will propose *(II) a new electrical model that explains the improved junction quality*.

Samples used to address the issues - Interface issues can have many origins. At the laboratory scale, our baseline is not an in-line process; the vaccum is broken between the growth of each layer and surface oxidation is inevitable. Moreover, mechanisms involved during the CIGS co-evaporation to produce high quality absorbers are complex. The Ga grading necessary to collect low-energy photons is impacted by the presence of Na, which comes from the glass by thermally activated mechanism through the Mo back contact layer. Many parameters can influence this process and the establishment of the grading, resulting in variations of the surface chemical composition. Simplifying the process to avoid the surface chemical composition variations is possible (see section 1.3.2). However, studying the effect of KF-PDT on such absorbers is not desirable, as CIGS morphological, chemical and electrical properties are highly process-specific. It is not sure that investigations on low quality absorbers would unveil the real effect of KF-PDT in very high efficiency devices. In this thesis we will therefore investigate and compare the

chemical and structural effects of KF-PDT in samples from Run#1 and #2 mentioned above. However in some cases we will focus our investigation on absorber without any compositional grading grown by one step process and referenced as Run#3.

Labels – For this work many samples have been synthesized and characterized. In the next chapters several samples which we believe to be representative and useful to address the issues will be investigated. For the sake of clarity they have been labelled uniformly as follows:

SampleType #Run (specificities)

Table 2.1, Table 2.2 and Table 2.3 detail the possibilities for each entry of the labels. If not specified by "SiN" the sample has been grown on SLG/Mo substrate. If not specified by "AG" the sample has been rinced with diluted ammonia (1 mol/L) in order to remove some contaminants or KF residual. For exemple, CIGS#1(SiN,K) corresponds to an absorber from Run#1 grown following the 3-stage process in alkali-free conditions, subjected to a KF-PDT and rinced with NH_3.

Table 2.1 - Details for the "SampleType" entry in sample labels

SampleType	Detailed structure
CIGS	SLG/Mo/CIGS
CdS	SLG/Mo/CIGS/CdS
Cell	SLG/Mo/CIGS/CdS/i-ZnO/ZnO:Al/grids

Table 2.2 - Details for the "#Run" entry in sample labels

#Run	Process	Effect of the KF-PDT	Ga grading
1	3-stage	Beneficial	Yes
2	3-stage	Detrimental	Yes
3	One step	Beneficial	No

Table 2.3 - Details for the "specificities" entry in sample label

Specificities	Details
SiN	Absorber grown in alkali-free conditions on SLG/SiN/Mo substrates
K	Absorber treated with KF
AG	"As grown" samples (not rinced with NH_3)
PE	Absorber subjected to a Cd^{2+} "Partial Electrolyte" treatment
B1	Absorber dipped 1min in the chemical bath
B3.5	Absorber dipped 3.5min in the chemical bath
B7	Absorber dipped 7min in the chemical bath

Methodology - According to SIMS analyses, K seems to diffuse into the CdS layer. The presence of this specie could then impact the growth of the buffer layer. After the completion of the device it is still present at the CIGS/CdS interface and within the whole absorber, probably at the GBs.

In chapter 3, we will firstly investigate the chemical and microstructural changes induce by the KF-PDT at the surface of the CIGS. Comparing the nature of the K-modified top layer in absorbers from Run#1

and #2, we will build the first step of our model (I) of the hetero-junction formation (modification of the CIGS surface)

In chapter 4, we will focus on the effects of the chemical bath on the surface of the absorbers from Run#1. We will compare the CdS growth on CIGS surfaces subjected or not to the KF-PDT and we will investigate the hetero-interface and the GBs in the complete devices from this run in order to build the second step of the model (I) of the hetero-junction formation (Interface formation during the CdS-modified growth).

Chapter 5 will be dedicated to the establishment of (II) a new electrical model for the improved-junction. Finally discussing model (I) and (II) will help us to address the questions (1) (what makes the KF-PDT sometimes detrimental?) and (2) (why CdS can be thinner?).

Table 2.4 summarizes the different issues addressed in this thesis and specifies the samples used in each chapter.

Table 2.4 - Summary of the issues adressed in this thesis, with corresponding samples used in each chapter

Chapter	Issues	Samples
3	(I) Hetero-junction formation: modification of the CIGS surface	CIGS#1 / CIGS#1(K) compared to CIGS#2 / CIGS#2(K)
4	(I) Hetero-junction formation: modified growth of the CdS	CIGS#1 / CIGS#1(K) CdS#1 / CdS#1(K) Cell#1 / Cell#1(K)
5	(II) Electrical model (1) What CIGS properties make the KF-PDT detrimental? (2) Why CdS can be thinner?	Cell#3 / Cell#3(K)

Chapter 3
Material changes induced by the KF-PDT at the surface of the absorber

In the previous chapter we have shown that two absorbers (from Run#1 and #2), grown similarly following the 3-stage process, and which both led to high efficiency if they remained untreated, can result in higher or lower efficiencies after KF-PDT. We refer to these as case#1 and #2, respectively. The purpose of this chapter is to compare the nature of the surface layer after KF-PDT in both cases in order to (i) model the chemical effect of this treatment on the CIGS surface, (ii) explain how these changes improve or deteriorate the hetero-junction and (iii) highlight eventual differences between reference absorbers that would explain why KF-PDT can have such different effects on the electrical performance of the related solar cells.

In section 3.1 the chemical and compositional changes induced by the KF-PDT at the surfaces of the absorbers are compared. The two following sections discuss the structural changes in this region. Finally in section 3.3.3 we formalize the chemical reactions that occur during the KF-PDT and propose a chemical and structural model of the absorber near-surface region in both cases.

3.1 Chemical and compositional changes

In this section we focus on the chemical and compositional changes induced by the KF-PDT at the CIGS surface. This issue has been addressed with the help of X-ray photoemission spectroscopy (XPS) measurements. Technical details about the XPS setup and the spectra analyses are given in Appendix A. For all investigated samples, a summary of all fitted contributions can be found in Appendix A and a quantification of the relevant effects of the KF-PDT on the CIGS surface chemistry as well as a summary of the most important XPS results are given in section 3.1.4.

In section 3.1.1 we propose a systematic comparison of the chemical composition of absorbers from Run#1 and Run#2, before and after the KF-PDT. Then we focus on the strong interactions that exist between Na and K, as it has already been shown by SIMS (see section 2.4.2). We analyse, in both absorbers, (i) the effect of the KF-PDT on the Na 1s XPS peak and (ii) the effect of the amount of Na present prior to the KF-PDT on the K 2p XPS peak. Finally we will investigate the effect of rincing the KF-treated absorbers with diluted ammonia. This study will allow us to discriminate the issues that result from the KF evaporation and those which result from the first moments in the chemical bath.

3.1.1 Comparison of the CIGS surface chemistry in the case of beneficial and detrimental effect of the KF-PDT

The chemical effects of the KF-PDT on the surface of absorbers from Run#1 grown in the presence of Na or not, i.e. on SLG/Mo or on SLG/SiN/Mo structures respectively, are very similar, but are more pronounced in the Na-free case. Neither shifts or widening of photoemission lines nor appearence/vanishing of contributions have been found in every investigated core-shells of the CIGS#1(K) compared to those of the CIGS#1(SiN,K). For the sake of clarity in this manuscript we do not show the XPS spectra performed on CIGS#1 and CIGS#1(K) in this section. The comparison will be performed between CIGS#1(SiN,K) and CIGS#2(K). However, a discussion on the effect of the presence of Na at the CIGS surface during the KF-PDT will be part of section 3.1.2. In this section we aim at studying the CIGS surface as it should be in the first moments of the deposition of the subsequent CdS layer in the chemical bath. For this we rinced all of the samples for one minute in diluted ammonia after their synthesis and transferred them into the XPS analysis system.

Figure 3-1, Figure 3-2, Figure 3-3 and Figure 3-4 show the effects of the KF-PDT on the Ga $2p_{3/2}$, In $3d_{5/2}$, Cu $2p_{3/2}$ and Se 3d XPS peaks of absorbers from Run#1 and Run#2, respectively. Main contributions in In $3d_{5/2}$ and Ga $2p_{3/2}$ XPS peaks, labelled In-1 and Ga-1 respectively, correspond to the environment of In and Ga in chalcopyrite [143]. In all investigated samples a contribution labelled In-2 (445.3 ± 0.1 eV) is detected. The comparison of the position of the In-2 component to those from the literature is consistent with the formation of In_2O_3 reported by Liu *et al.* [144]. In samples from Run#2, we have also found another contribution labelled Ga-2 at higher BE (1118.5±0.1eV) in Ga $2p_{3/2}$ XPS peak which can be attributed to a Ga oxide. Both as-received samples (CIGS#1 and CIGS#2) exhibit a well defined Cu $2p_{3/2}$ peak (Cu-1, 932.2 ± 0.1 eV) and Se 3d doublets with 2 contributions Se-1 (54.2 ± 0.1 eV) and Se-2 (54.9 ± 0.1 eV) which, in good agreement with the literature [145], have been attributed to the environments of Cu and Se in chalcopyrite, respectively.

Ga depletion – Although Ga $2p_{3/2}$ peaks are broader in absorbers from Run#2 due to the presence of gallium oxides, the amount of Ga detected at the surface of both of the reference absorbers is similar, as can be seen in Figure 3-1. In both cases, the KF-PDT leads to a strong Ga depletion, as reported in [130], [138]. The Ga oxide content in absorbers from Run#2 strongly decreases after the KF-PDT.

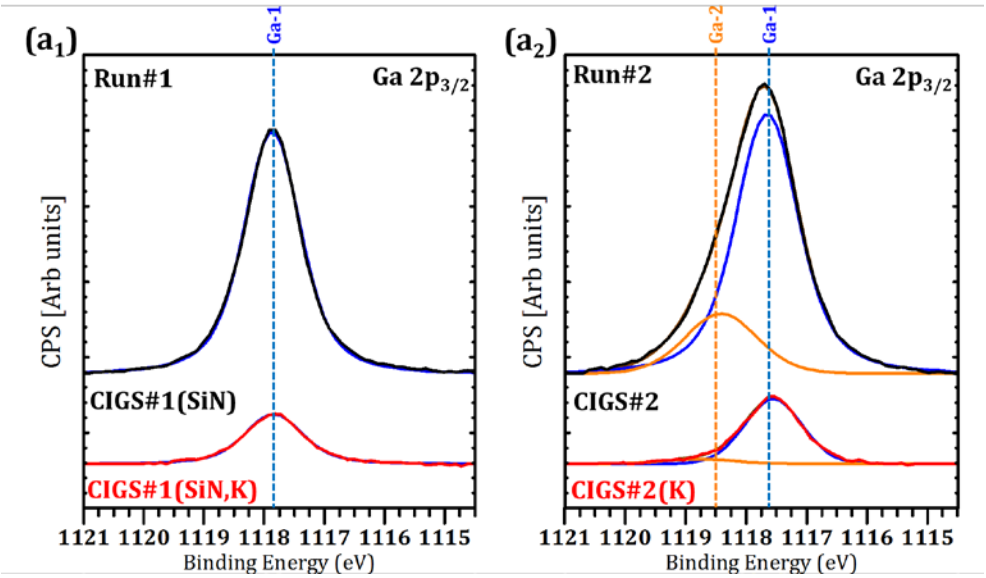

Figure 3-1 – Ga $2p_{3/2}$ XPS spectra of untreated (black) and KF-treated (red) absorbers from (a_1) Run#1 and (a_2) Run#2

In enrichment – Figure 3-2 shows that the amount of In detected at the surface of CIGS#2 is higher than that detected at the surface of CIGS#1(SiN). Pistor *et al.*, as well as Chirilă *et al.*, report no significant changes on indium amount detected by XPS after KF-PDT. In the present study, we find that such treatment increases the amount of In detected at the surface in both cases. However, the origin of these increases is different in case#1 and #2. KF-PDT increases the amount of the main contribution In-1 in CIGS#1(SiN,K). This contribution is related to the strong In-Se bond, as found in chalcopyrite. Hence, this indium enrichment after KF-PDT could suggest a chalcopyrite with a lower Ga content or another indium-selenide based compound at the surface of the absorber. The increase of the $In3d_{5/2}$ photoemission line intensity in CIGS#2(K) is mainly due to the increase of the In-2 contribution related to indium oxides or hydroxides and no significant changes are found on the main contribution related to In-Se bonds.

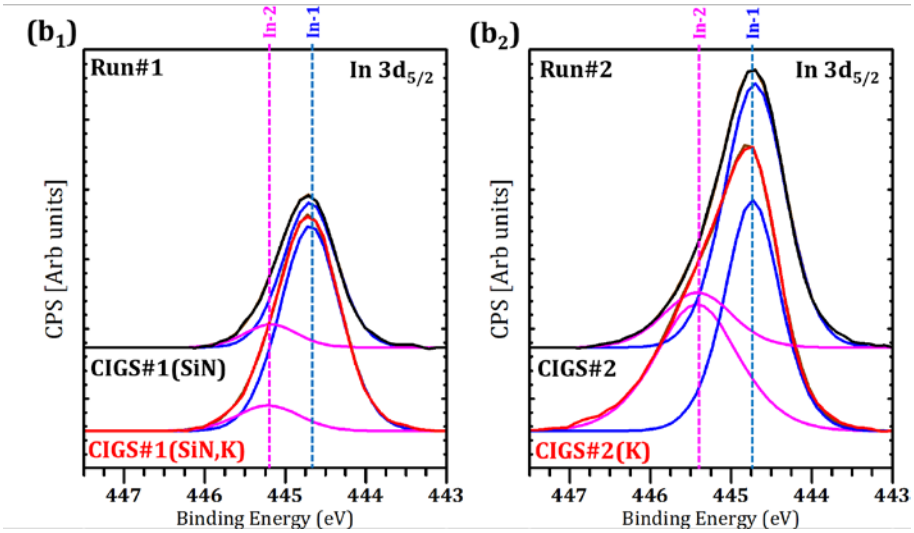

Figure 3-2 – In $3d_{5/2}$ XPS spectra of untreated (black) and KF-treated (red) absorbers from (a_1) Run#1 and (a_2) Run#2

Cu depletion – Figure 3-3 illustrates that the amount of Cu detected at the surface of CIGS#2 is higher than that in CIGS#1. The Cu depletion induced by the KF-PDT reported in literature [126], [129] is present only in CIGS#1(SiN,K). In CIGS#2(K) no depletion is found and a new contribution Cu-2 is detected. Cu-2 will be identified in the following.

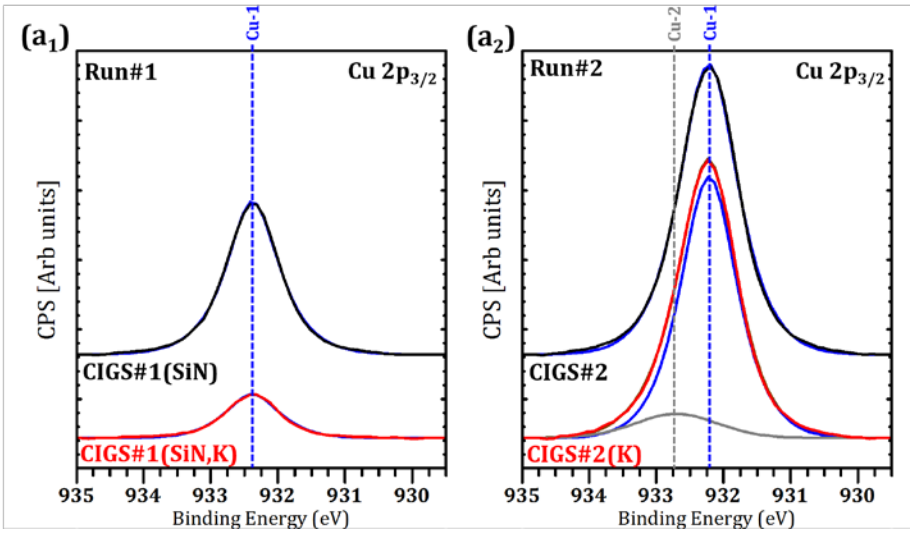

Figure 3-3 – Cu $2p_{3/2}$ XPS spectra of untreated (black) and KF-treated (red) absorbers from (a_1) Run#1 and (a_2) Run#2

Se-based new compounds– In both cases the KF-PDT induces the vanishing of the Se-2 contribution, as can be seen in Figure 3-4. One could suggest that this contribution is related to the Se environment at the outermost surface of the absorber and would disappear if new compounds (containing Se) cover the surface after the KF-PDT. In both cases the treatment leads to the appearence of the contribution labelled Se-3 identified at 55.2eV ± 0.1 eV. Se-3 corresponds very well to the Se $3d_{5/2}$ core level BE of metallic Se^0, as found in ref [145] or experimentally at the laboratory (not shown here). However, the amount of this -detrimental- elemental Se [146] is much lower in CIGS#1(SiN,K). Finally, the KF-PDT leads to the appearance of different new contributions in the Se 3d XPS peak in both cases:

(i) CIGS#1(SiN,K): The new contribution labelled Se-4 (53.5 ± 0.1 eV) could correspond to an indium selenide (In_xSe_y) compound, or at least to another In-Se bond in the material, as the Se $3d_{5/2}$ core level BE of 53.5eV has been reported for InSe and In_6Se_7 [147] and for co-evaporated In_2Se_3 [145]. One should notice that the In 3d core level BE of these compounds, reported by these same authors, is the same as that of CIGS, explaining why no other contribution is found in the In $3d_{5/2}$ XPS peak. Changes on the valence band spectrum corroborating the modification of the In-Se bonds in this samples will be detailed in the following.

(ii) CIGS#2(K): New contribution labelled Se-5 (54.7 ± 0.1 eV) corresponds quite well to a $Cu_{2-x}Se$ compound as Cu_2Se and $Cu_{1.83}Se$ have been reported to have Se $3d_{5/2}$ BE of 54.4 and 54.8 eV respectively [148]. Furthermore Se-5 is associated with the appearence of the new contribution labelled Cu-2 (932.9 ± 0.1 eV) in the Cu $2p_{3/2}$ XPS peak of CIGS#2(K). The 0.7 eV energy difference between Cu-1 and Cu-2 is the same as that found by Lyahovitskaya *et al.* [149] between the $CuInSe_2$ and Cu_2Se compounds. Hence Cu-2 and Se-5 have been attributed to the formation of -highly detrimental- $Cu_{2-x}Se$ compound at the surface of CIGS#2(K).

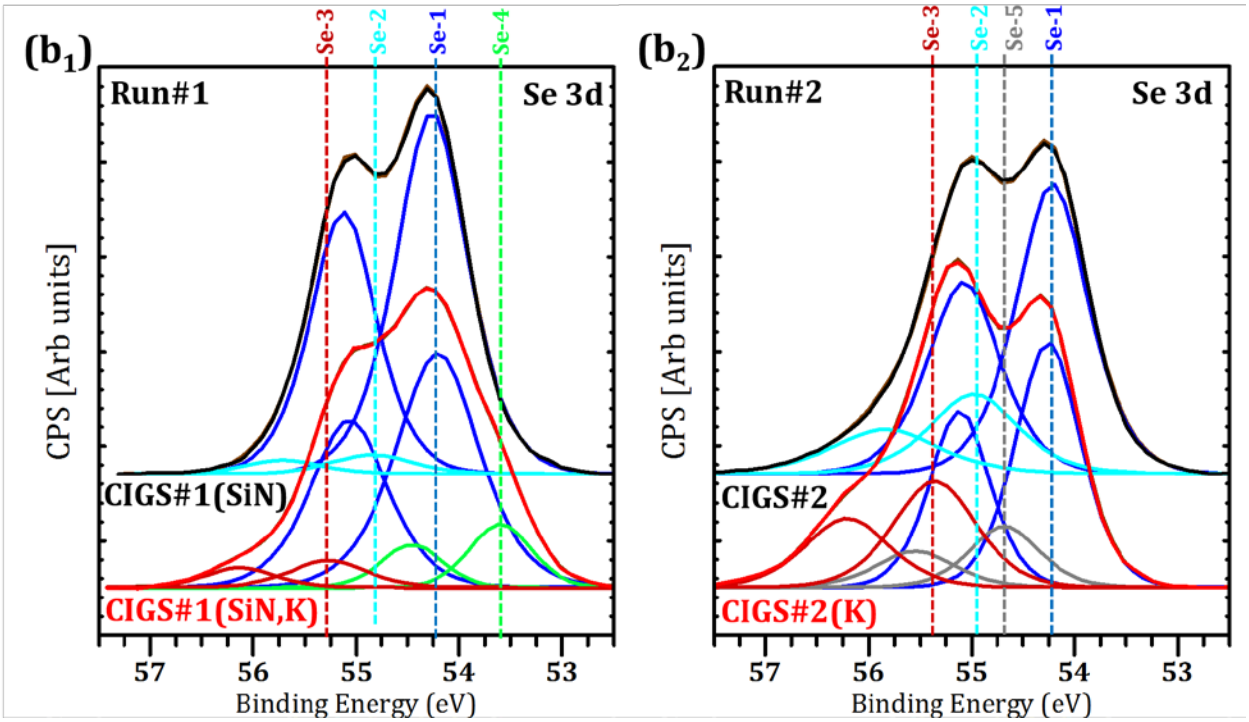

Figure 3-4 – Se 3d XPS spectra of untreated (black) and KF-treated (red) absorbers from (a_1) Run#1 and (a_2) Run#2

Valence band - Scans across the BE from 10 eV to -1 eV in reference and KF-treated absorbers from both Runs are displayed in Figure 3-5-a. Schmidt *et al.* explain in Ref [143] that photoemissions in the BE range 0-5 eV and 6.5-8.5 eV are related to the hybridization of the Se 4p core level with the Cu 3d and In 5s orbitals, respectively. In case#2, the spectra superimpose very well, confirming that CIGS#2(K) is not Cu depleted. Case#1 is very different. Figure 3-5-a_1 confirms the Cu depletion mentioned above, as the photoemission line is decreased in the 0-5eV BE range after KF-PDT. It also suggests that the In-Se chemical bonds are different at the surface material of treated and untreated samples, giving rise to the formation of a new indium selenide based compound. In the following we will focus on case#1 only.

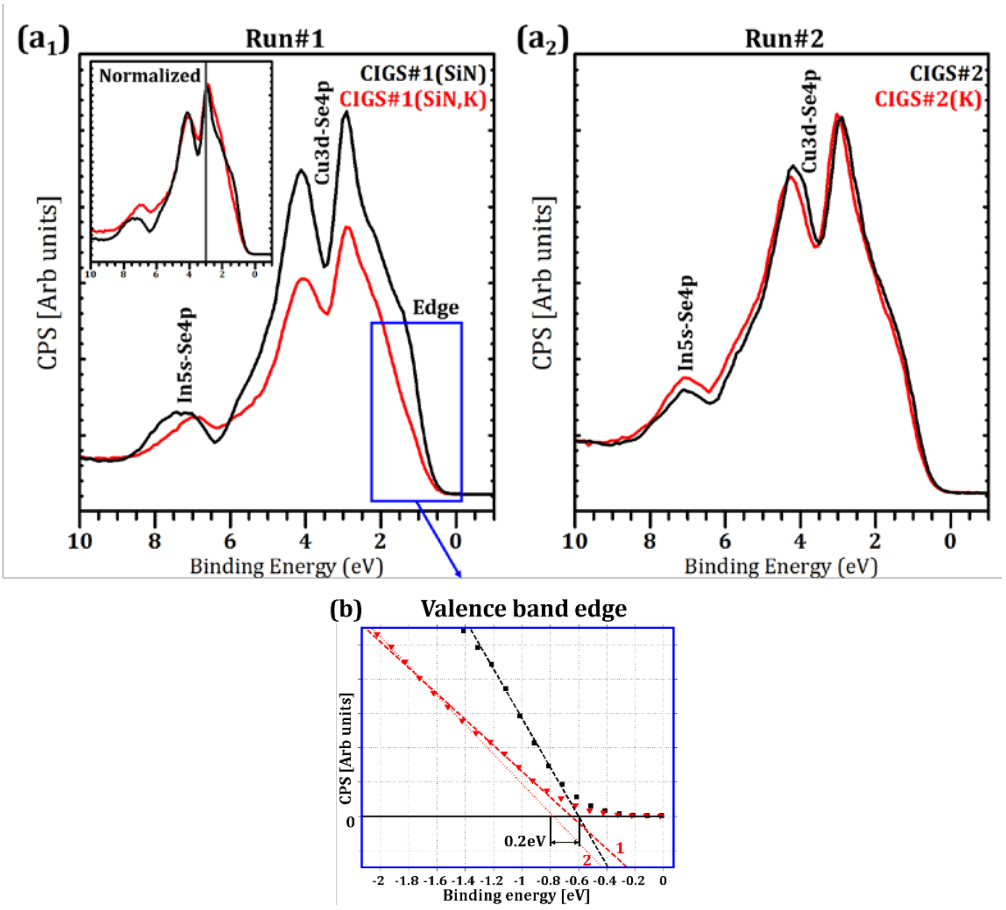

Figure 3-5 - Effect of KF-PDT on the valence band of absorbers from (a1) Run#1 grown in Na-free conditions and (a2) Run#2, subjected to KF-PDT (red lines) or not (black lines). Valence band normalized in intensity at 3eV is given in inset for case#1. (b) A zoom on the valence band edge (VBE) maximum is also given in that case. Black square and red triangle symbols corresponds to the experimental data of CIGS#1(SiN) and CIGS#1(SiN,K), respectively. Lines corresponding to the fit of experimental data in the BE range [0.7 - 1.4 eV] for the reference absorber and [0.9 - 1.3 eV] (line1) or [1.3 and 2eV] (line2) for the KF-treated absorber are also plotted to extract the energy of the VBE maximum in both samples.

Pistor *et al.* [130] report a widening of the band gap due to the KF-PDT. Linear fits of the Valence Band Edge (VBE) experimental data for reference and KF-treated absorbers have been performed. For the reference sample the edge is well defined and the intersection of the fit in the [0.7-1.4eV] BE region with the y axis gives the maximum of the VBE, this is about 0.6 ± 0.1 eV. The case of the KF-treated sample is not straightforward as two different slopes can be identified in the BE range of [0.9-1.3 eV] and [1.3-2 eV], respectively. According to the Se 4p inelastic-mean free path in CIGS calculated using the imfpwin code [150], the information depth in this energy range is about 85 ± 5 Å. If the K-modified top layer is thinner than this depth then the VBE in this absorber will result from the superposition of the VBE of this top layer material and that of the non-modified CIGS located below. Hence, fitting the experimental

data in the energy range [0.9-1.3 eV] leads to a similar VBE maximum than that in the reference sample; the shift in the VBE maximum extracted from line1 is below the uncertainities. However the VBE maximum extracted from line2 (fitting the 2nd slope in the BE range [1.3-2 eV]) is about 0.8 ± 0.1 eV.

This value has been determined considering the strong hypothesis that a K-modified top layer, that is not CIGS, exists but is thin enough so that the underlaying CIGS is still detected by XPS in this energy range. This assumption is corroborated by the normalized valence band given in the inset of Figure 3-5-a_1. It is clear that both photoemission lines do not superimpose so the surface material of KF-treated material is not simply an OVC layer. We then assume a shift of the valence band maximum after KF-PDT of about 0.2 eV, which is much lower than that found by Pistor *et al.* (0.37 eV). This could be due to the higher amount of KF evaporated in their case, resulting in a thicker top layer with no superimpositions of the VBE of the CIGS and that of this top layer, and thus a higher shift value.

In XPS, binding energies are relative to the Fermi level energy E_F so this shift of the VBE maximum can originate from (i) charging effects, (ii) a widening of the band gap or (iii) the shift of E_F closer to the conduction band. The latter effect could be explained by K-induced donor defects at the surface, a higher density of defects that would pin E_F, or a reduction of surface dipoles due to the presence of alkali that would then bend the valence band [118]. However the position of the In $3d_{5/2}$ was used as energy reference for both spectra. Although one could question this choice as In is not necessarily bonded similarly in the bulk and in the top layer, the Ga $2p_{3/2}$ and Cu $2p_{3/2}$ XPS peaks are at the same energy position in both samples. This allows us to exclude charging or band-bending effects. Assuming the strong hypothesis mentioned above the K-modified top layer could then have a wider band gap than that of the bulk CIGS.

Partial conclusion – The main difference between the reference absorbers from both Runs is the surface composition. CIGS#1 exibits a lower Cu and a higher Se content compared to CIGS#2. The KF-PDT leads to a strong Ga depletion in both cases, but other specific chemical effects are evidenced in each case:

(i) In the beneficial effect case (#1), a strong Cu depletion is detected and In-Se bonds are modified. These results suggest the formation of a new indium selenide-based layer at the surface that is not simply an OVC. Assuming the hypothesis that this layer is thin enough so that the underlaying CIGS is still detected by XPS, this surface material could have a wider band gap than the CIGS.

(ii) In the detrimental effect case (#2) no such Cu depletion is found after the treatment and $Cu_{2-x}Se$ phase is formed at the surface. The indium oxidation increases and the valence band is unaffected.

In both cases the formation of detrimental metallic Se^0 seems inherent to the KF-PDT. However in case#1 the amount of this specie is much lower than that formed in case#2.

3.1.2 Alkali interactions

In this section we firstly focus on the effect of KF evaporation on the Na amount and chemistry at the surface of the absorber. For that we will consider absorbers grown on SLG/Mo structure, i.e. CIGS#1 and CIGS#2. Then we investigate the effect of the presence of Na on the amount of K detected at the surface of the absorber by comparing Na-containing CIGS#1(K)/CIGS#2(K) with Na-free CIGS#1(SiN,K).

Influence of K on Na – Figure 3-6 shows the Na 1s XPS spectra in absorbers grown on SLG/Mo from both Runs. The amount of Na detected in CIGS#1 is much lower than that detected in CIGS#2. The y axis of Figure 3-6-a_1, showing the Na 1s XPS spectra of absorbers from Run#1, has been scaled (x10) so that the photoemissions lines can be compared to those from Run#2. It has been shown that the presence of a high amount of Na at the CIGS surface can inhibit the formation of the OVC (see section 2.1.2 and reference therein). This is in good agreement with the composition of CIGS#2 found in the previous section (high Cu content and lower Se content than that in CIGS#1). The higher amount of Na could also explain why CIGS#2 is more oxidized.

Surprisingly, although the amount of Na is much higher in CIGS#2, no Na is found after KF-PDT on the surface of CIGS#2(K) whereas a small amount of Na is still detected in CIGS#1(K). Two contributions have been identified at the surface of the untreated absorbers. Heske *et al.* [118] report two different Na species at the surface of absorbers grown on Mo-coated SLG substrates, one called "non reacted" and the other one called "reacted" or "passivated" at higher BE. In our study, these species would correspond to Na-1 and Na-2, respectively. After the KF-PDT, no trace of the "reacted" Na is found at the surface whereas the other contribution seems almost unaffected by the PDT in absorber from Run#1, as its area slightly decreases (-28%) and its energy position shift by only 0.15 eV.

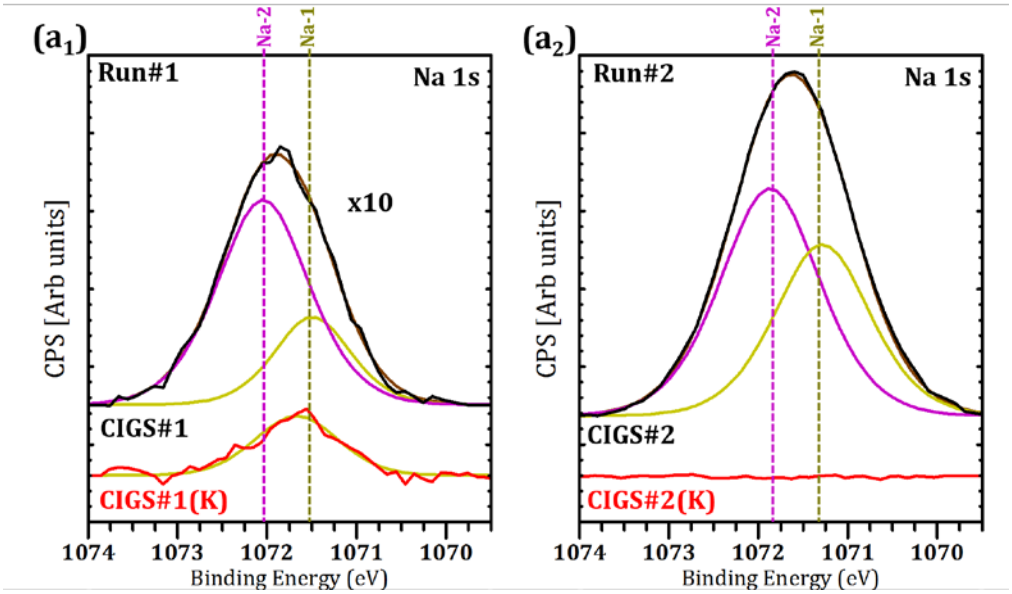

Figure 3-6 - Effect of the KF-PDT on the Na 1s XPS spectra in absorber from (a1) Run#1 and (a2) Run#2 subjected to KF-PDT (red) or not (black)

Influence of Na on K - KF-PDT has been performed simultaneously on absorbers grown with and without Na. Figure 3-7-a shows that the intensity of the K 2p peak[4] in all of the absorbers treated with KF. The highest amount of K is found on the Na-free sample CIGS#1(SiN), a lower amount is detected in CIGS#1(K) and no trace of K is found in CIGS#2(K). As shown previously CIGS#2 exhibits a large amount of Na detected by XPS at its surface. As a result it appears that Na lowers the amount of K detected by XPS at the surface of the absorbers. The question arising is to determine whether this is due to the presence of Na itself or to the eventual structural changes of the absorber surface induced by Na.

[4] Considering the relatively low amount of K in our samples, the K 2p XPS peak has been chosen because these transitions are the most intense. To be able to fit this peak, the Auger transition line Se LMM in CIGS#1 has been substracted from the photoemission lines in the K-treated samples, assuming the strong hypothesis that the Se LMM transition is not affected by the KF-PDT.

Oxidation of a K-containing compound - Figure 3-7-b shows the O 1s XPS peak in the absorbers treated with KF. The O1s XPS signal of CIGS#1 has been added for comparison. At least 3 contributions were necessary to obtain a good fit in the absorbers treated with KF. The O-1 (531.7 ± 0.1 eV, blue), O-2 (531.3 ± 0.1 eV, yellow) and O-3 (530.3 ± 0.1 eV, magenta) contributions have been attributed to In and Ga oxides or hydroxydes[5].

One can see that the area of the O-4 contribution is correlated to the amount of K detected in the absorbers. In CIGS#2(K) no such contribution is found. One could then suggest that the O-4 contribution is related to a K-containing compound. In the previous section we have shown that new In-Se bonds were formed due to the KF-PDT in case#1. One could then suggest that these bonds are related to the same surface compound. The investigation of the existing compounds that would fit these experimental indications will be presented in section 3.2.3.

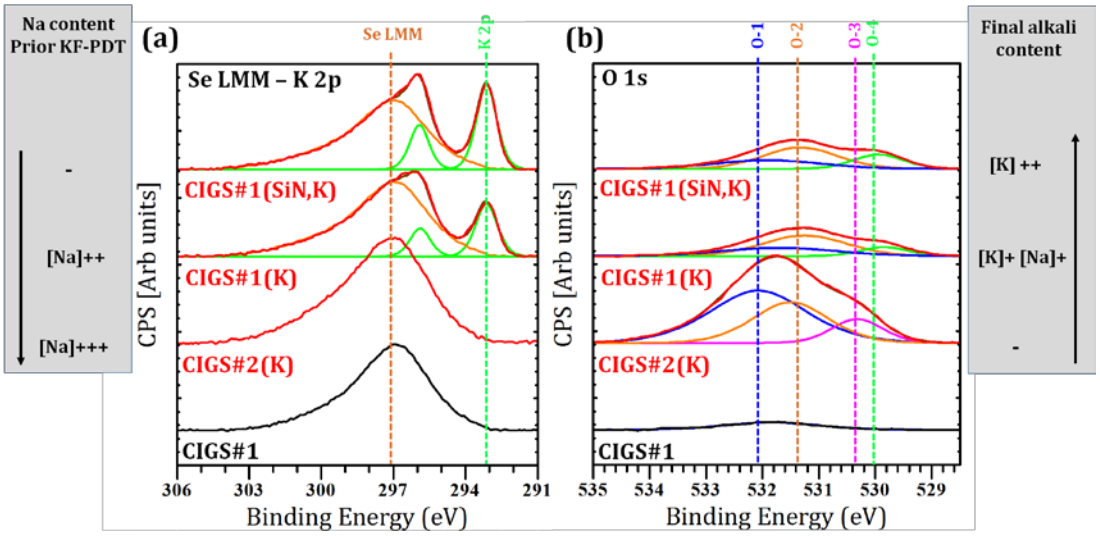

Figure 3-7 – (a) K 2p XPS peaks and Se LMM auger transition lines and (b) O 1s XPS peaks in absorbers from Run#1 (grown in presence of Na or not) and from Run#2 subjected to KF-PDT (red) or not (black).

Partial conclusion - Although KF was effectively deposited on CIGS#2, surprisingly no traces of K were found in CIGS#2(K) after rincing in diluted ammonia. This specific issue will be investigated in the next section 3.1.3. It seems that a competition exists between Na and K as K lowers the amount of Na at the CIGS surface (XPS measurements mentioned above) and at the GBs (SIMS measurements, see section 2.4.2). Na also lowers the amount of K deposited at the CIGS surface. This could suggest that both alkali tend to occupy the same sites at CIGS grain surfaces. A new surface compound containing K, In, Se and O is detected when K is detected at the surface of the treated absorbers. As a result it appears that the intensity of the effect of KF-PDT on the chemistry and composition of the CIGS surface depends on the amount of K really deposited and thus on the amount of Na present at the surface prior the PDT.

[5] As examples, $In(OH)_3$, Ga_2O_3 and In_2O_3 have been reported in literature to have O1s BE of 531.8 eV [151], 531.3 eV [152] and 530.3 eV [152] and could correspond to the O-1, O-2 and O-3 contribution, respectively. The O-1 and In-2 contributions seem correlated since both contributions are found in all of the investigated samples. The O-3 contribution in CIGS#2(K) is well correlated to the already mentioned broadening of the In $3d_{5/2}$ XPS peak in this sample. The amount of the O-2 contribution in samples from Run#2 is also well correlated to the amount of the Ga-2 contribution in such samples, attributed to the oxidation of Ga. This O-2 contribution is also found in CIGS#1(K) and CIGS#1(SiN,K) though the Ga $2p_{3/2}$ peak of these samples show no trace (from our fit) of the Ga-2 contribution. However, the amont of O-2 is lower in absorbers from Run#1 than in absorbers from Run#2.

3.1.3 Effect of rincing the K-treated layer

In this section we investigate the chemistry and the composition of the absorber right after the evaporation of KF and compare it to that after the rincing step in diluted ammonia (already studied in the previous section). Soluble compounds will be identified and will tell us whether this step is involved in the hetero-junction formation or if it is simply necessary to remove residuals from the evaporation. We will focus on samples from Run#2 as we also want to understand why in case#2 no K is detected by XPS at the surface (after rincing).

Figure 3-8 shows the XPS spectra of interest of an "as-grown" CIGS#2(AG,K) and rinced CIGS#2(K). A strong contribution labelled Ga-3 is found in Ga $2p_{3/2}$ peak of CIGS#2(AG,K) at 1119.3 ± 0.1 eV. We also find an isolated, and well defined, peak at 21.7 eV (not shown). This corresponds very well to the BE reported at 1119.4 eV [153] and 21.6 eV [154] for the Ga $2p_{3/2}$ and Ga 3d core levels of GaF_3, respectively. Ga-3 is thus attributed to GaF_3. A small contribution labelled In-3 is also found at higher BE (446.2 ± 0.1 eV) and has been attributed to InF_3 as it corresponds exactly to the reported BE of the In $3d_{5/2}$ for this compound [155]. Kawamoto *et al.* report BE of 685.8, 685.0 and 683.6 eV for the F 1s core levels of GaF_3, InF_3 and KF, respectively (see [156] and references therein). Figure 3-8-g shows the F 1s peak in CIGS#2(AG,K); only one contribution is found at 685.5±0.1 eV with a rather low FWHM of 1.35 eV. One could then suggest that the F-1 contribution corresponds to GaF_3 and not to KF.

F and O-assisted Ga depletion – Considering the amount of InF_3 and GaF_3 formed in the "as-grown" treated absorber, it seems that a preferential reaction occurs between Ga and F opposed to In and F. Both fluorides also seem to be soluble in ammonia since no trace of InF_3 or GaF_3 nor fluor are detected in rinced treated absorber. An important amount of GaF_3 is found at the surface of CIGS#2(AG,K), confirmed both by the Ga $2p_{3/2}$ and the F 1s peaks. Figure 3-8-e shows that an important amount of Ga oxides (O-2 contribution) is found in "as grown" treated absorber. After rincing, all the GaF_3 has been removed and the amount of Ga oxides is also lowered. Hence we assume that the Ga depletion observed in both cases is independent of the nature of the CIGS surface and is due to the formation of compounds soluble in amonia. These compounds are mostly GaF_3 but some Ga oxides are also formed.

Extreme surface evolution – Selenium oxides can be identified in Figure 3-8-d in the [58-61 eV] BE range. K 2p doublet of CIGS#2(AG,K) is shown in Figure 3-8-f. It is found at a higher BE (293.7 ± 0.1 eV) than in CIGS#1(K) (293.2 ± 0.1 eV) which means that K atoms are bonded differently in both cases. One could therefore suggest that, in case#2, K could not form the surface compound (containing K, In, Se and O) mentioned above in case#1. Therefore in case#2, K might only be solely located at the outermost surface. All of the atoms composing CIGS have corresponding XPS peaks lowered by the PDT before rincing. The Cu-2, Se-5 and Se-3 contributions seem to be less affected by this lowering. Hence, we suggest that, in case#2, the unrinced treated absorber is covered with a surface layer made of $Cu_{2-x}Se$, Se^0, Ga and Se oxides and an important amount of GaF_3 that lowers the detected intensity of photoemissions of atoms located below.

Thickness of the region modified by the KF-PDT - Figure 3-8-h shows the VB of CIGS#2(K,AG) and CIGS#2(K). The shape of the VB of the chalcopyrite is still detectable in CIGS#2(K,AG) (peaks at 3 and 4.2 eV) but is highly lowered. A new peak at 8.6 eV is in good agreement with the VB of GaF_3 reported by Varekamp et al. [157]. The thickness of the extreme surface layer formed before rincing (in CIGS#2(K,AG)) should then be of the same order of magnitude than the XPS information depth (ID) at this energy range. According to the inelastic mean free path in GaF_3, calculated for the 10 eV BE using the imfpwin code [150], this ID is about 11 ± 0.5 nm.

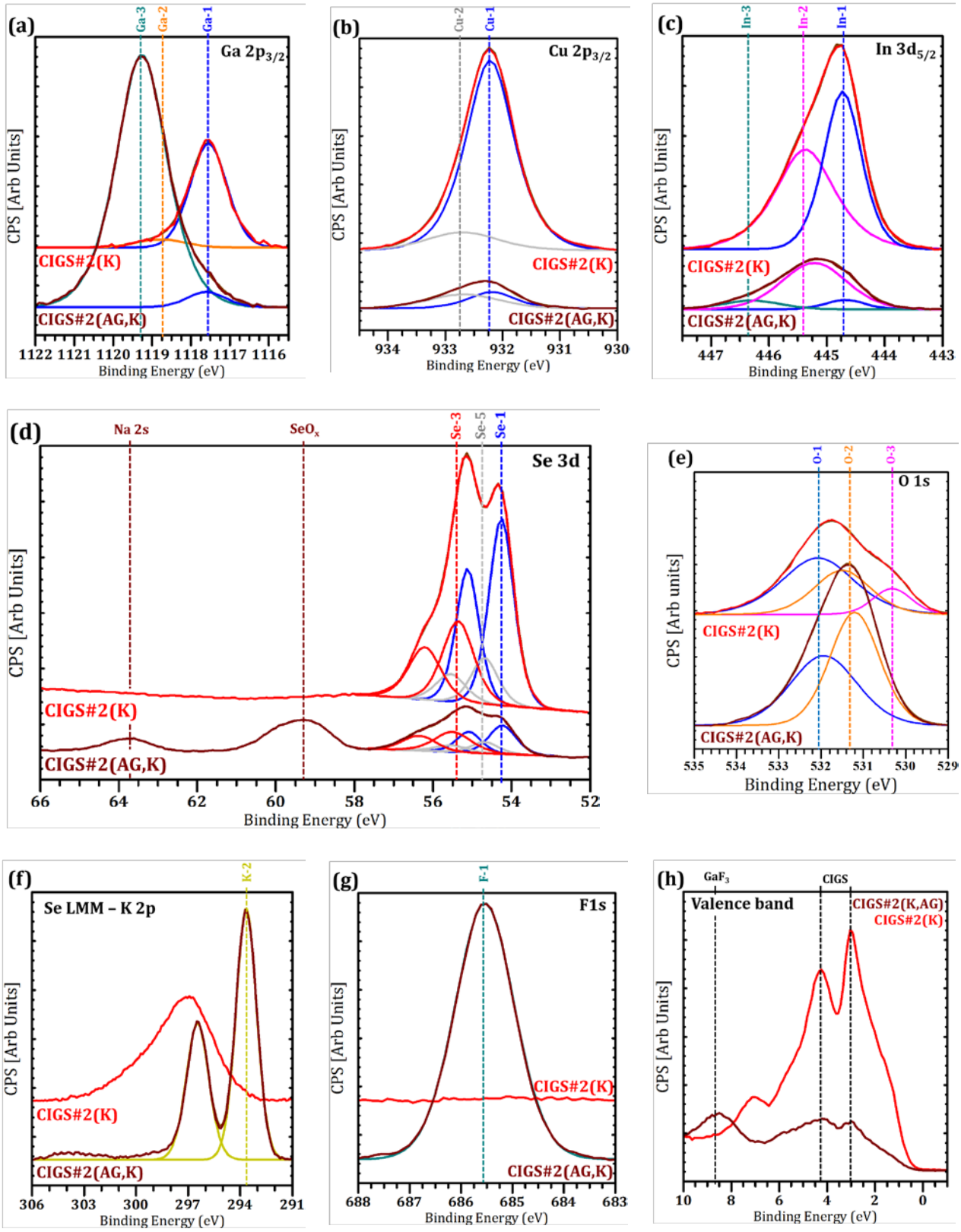

Figure 3-8 - Effect of rincing the KF-treated absorbers from Run#2 in diluted amonia on (a) Ga $2p_{3/2}$, (b) Cu $2p_{3/2}$, (c) In $3d_{5/2}$, (d) Se 3d, (e) O 1s, (f) K 2p, (g) F1s and (h) valence band XPS spectra.

Partial conclusion - After rincing CIGS#2(K,AG), all the fluorides and most of the Ga oxides are removed, resulting in a Ga-depleted CIGS layer with Se^0 and $Cu_{2-x}Se$ compounds remaining on top. We assume a similar mechanism involved in case#1. In case#1, the Ga depletion is also due to the solubility of Ga fluorides (and oxides) formed during the KF-PDT except that in this particular case a compound containing K, In, Se and O, not removed by the ammonia solution, is formed instead of $Cu_{2-x}Se$.

3.1.4 Summary on XPS results

Absorbers prior the KF-PDT – CIGS#2 exhibits a much higher Na content at its surface compared to that at the surface of CIGS#1. This could possibly explain why it is also much more oxidized and why it has a higher Cu and lower Se content (Na is reported to inhibit the OVC formation).

Absorbers after the KF-PDT - Table 3.1 assesses the chemical effects induced by the KF-PDT which we believe relevant to explain the beneficial or detrimental effects of this treatment. For the three treated absorbers, we quantify the depletions or enrichments relative to the references, the amount of K found after rincing, as well as the proportion of new contributions relative to the total related XPS peak.

Table 3.1 - Quantification of chemical effects of the KF-PDT in K-treated investigated samples

Samples	Evolution of XPS peak areas in K-treated samples relative to that in the references [%] (after rincing)				K amount	New compounds			
					K 2p areas relative to that in Run#1 on SiN	Proportion of new Se-based compounds peak area relative to the total Se3d peak area [%]			Proportion of the O-4 contribution peak area relative to O1s [%]
	$\Delta A_{Cu\ 2p3/2}$	$\Delta A_{Ga\ 2p3/2}$	$\Delta A_{In\ 3d5/2}$	ΔA_{O1s}	$A_{K2p_{3/2}}$	$\frac{A_{Se-3}}{A_{Se3d}}$ (Se^0)	$\frac{A_{Se-4}}{A_{Se3d}}$	$\frac{A_{Se-5}}{A_{Se3d}}$ ($Cu_{2-x}Se$)	$\frac{A_{O-4}}{A_{O1s}}$
Run#1 on SiN	-71%	-79%	+52%	+360%	1	8%	15%	-	16%
Run#1 on Mo	-56%	-65%	+37%	+171%	0.68	5%	9%	-	12%
Run#2 on Mo	-13%	-82%	+21%	-18%	-	30%	-	15%	-

In both cases (Run#1 and Run#2) the KF-PDT leads to a similar Ga depletion mainly due to the preferential formation of a soluble GaF_3 compound. Formation of -detrimental- Se^0 seems inevitable. This Se^0 could result from either the segregation of the evaporated Se (treatement under Se excess) on the substrate or the chemical reactions induced by the KF-PDT. However, considering the substrate temperature during the KF-PDT, it is surprising that the Se^0 remains on the surface after cooling. This could suggest that the kinetics of the reactions involved during the KF-PDT are slow. Hence, incomplete reaction during the cooling of the substrate could lead to remaining Se^0 at the surface. This is in agreement with the already reported minimum duration of the KF-PDT (see section 2.2). Although in case#1 the amount of Se^0 formed at the surface is correlated to the amount of K effectively deposited onto the absorber surface, it is much higher in case#2 where no K is found at the surface. It has been shown that the treatment does not lead to the formation of the same compounds at the surface in both cases. Almost no Cu depletion is detected in CIGS#2(K), the surface is chalcopyrite with a low Ga content and $Cu_{2-x}Se$ formation is highlighted (proportion of Se-5 contribution).

A strong Cu depletion is found in CIGS#1(K). A new compound containing K, In, Se and O, revealed by the In enrichment and the appearence of new chemical environments for the Se (Se-4), K (K-1) and O (O-4) atoms, is formed at the surface. This compound is not chalcopyrite and appears to exhibit a higher band gap than the underlaying CIGS. The amount of such compound depends of the amount of K effectively adsorbed at the surface (see the increase of the proportion of the Se-4 and O-4 contributions between CIGS#1(SiN,K) and CIGS#1(K)).

Finally Table 3.2 summarizes the most important experimental differences revealed by XPS between the surface chemistry of absorbers from Run#1 and Run#2 prior and after the KF-PDT.

Table 3.2 – Summary of XPS experimental findings in investigated samples

	Run#1	Run#2
Prior PDT	- Lower Cu content and higher Se content than those in Run#2	(- Higher Cu content and lower Se content than those in Run#1) - Higher Na amount at the surface
After PDT	- Cu & Ga depletion - In enrichement (More In-Se bonds) - Se^0 - GaF_3/GaO_x prior rincing - Modified valence band (not chalcopyrite with higher Eg)	- Ga depletion - In enrichement (More oxides) - Se^0 (higher amount) - GaF_3/GaO_x prior rincing - $Cu_{2-x}Se$ - Unchanged valence band (chalcopyrite)

3.2 Structural investigations

It has been shown previously that the chemical reactions involved during the KF-PDT are different on CIGS#1 and CIGS#2, resulting in different formed compounds and different electrical performance for both cases. The KF-PDT were performed in exactly the same conditions so the origin of such different chemical reactions has to come from the absorbers. We highlighted differences in the composition and the Na content (which is reported to inhibit the formation of the OVC). The purpose of this section is therefore to identify (i) structural differences at the surface of the reference absorbers and (ii) the new phase formed in case of CIGS#1(K). These issues have been addressed with the help of Raman scattering and Grazing Incidence X-Ray Diffraction (GIXRD) on both the reference and the K-treated absorbers from both runs, both grown on SLG/Mo.

Setup – Micro-Raman scattering measurements at 514.5 nm excitation wavelength have been performed using a T64000 Horiba Jobin-Yvon spectrometer equipped with a microscope in backscattering configuration. The information depth at this excitation wavelength is about 80 ± 5 nm. The focused spot size on the measured surface was about few μm^2. In order to minimize thermal effects, the Raman measurements have been performed at low power density. GIXRD has been performed at the Charles Coulomb laboratory located at the Université de Montpellier. Sample size of 2x1.5 cm^2 and grazing angles from 0.1° up to 5° were used.

3.2.1 Structural differences in the references

Figure 3-9 displays the Raman spectra of (a) CIGS#1 and (b) CIGS#2 normalized to the maximum intensity of the CIGS A1 mode. One can clearly see that a broad shoulder at about 155 cm^{-1} is present in CIGS#1 in addition to the CIGS A1 mode, which has been shown to be the signature of ordered defect

compounds like $Cu(In,Ga)_3Se_5$ [158]. No such broad shoulder is present in CIGS#2, suggesting that the OVC is not present in this absorber, or is too thin to be detected by Raman scattering. Recently, this technique has been used to study the effect of the presence of Na on the formation of the OVC [159]. This study confirms the already reported result that a sufficient amount of Na inhibits the formation of the OVC [29], [111], [112].

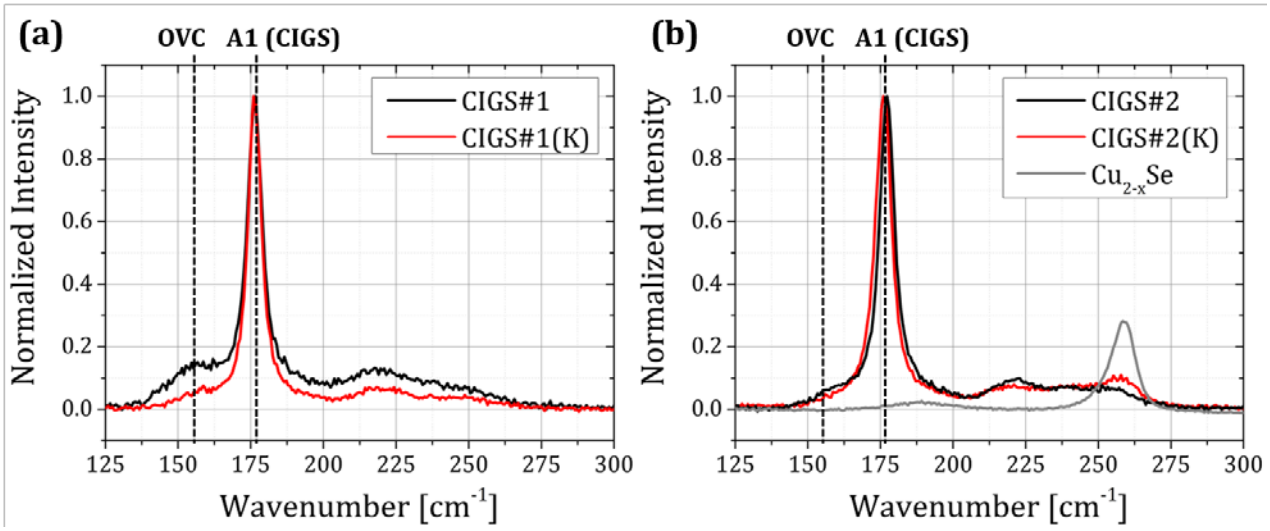

Figure 3-9 -- Effect of KF-PDT on RAMAN spectra of CIGS#1 and CIGS#2

3.2.2 Structural effects induced by the KF-PDT

Figure 3-9 also illustrates the effect of the KF-PDT on the Raman spectra in both cases. In case#1 the broad shoulder at about 150cm^{-1} vanishes after the KF-PDT. We observe a shift of the peak relative to the CIGS A1 mode towards lower wavenumber in case#2 that we do not observe in case#1. An additional phase (corresponding peak at 260 cm^{-1}), identified in the following, is detected in CIGS#2(K).

Ga content – The dependency of the Raman A1 peak position on the Ga content has been studied [160], showing that the corresponding wavenumber of the phonon peak shifts from 174 cm^{-1} up to 185 cm^{-1} when x is varied from 0 (pure CIS) to 1 (pure CGS). The position of this A1 peak can depend also on the Cu content [158]. However, XPS measurements have shown that the Cu content is similar in both CIGS#2 and CIGS#2(K). Hence, the shift towards lower wavenumber reported in case#2 after PDT can be interpreted as a lowering of the Ga content in the near surface region of this absorber. This suggests that the Ga surface depletion highlighted by XPS does not only result from the formation of new surface compounds (which do not contain Ga), but also from an underlaying chalcopyrite with lower Ga content. One could expect a similar shift in CIGS#1 as the same Ga depletion was evidenced in both cases. Surprisingly the CIGS A1 peak remains at the exact same position in that particulary case. This confirms that the top layer is not made of CIGS and does not contain Ga. It also suggests that the CIGS below this top layer has the same Ga content than that in the reference.

New phases – A new phase is identified in CIGS#2(K). Witte *et al.* show that Cu-rich films with y>1 exhibits a non-chalcopyrite mode at 260 cm^{-1}. In this paper they assign this contribution to $Cu_{2-x}Se$. We have also performed Raman scattering measurements in the same conditions on $Cu_{2-x}Se$ film co-evaporated in our laboratory. The grey Raman spectrum in Figure 3-9-b corresponds to this co-evaporated $Cu_{2-x}Se$ film. CIGS#2(K) exhibits the $Cu_{2-x}Se$ mode at 260 cm^{-1}. This confirms the formation of such phase in case#2 already evidenced by XPS.

The absence of the broad shoulder on the Raman spectrum of CIGS#1(K) suggests that the KF-PDT suppresses the OVC present in CIGS#1. The fact that the OVC is no more present in CIGS#1(K) should increase the Cu content globally detected by XPS in this sample, as the relative Cu content is lower in the OVC than in the α-phase chalcopyrite (see section 1.2.1). However, XPS reveals a strong Cu depletion. This gives rise to the formation of a top layer that is not CIGS and does not contain Cu.

We have performed GIXRD measurements on absorbers either "as grown" or treated with KF. In order to avoid the widening of the XRD peaks we performed these measurements on absorbers without Ga grading. For these samples, labeled CIGS#3 and CIGS#3(K), the KF-PDT is highly beneficial as in this case all of the parameters are increased. The electrical effects of the treatment on these samples will be debated in section 4.5. Figure 3-10 shows the XRD patterns of these samples between 26 and 27.5°. The peaks are not symmetric, suggesting at least two different reflexions. Fits of the peaks with two gaussians labelled P-1 and P-2 are proposed for both samples. They are centered at 26.95 ± 0.05 ° and 26.75 ± 0.05 °, respectively, corresponding very well to the 112-reflexions of the $CuIn_{0.7}Ga_{0.3}Se_2$ and the $CuIn_3Se_5$, respectively[6]. The reflexion corresponding to the OVC is highly decreased by the KF-PDT, confirming the results obtained with Raman scattering.

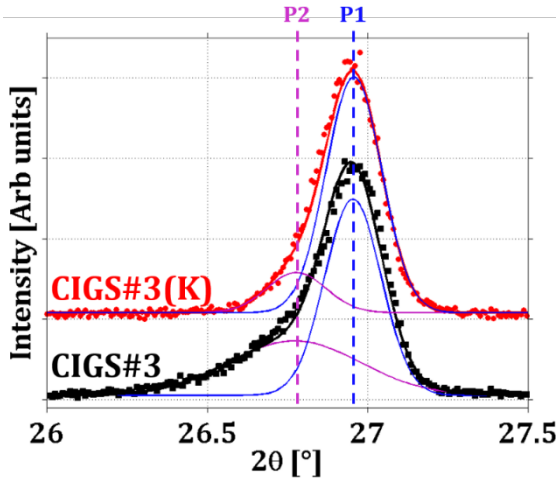

Figure 3-10 - GIXRD patterns of absorbers treated with KF (red) or not (black)

3.2.3 Summary on the structural investigations

Table 3.3 summarizes the structural experimental findings evidenced by the use of Raman scatterings and GIXRD measurements on absorbers from both Run#1 and #2 before and after the KF-PDT. For Run#1 the KF-PDT results in the removal of the OVC and no compositional changes on the underlaying CIGS. For Run#2 no OVC was present prior the KF-PDT. The KF-PDT results in the formation of a new $Cu_{2-x}Se$ phase and lowered Ga content in the CIGS.

Table 3.3 – Summary of structural experimental findings in investigated samples

	Run#1	Run#2
Prior PDT	- OVC	- No OVC
After PDT	- No OVC - Same Ga content for the CIGS	- No OVC in treated absorber - Lower Ga content for the CIGS - $Cu_{2-x}Se$

[6] An asymetric peak is also found at 44.7°, corresponding to the sum of the 204-reflexions of the $CuIn_3Se_5$ and the $CuIn_{0.7}Ga_{0.3}Se_2$, respectively

3.3 K-containing chalcogenide

A top layer containing K, In, Se and possibly O (or OH) has been previously evidenced on a KF-treated absorber from Run#1. If a material containing such species exists it has to be synthesisable at the rather low substrate temperature used during the KF-PDT, which is about 350°C. Cu and Ga depletions have been highlighted by XPS in such a sample but one cannot completly exlude their presence in this top layer. In the following, we will review the ternary chalcogenide materials that contain these elements that would potentially match the experimental features mentioned above. Then we will present the results of an X-ray Absorption Spectroscopy experiment at the K-edge performed on these samples at the Soleil synchrotron facility. Finally, we will propose a material with a structure that would fit the experimental findings related to the KF-PDT.

3.3.1 State of the art

The ternary chalcogenides AMQ_2 (A = alkali or alkaline-earth metal; M = Al, Ga, In; Q = S, Se, Te) have attracted much attention due to their rich structural chemistry and interesting physical properties (see [161] and references therein).

Adamentane structure – $KInSe_2$ [162] and $KGaSe_2$ [161] as well as $KInS_2$ [163] or $KGaS_2$ [164] have been synthesized and characterized. They are isostructural and crystallize in the monoclinic space group C2/c. Their structure exhibits both two-dimensional (layered) and three-dimensional structural features. Each $[M_4Q_{10}]$ unit is comprised of four vertex-sharing $[MQ_4]$ tetrahedrals surrounding an empty octahedral site. One $[In_4S_{10}]$ unit is illustrated in Figure 3-11-a and the global polyhedral representation of the layers of vertex-linked $[In_4S_{10}]$ units in $KInS_2$ is given in Figure 3-11-b.

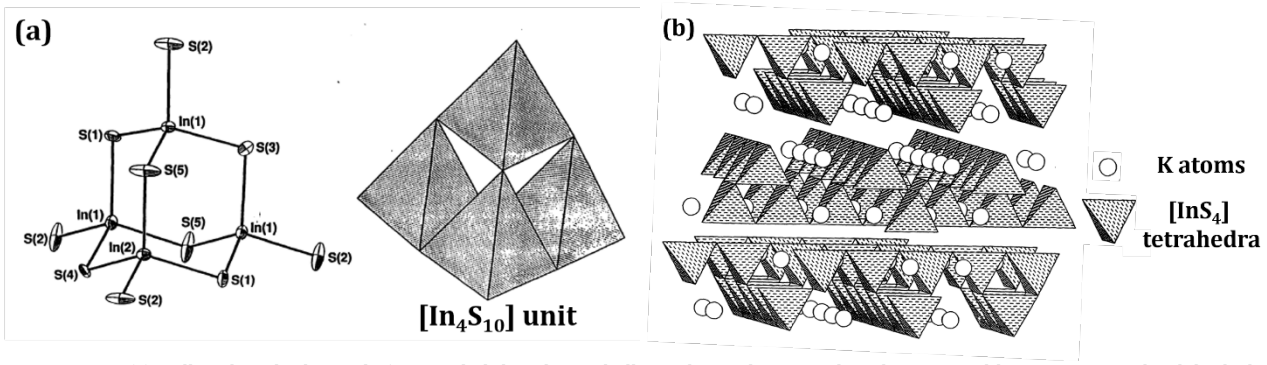

Figure 3-11 – (a) Ball-and-stick plot with 50% probability thermal ellipsoids emphasizing the adamantane-like structure and polyhedral plot of the $[In_4S_{10}]$ unit in KInS2; (b) (a) Polyhedral representation of the layers of vertex-linked $[In_4S_{10}]$ units in $KInS_2$. Each layer is rotated 90° relative to neighboring layers. The edges of the large $[In_4S_{10}]$ units in one layer nestle into the channels of the layers. After [163]

In such a structure, K is located in two different crystallographic sites. These atoms are coordinated to a bicapped trigonal prism of eight chalcogenes, resulting in K-Q (Q=Se, S) bond distances ranging from 3.264(2) to 3.917(2) Å in $KGaSe_2$ and 3.174 to 3.997 Å in $KInS_2$.

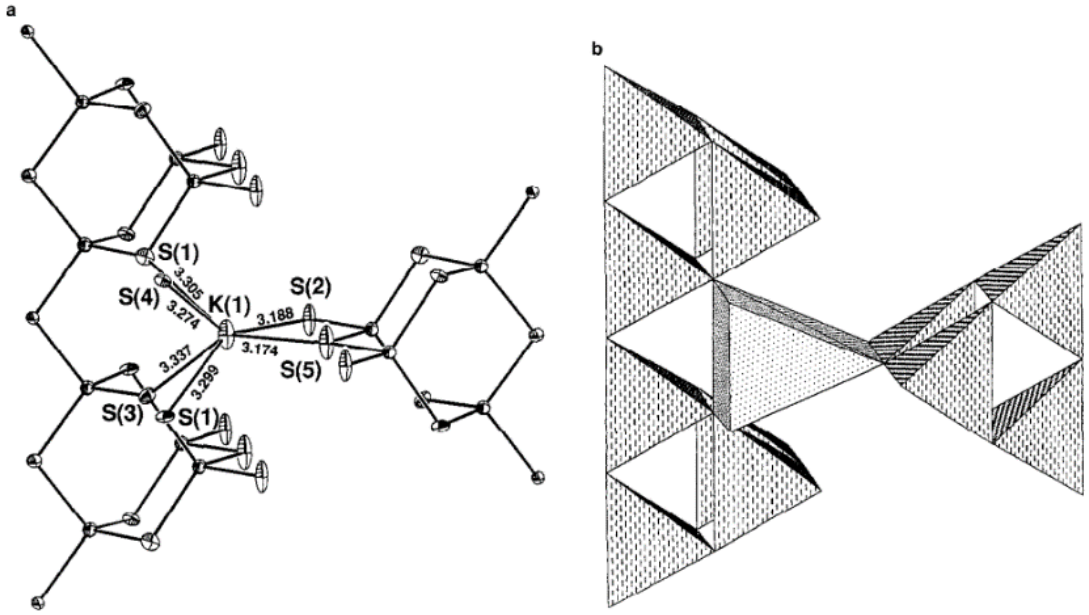

Figure 3-12 - Views along the channels of potassium atoms showing the interlayer connections in KInS2. (a) Ball-and-stick plot with 50% probability ellipsoids and with the 6 shorter interatomic distances noted; (b) polyhedral plot.

Kish *et al.* report that $KInSe_2$ has relatively low melting entropy and enthalpy values and is photosensitive. They assume that the In_2Se_3-K_2Se system is characterized by the formation of three intermediate phases where $KInSe_2$ and $K_4In_2Se_5$ melt congruently and KIn_3Se_5, incongruently [165]. In case of K/Ga/Se system, three compounds (i.e. $KGaSe_2$, $K_6Ga_2Se_6$ and K_5GaSe_4), have been found so far (see [161] and references therein). $KGaSe_2$ is the only compound that exhibits the two-dimensional layer structure. The lower the Ga content in the structure, the sparser the $GaSe_4$ tetrahedra connectivity.

Band gap – Electronic structures of such compounds have been calculated [161], [166], revealing that the band gap energy Eg is mainly determined by the $[MQ_2]$ (M=In, Ga and Q=S, Se) layers. Hence, direct band gap energies of Eg=2.0, 2.4 and 2.8 eV have been reported for the $RbInSe_2$, $KGaSe_2$ and $RbInS_2$ compounds, respectively.

Oxides – Feng *et al.* explain that since there are no Se-Se bonds in these structures, the oxidation states of +1, +3 and -2 can be assigned to K, Ga or In, and Se, respectively. Recently Lee *et al.* [167] synthesized new quaternary alkali-metal indium selenites, $AIn(SeO_3)_2$ (A=Na, K, Cs) through standard solid-state and hydrothermal reactions. They report that these materials are stoichiometrically equivalent but crystallographic data indicate that $NaIn(SeO_3)_2$ and $KIn(SeO_3)_2$ exhibit three-dimensional framework structures (centrosymmetric space group Pnma (No. 62)), whereas $CsIn(SeO_3)_2$ possesses a layered structure that allows efficient ion-exchange mechanisms.

Cu-containing compound – Ma *et al.* reported the synthesis of $K_2CuM_3Se_6$ (M=In, Ga) compounds that also crystallize in the space group $C2/c$ of the monoclinic system [163]. In these compounds, some of the $[MSe_4]$ units are simply replaced by $[CuSe_4]$ units. They report an optical band gap of 1.68 and 1.72 eV for these compounds, respectively.

Synthesis temperature – Rather low temperatures have been reported for the synthesis of these compounds. For examples, $RbInQ_2$ compounds were synthesized by heating a reaction mixture of pure elements in NH_3 at 773K in a sealed fused-silica tube, $K_2CuM_3Se_6$ was synthesized by heating a Pyrex ampoule containing the constituent powders at 793K.

3.3.2 XAS study of K in KF-treated CIGS

X-ray Absorption Spectroscopy experiments at the K-edge of the potassium (~3.6 keV) have been performed on the "Line for Ultimate Characterisation by Imaging and Absorption" (LUCIA) beamline (0.8-8 keV), at the Soleil synchrotron facility, on CIGS#1(K). We have acquired the signals in the fluorescence mode. In this detection mode, we may consider that we observe a large fraction of the thin film, limited by the absorption of the incoming X-rays, and the escape depth of the fluoresced X-ray, which is about 3 µm at the energy of the K-edge of the potassium.

Figure 3-13 shows the spectrum corresponding to the X-ray absorption[7] of the potassium in the surface layer of CIGS#1(K), corresponding to the sum of 3 acquisitions with 8 fluorescence detectors. The spectrum has been normalized. It is elemental specific (inherent from the technique, here the K) and can be divided in two parts: (a) the"X-ray absorption near edge structure" (XANES), which is characteristic of the environment and the valence state of the electronic cloud of K in the structure, and (b) the "Extended X-Ray Absorption Fine Structure" (EXAFS), which depends of the atomic pair distribution (i.e. interatomic distances) in the environment of the selected element. The theory of EXAFS explains that the oscillations of this signal correspond to the final state of the excited photoelectron in the high kinetic energy range (100-1000 eV), which is determined only by single backscattering events. The frequency of the oscillations is directly related to the interatomic pair distances, which makes this technique a powerful tool for local structure determination, even for poorly crystallized phases.

One can see that the EXAFS signal of the CIGS#1(K) shows no oscillations. This is surprising because Se is a heavy element that should induce oscillations on the EXAFS signal. The adamentane-like $KInSe_2$ structure could explain this flat response. The EXAFS signal of K in this adamentane-like structure is the sum of the responses of all of the chemical bonds involved in the structure. Considering the 8 different K-Se bond distances, ranging from 3.264(2) to 3.917(2) Å, and thus the very different induced frequencies of each contribution, the total EXAFS signal of such a structure could not show oscillations.

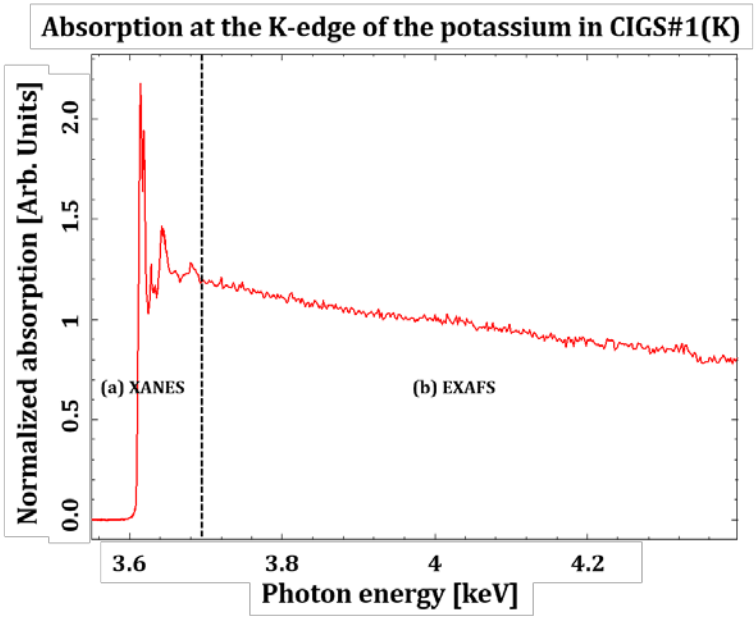

Figure 3-13 – X-ray absorption at the K-edge of the potassium in CIGS#1(K)

[7] Indeed the signal is the fluorescence of the sample induced by the X-ray absorption.

3.3.3 Discussion

An enhanced Cd in-diffusion, as well as a modified CdS growth was reported in the case of the KF-treated samples (see the review section 2.2.3 and the investigations performed in the framework of this thesis in the following section 4.2.2). Considering the ionic radius of Cd (109 pm) and that of K (152 pm), the layered structures mentioned above could explain why a higher amount of Cd is found in the top layer of treated absorbers: Cd could replace K in the adamentane structure involving an ion-exchange mechanism.

The very long and different distances for the chemical bonds involving K in the adamentane structure could explain why the EXAFS signal at the K-edge in the investigated sample exhibits a flat response.

Based on this analysis, in the following we assume that the top layer formed in case#1 is composed of adamentane-like $KInSe_2$. The higher oxidation of the KF-treated absorbers compared to the reference samples could then result in formation of $KIn(Se,OH)_2$. Ga and Cu containing compounds exhibiting the same adamentane structure exist and could possibly form a diffuse layer that could exhibit a decreasing Ga and Cu content from the surface towards the bulk. However, considering the strong Ga and Cu depletions revealed by XPS, we simplify the model by assuming an abrupt interface between non-modified CIGS and a pure $KInSe_2$ top layer.

3.4 Reaction mechanisms involved during the KF-PDT at the surface of the absorber

In this section we intend to formalize the chemical reactions that occur at the surface of the absorber in case#1 and case#2. We propose the formation of an adamentane-like $KInSe_2$ layer when the absorber exhibits a thick enough OVC. We do not consider the eventual formation of $KGaSe_2$, $K_2CuInSe_2$ or $K_2CuGaSe_2$ phases nor oxidation mechanisms. In case#2 we consider that the absorber is composed only of α-phase $Cu(In,Ga)Se_2$ and therefore the Cu cannot diffuse into the bulk.

In both cases we assume the following hypothesis:

- Higher reactivity of Ga than In with F to form GaF_3 instead of InF_3
- Gallium content of 33% relative to group III elements at the surface

3.4.1 Case#1 – beneficial effect

Hypothesis : - Thick OVC phase $Cu(In,Ga)_3Se_5$ present at the surface

For a qualitative approach, the reaction mechanism is artificially divided into two steps (i) formation of the top layer and (ii) consumption of the OVC:

$$\text{(i)} \quad CuIn_2GaSe_5 + 3\,KF \xrightarrow{Se\ flux} GaF_3 + 2\,KInSe_2 + \overrightarrow{Se} + \overrightarrow{Cu} + \frac{1}{2}K_2Se \tag{3.1}$$

$$\text{(ii)} \quad \frac{1}{2}CuIn_2GaSe_5 + \overrightarrow{Cu} + \overrightarrow{Se} \xrightarrow{Se\ flux} \frac{1}{2}Cu_3In_2GaSe_6 + \frac{1}{2}Se^0 \tag{3.2}$$

Where $\overrightarrow{Cu}$ and $\overrightarrow{Se}$ denote copper and selenium released during the formation of the top layer, not considering the charge state involved in these artificial steps, and finally the whole reaction can be written as:

$$\frac{3}{2}CuIn_2GaSe_5 + 3\,KF \xrightarrow{Se\ flux} GaF_3 + 2\,KInSe_2 + \frac{1}{2}Cu_3In_2GaSe_6 + \frac{1}{2}Se^0 + \frac{1}{2}K_2Se \qquad (3.3)$$

3.4.2 Case#2 – Detrimental effect

Hypothesis : - No OVC present at the surface

$$Cu_3In_2GaSe_6 + 3\,KF \xrightarrow{Se\ flux} GaF_3 + 2\,CuInSe_2 + \frac{1}{2}Cu_2Se + \frac{3}{2}Se^0 + \frac{3}{2}K_2Se \qquad (3.4)$$

3.4.3 Discussion

K and Cu coexistence – Considering the ionic radius of K it is unlikely that K could occupy any tetrahedral site in the chalcopyrite structure. Moreover due to its electronic structure Cu has a very similar chemical behavior to that of alkaline species. Therefore it is not surprising that K tends to repulse Cu from the surface of the absorber where it is supplied through PDT. In case#1, Cu can migrate easily within the OVC phase that contains an important amount of V_{Cu}. K might impose a new structure and a strong Cu depletion is found at the surface. In case#2, the amount of available V_{Cu} is much lower due to the absence of the OVC, Cu might not migrate similarly and K cannot form a new phase. This could help to explain why in this case no K is found at the surface after rincing with NH_3.

Consumption of the OVC – It is assumed that the Cu and Se released during the formation of the top layer in case#1 react with the OVC to form the α-phase CIGS. This reaction is likely to happen as the same process is involved during the second step of the 3-stage co-evaporation process that can be performed at a rather low temperature.

Selenium – Considering the temperature of the PDT (350°C) the Se released during the formation of the top layer could possibly evaporate and not react with the OVC to form the α-phase CIGS. This could explain why the PDT has to be performed under Se flux.

Conclusion – The above hypothesized equations are in good agreement with the experimental findings summarized in Table 3.4. In the case#2, they explain why a higher amount of Se^0 is formed. In the case#1, the underlaying CIGS layer (below the non-CIGS top layer) has the same Ga content as its reference (not including the OVC phase that does not respond in the same mode in Raman scattering). The Ga content in case#2 after KF-PDT is effectively lower than that in the corresponding reference. We do explain the formation of the new $Cu_{2-x}Se$ phase evidenced both with the help of Raman scattering and GIXRD.

Table 3.4 - Summary of the most important experimental findings in investigated samples

Technique	Run#1	Run#2
XPS	Low Na amount at the surface in the reference Cu & Ga depletion In enrichement Se^0 GaF_3/GaO_x prior rincing Modified valence band (non chalcopyrite with higher Eg)	High Na amount (and oxides)at the surface in the reference Ga depletion In enrichement Se^0 (higher amount) GaF_3/GaO_x prior rincing $Cu_{2-x}Se$ Non modified valence band (chalcopyrite)
RAMAN/GIXRD	OVC in the reference No OVC in treated absorber Same Ga content for the CIGS	No OVC in the reference No OVC in treated absorber Lower Ga content for the CIGS $Cu_{2-x}Se$

Figure 3-14 proposes a schematic view of the reaction mechanisms that occur during the KF-PDT and during the first moments in the chemical bath (rincing with NH_3)

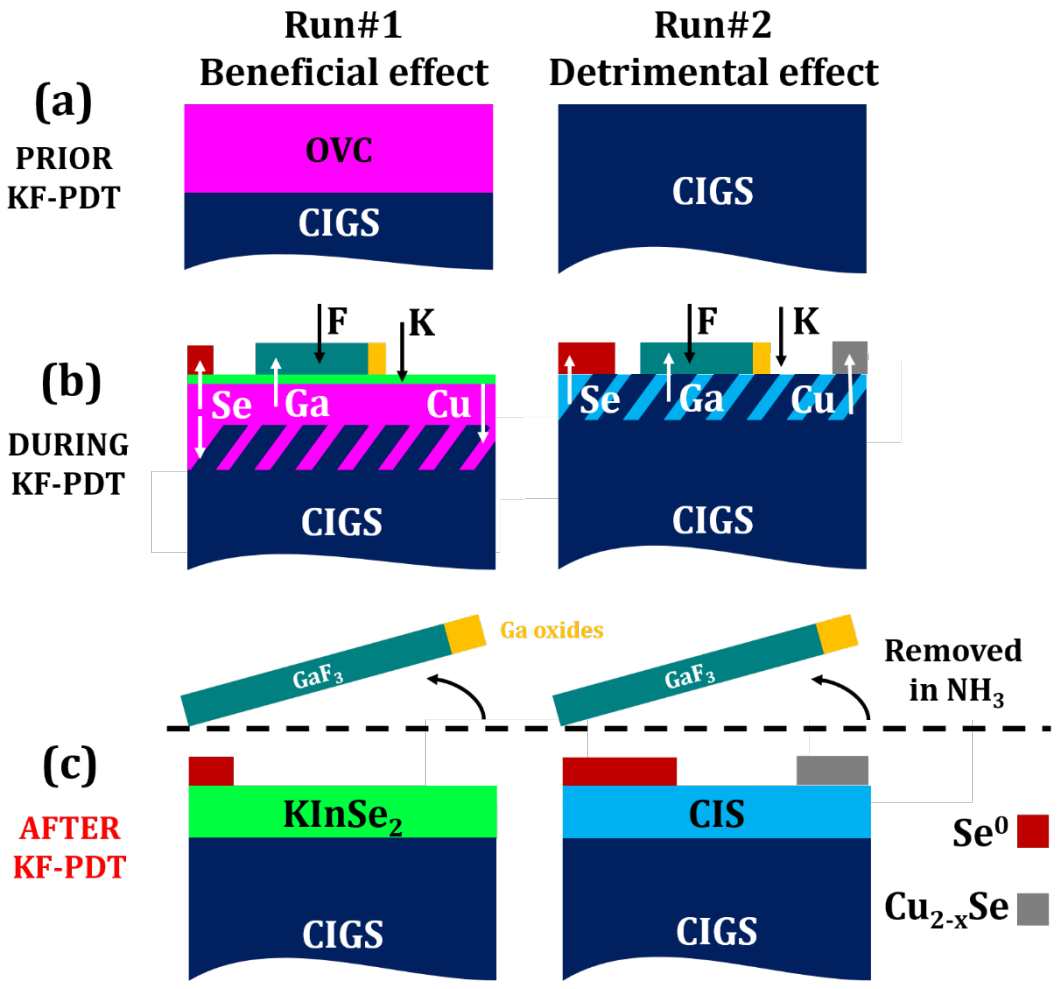

Figure 3-14 - Model of the chemical modification induced by the KF-PDT in absorbers from Run#1 (beneficial effect) and Run#2 (detrimental effect). Scheme of near-surface absorber are given (a) prior (b) during and (c) after the rincing step of the KF-PDT

Chapter 4
Material changes induced by the KF-PDT at CIGS interfaces

In the previous chapter we have investigated both the compositional and the structural changes induced by the KF-PDT at the surface of the absorber. We have shown that the involved chemical reactions depend on the properties of the absorber prior the treatment. We have concluded that the presence of an OVC phase at the surface of the absorber prior the KF-PDT is necessary to allow the formation of a thin $KInSe_2$ surface layer with potentially a layered adamentane-like structure. If no OVC is present prior to the KF-PDT then no such $KInSe_2$ material is synthesized and $Cu_{2-x}Se$ phase is formed instead. In all cases, KF-PDT induces the formation of Se^0 at the outermost surface.

The purpose of this chapter is to investigate the additional material changes that result from the KF-PDT at all CIGS interfaces after the completion of the device. We will focus on samples from Run#1 where the KF-PDT has a beneficial effect on device performance. This chapter will consist of two parts:

(I) In Part I we will focus on the *CIGS/CdS hetero-interface*. First we perform a compositional and structural assessment of this interface for complete devices (Cell#1 and Cell#1(K)). Then we will compare the (CBD)CdS growth on treated and untreated CIGS surfaces. Based on this analysis, we will synthesize and investigate the properties of a new material we suggest to be formed during the chemical bath deposition on the KF-treated CIGS surfaces. Finally we will formalize the chemical reactions that occur during the (CBD)CdS growth and propose a model for the hetero-junction formation in Cell#1 and Cell#1(K).

(II) In Part II we will investigate the *CIGS/CIGS homo-interfaces*, i.e. the properties of the CIGS grain boundaries (GBs). Two kinds of GBs, those located (i) in the near CIGS/CdS interface region and those located (ii) deeper in the CIGS, will be presented.

PART I – CIGS/CdS hetero-interface

The purpose of this first part is to investigate and model the material changes induced by the KF-PDT during the chemical bath deposition of the buffer layer. We focus on samples from Run#1 and hence we assume the presence of the $KInSe_2$ surface layer in CIGS#1(K) prior the CdS deposition. In section 4.1 we will investigate the CIGS/CdS interface of Cell#1 and Cel#1(K) by Transimission Electron Microscopy (TEM). In section 4.2 we will show the morphological (SEM) and chemical (XPS) changes on the surfaces of CIGS#1 and CIGS#1(K) after several dipping durations in the CBD. In section 4.3 we will present the electrical, optical and structural properties of a new material present at the CIGS/CdS interface of Cell#1(K). In section 4.4 we will model the hetero-junction formation in Cell#1 and Cell#1(K).

4.1 CIGS/CdS interface region in complete devices

In this section we focus on the CIGS/CdS interface region in Cell#1 and Cell#1(K). Thin cross section slices were prepared using the Focused Ion Beam (FIB) technique. Ion beam energy and current density were adjusted at the end of the milling in order to minimize the segregation of Cu condensates at the surface, usually observed with this material [168]. The cross sections were then transferred into a FEI Titan Transmission Electron Microscope (TEM) to perform composition analysis and imaging near this interface by using techniques such as Energy Dispersive X-ray Spectroscopy (EDS), High Resolution Transmission Electron Microscopy (HRTEM), and High Angle Annular Dark Field imaging (HAADF). Additional EDS mappings of the near CIGS/CdS interface region in Cell#1 and Cell#1(K) can be found in Appendix B.

4.1.1 CdSe segregation

Figure 4-1 shows the HAADF low magnification micrograph of the near CIGS/CdS interface region for the investigated devices. Two main differences can be observed between these two samples:

(i) The bright areas present within the CdS layer in Cell#1(K). These areas are about 60-80 nm size and are distributed along the CIGS/CdS interface. They are not observed in Cell#1. This TEM mode is sensitive to the chemical contrast: roughy the intensity in HAADF micrograph is proportional to Z^2 with Z the mean atomic number along the viewing direction. This means that a compound with an average atomic number higher than that of CdS segregates within the buffer layer.

(ii) We interpret the dark areas[8] at the CIGS/CdS interface of Cell#1(K) in the framework of the suggested $KInSe_2$ surface layer synthesized during the KF-PDT. According to Feng *et al.* [161], this material has a much lower density (3.96 g/cm^3 for the similar material $KGaSe_2$) than that of CdS (4.82 g/cm^3) or CIGS (~5.7 g/cm^3) because it has a layered structure with large inter-layer distances. Therefore, it is not surprising that such material would evolve under the beam. This interpretation suggests that a material with

[8] High intensity focused electron beam can interact and deteriorate the sample; in worst scenario it creates holes that darken the contrast of the micrograph. However it appeared that the CIGS/CdS interface was much more unstable under the focused electron beam in Cell#1(K) than in Cell#1.

similar structure, or at least with a lower density than that of CdS, is still present at the CIGS/CdS interface after the completion of the device. Interestingly, such dark areas are also observed at GBs in Cell#1(K), suggesting that the material formed at the CIGS/CdS interface could also be formed at these interfaces.

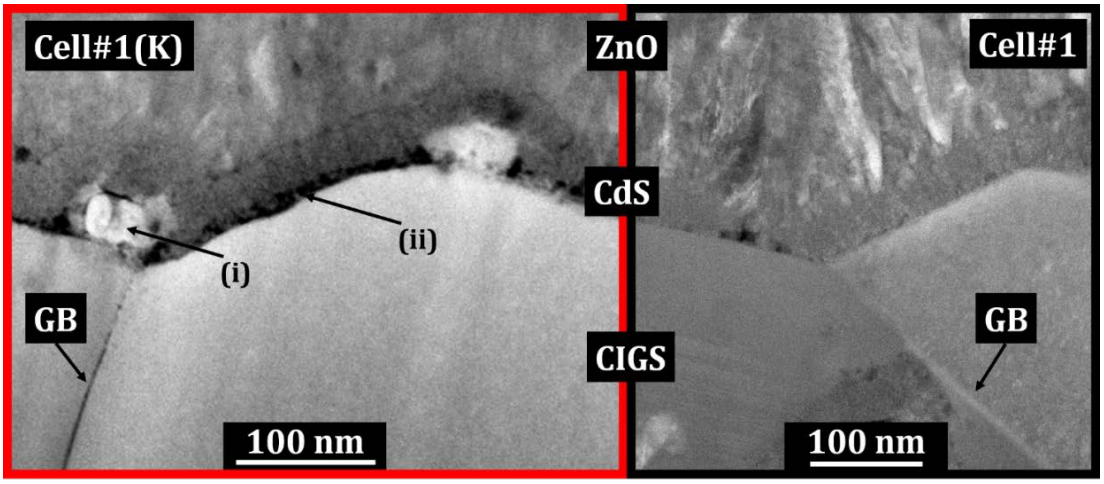

Figure 4-1 – Low magnification HAADF micrographs of the near CIGS/CdS interface regions in Cell#1(K) and Cell#1

An identification of the chemical composition of the compounds that segregate within the buffer layer has been performed by the use of EDS mapping techniques, centered on one of these condensates[9], as shown on Figure 4-2. One can clearly see that these compounds are composed of Cd and Se. We then suggest the formation of CdSe at the CIGS/CdS interface in Cell#1(K) during the chemical bath deposition. It seems that the CdS covers the CdSe. The dipping time in the chemical bath for these samples was 5 minutes. This means that the CdSe formation occurs at the very beginning of the chemical bath deposition. Sulfur and oxygen are clearly identified at an interface layer between the CdSe and the CIGS. The resolution of this mapping is not sufficient in order to identify the material at this interface. Therefore, quantifications obtained from EDS profiles recorded at higher magnification will be presented in the following.

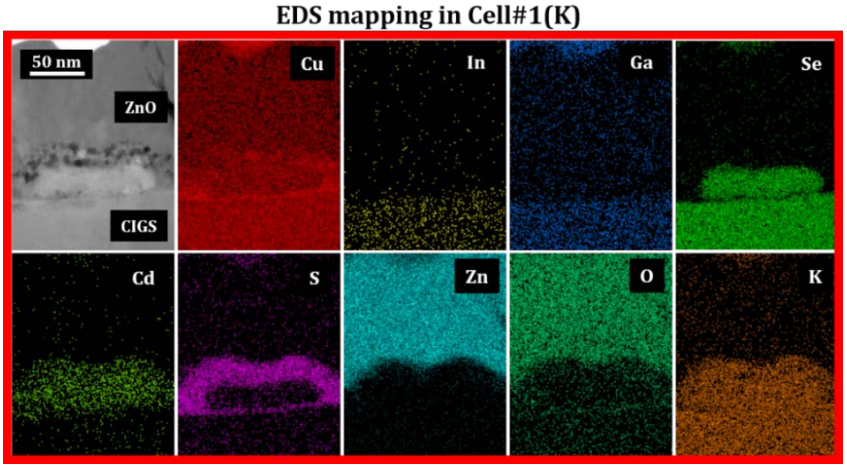

Figure 4-2 – EDS mapping of the near CIGS/CdS interface region in Cell#1(K)

[9] The presence of Cu above (in the CdS) and below (in the interface layer) the CdSe condensates is likely to be an artefact due to the use of Cu lift-out grids to support the cross-section lamella in the TEM. The mapping of K is not interpretable because the Kα line of the potassium (3.314 eV) is very close to the Cd Lα line (3.133 eV) and the In Lα line (3.286 eV). Therefore K signal is mixed up with these elements in the CIGS and the CdS.

4.1.2 Interface layer

Figure 4-3 shows a HRTEM migrograph of the absorber/buffer interface in Cell#1(K). One can clearly identify an interface layer with a thickness of about 5 nm. EDS spectra were recorded at the 3 zones indicated by the red circles (limited by the size of the probe) on the micrograph. The corresponding quantifications are given in the table adjacent to this figure. Once again, it appears that the proportion of Cu detected is too high, probably because of the Cu lift-out grid. For this reason, we have quantified the atomic percentage of the compounds of zone 1 and 2 excluding Cu. The proportions of S and O in the compound from zone 1 are very low and we can assume that this compound is CdSe. Considering that the diameter of zone 2 is greater than the thickness of the interface layer, fractions of the quantifications in the measurement of zone 2 come from zones 1 and 3. Nevertheless, the composition of this layer can be considered as close to that of the already reported $CdIn_2(Se,S,OH)_4$ material [169], [170].

Successful ion exchange experiments have been reported for this type of material [167]. Considering the fact that K is located in large "tunnel-like" sites in $KInSe_2$ (K-Se chemical bonds ranging from 3.174 to 3.997 Å) and the ionic radii of Cd (109 pm) and K (152 pm) the substitution of two K^+ by one Cd^{2+} in $KInSe_2$ (which can be written as $K_2In_2Se_4$) is likely to occur during the bath, thus forming $CdIn_2Se_4$. The proportion of Se, S and OH might suggest a sulfurization (iso-substitution of chalcogenide) and oxidation that are also very likely to happen in the alkaline (pH > 7, in CBD bath the pH is in the order of 12 [171]) chemical bath.

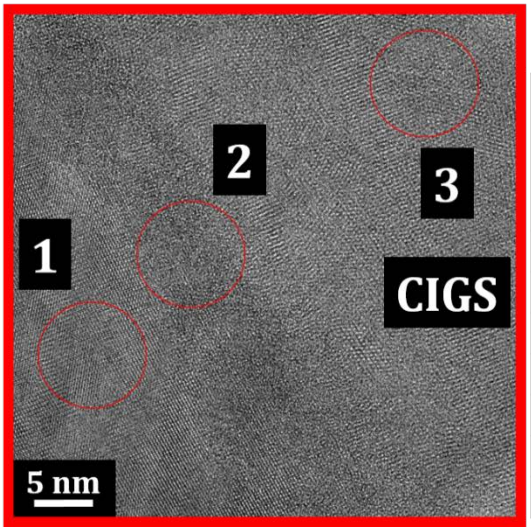

EDS quantification in Cell#1(K)

Zone / Element	1		2		3
	%at	%at Without Cu	%at	%at Without Cu	%at
Cu	36	#	46	#	45
In	0	0	14	27	15
Ga	0	0	1	1	4
Se	28	44	13	24	33
Cd	33	52	11	19	2
S	1	2	6	12	0
O	1	2	9	17	2

Figure 4-3 – TEM micrograph of the absorber/buffer interface in Cell#1(K). 3 red circles indicate the EDS probe size and the investigated zones. Table on the right gives the corresponding EDS atomic percentage quantifications excluding Cu or not.

Figure 4-4 shows the oxygen profiles centered on the CdS layer (without CdSe particle) from 50 nm deep in the CIGS towards 40 nm in the ZnO layer in the investigated samples. These profiles have been extracted from the EDS mapping represented on the left of the figure. The profiles have not been normalized and the amount of O in the CIGS and the ZnO is the same in both cases. One can notice an important amount of oxygen at the CIGS/CdS interface in Cell#1(K) that is not present in Cell#1, coherent with the oxidation of an interface layer. It seems that the surface material influences the subsequent CdS growth because a much higher amount of oxygen is also found in the CdS region of the Cell#1(K) compared to that in Cell#1. Assuming the substitution of K by Cd, the presence of K at the outermost surface of the sample could enhance oxidation of the growing CdS via catalytic effect as already shown by Kronik *et al.* [102].

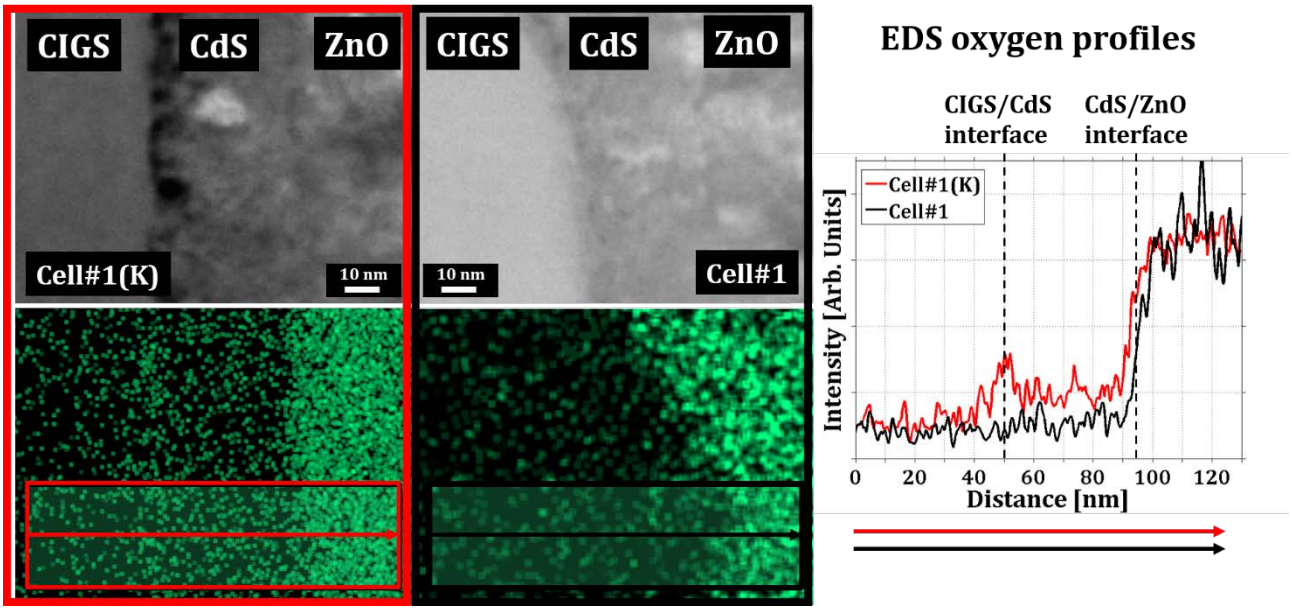

Figure 4-4 – TEM micrographs centered in the CdS region in Cell#1 and Cell#1(K) with the corresponding EDS mapping of the oxygen. Boxes represent the area of the mapping that has been considered to extract the profile of O in these samples given on the right.

4.1.3 CdS thickness

The buffer layers of Cell#1 and Cell#1(K) were deposited simultaneously in the same chemical bath for 5 minutes (see Appendix C for the experimental details of the CdS deposition). Figure 4-5 shows TEM micrographs of four different zones illustrating the CdS layer in these samples. No significant differences can be found in the buffer layer thicknesses, of about 40 ± 3 nm in both cases. In this mode (Bright Field TEM) the contrast is sensitive not only to crystallinity but also to the density of the material. One can clearly see the white "bubbles" at the absorber/buffer interface, corroborating the presence of an interface layer of lower density.

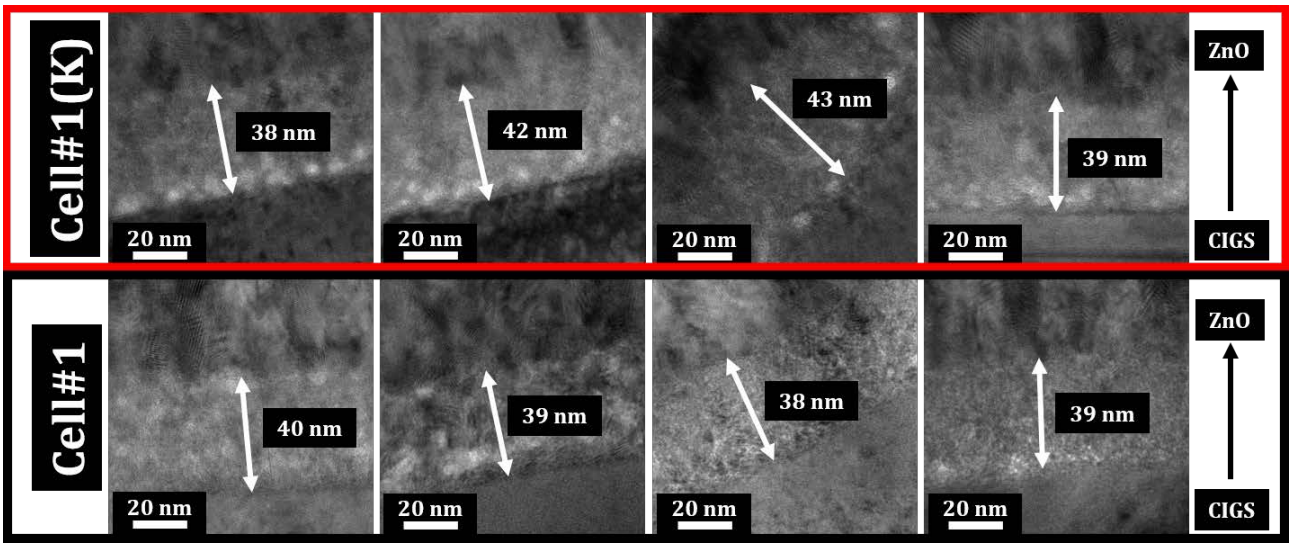

Figure 4-5 - TEM images of the CdS layer in both investigated cells

4.1.4 Micro-structural analysis

The morphology of the absorber/buffer interface is different in Cell#1 and Cell#1(K), as shown on the TEM migrographs given in Figure 4-6. Most of the investigated zones reveal a straight and abrupt interface in Cell#1 whereas some zones show less abrupt interfaces in Cell#1(K). One must add here that the morphological differences as well as the presence or not of "bubbles" at the interface of these two samples are not due to the lamella preparation by FIB or to the sample degradation during observation in a TEM with a too high accelerating voltage. They have been indeed also observed on cross section obtained by conventional TEM sample preparation in a 100kV TEM. This could help to understand what happens during the formation of the top layer. Due to its size and electronic structure the potassium might disorganize the chalcopyrite structure in the vicinity of the absorber surface. Following this, the overgrowth of the adamentane structure could result in an increased interface roughness.

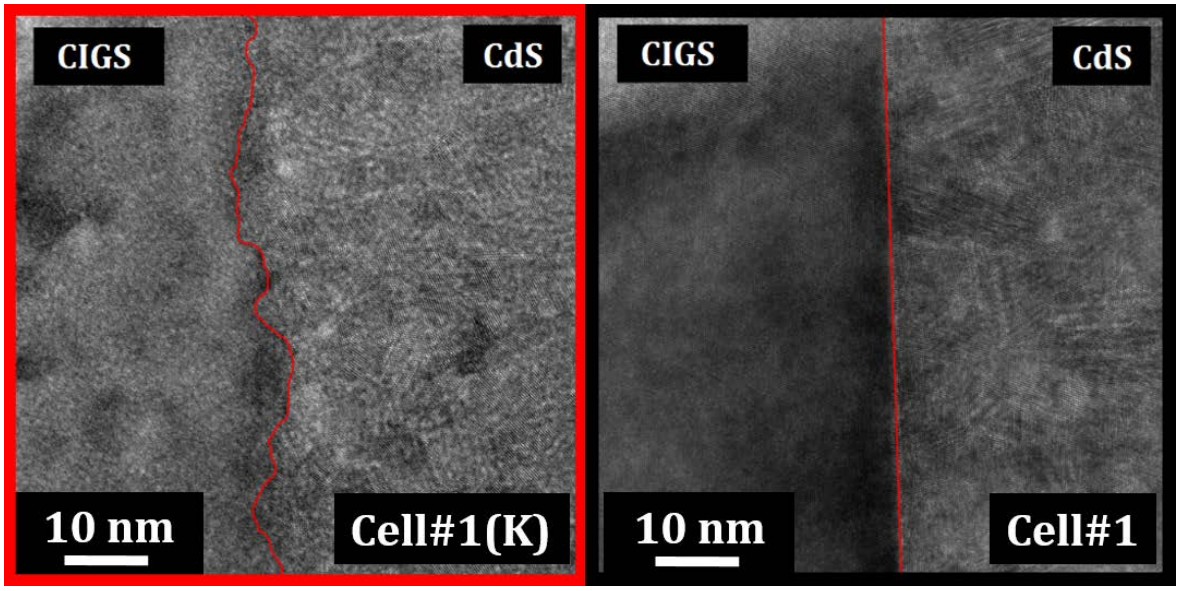

Figure 4-6 – TEM images of the CIGS/CdS interface in Cell#1(K) (left) and Cell#1 (right)

Figure 4-7-a shows the HAADF micrographs of the CIGS/CdS interface of Cell#1(K). Considering the chemical contrast of this mode one can see an intermixing of elements from the CIGS into the buffer layer. This could also suggest that the $KInSe_2$ surface layer reacts with the constituents of the chemical bath. The already suggested ion exchange mechanism between Cd and K could explain why the interface is revealed less abrupt in HAADF mode.

TEM micrographs at high magnification are also given in Figure 4-7-b. On the first one (Figure 4-7-b_1) an amorphous zone is highlighted, giving rise to the annihilation of the chalcopyrite structure due to the presence of K. Fast Fourier Transforms (FFT) are calculated in the CIGS, at the interface and in the CdS, from the second TEM micrograph (Figure 4-7-b_2). The results suggest an enhanced topotactic growth of the buffer layer onto the (112) planes of the surface of the treated absorbers. In most of the investigated zones the planes continue without discontinuities throughout the total thickness of the CdS. This implies an increased crystalline coherence of the buffer layer grown on KF-treated absorbers, with larger grains than those of the layer grown on the reference absorber (not shown). $CdIn_2(S,Se)_4$ material has been reported to have cubic (spinel) structure [169] and thus could explain the topotactic growth of cubic CdS.

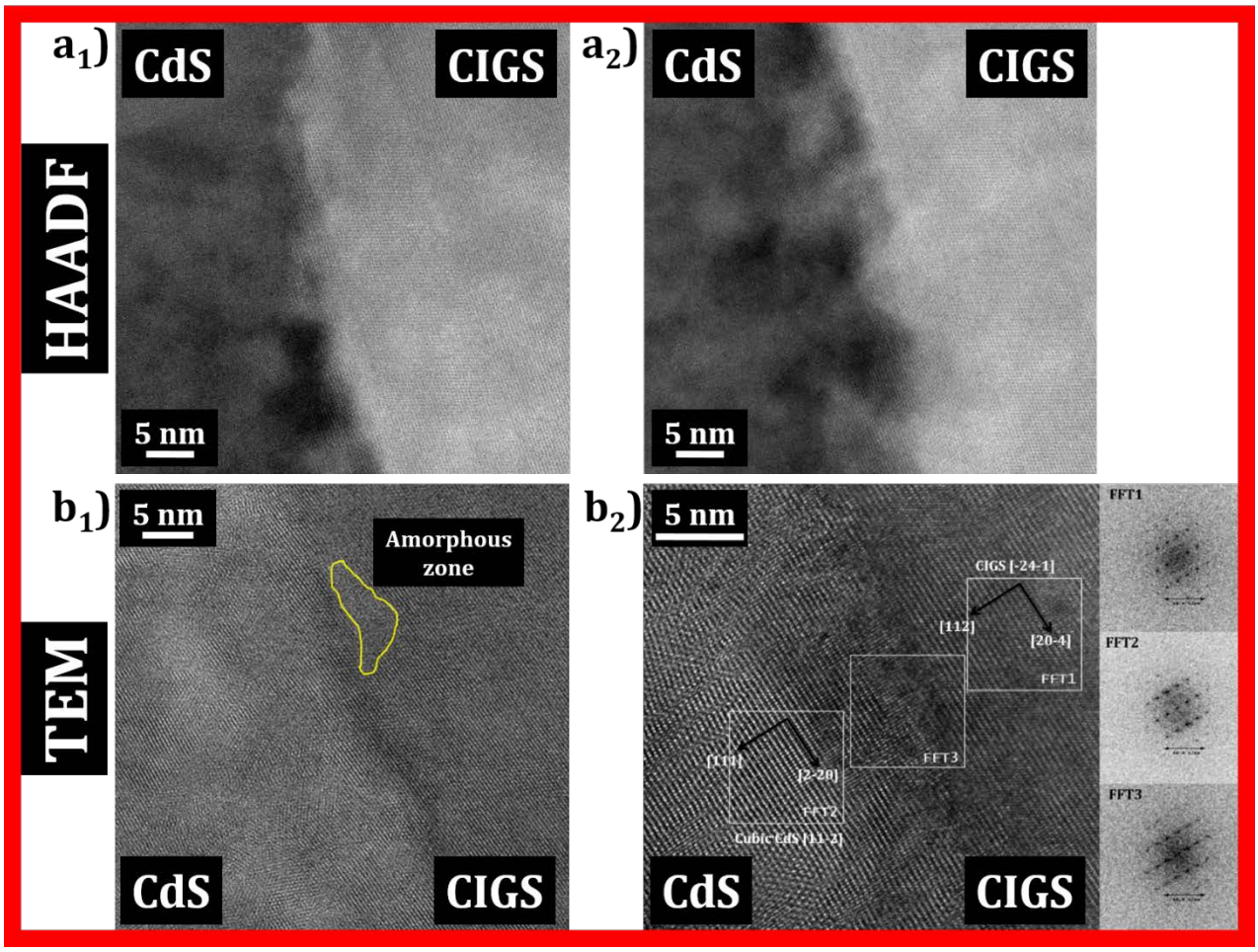

Figure 4-7 – HAADF (upper) and TEM (lower) micrographs of the CIGS/CdS interafce in Cell#1(K)

Partial conclusion – The TEM comparative study of the near absorber/buffer interface region reveals a more chemically diffused but enhanced crystalline CIGS/CdS interface in Cell#1(K) than in Cell#1. This induces a modified morphology of the CdS in Cell#1(K). We suggest that the $KInSe_2$ surface layer postulated in the previous chapter reacts with the chemical bath via substitution of K by Cd and Se by S. An enhanced oxidation of both the interface and the CdS layer is highlighted. Finally EDS measurements suggested the formation of a $CdIn_2(Se,S,OH)_4$ interface layer between the absorber and the buffer and the segregation of CdSe regularly distributed along the interface.

4.2 Comparative study of the chemical bath deposition

In this section we will compare the growth of CdS buffer layers by CBD on CIGS#1 and CIGS#1(K). As a first step, using XPS we will investigate the distinct effect of the Cd^{2+} ions from the solution, i.e. the reaction with the absorber surface and the diffusion into the absorber sub-surface via a Partial Electrolyte (PE) experiment [71]. We will then compare the growth of the CdS on both absorbers. A comparison of the chemical (XPS) and morphological (SEM) effects of different dipping durations in the bath will be proposed. Finally we will investigate the structural properties of the final CdS layer.

4.2.1 Cadmium partial electrolyte treatment

The absorbers CIGS#1(SiN) and CIGS#1(SiN,K) are immersed in a bath similar to the CdS deposition, but excluding the thiourea. The maximum temperature during the process, refered as the Cd PE treatment, was 80°C, and the total immersion time was 10 min. XPS spectra were recorded in the same conditions as the experiments presented in chapter 4 (p. 37). Technical details can be found in Appendix A.

Figure 4-8-a_1 and a_2 show the XPS spectra in the [0-22 eV] BE range before and after the Cd PE treatment of as-grown or KF-treated absorbers. Two main differences can be seen:

(1) The first difference concerns the Valence Band (VB) of these samples. The VB intensity of the as-grown absorber is just slightly lowered but not deformed by the PE, as revealed by the normalized VB given in inset. In 4d and Ga 3d XPS peak intensities are similarely decreased, suggesting the deposition of a thin layer during the Cd PE that induces signal attenuation of the non-modified chalcopyrite elements. On the other hand, the VB of the KF-treated absorber is markedly modified after the Cd PE, suggesting that the surface reacts with the bath. This gives rise to the presence of a non-CIGS surface material which, contrary to chalcopyrite, can react with the bath constituents. We suggest the substitution of K by Cd in the adamentane-like structure, resulting in the shift of the VB edge towards higher BE, as shown on Figure 4-8-b. For the same reasons as explained in section 3.1.1, this means a widening of the band gap.

(2) The second difference is related to the amount of Cd detected at the surface of these samples. One can clearly see from the area of the Cd 4d XPS peak that much more Cd is detected at the surface of CIGS#1(SiN,K,PE) than at that of CIGS#1(SiN,PE). Mainly three hypotheses can be proposed to explain this observation. The KF-PDT treatment could (i) change the surface terminations so the Cd^{2+} ions have more surface sites to which to bond, (ii) change the GBs properties so that the Cd can diffuse more easily through these defectives surfaces or (iii) allow K substitution by Cd in the hypothesized $KInSe_2$ surface layer. One should notice that (ii) and (iii) do not necessarily involve different processes. One can imagine that the $KInSe_2$ material is also formed at GBs and that Cd diffusion through GBs occurs via an ion exchange mechanism and the substitution of K.

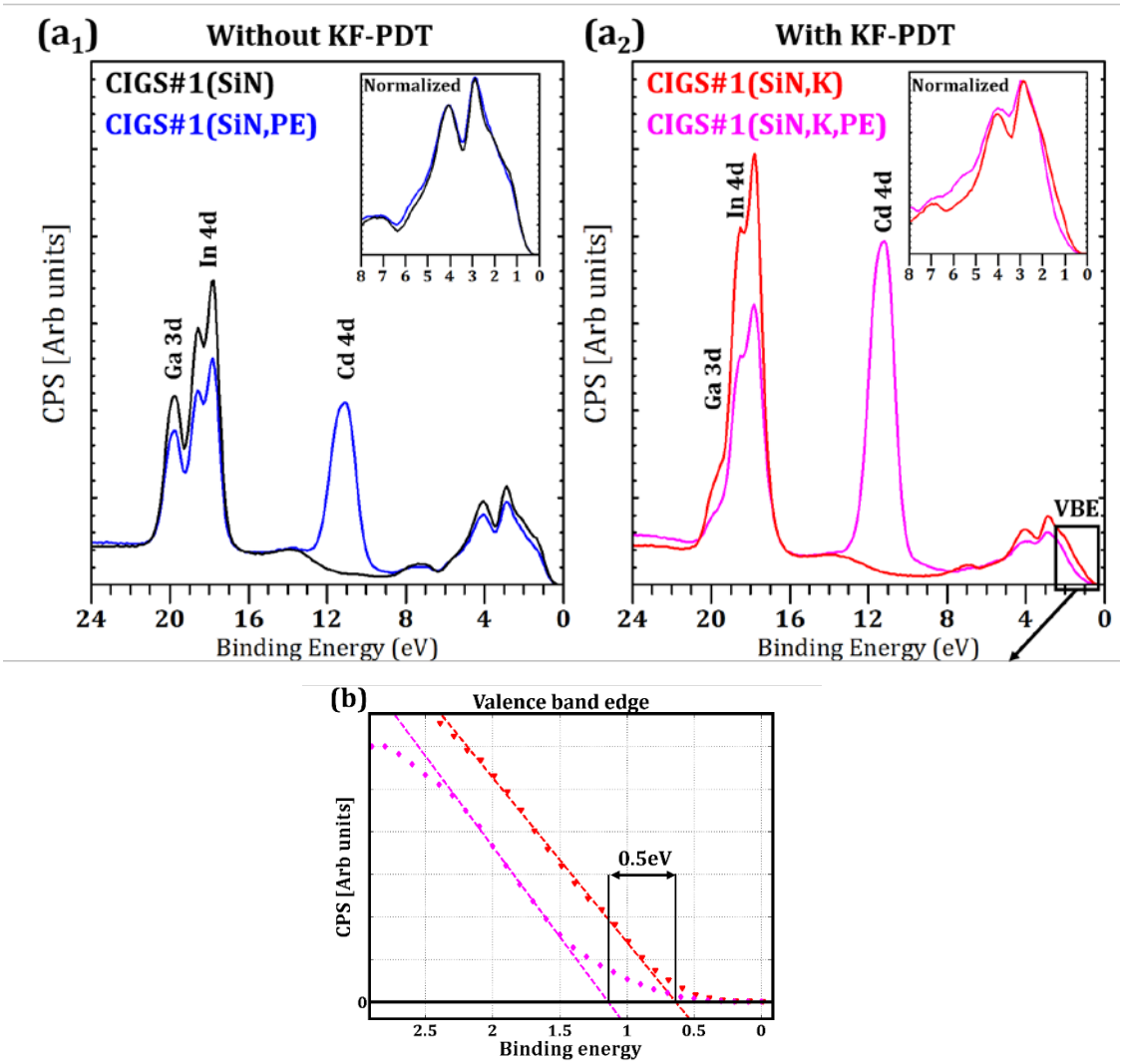

Figure 4-8 - Effect of the Cd PE on the photoemission lines corresponding to the valence band of absorbers from Run#1 grown in Na-free conditions and (a1) not subjected to KF-PDT (a2) subjected to KF-PDT. Valence band normalized at 3eV is given in inset. (b) A zoom on the valence band edge (VBE) maximum is also given for absorbers subjected to KF-PDT. Symbols corresponds to the experimental data. Dashed -lines corresponding to the fit of experimental data in the BE range [2 - 1 eV] for CIGS#1(SiN,K) and [2.3 - 1.5 eV] for CIGS#1(SiN,K,PE) are also plotted to extract the energy of the VBE maximum in both samples.

Substitution – As shown on Figure 4-9-a, the substitution of K by Cd at the surface layer is corroborated by the fact that K 2p doublet is not lowered by the Cd PE (whereas In 3d, not shown, is lowered). This suggests that K is not located below the Cd(Se,OH) deposited layer but at the outermost surface. We also suggest that the shift of the O-4 contribution (attributed to the oxidation of the surface layer) in the O1s XPS peak, shown in Figure 4-9-b, could also be due to the replacement of K by Cd in the structure.

Elemental Se - One can notice in Figure 4-9-c that the contribution corresponding to Se^0, present in KF-treated absorbers, disappears after the Cd PE. Two interpretations can be proposed: (i) Se^0 reacts with the bath and forms CdSe condensates, as revealed by the TEM study presented in the previous section or (ii) Se^0 is etched by the bath (presence of NH_3 in the bath, 80°C).

Surface sites for Cd adsorption - The anions present at the surface of the samples are Se^{2-} and O(OH) groups. Therefore, possible chemical bonds involved with the Cd are Cd-Se and Cd-O(H). Hunger *et al.* [172] have shown by XPS that Cd PE treatments lead to the formation of a hydroxide-terminated CdSe surface layer of one monolayer thickness on CIGS exhibiting an OVC at the surface, as it is in the case of CIGS#1(SiN). Hunger *et al.* suggest that the contribution in O1s at high BE and the contribution in Se3d at low BE are related to Cd-OH and Cd-Se chemical bonds, respectively. This is in good agreement with the denoted O-5 contribution[10] (531.4 ± 0.1 eV) in the O1s XPS peak and the Se-6 contribution (53.8 ± 0.1 eV) in the absorbers treated with Cd PE, as shown in Figure 4-9-b and c, respectively. A higher amount of Cd-OH and Cd-Se bonds are found in CIGS#1(SiN,K,PE), suggesting that a higher amount of Cd(Se,OH) is deposited in this case. This can be understood in the framework of the adamentane-like structure of the postulated $KInSe_2$ surface layer. This structure is constructed from $InSe_4$ tetrahedra so the layers are effectively terminated by Se, on which Cd can bond. More surface sites for Cd adsorption are availbale at the surface of KF-treated absorbers, which should have an important effect on the growth of the CdS.

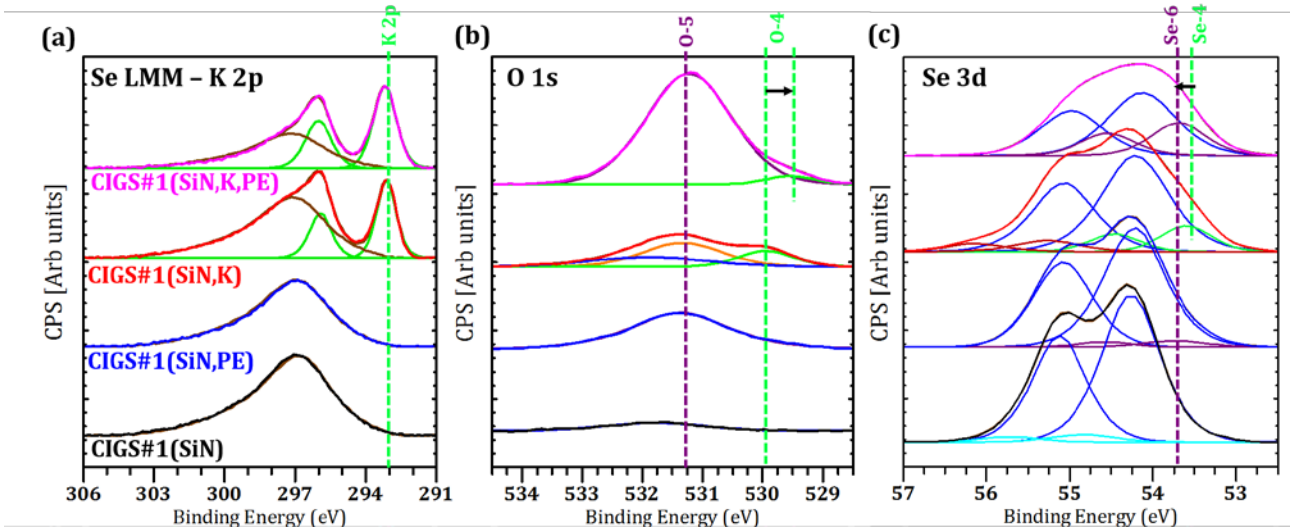

Figure 4-9 - Effect of the Cd PE treatment on the (a) K2p, (b) O1s and (c) Se3d XPS spectra of absorbers from Run#1 grown in Na-free conditions and subjected or not to a KF-PDT.

Cd penetration – We have investigated the penetration depth of the Cd into the absorber by XPS. Etching using an Ar^+ ion beam with 500eV energy and a 300x300 µm raster pattern was performed on the samples. In order to estimate the thickness etched by each etching cycle (60s), we determined the etching speed in these conditions by etching a 2µm thick CIGS/Mo structure and verifying after each cycle that the Mo $3d_{5/2}$ photoemission line was not detected. The atomic concentration of Cd was calculated considering the following photoemission lines (with respective Relative Sensibility Factor): $Cu2p_{3/2}$ (3.55), $In3d_{5/2}$ (4.36), $Ga2p_{3/2}$ (3.72), Se3d (0.50) and O1s (0.78). One should notice that no correction concerning the different information depths was considered, resulting in errors in the concentrations of the elements. However, this method allowed us to calculate a profile of the Cd atomic concentration in the investigated samples.

[10] The O-5 contribution is found at the same BE as the O-2 contribution attributed to Ga oxide or hydroxide. However, no Ga is found in absorber treated with KF so this increase of the O1s XPS peak cannot be related to Ga oxides or hydroxides.

Figure 4-10 shows the atomic Cd concentration in the first 20 nm of the CIGS#1(SiN,PE) and the CIGS#1(SiN,K,PE). Cd concentration is high at the surface due to the presence of the Cd(Se,OH) monolayer deposited on the Se-terminated surfaces. We find again a higher Cd concentration at the surface of the KF-treated. Excluding the point at the surface (which does not correspond to Cd that has effectively diffused into the absorbers) the Cd profiles can be fitted very well with an exponential decay (which is the signature of diffusion process). After 20 nm the concentration was below the detection limit of the technique in both cases. If we choose a concentration above 1% atomic as criterion for the penetration depth δ of Cd, δ is found to be 5 ± 1 nm and 9 ± 1 nm for the as-grown and the KF-treated absorbers respectively. This difference is important since Cd penetrates almost twice deeper into the absorber due to the KF-PDT. However, the 4 nm difference between δ in both cases is close to the thickness of the interface layer evidenced in the previous section. Therefore we suggest that the enhanced Cd in-diffusion into the treated absorber might be mainly due to the substitution of K by Cd in the adamentane material rather than an effective higher penetration of Cd into the chalcopyrite.

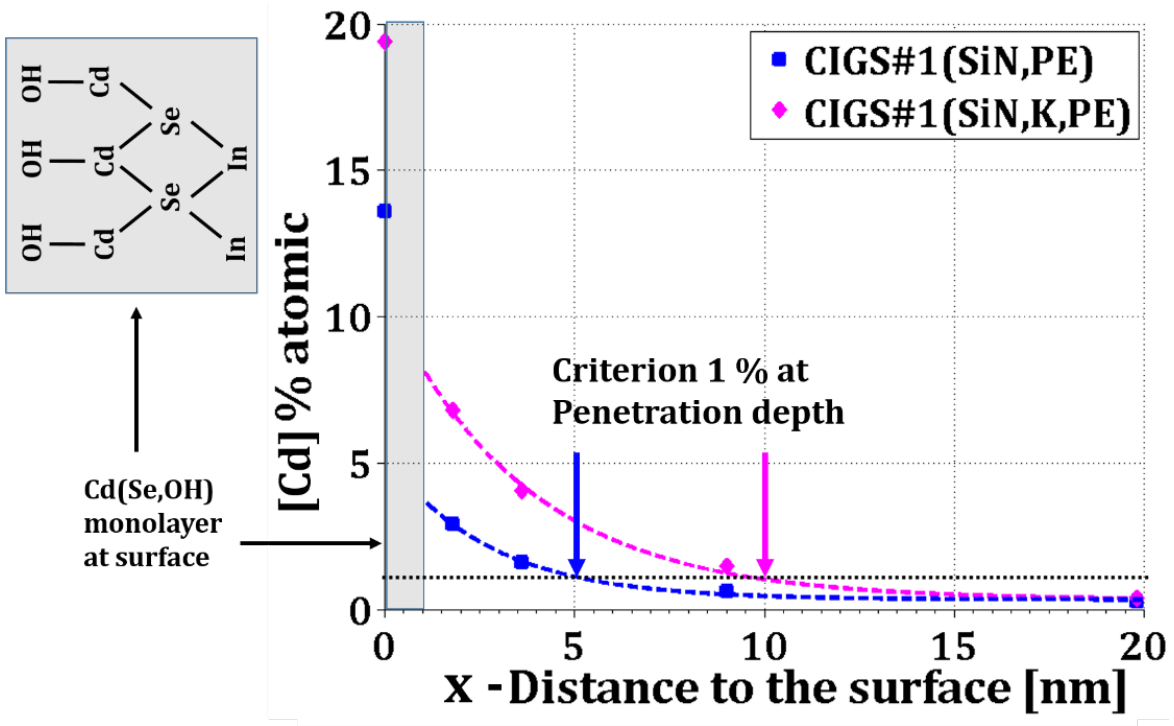

Figure 4-10 – Profile of the Cd atomic concentration in reference and KF-treated absorbers from Run#1 grown in Na-free conditions and subjected to a Cd PE. The Ar+ ion etching was performed at 0.5keV energy. The etching speed has been calculated through the complete erosion of a 2 µm thick CIGS layer. Dashed lines correspond the fit of experimental data (excluding first point) following an exponential decay. A criterion of 1% atomic has been chosen to define the penetration depth of the Cd into the absorber

Partial conclusion – Performing Cd PE treatment on as-grown and KF-treated absorbers has allowed us to corroborate the deposition of a Cd(Se,OH) monolayer onto the surface. The coverage seems higher on KF-treated samples (higher amount of Cd detected and stronger lowering of other XPS peaks), probably due to the higher availability of Se-terminated surfaces for the surface material than for the chalcopyrite. Several experimental findings suggest the substitution of K by Cd in the surface material. Among them, the VB shape modification, the shift of the VBE (0.5 eV) as well as the presence of K at the outermost surface of the absorbers are strong arguments showing that the surface material of KF-treated absorbers reacts during the Cd PE.

4.2.2 Modified CdS growth

In this section we will compare the CdS growth on CIGS#1 and CIGS#1(K) (grown on SLG/Mo, i.e. in the presence of Na). We will focus on the morphological and chemical differences induced by the CBD process using three deposition durations in order to highlight the growth differences onto the two absorbers. All of the investigated samples have been dipped in the same bath. CIGS#1(B1) and CIGS#1(K,B1) were removed from the bath after one minute, rinced with deionized water, dried with inert gas and both transfered in a Scanning Electron Microscope (SEM) and in the X-ray Photoelectron Spectrometer (XPS). CIGS#1(B3.5) and CIGS#1(K,B3.5) undergo the same process but have been removed from the bath after 3.5 minutes and CIGS#1(B7) and CIGS#1(K,B7) after 7 minutes.

Morphological effects – Figure 4-11 shows the plane view SEM micrographs of the 6 investigated samples obtained using a 5kV acceleration voltage and a 60,000x magnification. We added the micrographs of "as-grown" (non rinced) absorbers.

The surface of CIGS#1(K,AG) shows a very different morphology from that of CIGS#1(AG). Terraces in the chalcopyrite structure, visibles in CIGS#1(AG), cannot be detected in CIGS#1(K,AG) because they seem to be covered by a layer of very small grains. We also detect larger aggregates, already reported in [134], which we suppose to be fluoride compounds (see section 3.1.4). After 1 minute in the bath these aggregates are removed from the surface of CIGS#1(K,B1), revealing dark stains on SEM micrograph in secondary electron mode or Back-scattering Electron Imaging (BEI) mode (not shown). These stains are interpreted as holes in the literature.

After one minute in the bath, the surface of CIGS#1(K,B1) is smooth, as if covered by a very thin layer, whereas for CIGS#1(B1) the CdS seems to start growing at the edges of the terraces. After 3.5 min this inhomogeneous deposition of CdS on the untreated sample is highlighted. Recently, Witte *et al.* [173] have investigated the (CBD)CdS growth on CIGS surfaces and have shown that the coverage density of the CIGS grains by CdS depends on their orientation and the type of plane that terminates the surface. They have shown that the non-polar {220}/{204} planes terminated with both metal and Se species show a much denser coverage than that of the polar –metal terminated- {112} planes. This could help to understand why the coverage is much more homogeneous on CIGS#1(K,B3.5). On this sample the CdS covers all of the surface. As already mentioned, the surface of the adamentane material should exhibit a high density of Se/metal terminated planes and thus could explain the better coverage by the CdS. Finally, at seven minutes both samples are completly covered with CdS. The CdS grains are larger on CIGS#1(K,B7) than on CIGS#1(B7).

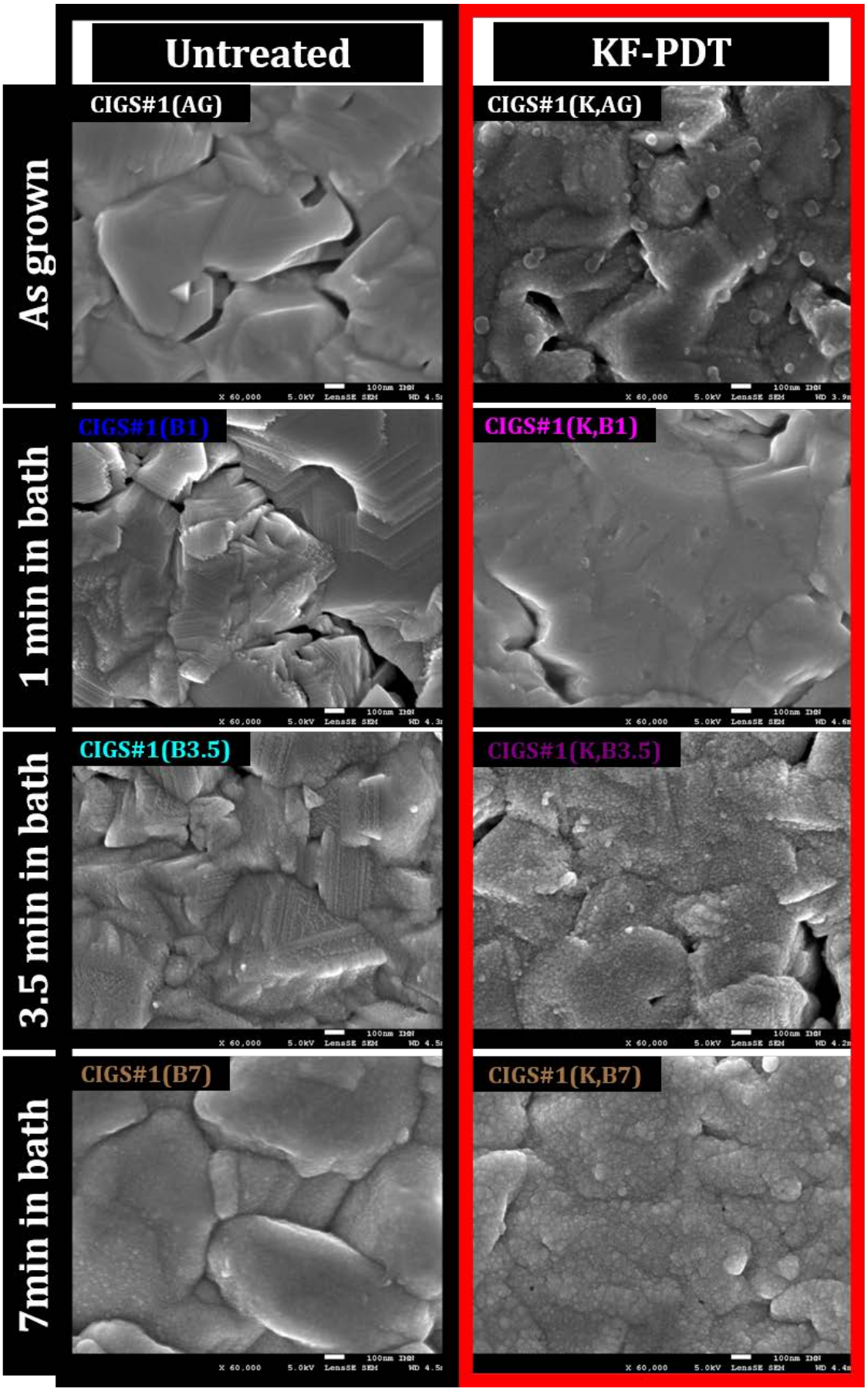

Figure 4-11 - Plane view SEM micrographs of absorbers treated (right) or not (left) with KF and dipped into the chemical bath for 0, 1, 3.5 and 7 min (from upper to bottom)

Growth mechanisms - Figure 4-12-a shows the XPS spectra of the 6 investigated samples in the [0-21] eV range. Surprisingly it appears that the amount of Cd detected at the surface of the KF-treated absorbers is always slightly lower than that detected on the untreated one. This is very different from the PE experiment in which a much higher amount of Cd was detected on the KF-treated samples. However the dipping duration and conditions in the chemical bath are different from those during the PE so the comparison of the Cd adsorbtion for both cases is hazardous. The purpose of the PE experiment was to show that a much larger amount of Cd-OH bonds are formed on KF-treated absorbers. This is also confirmed in the bath as a higher amount of oxygen is detected in treated samples (see Figure 4-12-b). This could explain why lower quantities of Cd and S (see Figure 4-13-b) are detected by XPS in all cases for the KF-treated samples (relative to the untreated ones). SEM micrographs reveal a dense coverage of the CdS on CIGS#1(K,B3.5). This is confirmed by the VB shape of this same sample (Figure 4-12-a). The VB of CIGS#1(K,B3.5) superimposes that of CIGS#(K,B7). This means that the surface of the treated absorber is already fully covered by a CdS layer after 3.5min. This is not the case in untreated samples where it is shown that the CdS growth is much more heterogeneous, with a large part of the OVC surface not covered by CdS after this 3.5 min dipping duration. The valence band of CIGS#1(B3.5) does not superimpose that of CIGS#1(B7) because the OVC is still detected after these 3.5 minutes of dipping duration. This also explains why Se (see the Se 3s XPS peak in Figure 4-13-b_1), In (see Figure 4-14-1), Cu and Ga (not shown) are still detected by XPS after this dipping duration in CIGS#1(B3.5).

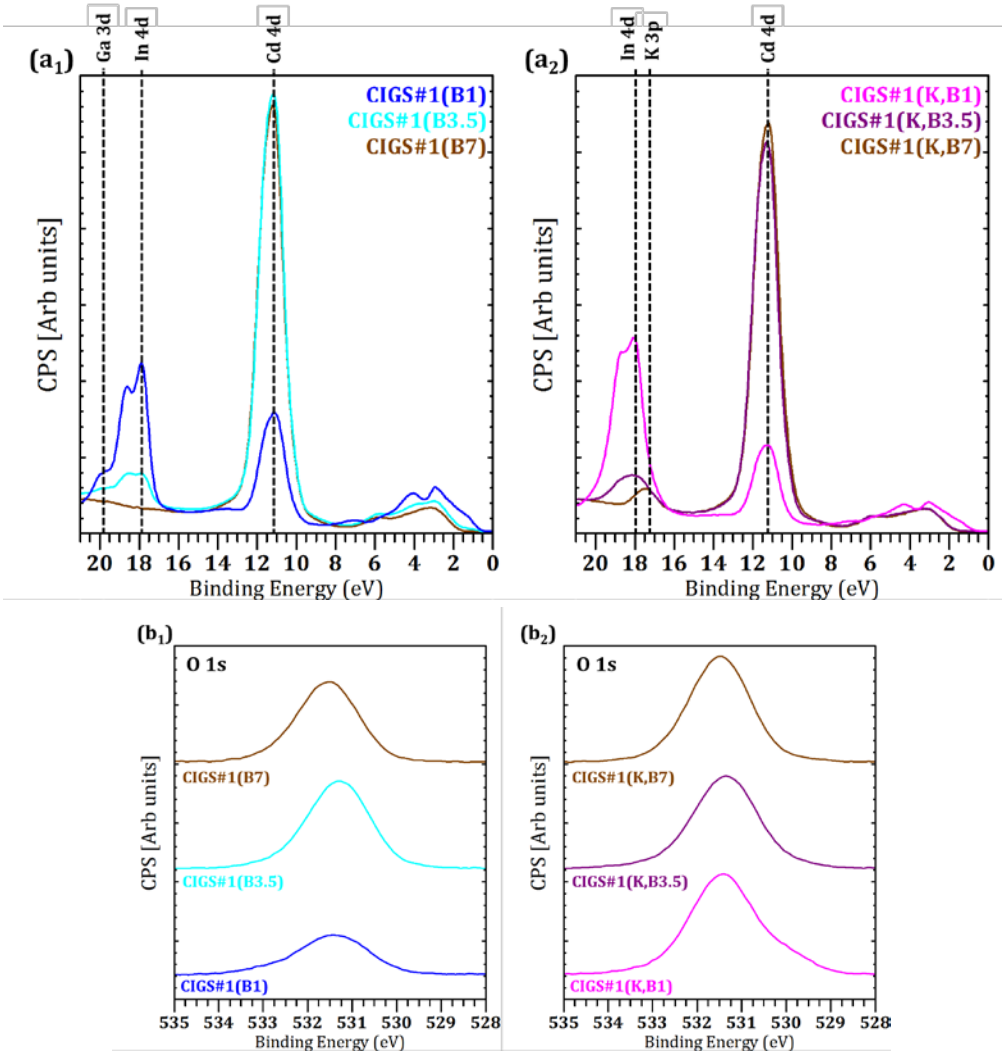

Figure 4-12 –Effect of dipping 1, 3.5 and 7 minutes in the chemical bath the untreated (left, subscript 1) and the KF-treated absorbers (right, subscript 2) on their (a) XPS spectra in the [0-21 eV] BE range and (b) O1s XPS spectra

Substitutions - One can notice in Figure 4-13-b that the amount of Se (see the area of the Se 3s XPS peak) is lesser in CIGS#1(K,B1) than in CIGS#1(B1) whereas it was similar before the chemical bath dipping. One can therefore suggest that a substitution of Se by S in the adamentane material occurs during the chemical bath deposition. Figure 4-13-a_2 shows that K is found at the outermost surface of the treated absorber for all explored dipping durations of the bath. The amount of K is equivalent to that found in CIGS#1(K) (not shown) which was not dipped into the bath. This again suggests that Cd substitutes K in the surface material. We suggest that the K at the surface react with OH^- hydroxides present in the bath to form KOH.

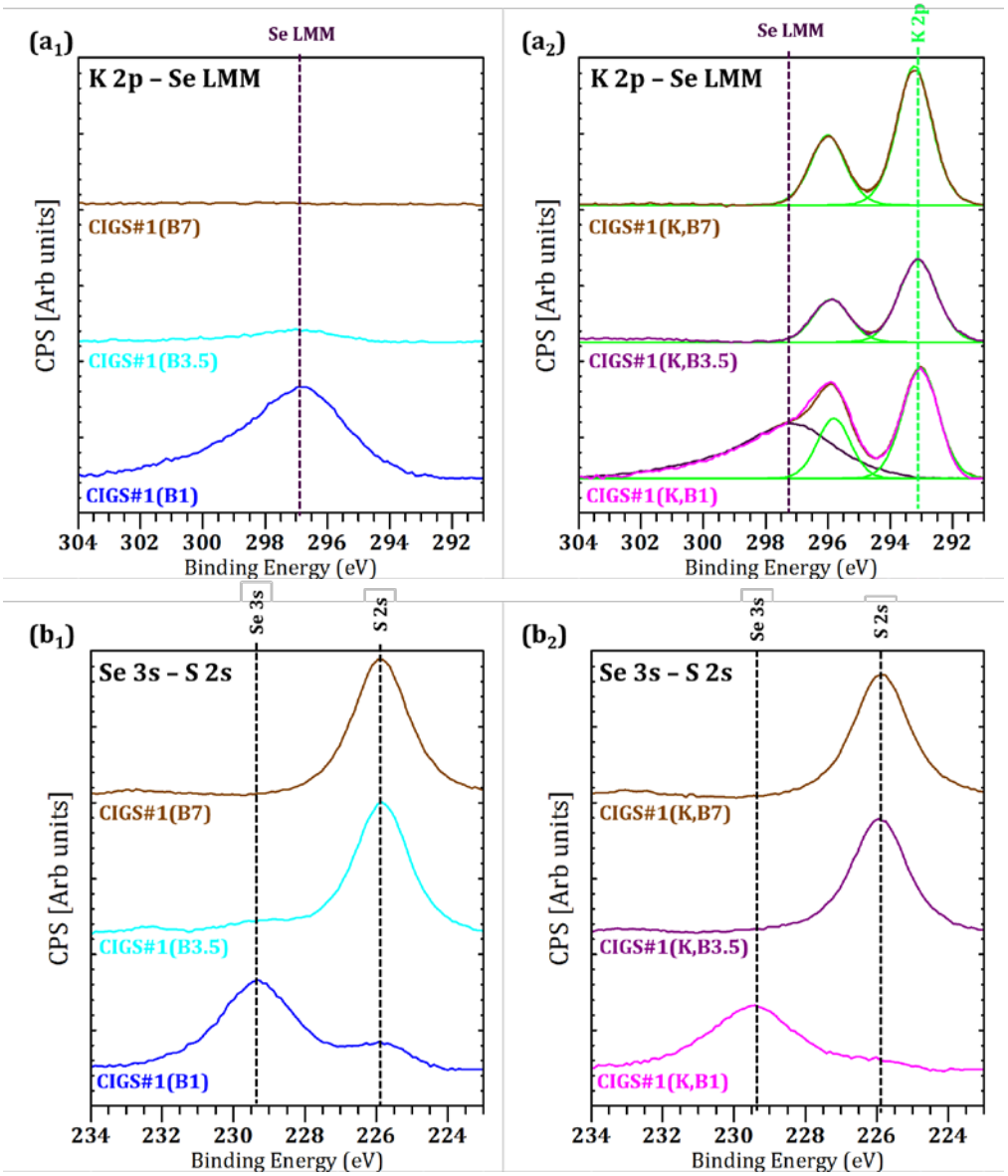

Figure 4-13 - Effect of dipping 1, 3.5 and 7 minutes in the chemical bath the untreated (left, subscript 1) and the KF-treated absorbers (right, subscript 2) on their (a) K 2p and (b) Se3s and S2s XPS spectra

Resulting CdS - Finally, after 7 minutes dipped in the CBD, both samples, treated or not with KF, are very similar since the VB of CIGS#1(B7) and that of CIGS#1(K,B7) superimpose very well (not shown) and correspond to that of standard CdS. Only Cd, S and O are detected. The unique difference concerns the higher amount of oxygen found in the treated absorber. We suggest that the K detected at the surface catalyses the surface oxidation.

Interface layer containing In - Figure 4-14 shows the In $3d_{5/2}$ XPS spectra of all the investigated samples. Although the spectra of untreated and KF-treated samples after 3.5 min in the bath seem similar, the interpretation of the origin of the detected In in both cases is not straightforward. In CIGS#1(B3.5), the detection of In originates from the incomplete coverage of the OVC surface with CdS. On the other hand, the surface of CIGS#1(K,B3.5) has been shown to be fully covered with CdS. One could suggest that the detection of the In in this sample could originate from the surface material induced by the KF-PDT on top of the CIGS (containing also K and Se, we postulated the formation of $KInSe_2$). However, no Se is detected in CIGS#1(K,B3.5) (see Figure 4-13-a2 and Figure 4-13-b2 for the Se LMM Auger transition and the Se 3s core level photoemissions[11], respectively), nor Cu and Ga (not shown).

Basically, two interpretations can be proposed:

(i) All of the Se has been substituted by S in the surface layer induced by the KF-PDT (which contains In) and the CdS that covers the surface is thin enough to allow the detection of the new material $CdIn_2S_4$ (assuming a $KInSe_2$ composition for the surface layer and a complete substitution of the K by Cd, which is not probably the case)

(ii) In diffuses from the surface layer into the forming CdS. The CdS after 3.5 min in the bath is thick enough to prevent the detection of the Se from the Se-containing materials (e.g. CIGS) located below.

In both cases this is a very interesting result as a material containing exclusively Cd, In and S is detected in CIGS#1(K,B3.5).

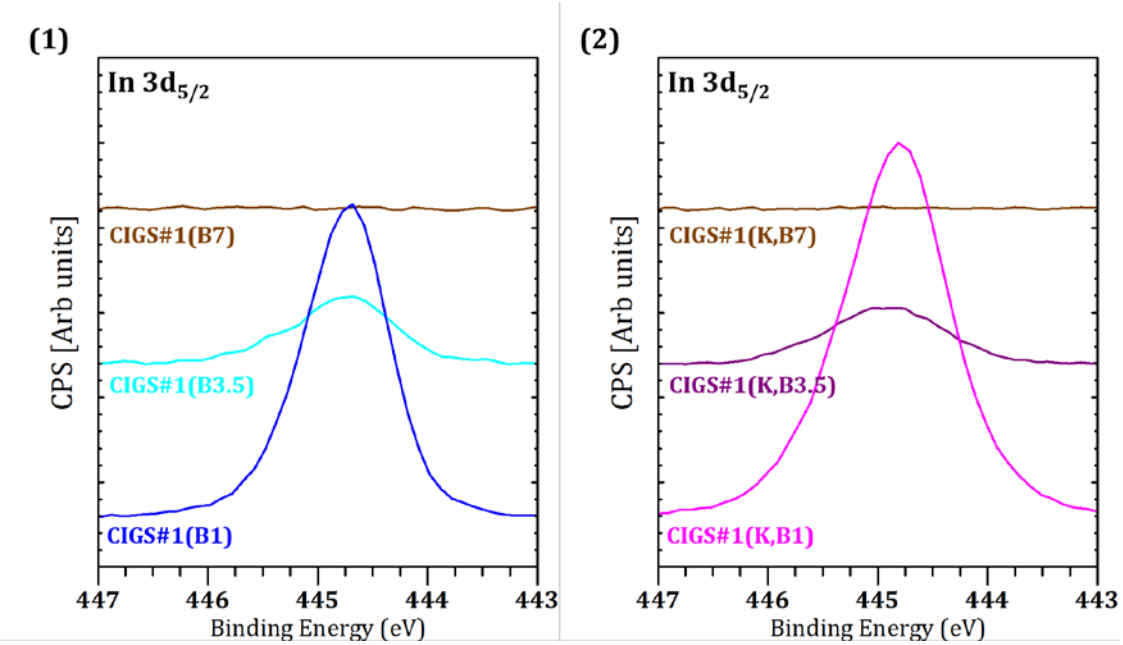

Figure 4-14 - Effect of dipping 1, 3.5 and 7 minutes in the chemical bath the untreated (1) and the KF-treated absorbers (2) on their In$3d_{5/2}$ XPS spectra

[11] Se 3s is not detected in CIGS#1(K,B3.5). This means that the thickness of the CdS layers covering the absorber is at least 7 ± 1 nm (considering the XPS ID in this energy range).

Partial conclusion – SEM and XPS measurements show a different (CBD) buffer layer growth mechanism onto untreated and KF-treated absorbers. The resulting CdS layers on both absorbers after 7 min exhibit similar Cd and S content and the same VB shape though a higher content of oxygen is found in CdS deposited on KF-treated absorbers. However, the resulting CdS are morphologically different since larger CdS grains are found in CIGS#1(K,B7) relative to those in CIGS#1(B7). The most important difference occurs during the first part of the deposition. The growth is much more homogeneous on KF-treated absorbers and we highlighted a compound containing only Cd, S and In in that case.

According to the SEM and XPS characterizations, in the framework of the postulated $KInSe_2$ surface layer induced by the KF-PDT, and assuming that In does not diffuse into the CdS, we propose a schematic plane view model of the CdS growth on untreated and KF-treated absorbers:

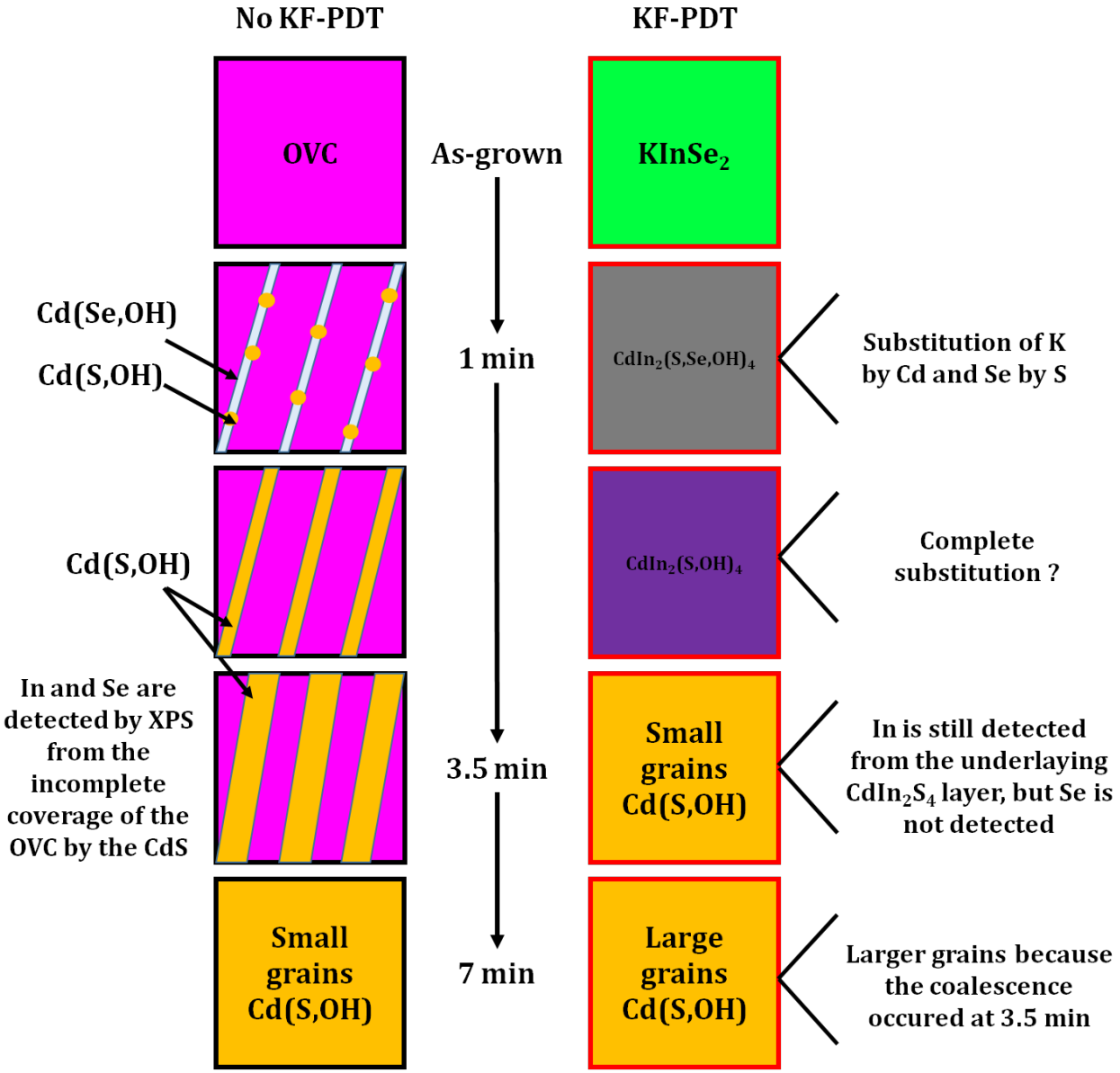

Figure 4-15 - Schematic plane view model of the CdS growth on untreated and KF-treated absorbers

Table 4.1 summarizes the important differences concerning the CdS growth found in these samples.

Table 4.1 - SEM and XPS principal results from the comparative study of the CdS growth on untretaed and KF-treated absorbers

	CIGS#1	CIGS#1(K)
CdS growth mechanisms	- Preferential (heterogeneous) on certain CIGS planes - Not fully covered after 3.5 min	- Homogeneous on non faceted surface - Fully covered after 3.5min
Morphology	- Small grains after 7min	- Large grains after 7min
Buffer material	- CdS	- interface compound: K/Se substitution by Cd/S, compound containing only In, Cd and S - CdS (No indium detected after 7min) - More oxygen detected

4.2.3 Structural properties of the CdS

CdS layers have been simultaneously grown by CBD (7 minutes) on CIGS#1 and CIGS#1(K). Figure 4-16 shows the Raman diffusion spectra of these samples. This technique does not reveal any structural changes since no shift or widening of the Raman peak corresponding to the CdS layer are found between the two investigated samples. If a new phase exists it is too thin or not sufficiently cristallized to be seen by the Raman scattering measurements. The Raman spectra normalized to the maximum intensity of the A1 mode are given in inset in Figure 4-16. As a result, structural changes induced by the KF-PDT (vanishing of the OVC) remain after the CdS deposition.

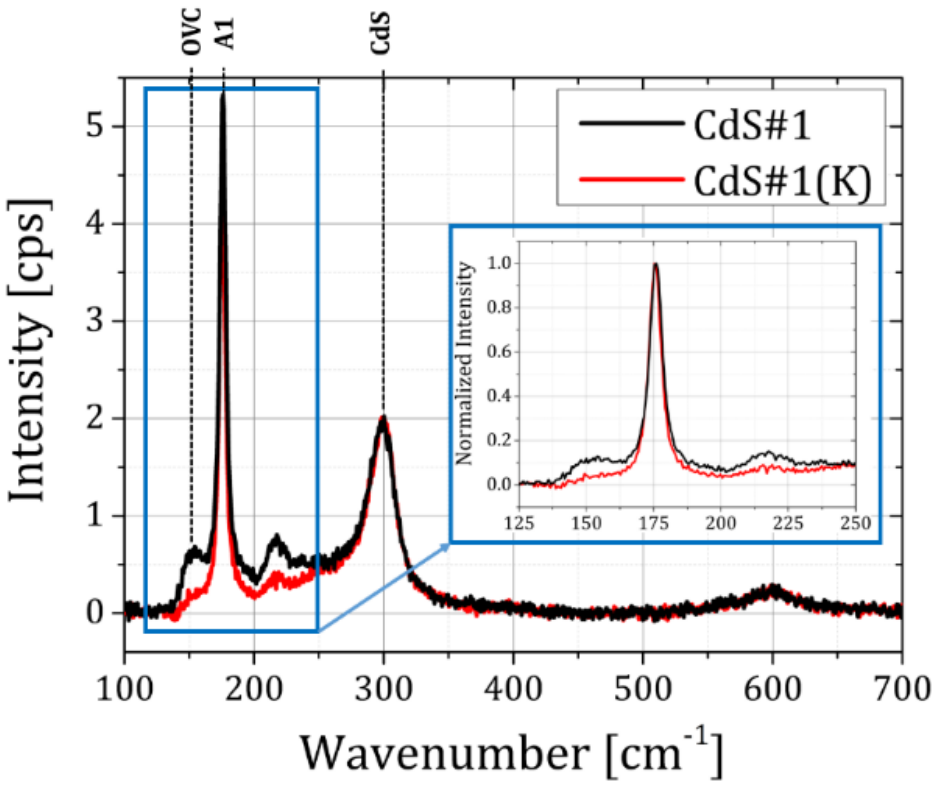

Figure 4-16 - Raman diffusion spectra of CIGS#1(K)/CdS (red) and CIGS#1/CdS (black) samples. Raman spectra normalized at the maximum intensity of the A1 mode are given in inset.

4.3 CdS grown on indium selenide

In the previous sections we evidenced the presence of a very thin interfacial layer in the KF-treated samples. The thickness of this layer, and the presence of the Mo/CIGS, make the study of the material and electrical properties of this layer very difficult. Ideally the study of such a material would require the growth of a thin film on glass in order to characterize the optical, structural and electrical properties independently of those of the CdS, CIGS and Mo layers.

It seems that the formation of this layer is due to the presence of the top material $KInSe_2$ induced by the KF-PDT of the absorber. XPS measurements show that most of the potassium leaves the structure during the chemical bath deposition. The result, after the deposition of the buffer layer, is the presence of a layer with a composition close to $CdIn_2(S,Se,OH)_4$. The question that arises is to know whether K has (i) a direct role in the formation of the layer, involving for instance ion exchange mechanisms, or (ii) an indirect role. In the latter case the role of K would be to help forming an indium selenide compound on top of the absorber that will react with the bath constituents and form the $CdIn_2(S,Se,OH)_4$ layer.

The purpose of this section is to address this question. Hence we have tried to reproduce the growth conditions of the (CBD)CdS on the KF-treated absorber surface but avoiding the CIGS layer. To do so we have co-evaporated a very thin indium selenide layer on SLG substrates (15 nm as measured by a profilometer, not shown). We then have deposited CdS layers by CBD in our standard conditions. The structural, optical and electrical properties of the material formed during this chemical bath deposition will be presented and discussed. As a first step we present a literature review on indium containing cadmium sulfoselenide.

4.3.1 Literature review

Indium-doped Cd(S,Se) refers in the literature to cadmium sulphoselenide containing up to 10% at of In. Such materials have been synthesized by several techniques including spray pyrolysis [174], co-evaporation of In and CdS [175], [176], thermal evaporation of In onto (CBD)CdS [177], thermal diffusion of In into single CdS crystal [178], pulsed laser deposition [179], [180] and pure solution-based growth (using In trichloride) [181], [182]. Electrical, optical and structural properties of these compounds are reported:

(a) *Electrical properties* - Although the properties of the films depend on the synthesis technique, all of these studies report an increase of several orders of magnitude of the n-type doping and conductivity of the film with increasing the In concentration. The carrier concentration in CdS:In has been shown to depend on the film thickness [182].

(b) *Optical properties* – The energy band gap in polycrystalline materials depends on many parameters such as the grain size or the properties of the GBs. Considering the diversity of the deposition techniques it is then not surprising that inconsistent tendencies have been reported for the variation of the optical band gap with the incorporation of In. In fact, the energy band gap of In-containing CdS is reported both to increase [176], [181] or decrease [177] with increasing the In concentration.

(c) *Structural properties* - Incorporation of In has been reported to increase the cristallinity of the material for low In concentrations [181] but it can also increase the structural disorder [179] or even result in amorphization for higher concentration [181].

$CdIn_2(S,Se)_4$ – This material cannot be considered as an "indium-doped Cd(S,Se)". It has been widely studied between 1970 and 1990. CIS/$CdIn_2S_4$ hetero-junction have already been synthesized since $CdIn_2S_4$ is a semiconductor with a n^+ type conductivity [170]. Lithium can be intercalated in $CdIn_2S_4$, making this material potential candidate in the development of batteries [183].

(a) *Optical properties* – An optical band gap of 1.95 eV has been reported for the $CdIn_2Se_2S_2$ [184]. According to Srivastava et al. [169], the band gaps of the $CdIn_2S_{4-x}Se_x$ ($1.75<x<2.75$) compounds are in the range 1.57-1.77 eV. Pure $CdIn_2S_4$ has been reported to have a band gap varying in the range 2.0-2.3 eV (see [185] and references therein)

(b) *Structural properties* - $CdIn_2S_4$ has been reported to crystalize in the cubic spinel structure Fd3m (JCPDS # 00-0027-0060). According to [169], layered materials $CdIn_2S_{4-x}Se_x$ ($1.75<x<2.75$) can also crystalize in the $ZnIn_2S_4$ structure with space group *R*3*m*. The unit cell consists of three slabs built from two layers of tetrahedra connected to a central layer of octahedra. The slabs are separated by a van der Waals gap.

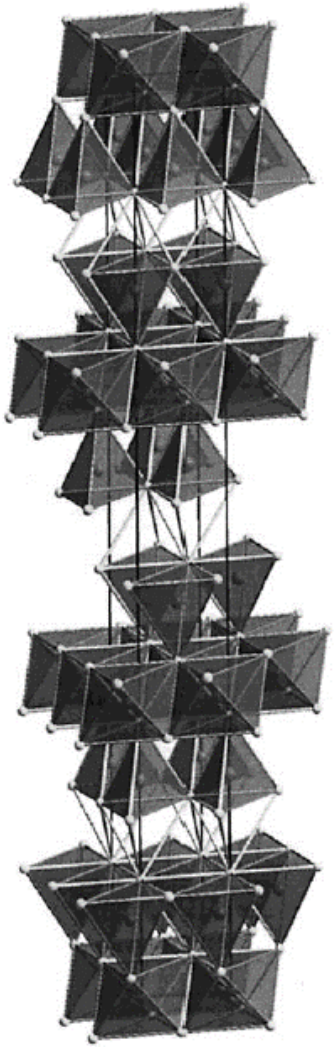

Figure 4-17 - Layer type ZnIn2S4 (IIIa) structure of the $CdIn_2S_{4-x}Se_x$ compounds, after [169]

(c) *Electrical properties* – A very high electron trap density ($\sim 10^{20} cm^{-3}$), as well as an important photoconductivity have been reported in $CdIn_2S_4$ single crystals [186].

4.3.2 Properties of the (CBD)CdS grown on indium selenide

In order to investigate the impact of the presence of indium selenide on the growth of the buffer layer, two samples have been synthesized. The first one, labeled "BufferA", will refer to a CdS thin film grown by CBD following our standard process (see Appendix C) on a clean SLG substrate. The second sample, labeled "BufferB", will refer to a CdS thin film grown in the same bath for the same duration but on a 15 nm-thick indium selenide In_xSe_y thin film co-evaporated at 350 °C on a clean SLG substrate. In this section we will compare the morphological, structural, optical and electrical properties of the BufferA and the BufferB.

Morphology – The thicknesses of the layers have been estimated by cross-section SEM micrographs depicted in Figure 4-18. The BufferA has the expected thickness of about 70 nm for the 7 minutes dipping duration following our CBD process whereas for the BufferB the estimated thickness is about 125 nm. This increase (+78%) is not simply due to the additional thickness of the indium selenide thin film (15 nm) and suggests that (i) the presence of the indium selenide thin film modifies the CdS growth kinetic and/or (ii) the deposited material is not "pure" CdS phase. The latter case includes the possibility of the synthesis of two separate phases, with one phase resulting from the reaction between the indium selenide with the bath and another constituted of pure CdS. The inset in Figure 4-18 shows the cross-section of the BufferB recorded at lower magnification. It suggests the presence of two layers (1) and (2), supporting the hypothesis (ii) that two separate materials are formed during the CBD.

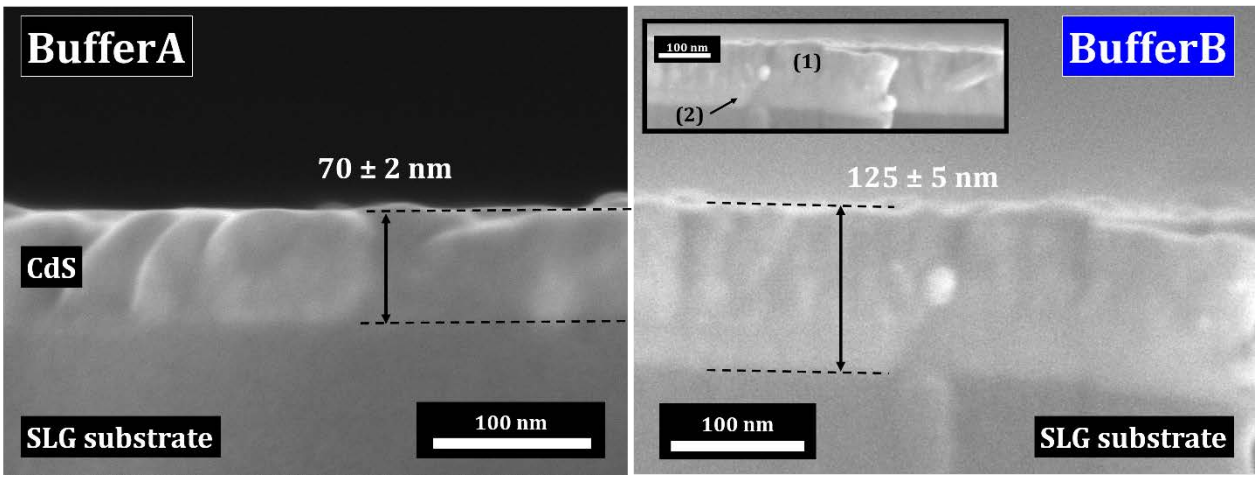

Figure 4-18 - SEM micrographs of the BufferA ((CBD)CdS on SLG substrates) and the BufferB ((CBD)CdS on SLG/In_xSe_y) cross-sections. A micrograph recorded at lower magnification for the BufferB is given in inset.

Structural properties - The SEM cross section views of these samples tend to show a bilayer structured BufferB (total thickness of 125 nm), whereas BufferA looks like standard narrow grained (CBD)CdS. This observation arises several questions concerning the BufferB:

(a) Does the (CBD) deposited CdS effectively react with the indium selenide thin layer? If yes, what is the resulting material?

(b) Is the new material more stable than the CdS? This can also be formulated as: do the In atoms diffuse throughout the whole CdS layer or are they "trapped" within the 'new phase', which can be assumed as to constitute the interface layer detected at the CIGS(K)/(CBD)CdS hetero-junction?

In order to answer these questions, the BufferA and the BufferB have been investigated by X-Ray diffraction in the regular Bragg-Brentano configuration. Figure 4-19 plots the XRD diagrams of both BufferA and BufferB, that are (CBD)CdS deposited on SLG and on SLG/In_xSe_y, respectively. As additional information, the angle positions of $CdIn_2S_4$ spinel phase lines are also represented[12]. From this figure, one can clearly observe that the presence of the In_xSe_y layer strongly impacts the crystalline characteristics of the resulting buffer. Indeed, if the (CBD)CdS appears amorphous (for the standard XRD studies), that grown onto the even very thin In_xSe_y shows much larger grains (longer coherence length). The lines do not correspond to In_xSe_y. They do fit rather well with those of $CdIn_2S_4$, although they are shifted toward shorter angles, denoting larger lattice parameters, whatever the crystal inter-planes. This latter observation is consistent with the presence of both Se and S within the layers.

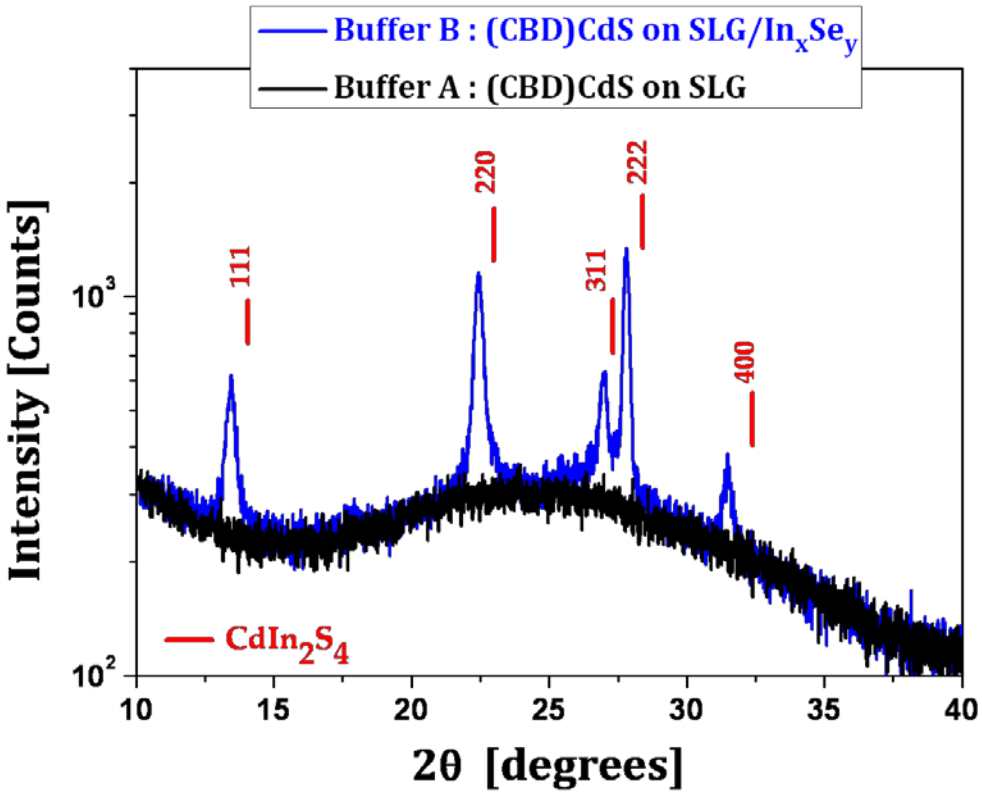

Figure 4-19 - XRD patterns (Bragg-Brentano configuration) of the BufferA and the BufferB. Positions of the relevant lines of the $CdIn_2S_4$ are dispayed in red

Although the above mentioned layers grown by CBD are the closest to the actual phases formed at the CIGS(K)/CdS interface, it appears relevant to check whether the bilayered structure evidenced by the SEM corresponds to two different materials. With this aim, CdS has also been evaporated onto the same SLG/In_xSe_y and bare SLG, and will be referenced to as BufferB' and BufferA', respectively. The XRD patterns shown in Figure 4-20 highlight the presence of both $CdIn_2S_4$-like and CdS lines for the BufferB'. This observation corroborates the co-existence of the two phases. From these spectra, it has not been possible to discriminate if the CdS phase was cubic or hexagonal.

[12] Lines of the spinel $CdIn_2S_4$ are extracted from the JCPDS #27-0060

In the BufferB', the (111)-cubic CdS (and thus (002)-hexagonal CdS) XRD peak is wider than the one in the BufferA'. However, this widening originates from the presence of the (311) reflexion of the $CdIn_2S_4$ at 27.25 ± 0.05°. The CdS peak in the BufferA' and the BufferB' might then be similar. As a shift of the XRD peaks is detectable if the composition changes in the range of the percent, we suggest that the indium content in the CdS is very low (or even null). The indium of the $CdIn_2S_4$-like phase seems not to diffuse in the CdS, suggesting that the $CdIn_2S_4$-like phase is stable.

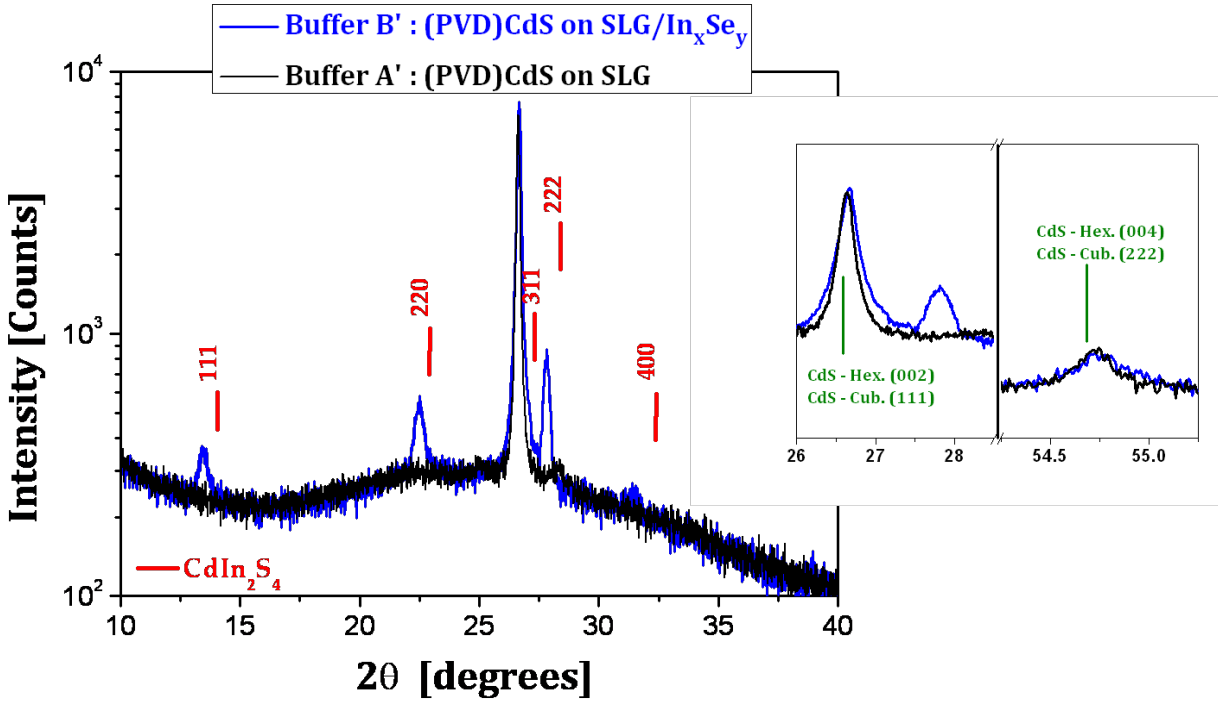

Figure 4-20 - XRD patterns (Bragg-Brentano configuration) of the BufferA' and the BufferB'. Positions of the relevant lines of the $CdIn_2S_4$ are dispayed in red. Zooms on the angular position of peaks related to the CdS are given in inset.

We have performed Raman scattering measurements on the BufferA and the BufferB, using a 532 nm wavelength excitation (see section 3.2 for the detailed setup). Figure 4-21 shows the Raman spectra of the BufferA and the BufferB. One can see that the intensity of the CdS Longitudinal Optical (LO) peak at 300 and 600 cm^{-1} are increased in the BufferB compared to those in the BufferA. The width of the LO peaks, as well as the ratio between LO1 (peak at 300 cm^{-1}) and LO2 (peak at 600 cm^{-1}), are similar in both samples, suggesting that the size of the grains is equivalent in the BufferA and the BufferB. The increase of the intensity of the LO peaks in the BufferB could therefore originate from a variation of the band gap E_g of the CdS in this sample. If E_g is close to the energy of the laser (about 2.3 eV for the 532 nm wavelength excitation) then a Raman resonance scattering can occur.

The BufferB exhibits at least two additional Raman peaks at about 150 cm^{-1} and 250 cm^{-1}. This confirms the presence of a secondary phase within the BufferB layer. These Raman peaks at 150cm^{-1} and 250 cm^{-1} are a signature of the In-Se bonds vibration [187]. It could mean that the In_xSe_y thin film deposited on the SLG (prior the CBD) has not comptetly reacted with the bath constituents and some of the InxSey was still present within the final BufferB layer. However, in this case, the XRD pattern of the BufferB should exhibit the peaks corresponding to the In_xSe_y. They are not observed. Hence, we suggest that these In-Se bonds originate from the $CdIn_4S_4$-like material evidenced by XRD measurements. The material should contain Se and it will be refered to $CdIn_2(S,Se)_4$ in the following.

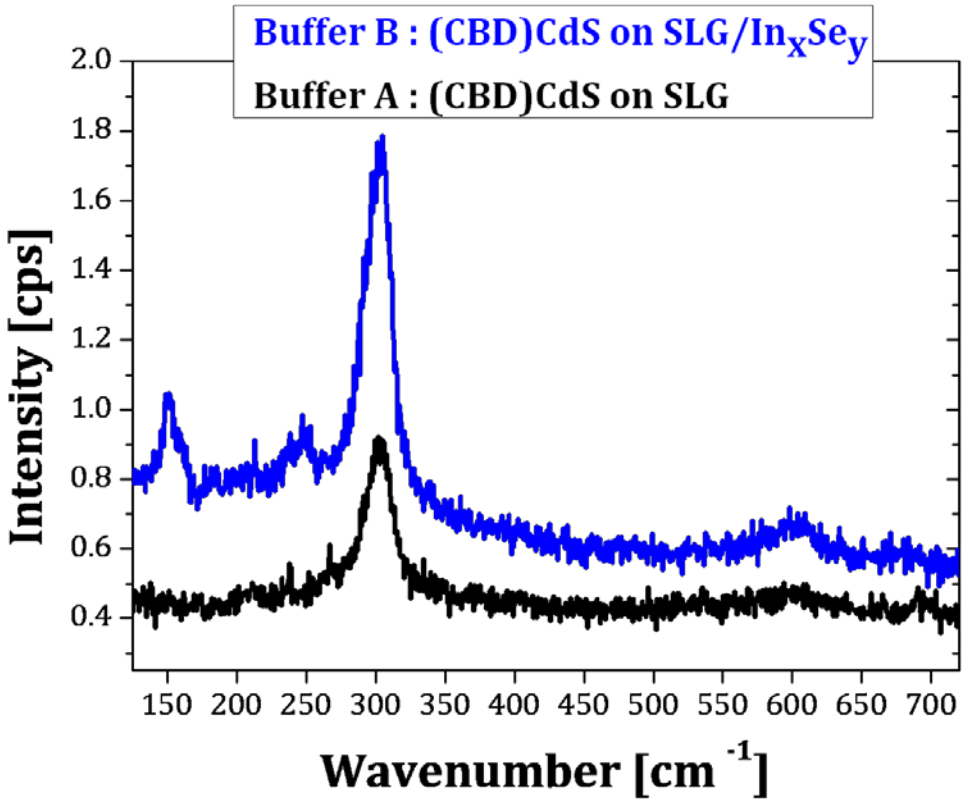

Figure 4-21 - Raman spectra of the BufferA and the BufferB

Optical properties – The optical properties of the thin films have been determined from specular $R(\lambda)$ (near normal incidence) and specular $T(\lambda)$ (normal incidence) measurements performed in the spectral range 350–1500 nm using a Perkin-elmer LAMBDA 1050 spectrophotometer. From these data, the refractive index (n), the extinction coefficient (k) and the thickness (d) have been determined using the "Fresnel coefficient method". This method consists in writing R and T of a single film[13] on a thick substrate surrounded by air as a function of the Fresnel coefficients r_{ij} (reflection between media i and j) and t_{ij} (transmission from i to j). An algorithm minimizes the Root Mean Square (RMS) error between the experimental and fitted data. This calculation at each wavelength provides the complex refractive index $N_f=n_f+ik_f$ and the thickness d_f of the thin film. The contribution of the glass substrates has been subtracted according to [188]. Furthermore, in order to improve the accuracy of the results, as the light is scattered by rough interfaces, the influence of the film surface roughness (σ) has also been accounted through the use of scalar scattering theory. A correction factor containing the RMS roughness between the air and the film is introduced. From $k_f(\lambda)$ the wavelength dependence of the absorption coefficient α_f has been calculated through the relation $\alpha_f=4\pi k_f/\lambda$.

[13] The BufferB could be composed of two separate layers. Considering the thicknesses of each layers we preferred to use a simple model consisting of one single layer instead of a more complicated multi-layer model. With this method, we minimize the fit errors on the n(λ) and k(λ) parameters. However, the possibility of a multiple layer stack for the BufferB will be taken into account during the interpretation of the results.

Figure 4-22 shows the absorption coefficient α_f of the BufferA and the BufferB. A well defined absorption edge is found in the BufferA at 2.40 ± 0.05 eV, corresponding to the well known CdS optical band gap. On the other hand, the BufferB exhibits three different absorbtion edges at 1.60 ± 0.05 eV, 1.90 ± 0.05 eV and 2.30 ± 0.05 eV, respectively[14]. The presence of several absorption edges corroborates the presence of different materials in the BufferB, as suggested by SEM, XRD and Raman scattering characterizations. Attributing these absorption edges to specific compounds is not straightforward. Indeed, according to Mane *et al.* [189], increasing the Se content z in $CdS_{1-z}Se_z$ from z=0 (pure CdS) to z=1 (pure CdSe) decreases the band gap from 2.5 to 1.8 eV. Furthermore, it has been reported in section 4.3.1 that the band gap of $CdIn_2S_{4-x}Se_x$ can lie from 2.30 to 1.57 eV by varying x from 2.75 to 0 (pure $CdIn_2S_4$). However, the XRD and Raman characterizations have revealed the presence of CdS in the BufferB. Therefore, the 2.3 eV absorption edge is attributed to the band gap of the CdS. The lowering of this CdS band gap in the BufferB compared to that in the BufferA could result from the incorporation of small amounts of either In or Se into the CdS. These elements, or crystalline defects induced by the presence of In_xSe_y substrate, could act as dopants and introduce shallow electronic defects, which would reduce the optical band gap. The 2.3 eV CdS band gap value in the BufferB explains the higher intensities of the LO peaks in the Raman spectrum (excited with a 532 nm laser) of this layer compared to those of the BufferA. In conclusion, the optical measurements do not contradict the suggested model of a bilayer structured BufferB composed of two different materials. For the BufferB, the absorption edge at 2.3 eV can be attributed to a modified CdS and additional absorption edges could correspond to the $CdIn_2(S,Se)_4$.

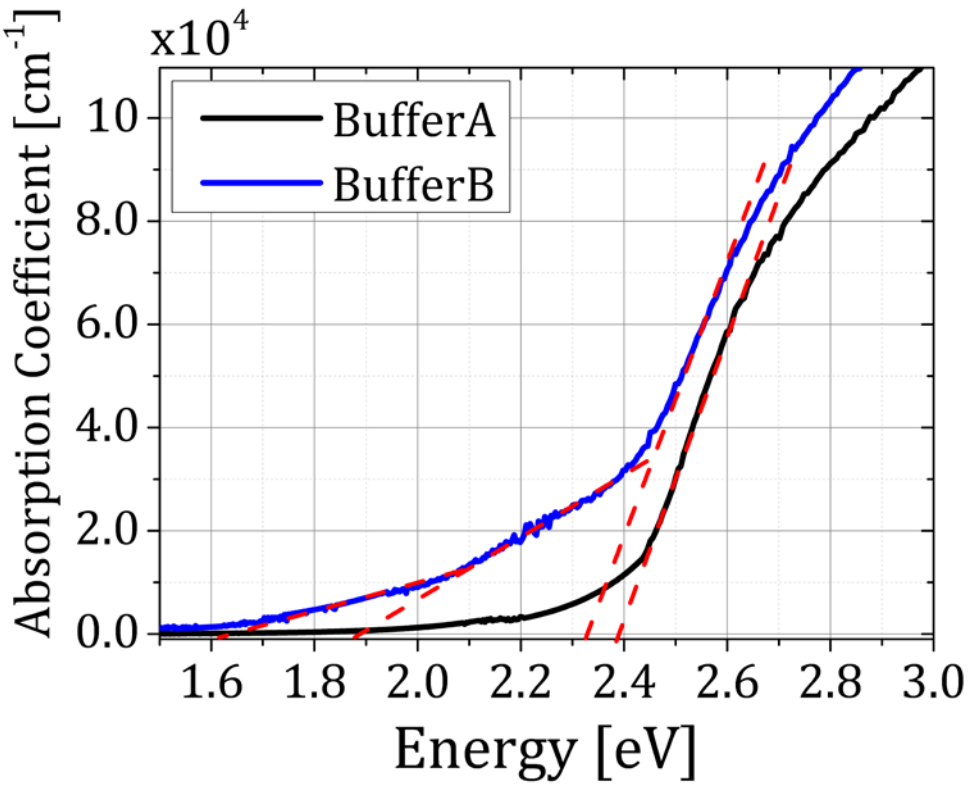

Figure 4-22 - Absorption coefficient versus photon energy in the BufferA and the BufferB

[14] In the BufferA, the absorption edge is not abrupt due to the presence of a band tail, typically found in (CBD)CdS thin films. Such a band tail is likely present in the BufferB and could correspond to the first slope of the absorption coefficeient (at 1.6 eV) of this layer.

Electrical properties – Figure 4-23 shows the I-V responses of the BufferA and the BufferB in dark and under AM1.5 illumination. These curves exhibit an ohmic behavior and it has been possible to extract the corresponding resistance of the samples from the slopes of the JV curves. Considering the geometry of the contacts given in inset of this figure, we have calculated the global resistivity (and thus the conductivity) of these samples.

In both BufferA and BufferB, the materials show a high photosensitivity as the conductivity is increased by two orders of magnitude when the samples are illuminated. For BufferB the conductivity is higher by three orders of magnitude (both in dark and under illumination) than for BufferA. This increase of the conductivity can originate from to the presence of a n^+ semiconducting layer[15] below the CdS.

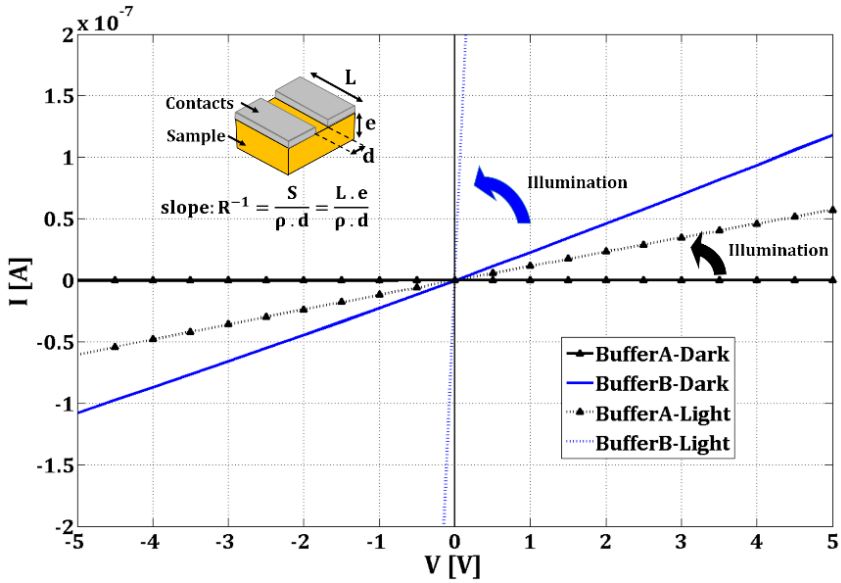

Resistivity ρ [Ω.m]

Sample	Dark	Light
BufferA	2.00 10^4	38.1
BufferB	1.50 10^2	1.20

Conductivity $\sigma = \frac{1}{\rho}$ [S]

Sample	Dark	Light
BufferA	4.99 10^{-5}	2.63 10^{-3}
BufferB	6.66 10^{-2}	0.83

Figure 4-23 - I-V measurments of buffer layers grown on SLG and SLG/In_xSe_y substrates. Tables on the right give the corresponding resistivity and conductivity extratacted from these curves considering the geometry of samples given in inset

4.3.3 Summary

We have shown that the presence of indium selenide on the substrate modifies the (CBD)CdS growth. A new crystalline phase is formed during the CBD, resulting in a bilayer structure composed of this new phase with CdS on top of it. We have highlighted that this bilayer structure has a lower band gap and a higher conductivity than those of the pure CdS. These properties are consistent with the XRD characterizations, which show that the new material below the CdS is likely a $CdIn_2S_4$-like spinel. This new structure is stable enough to not mix with the CdS. As the the $CdIn_2S_4$ has been reported to have a n^+ type conductivity, the presence of such a layer between the CIGS and the CdS in the device would have important effects on the electrical behaviour of the hetero-junction and will be discussed in the next chapter.

[15] In this thesis, a n^+ conductivity will refer to a high n-type conductivity ($n \sim 10^{18}$ - 10^{19} cm^{-3}). In particular it will not refer to degenerated semiconductors ($n > 10^{20}$ cm-3)

4.4 Hetero-junction formation

In this section we intend to firstly formalize the chemical reactions that occur between the surface materials of the absorber (from case#1) with the ions contained in the bath used for the deposition of the buffer layer. We will then propose a growth model for the CdS for both KF-treated or untreated cases.

4.4.1 Reaction with the top surface material

In the following, we will consider a complete substitution of K by Cd and Se by S although, in practice, these substitutions may only be partial, as Chirilă *et al.* [126] still detect K by XPS at the absorber/buffer interface after CdS deposition. Moreover, our TEM study has revealed the presence of Se in the interface layer in complete devices. The Se^0 resulting from KF-PDT at the surface might either react or be removed in the bath as such a specie is not detected after one minute by XPS. A reaction with Cd to form CdSe might occur but this is not taken into account in the following:

K/Cd Ionic exchange $$2\,KInSe_2 + Cd^{2+} \rightarrow CdIn_2Se_4 + 2\,K^+ \quad (4.1)$$

Chalcogene substitution $$CdIn_2Se_4 + 4\,S^{2-} + 4\,Cd^{2+} \rightarrow CdIn_2S_4 + 4\,CdSe \quad (4.2)$$

Formation of KOH $$K^+ + OH^- \rightarrow KOH \quad (4.3)$$

Finally $$2\,KInSe_2 + 4\,S^{2-} + 5Cd^{2+} + 2OH^- \rightarrow CdIn_2S_4 + 2\,KOH + 4\,CdSe \quad (4.4)$$

4.4.2 Model of the buffer layer growth

Figure 4-24 depicts a schematic view of the suggested growth mechanisms involved during the chemical bath deposition of the buffer layer onto the untreated and the KF-treated absorbers. We assume the presence of the suggested adamentane-like $KInSe_2$ layer on top of KF-treated absorbers.

Start – On the KF-treated absorbers a substitution of K by Cd and Se by S occurs in the top surface adamentane material, resulting in K and Se ions released at the surface. The latters will react with Cd ions to form CdSe as evidenced by TEM. The presence of K at the outermost surface catalyses the oxidation of this surface, which helps the formation of CdS. Indeed, it has been postulated [190] that $Cd(OH)_2$ precipitates on the CIGS surface as a first step of the heterogeneous nucleation leading to the formation of CdS by subsequent sulfurization. Simple columnar growth model has been proposed in this case [191] in order to describe the growth of these forming islands up to the coalescence. The adamentane structure shows surface termination planes with more chalcogenide available to bond with the Cd. Finally, both the higher amount of chalcogenes and hydroxides at the surface of the treated absorber explains the more homogeneous growth of the CdS evidenced by the SEM and the XPS measurements.

On the untreated CIGS surfaces, CdS starts to grow on certain planes only, depending on their polarity and the availability of Se or hydroxide to form Cd-Se or Cd-OH bonds.

CdS growth – From these starting points the CdS nuclei can grow. On untreated absorbers the limited number of nucleation sites also limits the size of the nuclei. After 3.5 min in the bath, this results in a partially and fully covered surface by CdS on the untreated and the treated surface, respectively. Finally, at the end of the deposition, the CdS grains are larger on the treated absorbers, as it is shown by the SEM observations. The presence of K at the surface of the growing CdS (see XPS measurements) implies a more hydroxidized CdS layer in case of KF-treated absorbers.

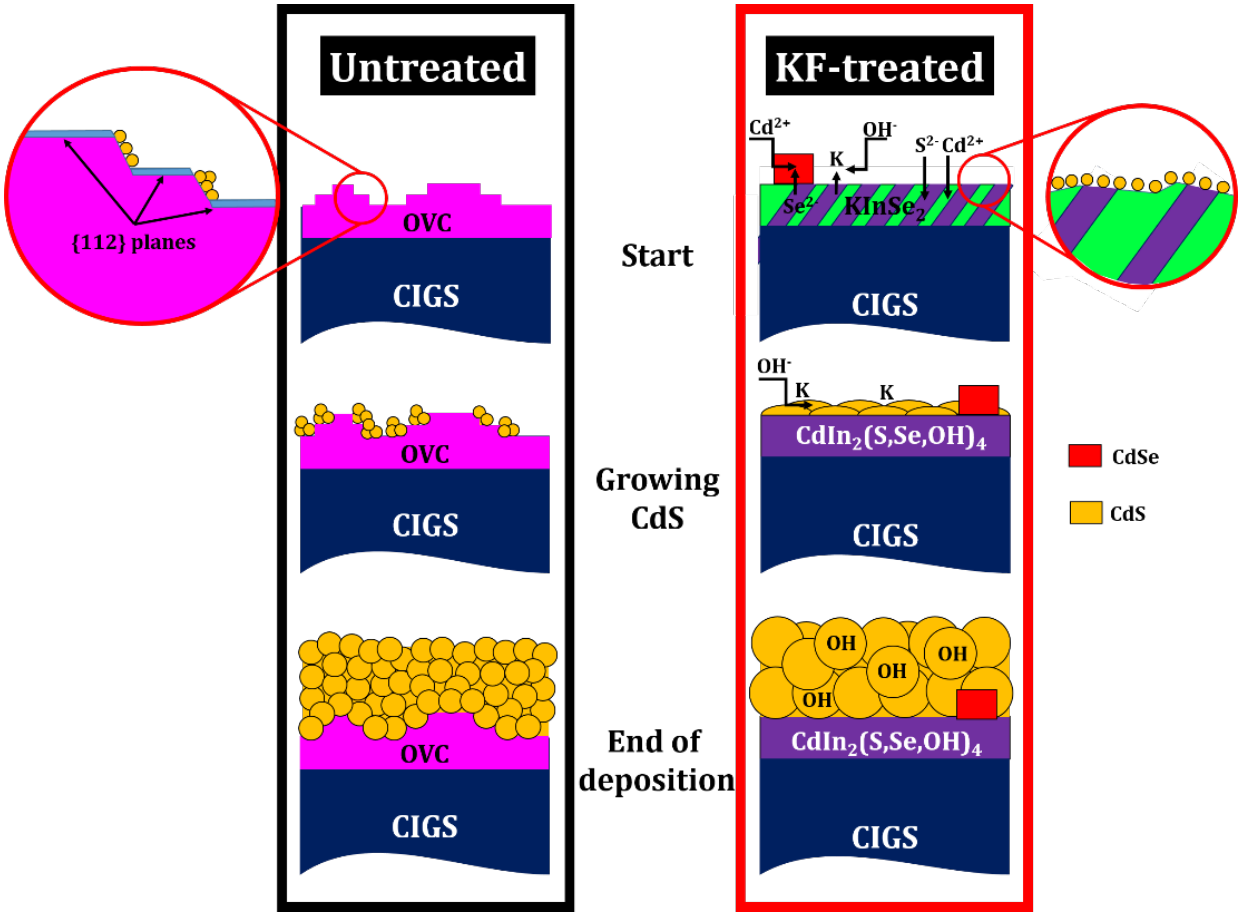

Figure 4-24 – Model of the buffer layer growth in the chemical bath onto untreated or KF-treated absorbers

4.4.3 Discussion

CdS thickness - For CBD durations of 3.5 min, the KF-treated and the untreated absorbers show different CdS coverage. For these two samples (CIGS#1(K,B3.5) and CIGS#1(B3.5)) different growth mechanisms have been proposed explaining the different CdS coverage. However, TEM cross-sections show that after 5 minutes the thickness of the CdS layers is similar in both cases. Hence, at least for short deposition duration, the CdS growth mechanisms are different but the resulting thicknesses are similar.

Interface layer - The most important effect resulting from the KF-PDT is the presence of a thin interfacial layer between the non-modified CIGS and the CdS. We suggest the nature of this layer to be $CdIn_2S_4$-like spinel phase, resulting during the CBD from the substitution of K/Se by Cd/S in the postulated adamentane-like $KInSe_2$ material (formed during the KF-PDT). We have demonstrated that the (CBD)CdS layer growth on an indium selenide thin layer results in a bilayer structure composed of such a $CdIn_2S_4$-like phase and CdS. The investigation of the properties of this bilayer structure have revealed a higher conductivity and a lower band gap than those of pure (CBD)CdS.

Role of the K – We suggest that the formation of the bilayer structure $CdIn_2S_4$-like phase/CdS on SLG/In_xSe_y is representative to what occurs on KF-treated absorbers. The role of K in the formation of the thin $CdIn_2S_4$-like phase layer between CIGS and CdS device might then be indirect. Indeed, it was possible to grow this material on indium selenide without any K added intentionally. Therefore one could suggest that the K creates the favourable conditions for the growth of this material during the chemical bath deposition of the buffer. K would repel copper from the surface by forming a $KInSe_2$ layer. During the CBD it leaves the structure, rendering the In available to react with the ions in the bath to form the $CdIn_2S_4$-like material. Finally, we have modelled the formation of the $CdIn_2S_4$-like material by the substitution of K by Cd and Se by S in the $KInSe_2$. It might mean that K enhances (or facilitates) the formation of the $CdIn_2S_4$-like material. However we suggest that this $CdIn_2S_4$-like material should also be formed if an indium selenide compound could exist at the surface of the CIGS (without Cu migrating at the surface) without the presence of the K.

PART II – CIGS/CIGS homo-interfaces

In chapter 4 we have shown that the KF-PDT leads to the formation of a thin $KInSe_2$ layer at the surface of the absorber. K has been shown to segregate at GBs (see section 2.2), and therefore the question is whether $KInSe_2$ phase is also formed at these GBs. Moreover, we have shown in the previous part of this chapter that $KInSe_2$ reacts with the constituents of the chemical bath to form an n^+-type $CdIn_2S_4$-like phase layer. Cd diffuses into the absorber preferentially through the GBs (see section 1.4.2) and this diffusion is enhanced by the KF-PDT (see section 4.2.1). Hence, one can question whether such $CdIn_2S_4$-like n^+ material could also be formed at the GBs and change their electronic properties.

The purpose of this present part II is to investigate the composition of the GBs in Cell#1(K). If the chemical bath has an influence on such defective surfaces, then it should be restricted to the near CIGS/CdS interface region where Cd and/or S can diffuse (see section 4.2.1). Therefore, two GBs will be investigated:

(i) *GB close to the CIGS/CdS interface* (<100nm from the CIGS/CdS/interface). The composition will be addressed by the use of EDS mapping in a TEM.

(ii) *GB located deeper in the bulk* (>100nm from the CIGS/CdS/interface). The composition will be addressed by the use of Atomic Probe Tomography (APT) measurements[16].

4.5 K-induced material changes at the grain boundaries in the near CIGS/CdS interface region

Depletions - Figure 4-25 shows the EDS mapping of the Cu, In, Ga, Se, Cd, S, K and O elements in the near-surface region of Cell#1(K). One can notice that the CdS is present at the top of this region. We focus our interest on the GB between the two highlighted CIGS grains. One can clearly see a Ga depletion at the GB whereas no In enrichement or depletion can be detected[17]. Even in the CdS region the In signal is still higher than those of Ga, Cu or Se. This confirms the presence of an indium-containing CdS material at the interface between the CIGS and the CdS. Finally, the mapping suggests a slight Cu and Se depletion at the GB.

Presence of K at GBs - We have already discussed the artefacts that could lead to the misunderstanding of the EDS K mapping. In fact, the mapping of K in Figure 4-25 corresponds in reality to that of In. However, if K was present in sufficient amount the mapping would show a strengthening of the signal where K segregates. Figure 4-25 does not reveal any K segregation at the GB close to the surface. However, the GB investigated in Figure 4-25 is very close to the CIGS surface. Therefore, K might have segregated at this GB but could have been removed during the chemical bath deposition due to the proximity to the surface. For this reason we further investigate another GB located deeper in the bulk.

[16] It was not possible to study the GB (i) close to the CIGS/CdS interface with this technique because in this case the "needle" APT sample has to contain both CIGS and CdS. These two different materials do not need the same electric field to evaporate and most of the time the sample is broken during the analysis.
[17] Contrary to superposition of K signal with Cd and In, energy range chosen for In and Cd mapping are well separated (Cd Kα : 23.029 – 23.319 keV, In Kα : 24.062 – 24.358 keV)

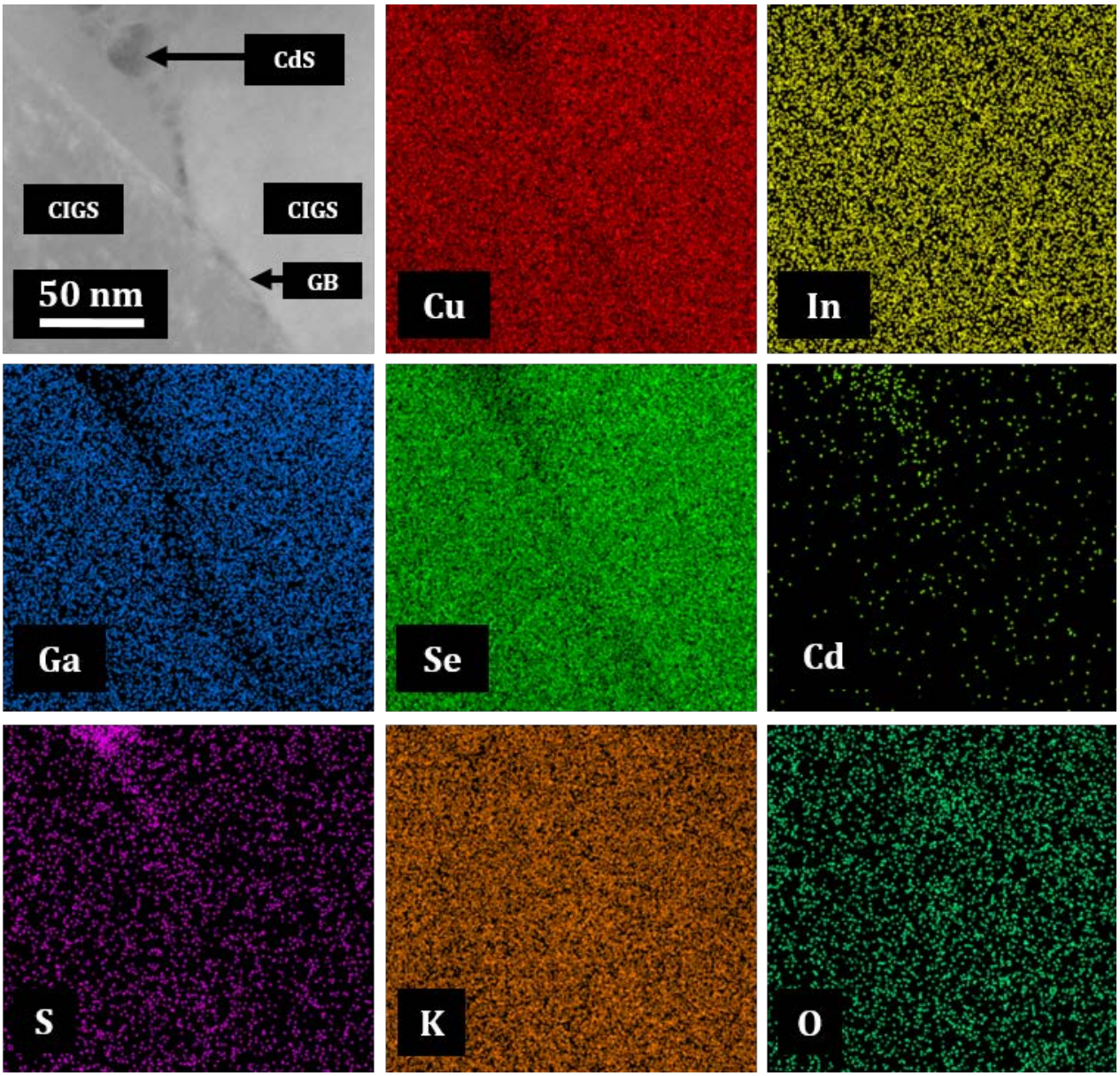

Figure 4-25 - EDS mapping of different elements in the vicinity of a GB close to the absorber surface in CIGS#1(K)

Figure 4-26 shows the EDS K mapping of such a GB. In this case, the mapping shows strengthenings of the signal, suggesting a segregation of K at the GB and at the interface; profiles along these two regions are given. However we also show the EDS mapping of the addition of Cd and In signals. One can clearly see an overlapping of the signal of In and Cd at the interface that could originate from the indium-containing CdS layer. We also plot the superposition of Zn and S signals showing another overlapping at the CdS/ZnO interface. This means that the interface was not perfectly oriented parallel to the TEM optical axis. We cannot conclude on the presence of K at the CIGS/CdS interface after the completion of the device. However, there is no doubt on the presence of K at the GBs (profile#2), at least deep in the bulk (80-100 nm from the CIGS surface in this particular case) as in this area there is no strengthening of the Cd+In signal.

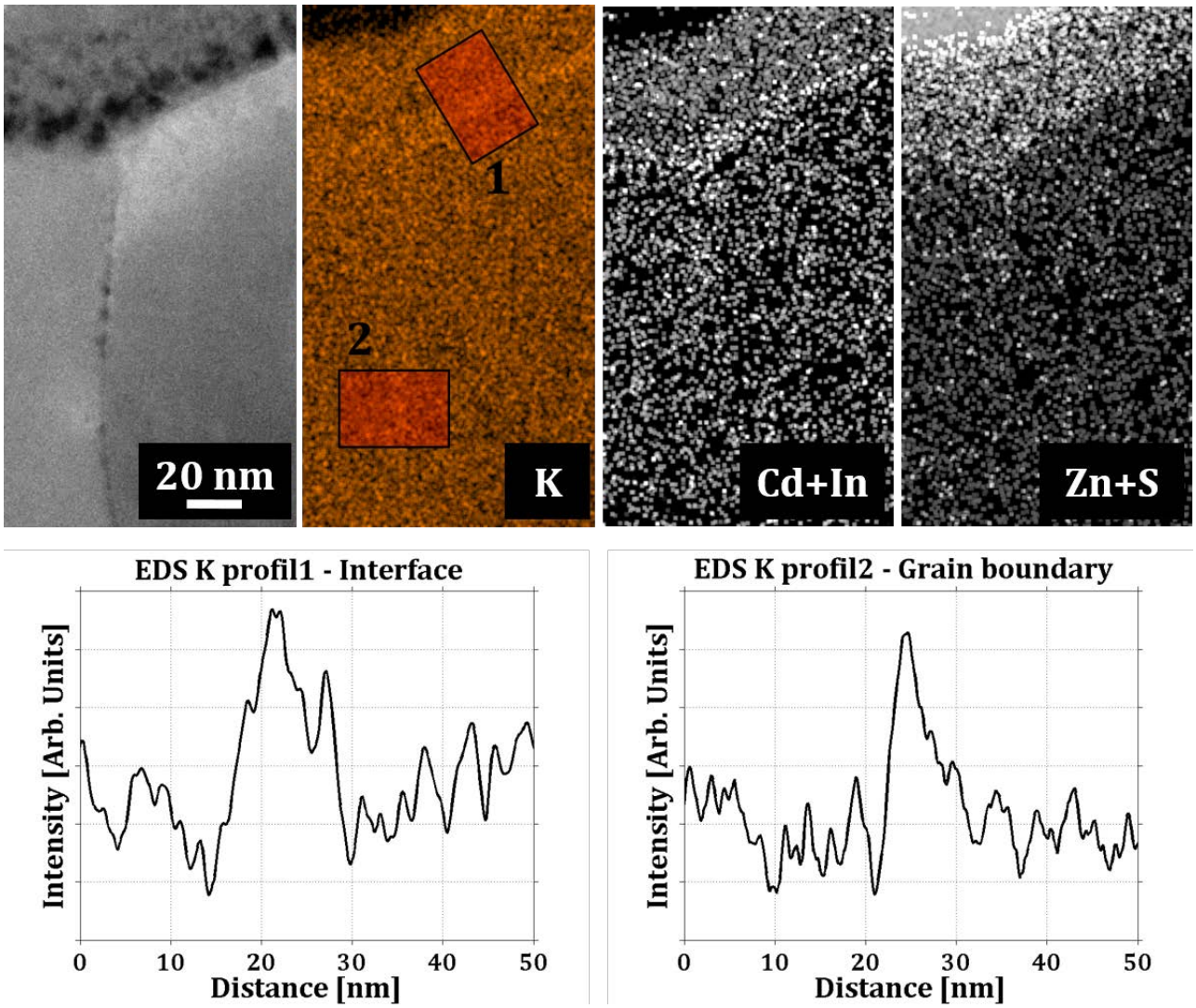

Figure 4-26 – Segregation of K in Cell#1(K), profiles at the interface and at a GB extracted from EDS mapping.

4.6 K-induced material changes at grain boundaries deep in the absorber

The EDS resolution in TEM was not sufficient in order to properly investigate the composition of the GBs. Furthermore, a strong interaction between these regions and the electron beam deteriorates the KF-treated samples. We have then decided to address the chemical study of the GBs with the help of APT measurements performed by E. Cadel at the "Groupe de Physique des Matériaux" at Université de Rouen. APT samples were prepared from complete devices from Run#1 in a Zeiss NVision 40 CrossBeam FIB using a lift out method [192]. APT investigations have been carried out at 50K using a CAMECA laser assisted wide angle tomographic atom probe (LaWaTAP). For more details about the setup and the analytical treatments performed on the recorded mass spectra in order to identify the different elements present in the samples one should refer to Ref[106] and references therein.

Figure 4-27 shows the typical 3D distribution mappings resulting from these APT analyses in Cell#1(K) in a region burried 300-400nm below the CIGS/CdS interface. Corresponding profiles for Cu, In, Ga, Se as well as for K and Na atoms are given across a GB. Results clearly highlight an important 5%at segregation of K at this GB. The amount of K is even higher than that of Na. As far as the CIGS constituents are concerned, APT measurements reveal that KF-PDT induces a strong Cu depletion and a slight Se enrichment. In that case we do not evidence Ga depletion probably because the GB is too far from the surface and fluorine could not react with Ga. The most important result concerns the In profile. As In enrichment is generally observed at GBs in CIGS [193] it is very surprising that such an enrichment is not observed after the KF-PDT.

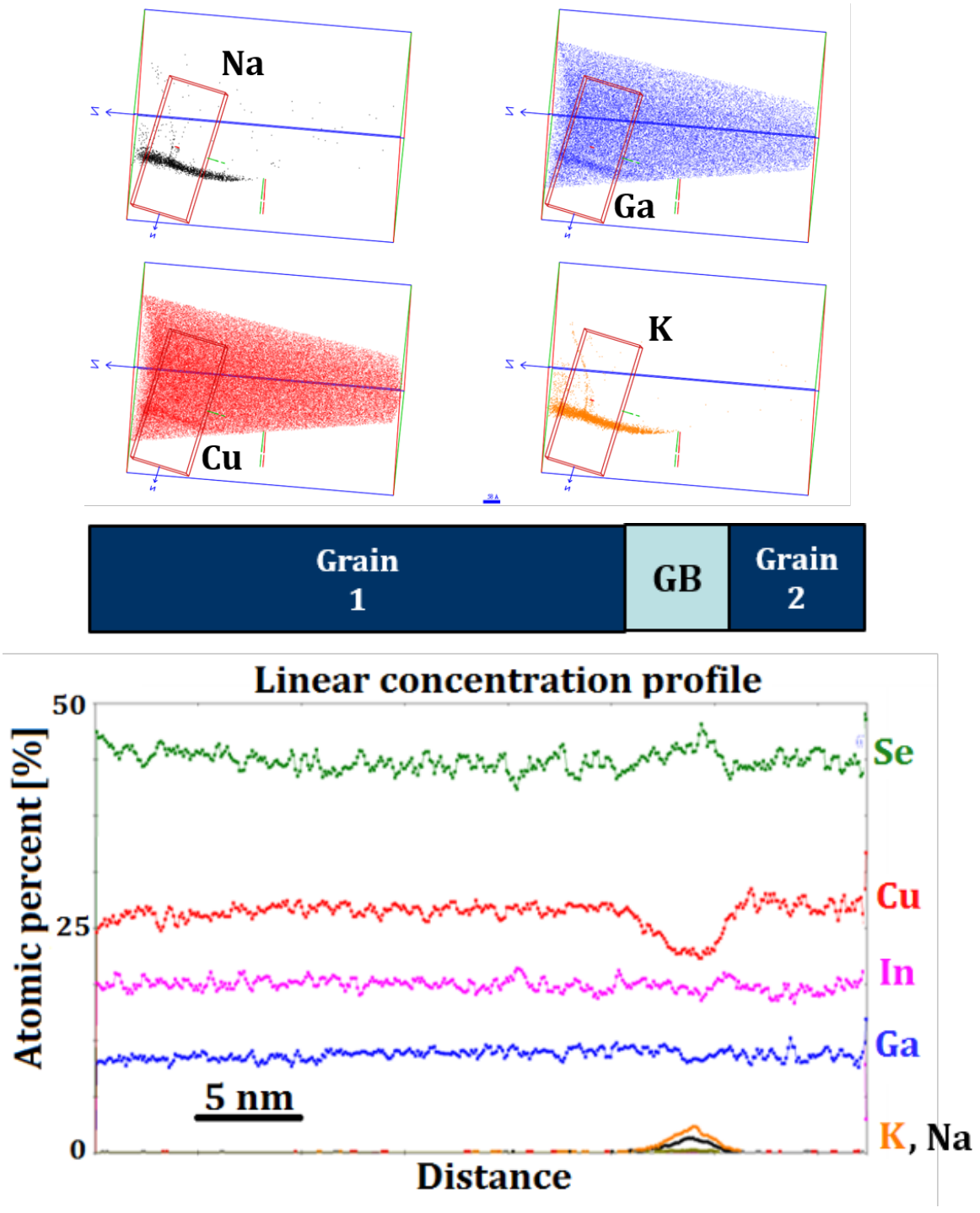

Figure 4-27 – Segregation of K in Cell#1(K), profiles at the interface and at a GB extracted from EDS mapping.

4.7 Summary of the chapter

Interfaces - In this chapter, two kinds of interfaces have been investigated in complete solar cells. Compared to the reference devices (not treated with KF), the KF-treated solar cells exhibit the following differences:

(1) *The CIGS/CdS interface* – We have evidenced by TEM the presence of a thin 5 nm-thick interface layer between the CIGS and the CdS. HAADF contrast suggests that this layer has a low density. EDS measurements suggest the nature of this layer to be $CdIn_2(S,Se,OH)_4$. This layer induces a high crystalline coherence of the buffer layer. A high amount of oxygen is found both at the interface and in the buffer layer. We have highlighted the segregation of CdSe regularly distributed along the interface.

(2) *The CIGS/CIGS interfaces* – We have evidenced that K segregates at the GBs located deeper than few tens of nm. These GBs show an important Cu depletion but surprisingly no In enrichement. The GBs located close to the CIGS/CdS interface exhibit an additional Ga depletion probably due to the reaction with F during the KF-PDT.

Properties of the interface layer – We have reproduced the synthesis of the interface layer material avoiding the presence of K. To do so we have grown CdS onto an indium selenide thin film. It has resulted in a $CdIn_2S_4$-like material/CdS bilayer structure. In this structure, the CdS properties are comparable to those of CdS grown on SLG. This bilayer structure exhibit a high photoconductivity and has a lower band gap than the CdS. As $CdIn_2S_4$ has been reported to have an n^+ type conductivity in the literature, the presence of such a thin layer between the CIGS and the CdS in real device should have important effects on the electrical transport. This will be discussed in chapter 5.

Buffer layer growth - In this chapter we have also studied the buffer layer ((CBD)CdS) growth mechanisms on both KF-treated and untreated absorbers. The presence of a surface layer $KInSe_2$, induced by the KF-PDT (evidenced in the chapter 3), induces a much more homogeneous growth of the buffer layer. The full coverage of the absorber surface is reached sooner than on the untreated surfaces, resulting in larger CdS grains. Finally the suggested models of the hetero-junction structures in both cases are depicted in Figure 4-28. The n-type buffer in KF-treated devices is composed of a $CdIn_2S_4$-like material/CdS bilayer. No OVC is present in KF-treated devices.

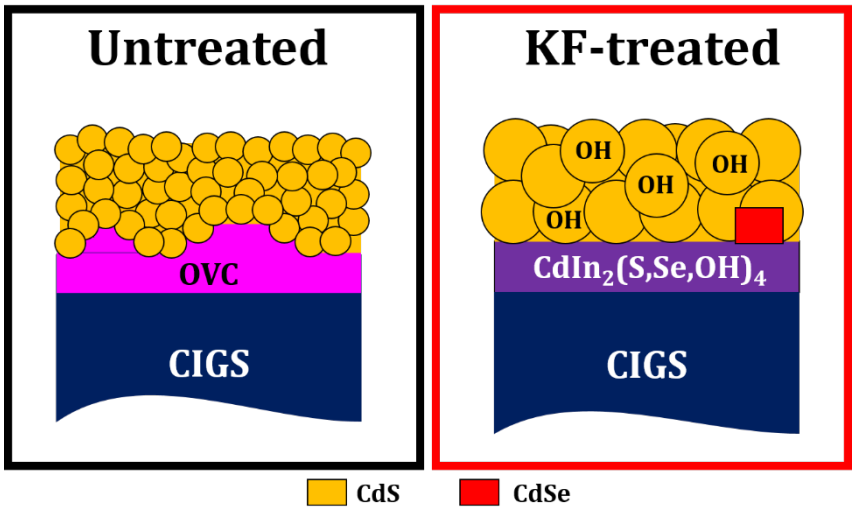

Figure 4-28 - Model of the hetero-junction in KF-treated (red, right) and untreated (black, left) devices

Chapter 5
Impact of the material changes induced by the KF-PDT on the opto-electrical performance of the related devices

In the previous chapters, we have investigated the material changes induced by the KF-PDT on the surface chemistry of the absorber, in the case of a beneficial effect (increase of the V_{oc}, similar FF and J_{sc}) and a detrimental effect (lowering of all the photovoltaic parameter) of the treatment. We have highlighted that the presence of an OVC at the surface of the absorber prior the KF-PDT was necessary to take advantage of this treatment. In the case of the beneficial effect of the treatment, we have studied the hetero- (CIGS/CdS) and the homo-interfaces (CIGS/CIGS) material properties of the complete devices. We have also studied the hetero-junction formation in the CBD and we have modelled the chemical reactions occurring during the chemical bath deposition of the CdS. The material model of the hetero-junction formation, summarizing the conclusions of the chapter 4 and 5, is shown in Figure 5-1.

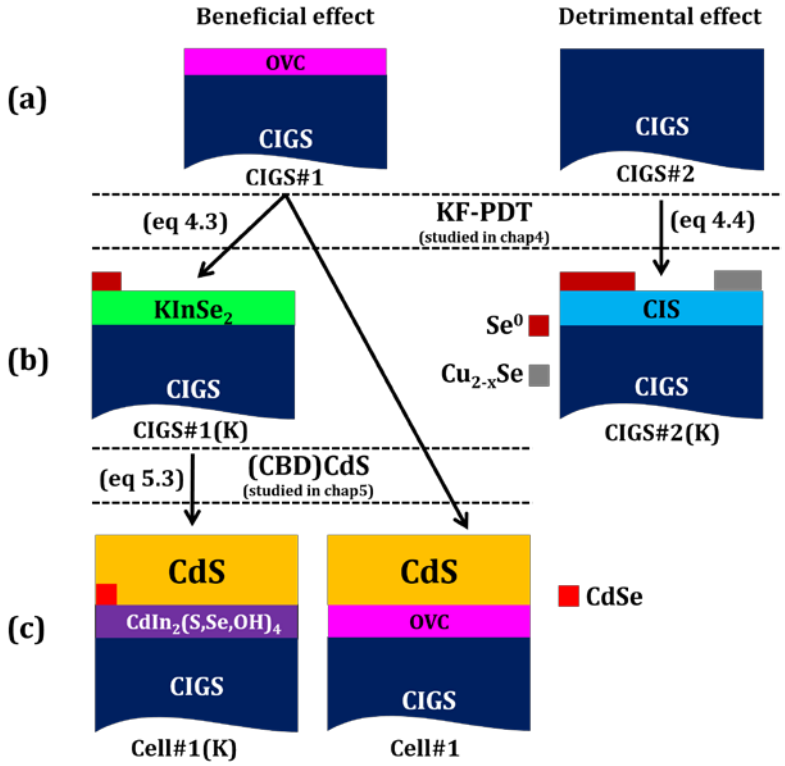

Figure 5-1 – Material model of the effect of the KF-PDT on the hetero-junction formation, built from the investigations shown in chapter 4 and 5. (a) Suggested absorbers prior the KF-PDT, leading to a beneficial or detrimental effect of the treatment. (b) New compounds formed at the surface of the absorber in both beneficial and detrimental effect of the treatment (studied in chapter 4). (c) Effect of the (CBD)CdS on the formation of the junction with untreated and treated absorbers, in case of a beneficial effect of the KF-PDT (studied in chapter 5).

We have highlighted several major differences between Cell#1 and Cell#1(K), including the presence of a thin $CdIn_2(S,Se,OH)_4$ layer at the absorber/buffer interface in Cell#1(K). We have reproduced the synthesis of this material on indium selenide coated glass substrates and we have shown that the interface layer material is highly photoconductive, with a lower band gap than the CdS. The $CdIn_2(S,Se)_4$ has been reported in the literature to have an n^+ type conductivity (not degenerated). We have also demonstrated that the presence of K at the GBs highly affects their composition. The GBs in Cell#1(K) are highly Cu depleted and show a Se enrichment but no enrichment of In compared to those in devices untreated with KF.

In this chapter, we will first discuss the results of temperature-dependent opto-electrical measurements. Based on the study of the electrical transport in Cell#1(K) and the results from the material assessment shown in Figure 5-1, we will propose a model for the hetero-junction based on KF-treated absorbers and (CBD)CdS buffer layers that could explain the electrical improvements induced by the KF-PDT. Finally we will discuss the (I) material and (II) electrical proposed models in order to answer the questions of chapter 3 (p.19):

(1) What are the absorber properties that make the KF-PDT beneficial or detrimental for the device efficiency?

(2) Why can we reduce the CdS chemical bath deposition duration without lowering the photovoltaic parameters and why a minimum amount of KF has to be provided to do so?

5.1 Electronic transport

The purpose of this section is to model the origin of the increase of the photovoltaic parameters. We do not focus on the fill factor (FF) since, in the present work, KF-PDT yields either decreased or unchanged FF (no improvement). We first analyse the transport mechanism in Cell#1 and Cell#1(K) from capacitance and temperature-dependent J(V) measurements in order to explain the increase of the open-circuit voltage (V_{oc}). The increase of the short circuit current density J_{sc} in the short wavelength region through the reduction of the buffer layer deposition duration (and thus thickness) has already been reported and will be debated in section 5.2.2. Here we report an increase of the J_{sc} due to a better collection of the carriers photogenerated by low energy photons in devices without any grading.

5.1.1 Increased open-circuit voltage

Possible origins of the V_{oc} increase - KF-PDT has been shown to significantly increase the V_{oc} (+30/40 mV). It has been shown in section 1.1.3 that V_{oc} is driven by the following equations:

$$V_{oc} = \frac{E_a}{q} - \frac{AkT}{q}\ln\left(\frac{J_{00}}{J_L}\right) = \frac{AkT}{q}\ln\left(\frac{J_{sc}}{J_0}\right) \quad (5.1)$$

Where E_a is the activation energy of the dominant recombination path, k the Boltzman constant, A the ideality factor, J_{00} a weakly temperature-dependent prefactor, J_L the photogenerated current and J_0 the saturation current density of the recombination current J_R (dark current). Basically, the V_{oc} would increase if the recombinations decrease or if the band gap is increased.

Depending on the dominant recombination mechanism in the related devices the explanation for the origin of such increase of the V_{oc} might be different:

(i) *Recombinations in the space charge region (SCR):* ($1 \leq A \leq 2$; $E_a = E_g$)

The V_{oc} can be increased by increasing either the band gap (increase of the activation energy) or the doping since it will shrink the space region width W_{SCR} and thus reduce the recombination current $J_R = q \int_0^{W_{SCR}} R \, dx$ (with R the recombination rate in the SCR).

(ii) *Recombination at the CIGS/CdS interface:* ($A \sim 1$, $E_a = \Phi_b$)[18]

V_{oc} can be increased by increasing the barrier for recombinations Φ_b at the interface or by passivating interface defects that would assist these recombinations.

Dominant transport mechanism – We have determined the dominant recombination path with the help of temperature-dependent J(V) measurements. Cell#1 and Cell#1(K) were cooled down with liquid nitrogen to temperatures from 200 K to 330 K in a Janis cryostat equipped with windows transparent to wavelength from 280 to 2000 nm. Since the devices were frozen at low temperature, the electrical state of the device before lowering the temperature was important. In order to study the transport mechanisms in conditions close to the real operating point of the devices, we have illuminated the cells for 10 min at room temperature under AM1.5 solar spectrum at maximum power point ($V=V_{max}$, $J=J_{max}$, see section 1.1.2) and cooled them down to low temperature (under illumination)[19]. This so called light-soaked electrical state is used to calculate the certitfied energy conversion efficiency of champion cells.

J(V) responses were fitted according to the one-diode model (see section 1.1.3). It appeared that the ideality factors were always higher than one, giving rise to recombinations in the SCR in both cases. Figure 5-2 shows the evolution of the V_{oc} with the temperature in Cell#1 and Cell#1(K). The activation energy of the recombination in the SCR is 30 meV higher in Cell#1(K). This is consistent with the typical value of the increase of the Voc due to the KF-PDT treatment (30/40mV). Since recombinations mostly take place in the SCR of the devices, it might suggest that the average band gap in the SCR of Cell#1(K) is higher than that in the SCR of Cell#1.

[18] In that case $A = 1 + \frac{N_A}{N_D}$ with N_A and N_D the effective hole and electron concentrations in the CIGS and the CdS. For typical CIGS/CdS hetero-junctions, we have $N_D >> N_A$ and therefore $A \sim 1$. Φ_b represents the barrier for recombinations at the interface, see section 1.1.3.

[19] In that case the illumination yields creation of electron-hole pairs and Fermi level splitting, inducing the charging of some defects. In particular, metastable and amphoteric defects related to Se vacancies can convert from donor configuration into acceptor configuration and thus increase the effective doping under illumination [38].

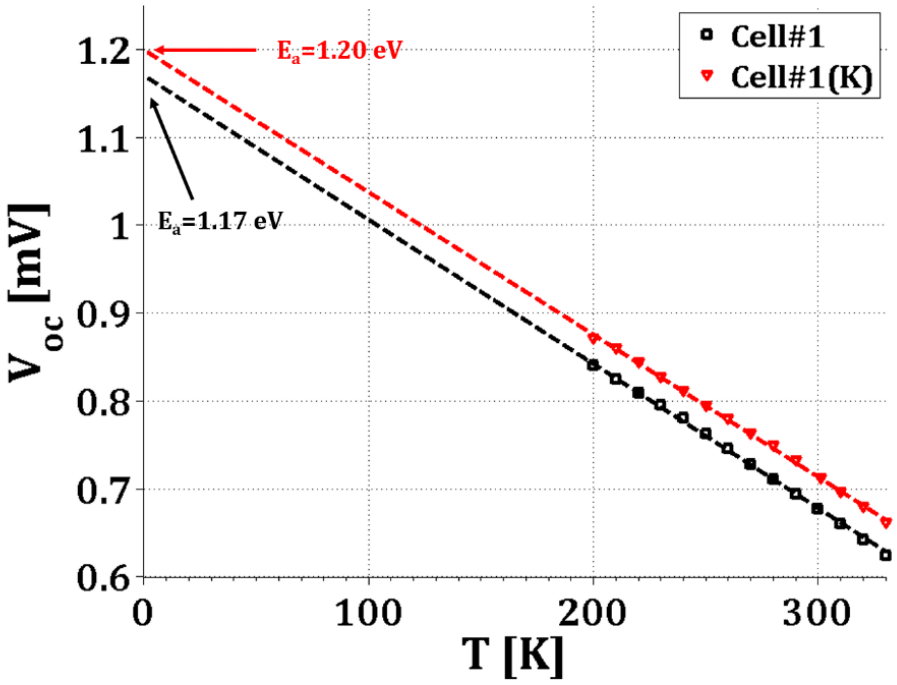

Figure 5-2 - Evolution of the Voc with the temperature in Cell#1 and Cell#1(K) after white light soaking

Estimating the band gap in the SCR of the devices requires to know the band gap in such graded absorber and the actual in-depth extension of the SCR. In the following, the width of the SCR will be estimated from capacitance measurements and the value of the band gap via the calculation of the Ga content (see section 1.2.2) extracted from SIMS measurements.

"Doping" and space charge region width - The net hole concentration (N_A) and the width of the space charge region (W_{SCR}) have been estimated through Drive-Level Capacitance Profiling (DLCP) measurements performed at Warsaw University of Technology. N_A and W_{SCR} have been estimated by the y coordonate in the flat part of the profile and the x coordinate maximum[20] of the non-uniform profiles (as indicated in Figure 5-3), respectively. The measurements have been performed on light-soaked devices at 100 K in order to avoid hysteresis effects. Applied DC-voltage has been varied from -2 V up to 0.8 V. The frequency of the AC-voltage was 100 kHz. Details of the technique and the method to plot the DLCP profiles can be found in Ref [194].

The DLCP profiles of Cell#1 and Cell#1(K) are shown in Figure 5-3. The profile of the Cell#1 is quite uniform. The effective hole concentration is about 2.5 10^{16} cm^{-3}, with a corresponding SCR width of about 380 nm. On the contrary, the in-depth capacitance profile of Cell#1(K) is highly non-uniform. Two parts of the KF-treated absorber have to be considered. The part of the profile between 30 nm and 100 nm (Part A) gives an effective hole concentration of about 2.0 10^{17} cm^{-3}, which is a decade higher than that in Cell#1. The part between 0 and 30 nm (Part B) shows an increase of the N_{DLCP} up to 7 10^{18} cm^{-3}.

[20] In capacitance measurements we do not discriminate positive or negative charges. Therefore we assume that the flat part on the right of the profiles corresponds to the capacitance in the absorber and thus to N_A. The SCR width is overestimated since it corresponds to the width of the SCR with an applied bias voltage of -2 V.

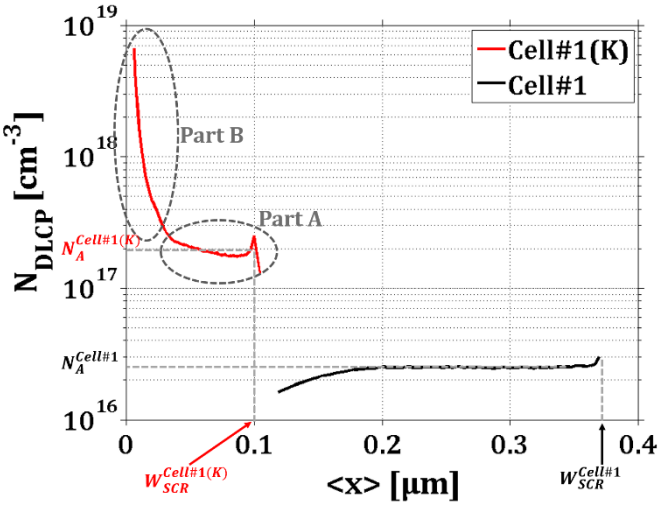

Figure 5-3 -- Drive-level capacitance measurements in Cell#1 (black) and Cell#1(K) (red) after white light soaking

Table 5.1 - Effective hole concentration and width of the SCR in Cell#1 and Cell#1(K) after light soaking

Sample	N_A [cm^{-3}]	W_{SCR} [nm]
Cell#1	2.5 10^{16}	380
Cell#1(K)	2 10^{17}	100

Origin of the increase of the doping – The "doping" in the Part A can reasonably be attributed to the net hole concentration in the p-part of the junction (absorber). The increase of the net hole concentration in the SCR "far" from the hetero-interface due to the KF-PDT can have many origins. The K may have the same effects as the Na (see the detailed section 2.1.3 on the increase of the free hole density due to the presence of the Na). However, due to the already mentioned steric reasons, K may not occupy any site in the CIGS lattice. Furthermore, K is added by PDT after the completion of the CIGS film and diffuses at GBs. Therefore, K should not change the bulk properties. Hence, we suggest that K should increase the free hole density via the changes it induces at GBs (e.g. passivation of deep donor defects).

From the capacitance technique, it is not possible to discriminate whether the carriers involved in the Part B of the profile originate from the n- or the p-side of the junction. Indeed, in the case of an asymmetric doping, the capacitance is representative of the lower doped part of the junction. However, considering the width of the SCR, the doping of the n- and p-side may be comparable. Therefore, two interpretations of the increase of the doping in the Part B of the profile have to be considered:

- The light-soaked state of the devices could have induced an important photoconductivity in the n^+ $CdIn_2(S,Se,OH)_4$ interface layer and the increase in N_{DLCP} is due to the n-part of the junction.
- Due to the presence of the n^+ $CdIn_2(S,Se,OH)_4$ interface layer, the Fermi level at the absorber/CdS interface should be close to the conduction band. It has been shown that this particular position of the Fermi level can induce the conversion of metastable defects from donor to acceptor configuration, thus increasing the p-type conductivity of the absorber in the vicinity of the absorber surface [20], [38].

Tunneling - The increase of the doping in Cell#1(K) yields the shrinking of the SCR width. This width is less than 100 nm. It is very surprising that a device with such a small SCR exhibits a high efficiency. Indeed, the value of the electric field in the SCR must be four times higher in Cell#1(K) than in Cell#1. Assuming a built-in voltage (V_{bi}) roughly corresponding to the band-gap (1.2 V), an applied voltage (V_a) of 0.7 V (maximum power point) and a SCR width of 20 nm (changing the applied bias from -2 V to 0.7 V will shrink the W_{SCR} from 100 nm to a much lower value, probably even lower than the 20 nm considered here), one can estimate the maximum electrical field magnitude (at the metallurgical absorber/buffer layers interface):

$$\left|\vec{E}\right|_{max} \sim \frac{2(V_{bi} - V_a)}{W_{SCR}} \sim 250\ kV/cm$$

This important electric field at the metallurgical interface leads to recombinations assisted by tunneling (deduced from the temperature dependency of A, not shown) but it is not critical for the device performance. It suggests that the electrical pn junction is buried in the absorber so the dominant recombination mechanism is not interface recombination. Indeed, interface recombinations enhanced by this tunneling phenomenon would limit the device performance and Cell#1(K) would not exhibit the high electrical performance reported in section 2.4.1.

Band gap in the SCR – The Ga grading in the absorbers of Cell#1 and Cell#1(K) are shown in Figure 5-4. These Ga gradings have been calculated from SIMS in-depth profiles[21] carried out on peeled off CIGS/CdS/ZnO/ZnO:Al stacks. One can see that the Ga grading in both samples are typical of 3-stage processed CIGS. Moreover, both profiles are similar, the most important difference concerns the value of the Ga grading in the rear part of the absorbers but this difference will not change the value of the band gap in the SCRs. Assuming unchanging sputter cycles during the SIMS measurements in the absorbers we have estimated the distance from the Mo/CIGS interface (the measurement of the thicknesses of the absorbers have been performed both in a profilometer and in a SEM, not shown). This protocol allows us to estimate the band gap (see section 1.2.1) in the SCR of Cell#1 ($W_{SCR}^{Cell\#1}$~380 nm) and Cell#1(K) ($W_{SCR}^{Cell\#1(K)}$~100nm), assuming that the variation of the band gap comes from the variation of the Ga content only (no other chemical or electrical changes).

In Cell#1, the SCR extends to the notch position (see section 1.3.3 for the definition). The band gap in the SCR lies from 1.10 to 1.24 eV. The value of the activation energy in Cell#1 (1.17 eV) is then consistent with the values of the band gap in the SCR of this samples. The band gap in the SCR of Cell#1(K) is almost constant and about 1.24 eV. This value is higher than the activation energy (1.20 eV) found in Cell#1(K). However, the average value of the band gap in the SCR of Cell#1(K) is higher than that in Cell#1, corroborating our interpretation of the origin of the increase of the V_{oc} induced by the KF-PDT.

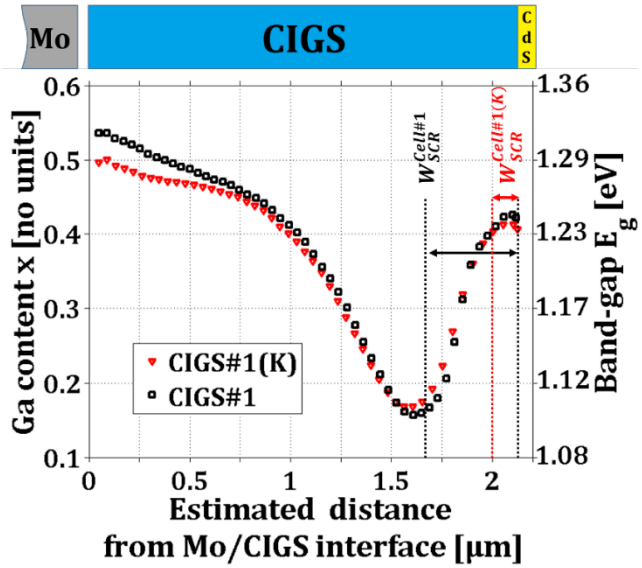

Figure 5-4 - Ga grading profiles (calculated from SIMS measurements) in absorbers from Cell#1 (black) and Cell#1(K) (red)

[21] From the ^{69}Ga and ^{115}In SIMS profiles in the investigated sample and measurements in standard samples with known composition (from EDS), it is possible to calculate the Ga content $x = {[Ga]}/{([Ga] + [In])}$

5.1.2 n+p hetero-junction

Based on the material model of the hetero-junction proposed in section 4.7, we propose an electrical model for the impact of the KF-PDT on the electrical transport in related solar cells. The electronic band diagrams of a standard solar cell (untreated with KF) and of a device treated with KF (corresponding to the assumed electrical model) are depicted in Figure 5-5. In order to simplify the understanding of this diagram we assume no Ga grading within the absorber. Furthermore we have no experimental indications for the band continuity at the $CdIn_2(S,Se,OH)_4$/CIGS interface so we have assumed the case with no band discontinuities. Considering the photoconductivity of the $CdIn_2(S,Se,OH)_4$, we suggest that the SCR in the n-side of the junction does not extend into the CdS so no electric field is present in the i-ZnO and the CdS (flat bands)[22]. Due to the n^+-type conductivity of the $CdIn_2(S,Se,OH)_4$ layer the position of the Fermi level at the interface with the CIGS is close to the conduction band E_c.

It is worth noting that in both untreated and KF-treated cases the electrical pn junction (where n=p) is buried into the absorber. However, the mechanisms leading to this burying of the electrical junction are different in both cases:

- *The untreated case* – The burying originates from the presence of an n-type OVC at the surface of the absorber. This material contains a high density of crystalline defects.
- *The KF-treated case* – There is no type inversion of the absorber surface. The burying originates from the position of the Fermi level close to the conduction band at the surface of the CIGS (due to the n+ conductivity of the $CdIn_2(S,Se,OH)_4$).

R. Klenk explains that an n^+p hetero-junction is the best configuration (considering the doping of the n- and p-side of the junction) to minimize interface recombinations, even in presence of a high interface recombination velocity [195]. According to this author "type inversion of the absorber surface by n-type doping [as in the case of the OVC] is neither required nor necessarily desirable. As soon as the above [configuration] is fulfilled, the cell will likely be limited by bulk properties and can be further optimised through, e.g. high optical absorption and good carrier lifetimes in the absorber". Moreover, according to J.F. Guillemoles [196], "when defects are introduced in the material [as it is the case in the defect chalcopyrite OVC] this may produce […] an increase in the concentration of recombination centers and traps". In conclusion, both the presence of an inverted n-type surface region of the absorber (OVC) and the position of the Fermi level close to the conduction band at the absorber surface (n^+p hetero-junction) will bury the electrical junction. However, in the second configuration (n+p hetero-junction) the electrical performance are better because the burying of the electrical junction does not involve defects within the absorber.

[22] Assuming that the free electron density in the $CdIn_2(S,Se,OH)_4$ is two decade higher than the free hole density in the CIGS, and a total W_{SCR} of about 100 nm, then the conservation of the charges imposes that the extension of the SCR in the n-side of the junction sould be in the order of the nanometer.

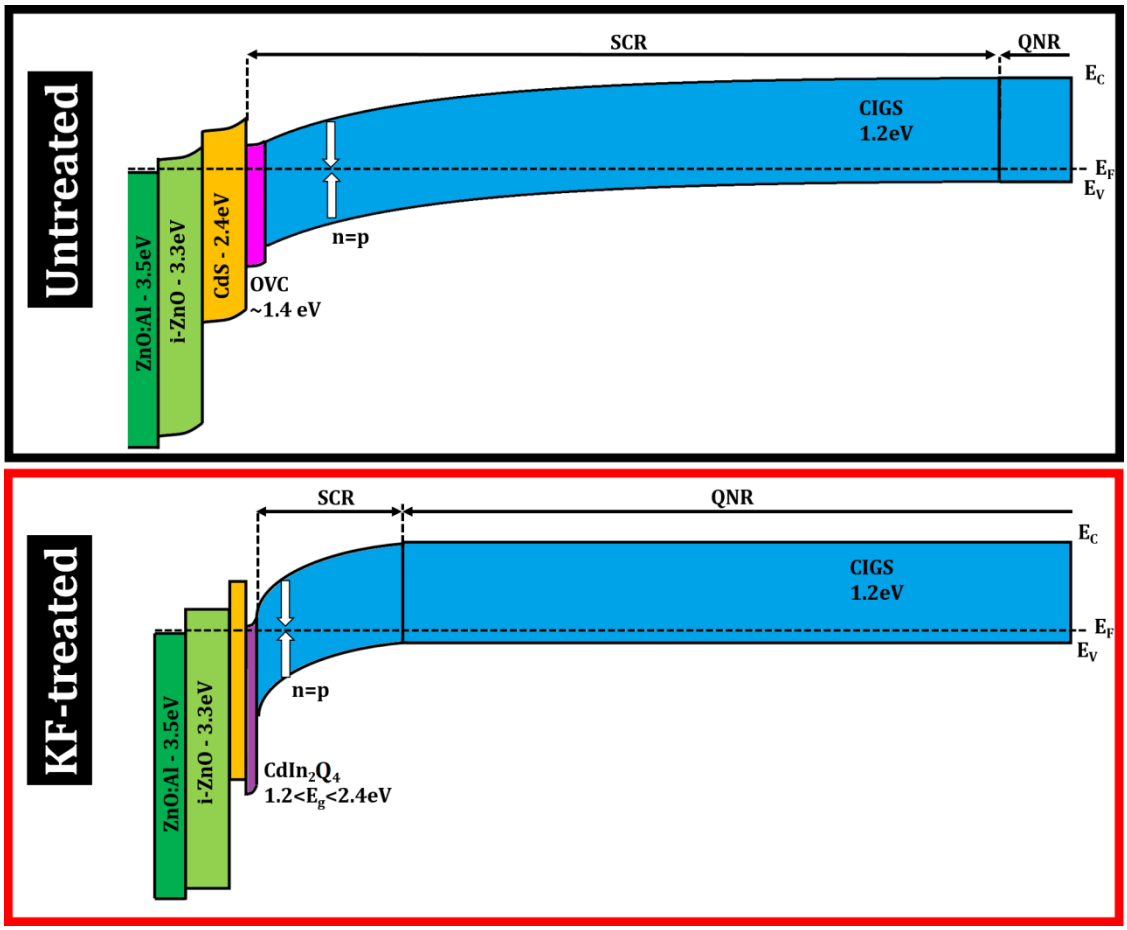

Figure 5-5 – Suggested electronic band diagrams of a standard solar cell (untreated with KF, in dark) and that of a device treated with KF, in red, in a light-soaked state and at 0 V bias. No grading of the absorbers is considered

The electrical model arises the following questions:

(a) Why the dramatic shrinking of the SCR in KF-treated devices does not limit the collection of the carriers photogenerated deep into the absorber (where no electric field is present to assist the collection)? This particular issue will be discussed in the following section.

(b) In absorbers with Ga grading (e.g. in CIGS#1 and CIGS#1(K)), the position of the "notch" separates the absorber into two parts, with two different "quasi-electric" fields ξ_F and ξ_R in the front and rear part, respectively (see section 1.3.3). The ξ_F tends to slow the minority electrons coming from the absorber towards the window. Usually (as it is the case in Cell#1), the electric field of the junction compensates the ξ_F and the presence of the ξ_F is not detrimental. In KF-treated absorbers with such a grading, the SCR does not extend to the "notch". Therefore, the ξ_F is not compensated and might become detrimental for the electronic transport. In 3-stage processed CIGS, the in-depth position of the "notch" can be tuned via the duration of the 3rd stage. However, as only In and Ga are evaporated during the 3rd stage, varying its duration changes also the final Cu content of the near-surface region of the absorber, which has been shown to be critical in order to take advantage of the KF-PDT. The engineering of the Ga grading independently of the Cu content is possible using alternative deposition processes of the absorbers (e.g. 3-stage in Na-free conditions or at low substrate temperature, "Copper Poor Rich Off" process (CUPRO), one stage with variation of the fluxes [197]). The influence of the position of the "notch" in KF-treated absorbers will be further investigated.

(c) In this modelled structure, the CdS seems unnecessary, or even detrimental (the introduction of an electronic barrier for the minority electrons transport due to a thick CdS will be discussed in section 5.2.2). According to C. Platzer-Björkman, the problem with CdS-free devices is the band alignement between the ZnO and the CIGS due to the presence of the Ga. Similar efficiencies can be achieved using CdS or avoiding it in CIS-based devices [198]. As far as CIGS-based devices are concerned, Olsen et al. have already reported efficiencies of 13.95% for direct MOCVD ZnO/Cu(In,Ga)Se_2 devices [199]. The introduction of the KF-PDT might allow the synthesis of CdS-free CIGS-based device with higher efficiencies since the treatment induces an important Ga depletion at the surface of the absorber. The thickness of the CdS layer has turned to be an issue in the framework of the KF-treated devices (e.g. reduction of the thickness without lowering the photovoltaic parameters). The duration of the CdS chemical bath deposition will be discussed in the section 5.2.2.

(d) Finally, if we assume the n^+ conductivity of the $CdIn_2(S,Se,OH)_4$, the presence of the ZnO bilayer may also be unnecessary. Avoiding ZnO in complete device would require a complete coverage of the absorber by the $CdIn_2(S,Se,OH)_4$. This would also question the stability of this material, which will be the subject of further investigations.

5.1.3 Improved collection without Ga grading

The capacitance measurements have shown that the KF-PDT yields shrinked SCR with a corresponding width in the order of a few tens of nm. In absorbers with a Ga grading (e.g. 3-stage processed CIGS), a "quasi-electric" field in the rear part of the absorber helps to the collection of the electrons photogenerated in this region and the reduction of the SCR might not influence the collection of these carriers. In absorbers without such a Ga grading, the collection of long-wavelength photogenerated carriers is low. Therefore, the effect of the SCR shrinking induced by the KF-PDT should become critical.

In this section, we will focus on samples from Run#3 grown following a one step co-evaporation process (see section 1.3.2). In such samples, no compositional grading is present within the absorber. No additional "quasi-electric" field induced by a band gap grading is then present in the bulk. This results in the poor collection of the carriers photogenerated with low-energy photons deep in the bulk, as it can be noticed on the EQE measurement of Cell#3 in Figure 5-6. However, after the KF-PDT, all the photovoltaic parameters are improved, including the J_{sc}, due to an increase of the long-wavelength photogenerated carriers collection. It can be seen in Figure 5-4 that the KF-PDT does not induce any additional Ga grading. Moreover, it has been shown in the previous section that this treatment reduces the space charge region width. Therefore this improved collection deep in the bulk might not origin from an electric field from the junction or induced by a compositional grading. One could suggest that this improved collection could result from an increase of the effective minority carriers diffusion length induced by the KF-PDT. As already discussed, it is very unlikely that K can occupy any site in the CIGS lattice. Hence, we suggest that the improved collection may result from the reported changes at the GBs. This issue will be discussed in section 5.2.1.

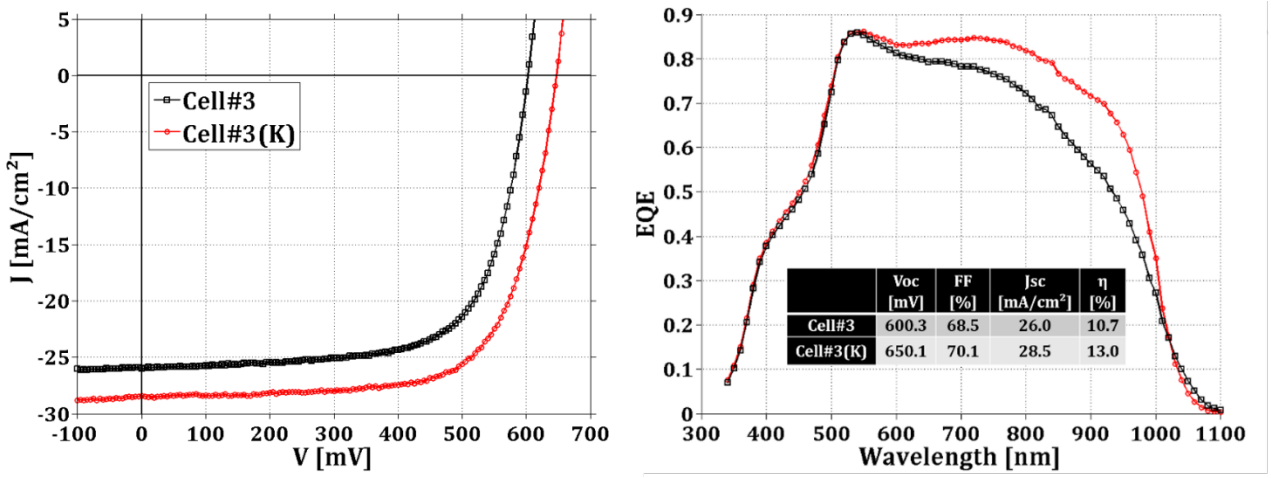

Figure 5-6 – J(V) curves and EQE of cells from Run#3 (no grading), treated (Cell#3(K)) or not (Cell#3)

5.1.4 Summary

The enhancement of the electronic transport results from the combination of at least three effects of the KF-PDT:

(i) *The increase of the free hole density* – We suggest that the changes induced by the KF-PDT at the GBs increase the free hole density in the CIGS. The W_{SCR} is dramatically reduced. If the transport is dominated by recombination in the SCR (role of the condition (ii)), then the V_{oc} is increased. In the particular case of graded absorbers, the reduction of the W_{SCR} leads to an additional (and beneficial) increase of the activation energy of the recombination current since the average band gap in the SCR is higher than that in the SCR of the untreated samples.

(ii) *The buried electrical junction* – The presence of the n^+ $CdIn_2(S,Se,OH)_4$) creates a n+p hetero-junction. It induces a position of the Fermi level close to the conduction band at the interface with the CIGS and therefore buries the electrical junction. This prevents the interface recombinations, which would be enhanced by tunneling mechanisms due to the high electrical field close to the metallurgical interface.

(iii) *The enhancement of the diffusion length* – Since the W_{SCR} is dramatically reduced, the collection of the carriers photogenerated far from the junction should be decreased. However, this collection in KF-treated devices is even higher than in the references. We suggest that this better collection originates from an enhancement of the diffusion length of the electrons in the CIGS due to the material changes induced by the KF-PDT at the GBs.

5.2 Discussion of the models

The purpose of this section is to discuss the proposed material and electrical models in order to address the issues of the chapter 3. Firstly, we will summarize the requested conditions in order to take advantage of the KF-PDT. The origins of the detrimental and beneficial effect will be discussed (issue (1)). Then we will discuss the influence of the CdS buffer layer thickness. We will answer why the CdS can be thinned in KF-treated devices (issue (2)) and discuss the question (c) of section 5.1.2 concerning the suggested detrimental effect of a too thick CdS on electronic transport.

5.2.1 (1) Beneficial and detrimental effect

New formed compounds– In the chapter 4 we have evidenced by XPS the formation of different compounds at the surface of the absorber during the KF-PDT, depending on the structural properties of the absorber prior the treatment. We have shown that the presence of an OVC at the surface of the absorber (prior the KF-PDT) is required to form $KInSe_2$ and avoid the formation of $Cu_{2-x}Se$. When $KInSe_2$ is formed, during the CBD it is transformed into $CdIn_2(S,Se,OH)_4$. In all cases, the KF-PDT leads to the formation of Se^0. The amount of formed Se^0 is much higher when no OVC is present before the KF-PDT (case #2). When an OVC is present (case #1), the amount of formed Se^0 is correlated to the amount of formed KInSe2. Table 5.2 is a summary of the correlation that exists between the evolution of the photovoltaic parameters (due to the KF-PDT), the presence of an OVC prior the treatment and the new compounds formed during the treatment.

Detrimental effect - $Cu_{2-x}Se$ is known to be highly detrimental for the device performance because it creates conducting shunt pathes, thus lowering the photovoltaic parameters. One could suggest that the formation of $Cu_{2-x}Se$ in the particular case of the KF-PDT is limited to the surface of the absorber and therefore may not create shunt paths throughout the all absorber. However, Virtuani *et al*. suggest that even nanoscale phase segregation in the SCR ("hot spot" in their paper), can decrease the shunt resistance [123]. Se^0 is also detrimental for the junction as it has been shown to lower the J_{sc} [146]. The deterioration of the performance in case#2 can therefore be explained by the presence of these compounds.

Beneficial effect - As far as absorbers from Run#1 (beneficial effect) are concerned, it seems that the increase of the V_{oc} is correlated to the amount of formed $KInSe_2$ (and thus to that of $CdIn_2(S,Se,OH)_4$), as a much higher relative increase of the V_{oc} is found in Na-free device. However, we have shown in section 5.1.1 that the increase of the V_{oc} in Cell#1(K) compared to that in Cell#1 is due to the increase of the effective hole concentration[23]. Therefore, it is not surprising that the gain in V_{oc} due to the KF-PDT is higher in Na-free devices, as the hole concentration (if not treated with KF) is lower in these devices than in Na-containing devices.

The FF and the J_{sc} are not modified by the KF-PDT in Cell#1(K) whereas these parameters deteriorate in CIGS#1(SiN,K) (Na-free sample). A possible origin of such deterioration could be the higher amount of Se^0 formed during the KF-PDT in Cell#1(SiN,K). One could suggest that the KF-PDT is therefore "self-limited". The formation of $KInSe_2$ that increases the V_{oc} leads to the formation of Se^0 that lowers the FF and the J_{sc}. Unless we find a way to avoid the Se^0 formation, it is not clear that the KF-PDT will lead to an increase of the V_{oc} higher than the 40/50mV already reported in literature in very high efficiency devices.

[23] In the particular case of graded devices (such as Cell#1(K)), the increase of the net hole concentration leads to an increase of the activation energy of the recombination current because the average band gap in the shrinked SCR is higher than that in the SCR of the untreated devices. In Na-free devices (such as Cell#1(SiN,K)), the grading should be much lower (the grading is induced by the presence of Na during the CIGS growth) and the activation energy should remain unchanged. This does not contradict the increase of the V_{oc} via the increase of the hole concentration.

Table 5.2 -- Correlation of the evolution of the photovoltaic parameters (due to the KF-PDT) with the presence of an OVC prior the treatment and the new compounds formed during the treatment

Samples	Presence of an OVC prior the KF-PDT	New compounds			Evolution of the photovoltaic parameters compare to that in the references		
		Proportion of new Se-based compounds peak area relative to the total Se3d peak area [%]					
		$\frac{A_{Se-3}}{A_{Se3d}}$ (Se^0)	$\frac{A_{Se-4}}{A_{Se3d}}$ ($KInSe_2$)	$\frac{A_{Se-5}}{A_{Se3d}}$ ($Cu_{2-x}Se$)	ΔV_{oc} (mV)	ΔFF (abs %)	ΔJ_{sc} (mA/cm^2)
Cell#1(SiN,K)	YES	8%	15%	-	+102	-3.5%	-1
Cell#1(K)	YES	5%	9%	-	+40	+1%	<1
Cell#2	NO	30%	-	15%	-240	-29%	-7

Grading – In the particular case of the graded devices, we have shown in section 5.1.2 that the narrowing of the SCR (induced by the KF-PDT) reduces the region where the electric field of the junction compensates the detrimental "quasi-electric" field ξ_F created by the Ga grading in the front part of the absorber. Hence, we suggest that the presence of an OVC prior the KF-PDT may not be sufficient to enable a beneficial effect of the treatment. The Ga grading has also to be engineered in order not to induce a barrier for minority carriers in the front part of the KF-treated absorbers.

Role of the GBs – In the particular case of non-graded CIGS-based devices (such as Cell#3(K)), the KF-PDT leads to the increase of all of the photovoltaic parameters. The increase of the V_{oc} and the FF can be explained with the same model as in the case of graded absorbers. A n^+p hetero-junction is formed between the $CdIn_2(S,Se,OH)_4$ and the CIGS that buries the electrical junction. Simultaneously, the net hole concentration is increased. The combination of these two effects leads to the increase of the V_{oc} (and the FF). However, it cannot explain the collection enhancement of the carriers photogenerated deep in the absorber (with low energy photons). We have proposed that this particular issue could be explained by an enhanced minority carrier lifetime. We have evidenced by APT measurements that the GBs of KF-treated CIGS were highly Cu depleted and did not exhibit the usual In enrichement. Two interpretations can be imagined in order to explain the suggested better minority carrier lifetime:

- The lower amount of In at GBs decreases the density of donor defect In_{Cu}. This decreases the band bending of the conduction band in the vicinity of the GBs, reducing the attraction of the electrons in these defective regions and therefore reducing the recombinations. Urbaniak *et al*. [103] also suggest that decreasing the band bending in the vicinity of the GB would increase the effective holes density in this region, which is consistent with the capacitance measurments.

- The important Cu depletion, as well as the width of the depleted regions at GBs, suggests that the material composing the GBs is not CIGS. Another phase (not CIGS) is formed at the GBs. This phase could either be KInSe2, $CdIn_2(S,Se,OH)_4$ or another compounds. This phase would have a beneficial effect on the electronic transport of the holes or the electrons.

These assumptions have to be confronted to experiments and the electrical behavior of the GBs in KF-treated devices will be further investigated.

Effect of the Cu and Ga content of the absorbers – Four absorbers have been grown on SLG/Mo following the 3-stage process. The first and second stages were identical for the four absorbers while the 3rd stage was changed in order to obtain high and low Cu and Ga contents in the near-surface region of the absorbers[24]. The devices based on these absorbers all lead to high efficiencies between 16 and 17% if they remain untreated with KF (not shown). A standard KF-PDT has been applied on the four absorbers. For technical reasons[25], it was not possible to simultaneously grow the subsequent buffer and window layers on the four absorbers. The CdS and ZnO layers have been grown simultaneously on the absorbers with identical Ga contents. This results in the variation of the absorption in the short wavelength region on the EQE of the corresponding devices shown in Figure 5-7.

From the J(V) and the EQE curves of the KF-treated samples depicted in Figure 5-7 it is clear that the final Cu content of the absorber (prior the treatment) is critical to take advantage of the KF-PDT. Both samples with a high y exhibit a poor FF with an additional barrier above V_{oc} and a reduced J_{sc} (compared to that in the sample with both low x and y). The first condition to form an OVC is to be Cu poor. This excludes the presence of an OVC in both samples with a high y. In these samples, $Cu_{2-x}Se$ phases should have been formed, explaining the poor electrical performance. In absorbers with low y, an OVC is present prior the KF-PDT (not shown). But then the Ga content becomes critical and poor performance are obtained on KF-treated absorbers with a high x. This could originate from a too strong gradient which would not be compensated by the electrical field of the junction (due to the reduced SCR, see question (b) at the end of the section 5.1.2) and would create an electronic barriers for the electrons in the CIGS. Finally, the sample with both low x and y exhibits very good performance.

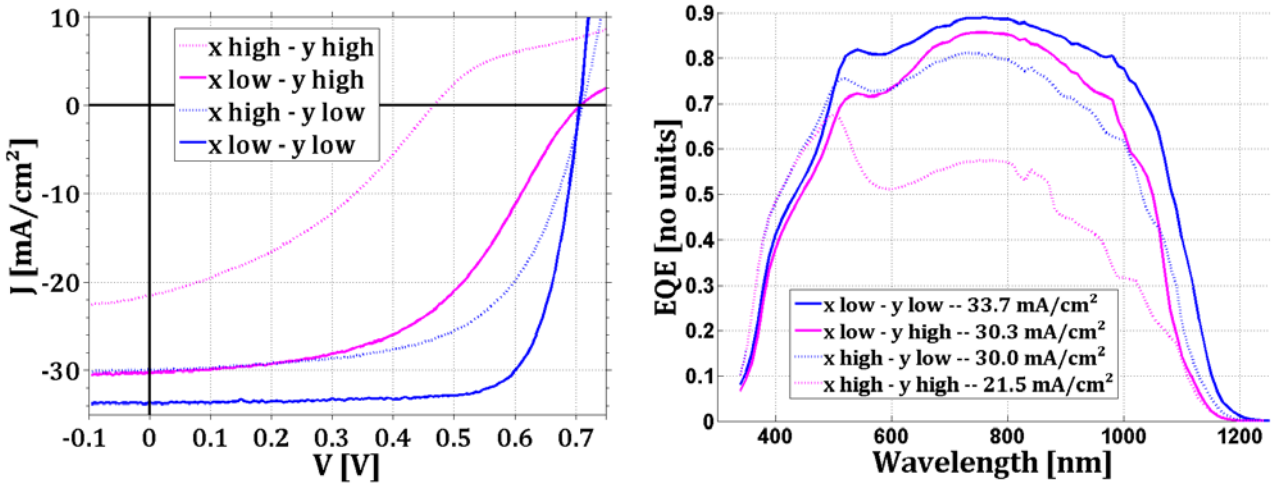

Figure 5-7 -- J(V) and EQE of KF-treated absorbers with various Cu content (y) and Ga content (x) at the surface

5.2.2 (2) CdS chemical bath deposition duration

In this section we will only consider the case of KF-treated absorbers.

Thinning the CdS – In the framework of the suggested model (material and electrical), the n-type semiconducting materials of the devices are the $CdIn_2(S,Se,OH)_4$, the CdS and the ZnO bilayer. The model also suggests that the $CdIn_2(S,Se,OH)_4$ is highly photosensitive and has an n^+-type conductivity so, under

[24] The Cu content was varied by changing the duration of the 3rd stage, since only Ga and In are evaporated (under Se excess) in this stage. The Ga content was changed by tunning the Ga and In fluxes ratio (constant during the 3rd stage). Varying the duration of the last stage induces different positions for the "notch" and different Ga gradings.
[25] (sharing of the co-evaporation chamber, a deposition of an absorber with a KF treatment takes a day at the lab)

illumination, the space charge region should not extend into the CdS. The electrical junction is then composed of the CIGS and the n^+-type semiconductor $CdIn_2(S,Se,OH)_4$. The CdS seems to be "unnecessary". Hence, it is not surprising that it appears possible to reduce the duration of the chemical bath deposition without lowering the V_{oc} and the FF. The dipping duration should be limited to the time needed to form the $CdIn_2(S,Se,OH)_4$. We have shown that the $CdIn_2(S,Se,OH)_4$ may result from the substitution of K by Cd and Se by S in the $KInSe_2$ at the beginning of the chemical bath deposition. Furthermore, it has been shown that once the $CdIn_2(S,Se,OH)_4$ is formed, the In does not diffuse into the forming CdS. Finally, according to the model, once the $CdIn_2(S,Se,OH)_4$ is formed, "unnecessary" CdS is deposited in the bath, explaining why longer CdS deposition duration do not lead to better V_{oc} and FF.

Too thick CdS - For devices with untreated absorbers, the V_{oc} and the FF are correlated to the CdS thickness. The thicker CdS, the higher the V_{oc} and the FF [200]. Since the electronic configuration is modified in KF-treated absorbers (see the band diagram in Figure 5-5, p 98), this may be different because a thick CdS might introduce an electronic barrier. For thin CdS, this should not modify the electronic transport because of the proximity with the electrical field of the junction. However, for too thick CdS the barrier may decrease the photovoltaic parameters.

Optimal CBD duration (in the IMN laboratory conditions) **-** Absorbers have been grown on SLG/Mo following the 3-stage process. The 3rd stage has been adapted in order to obtain an OVC at the surface of the absorbers. The absorbers have been separated into four parts. A quarter (corresponding to 18 cells after the completion of the devices) have been saved to serve as reference samples. A standard KF-PDT has been performed simultaneously on the other part of the absorbers. Then all of the absorbers have been dipped into the same CdS chemical bath. The untreated samples have been removed from the bath after seven minutes. The three sets of KF-treated samples have been removed from the bath after three, five and seven minutes, respectively. The ZnO bilayer has been grown simultaneously on all the samples.

Figure 5-8 shows the statistics (on 18 cells for each set of samples) of the V_{oc} and the FF. Figure 5-9 depicts the J(V) curves and the EQE of the best solar cells. In this experiment, the gain in Voc induced by the KF-PDT (of about 5mV) is not as high as in other experiments. However, the results clearly show the tendency on the effect of the CdS thickness. As can be seen on the EQE shown in Figure 5-9, the absorption by the CdS (for photons with λ<500 nm) is lowered as the dipping duration in the bath is reduced from seven minutes to three minutes. Outside of this wavelength region, the EQE are similar for the four type of samples. One can see from the statistics shown in Figure 5-8 that for the seven and the five minutes durations, the V_{oc} of the KF-treated devices are higher than those of the reference. The V_{oc} starts to decreases if the duration in the bath is reduced down to three minutes[26]. The dipping duration has a high influence on the FFs of the KF-treated devices. On these samples, best FFs (>75%) are obtained for five minutes in the bath, which is 28% shorter than the ideal duration on untreated absorber. Even more surprising, for the standard seven minutes duration, the FF of KF-treated devices is much lower than that of the reference. We suggests that this seven minutes duration leads to a too thick CdS deposited on top of the $CdIn_2(S,Se,OH)_4$, leading to an electronic barrier which limits the FF.

[26] In this experiment we do not vary the dipping time duration in the bath for untreated absorbers. However, the standard 7 minutes duration is an optimized compromise for the untreated absorbers. Longer durations lead to lower J_{sc} due to the absorption by the CdS and shorter durations induce a lowering of the V_{oc} and the FF. For 3 minutes in the bath, the "performance" of devices based on untreated absorbers are very low (V_{oc} anf FF lower than 300 mV and 50%, respectively). This emphasises the surprinsing honourable performance of the KF-treated samples for the 3 minutes dipping duration (V_{oc}~660 mV, FF~74%).

This result is representative of the performance obtained on most of the KF-treated devices based on a buffer layer deposited in seven minutes[27]. Finally, similar FFs as those of the reference samples (with a thick CdS resulting from seven minutes in the bath) can be obtained on treated samples with only three minutes in the bath. However, in this particular case, the spread of the statistics increases. Both poor and high FFs are obtained, suggesting an incomplete coverage of the buffer layer or an incomplete substitution to form $CdIn_2(S,Se,OH)_4$.

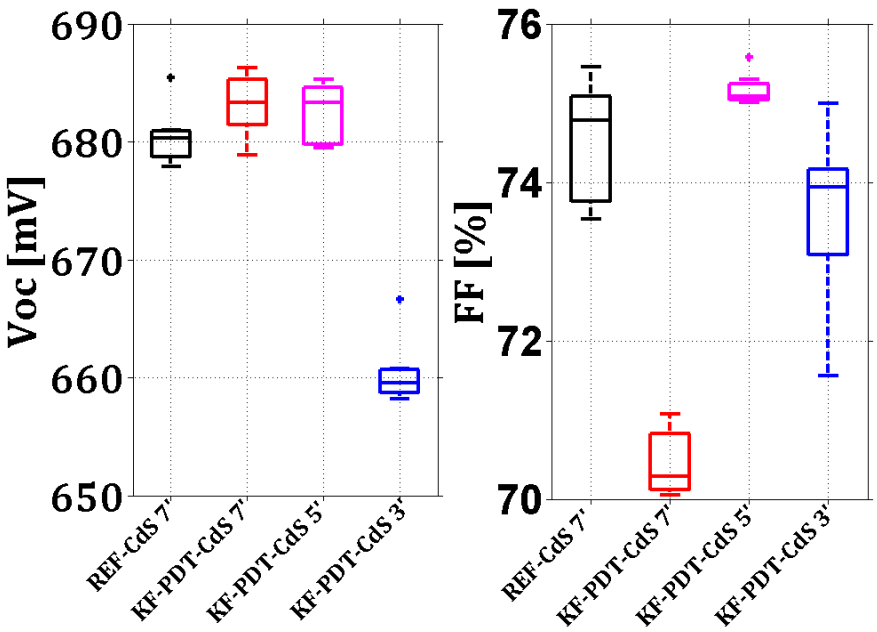

Figure 5-8 -- Voc (left) and FF (right) statistical results of solar cells with an absorber subjected to KF-PDT (red, magenta or blue) or not (black) and dipped into the CdS chemical bath for 3 (blue), 5 (magenta) and 7 minutes (red and black). Each box gives statistical results on 18 cells. The box has lines at the lower quartile, median and upper quartile values. Lines extending from each end of the box show the extent of the rest of the data

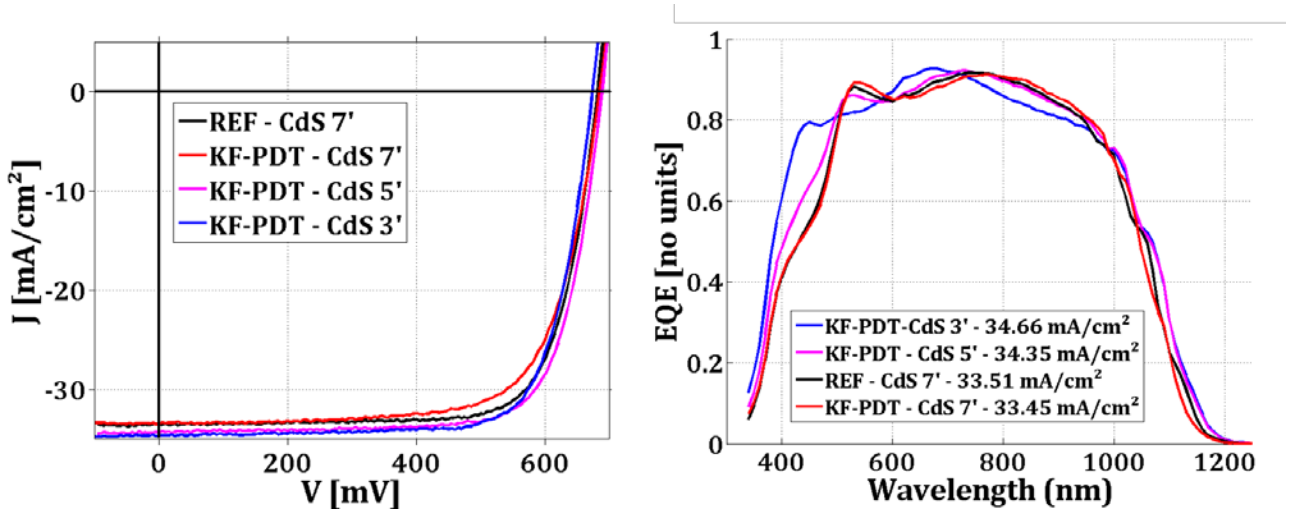

Figure 5-9 -- J(V) curves (left) and EQE measurements of solar cells with an absorber subjected to KF-PDT (red, magenta or blue) or not (black) and dipped into the CdS chemical bath for 3 (blue), 5 (magenta) and 7 minutes (red and black).

[27] For some runs (including the Run#1 presented in this manuscript) a thick buffer layer (seven minutes) did not decrease the overall performance compared to that in the reference, but shorter deposition time of the buffer layer always led to higher performance.

Minimum duration of the KF-PDT – A minimum duration of the treatment has been reported in order to be able to reduce the thickness of the CdS without lowering the V_{oc} and the FF. The KF has to be evaporated slowly (attempt to evaporate KF with high fluxes have failed, not shown), suggesting that the kinetic of the chemical reactions involved during the treatment are slow. Therefore the minimum duration for the KF-PDT can be interpreted in two ways:

- The KF reacts with a certain thickness of the CIGS. Once this amount of CIGS has react, the treatment has to continue in order to let the system stabilizing. Then the residuals of KF which did not react are etched in the bath. In particular, a long treatment will allow the –detrimental- Se^0 formed during the treatment (coming from the CIGS which have reacted) to leave the heated substrate.

- The $CdIn_2(S,Se,OH)_4$ interface layer has to be thick-enough in order to be able to thin the CdS. One could also suggest that the formation of such a layer is not homogeneous at the surface. A long treatment would minimize these inhomogeneities.

Partial conclusion – It appears that the dipping duration in the bath is critical in order to take advantage of the KF-PDT. The standard duration applied on untreated absorbers does not fit to the KF-PDT samples. From the experiment discussed above, it appears that, in the CBD conditions of the IMN, the duration has to be higher than three minutes, but shorter than seven minutes. In these CBD conditions, the kinetics of the reaction is too fast. It is not sure that both K and Se in $KInSe_2$ have been fully substituted before the CdS starts to grow. In conclusion, these results suggest that, beyond the optimization of the dipping duration, the CBD conditions have to be adapted in order to favor the formation of the interface layer $CdIn_2(S,Se,OH)_4$ before the deposition of the CdS.

5.3 Learning from the KF-PDT

The KF-PDT has been shown to modify both (i) the CIGS/(CBD)CdS hetero-junction and (ii) the GBs properties of the absorbers. These changes modify the electronic transport within the whole device, which increases the photovoltaic parameters (V_{oc} and FF) and allow the reduction of the CdS buffer layer (and thus the increase of the J_{sc}). The analysis of the effects of the KF-PDT on the material and electrical properties of the hetero- and homo-interfaces could help to unveil some of the issues that have animated the scientific community in the past. In particular, the role of the (CBD)CdS in the achievement of very high efficiencies in CIGS-based solar cells is an ongoing debate. The model proposed in this thesis, in the framework of the KF-treated devices, could help to understand the following issues concerning the untreated devices:

(i) Thick (CBD)CdS has to be grown on the absorber in order to obtain a high V_{oc} and FF. There is no consistent model that explains why it is not possible to thin the CdS layer in (untreated with KF) devices (assuming a complete coverage of the absorber with the CdS).

(ii) There is a correlation between the V_{oc} and the preferential orientation of the CIGS films.

(iii) Devices based on (PVD)CdS buffer layers are less efficient than those based on CBD.

KF-PDT has been shown to modify the surface of the absorber. KF-treated CIGS surfaces exhibit a higher amount of In and Se than that of the untreated absorber surfaces. We have also demonstrated that the (CBD)CdS growth on treated surfaces is much more homogeneous, with an additional formation of a $CdIn_2(S,Se,OH)_4$ interface layer. Witte *et al.* [173] have investigated the influence of the (untreated with

KF) CIGS grain orientation on the growth of the (CBD)CdS. They have shown that the non-polar {220}/{204} planes terminated with both metal (such as In) and Se species show a much denser coverage than that of the polar –metal terminated- {112} planes. The question that arises is to determine whether the growth mechanism of the CdS on such {220}/{204} planes is similar to that on the KF-modified surface. Assuming this hypothesis, the $CdIn_2(S,Se,OH)_4$ interface layer could also be formed in untreated devices. Figure 5-10 depicts the suggested model of the CdS growth on (untreated) faceted CIGS surfaces if we assume the hypothesis of the formation of a $CdIn_2(S,Se,OH)_4$ interface layer below the {220}/{204} CIGS planes. This model is consistent with several experimental observations:

- The observation of intermixing elements at the CIGS/CdS interface has been reported [33]. Models based on the n-type doping of the CIGS near-surface region, due to the in-diffusion (in the CIGS) of the Cd^{2+} ions from the chemical bath, have been proposed in order to explain the beneficial effect of the CBD (see sections 1.2.3 and 1.4). In the framework of this model, we do not know whether the Cd and the S penetrate into the CIGS or if the In diffuses into the forming CdS but a layer containing both In and Cd is formed.

- Using photoluminescence measurements, Bauer *et al.* have observed local inhomogeneities of $Cu(In,Ga)Se_2$/CdS structures in terms of material composition, metallurgical phases, and consequently of electronic and optical properties [201]. In the framework of the model of Figure 5-10, this could be interpreted as the different junctions (A) CIGS/CdS and (B) CIGS/ $CdIn_2(S,Se,OH)_4$/CdS.

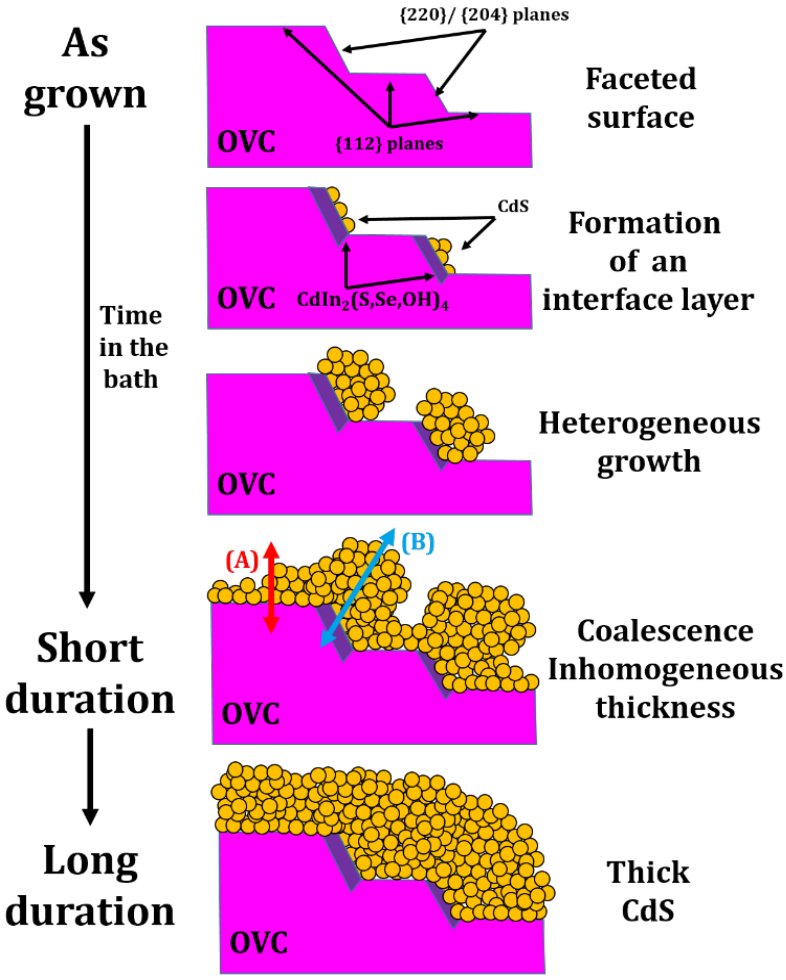

Figure 5-10 -- Growth model of thin (CBD)CdS on untreated absorber, assuming the formation of the $CdIn_2(S,Se,OH)_4$ interface layer

This model can also help to interpret the issues mentioned at the beginning of this section:

(i) Since the growth is inhomogeneous, a short deposition duration of the (CBD)CdS results in both thin (A) and thick (B) CdS. In the framework of this model, the thin CdS on {112} planes (mainly) originates from the coalescence of the CdS aggregates which grow on the {220}/{204} planes. Therefore, the CIGS/CdS interface (A) may show a high density of defects. Locally too thin and defective CdS could hence explain why it is not possible to short the CBD duration on untreated (with KF) absorbers.

(ii) A {220}/{204} preferential orientation of the CIGS film may induce more {220}/{204} planes at the CIGS surface, on which the CdS can grow, resulting in a more homogeneous thickness of the buffer. This also minimizes the detrimental junction type (A) and and may explain why such preferential orientation leads to higher V_{oc}.

(iii) The mechanisms leading to the formation of the $CdIn_2(S,Se,OH)_4$ may be specific to the CBD technique, involving for instance ion exchange mechanisms and preferential sites for chemical reaction. In PVD, it is not sure that such preferential reactions will occur (considering the low temperature deposition of the (PVD)CdS (200°C), the mobility of the species may not be sufficient) and ion exchange mechanisms are excluded. If the formation of the $CdIn_2(S,Se,OH)_4$ is required in order to have a good quality of the junction, this could explain why (PVD)CdS-based devices show lower efficiencies than the devices based on (CBD)CdS.

To conclude, we have shown that the KF-PDT may enhance a growth mechanism which may also be involved on untreated absorbers. The role of the KF-PDT may be to remove the copper from the CIGS surface, resulting in an enhanced availability of In (and Se) to form the beneficial $CdIn_2(S,Se,OH)_4$ interface layer and allow a homogeneous growth of the CdS. Considering that high quality hetero-junctions cannot be obtained with CIGS exhibiting a high Ga content, the role of the fluorine in this treatment may also be important as it has been shown to help to remove the Ga from the surface, hence increasing the availability of the In.

Summary and perspectives

Summary of material investigations - The KF-PDT consists in evaporating KF under Se excess at the surface of finished absorbers. Applying such a KF-PDT on a CIGS absorber before the deposition of a thin (CBD)CdS has been reported to improve all the photovoltaic parameters of the related solar cells. In particular, higher J_{sc} are reported because, in the KF-treated devices, it is possible to thin the CBD(CdS) buffer layer without lowering the V_{oc} and the FF, and therefore to lower the absorption in the CdS.

In this work, we have shown that the treatment could have either a beneficial effect (increase of the V_{oc}, similar FF and J_{sc}) or a detrimental effect (lowering of all the photovoltaic parameters), depending on the properties of the absorber. We have evidenced that the presence of an OVC at the surface of the absorber prior the treatment is necessary in order to take advantage of the treatment. If this condition is not fulfilled, the treatment induces the formation of the highly detrimental $Cu_{2-x}Se$. Whether the OVC is present prior the treatment or not, the KF-PDT induces an important Ga depletion at the surface due to the formation of soluble GaF_3 (removed during the subsequent CBD) and the formation of elemental Se^0, probably resulting from an incomplete reaction during the cooling of the samples after the KF-PDT. Hence, we explain the detrimental effect of the KF-PDT by the formation of a thin CIS layer (with a lower band gap than that of the CIGS) and the segregation of detrimental phases at the surface of the related absorbers.

If an OVC is present prior the treatment, we suggest that the KF-PDT leads to the formation of a non-chalcopyrite thin $KInSe_2$ surface layer on top of a stochiometric CIGS. This surface layer induces a much more homogeneous growth of the subsequent CdS layer, resulting in larger CdS grains with a higher crystalline coherence. Furthermore, we have highlighted the presence of a 5 nm-thick $CdIn_2(S,Se,OH)_4$ interface layer between the CIGS and the CdS in KF-treated devices. We suggest that this interface layer results, during the CBD, from the substitution of K by Cd and Se by S in the $KInSe_2$. We have reproduced the synthesis of this material on glass coated with indium selenide and we have shown that the interface layer material is highly photoconductive, with a lower band gap than the CdS. The $CdIn_2(S,Se)_4$ has been reported in the literature to have a n^+ type conductivity (not degenerated).

A higher amount of oxygen is found both at the CIGS/CdS interface and in the CdS compared to that in the untreated devices. Assuming the substitution of K by Cd, the presence of K at the outermost surface of the sample during the CBD could enhance the oxidation of the interface layer and that of the growing CdS. Finally, we have evidenced the presence of 100 nm-scale CdSe precipitates distributed all along the interface layer. We suggest that these compounds result from the substituted Se which reacts with the Cd ions present in the bath. Figure 5-1 (p. 91) shows the material model of the hetero-junction in both untreated and KF-treated cases.

An investigation of the composition of the GBs has revealed that, in KF-treated devices, these interfaces show a higher Cu depletion and a lower In enrichement compared to those in untreated ones.

Summary of electronic investigation - From this material assessment, and the analysis of the electronic transport in KF-treated and untreated devices, we suggest that the improvement of the photovoltaic parameters results from the combination of at least three effects of the KF-PDT:

(i) *The increase of the free hole density* – We suggest that the changes induced by the KF-PDT at the GBs increases the free hole density in the CIGS. The W_{SCR} is dramatically reduced. If the transport is dominated by recombination in the SCR (role of the condition (ii)), then the V_{oc} is increased. In the particular case of graded absorbers, the reduction of the W_{SCR} leads to an additional (and beneficial) increase of the activation energy of the recombination current since the average band gap in the SCR is higher than that in the SCR of the untreated samples.

(ii) *The buried electrical junction* – The presence of the n^+ $CdIn_2(S,Se,OH)_4$ creates a n+p hetero-junction. It induces a position of the Fermi level close to the conduction band at the interface with the CIGS and therefore buries the electrical junction. This prevents the interface recombinations, which would be enhanced by tunneling mechanisms due to the high electrical field close to the metallurgical interface.

(iii) *The enhancement of the diffusion length* – Since the W_{SCR} is dramatically reduced, the collection of the carriers photogenerated far from the junction should be decreased. However, this collection in KF-treated devices is even higher than in the references. We suggest that this better collection originates from an enhancement of the diffusion length of the electrons in the CIGS due to the material changes induced by the KF-PDT at the GBs.

Perspectives – The role of the KF-PDT has to be divided in two parts. The first part concerns the modification of the GBs. These interfaces play an important role in polycrystalline devices. The important Cu depletion induced by the treatment seems to have a beneficial effect on the electronic properties of the GBs. Since a higher amount of Cu is found at GBs of wide bandgap absorbers (high Ga content), this K-induced Cu depletion could help to understand why KF-treated absorbers with high Ga content can be used in high efficiency devices (see the results of the ZSW group). Moreover, we have suggested that the increase of the doping in the CIGS, which is, at least partially, at the origin of the increase of the V_{oc}, might originate from the changes induced by the KF-PDT at the GBs. The electronic properties of the GBs in KF-treated absorbers have therefore to be further investigated.

The modification of the voltage distribution induced by the treatment (due to the increase of the doping) within the absorber has been shown to be critical in the case of graded absorbers grown following the 3-stage process. The front grading in such absorber may not be compensated by the electrical field of the junction since the space charge region is dramatically reduced, resulting in a barrier for the minority carriers transport. It is worth to note that in the actual world record CIGS champion cell, the notch is very close to the CIGS surface, minimizing this barrier. The investigation of the influence of the position of the notch on the performance of KF-treated device has to be investigated.

The second part of the role of the KF-PDT concerns the modification of the CIGS/CdS hetero-junction. The material and electronic properties of the interface layer between the CIGS and the CdS have to be characterized and modeled since they could be at the origin of the outstanding performance of the device based on (CBD)CdS, even in untreated devices. Furthermore, the optimal growth conditions of this layer are still not fully understood. One of the roles of the KF-PDT could be to repel the Cu from the CIGS surface and therefore to render the In available to react with the bath constituents. This questions the role of In in the fabrication of high quality hetero-junctions with CdS as n-type partner material. It

may help to understand why absorbers which do not contain In, such as Copper Zinc Tin Sulfide (CZTS), do not lead to high quality junctions with CdS. Finally, the availability of In is not sufficient in order to obtain a $CdIn_2(S,Se,OH)_4$ interface layer and the synthesis conditions of this material have to be considered. In the case of KF-treated absorbers, the interface layer has been shown to result from the substitution of K and Se by Cd and S, respectively. The growth kinetics in the bath appears to be critical and the CBD conditions have to be adapted in order to favor the synthesis of the $CdIn_2(S,Se,OH)_4$ interface layer before the effective deposition of CdS.

A minimal duration (15 min) of the KF-PDT has been reported in the literature in order to take advantage of the treatment. This duration may be a serious issue in order to industrially implement the technique. Finally, going one step further, one could suggest that this interface layer could be synthesized without using a KF-PDT. Two methods can be considered:

- *Direct method* – A $CdIn_2S_4$ buffer layer could be directly sputtered on the CIGS. One should also try to replace the –toxic- Cd with Zn, as spinel $ZnIn_2S_4$ material exists.

- *Indirect method* - If the In is available to react with the Cd and the S, we should be able to form a $CdIn_2S_4$ compound, either with a CBD or PVD method, as suggested in this work by the synthesis (by these two methods) of a $CdIn_2S_4$-like material on indium selenide coated glass. The formation of the interface layer then requires the growth of an indium selenide compound at the surface of the CIGS, which means to minimize the Cu migration and suggest a growth at low temperature.

Conclusion – The KF-PDT has, in less than two years, allowed the improvement of the efficiencies of the CIGS based solar cells from less than 20 to almost 22%. This work is a first step towards the full understanding of the KF-PDT effects. There is no doubt that further improvements will come in the future because the analysis of the effects of this treatment opens up new pathways to CIGS-based solar cells fabrication. However, this work suggests that the synthesis methods used to grow the devices may not be adapted to the KF-PDT (3-stage, CBD(CdS)). Finally, the effects of the KF-PDT on the CIGS material (GBs properties) and at the CIGS/CdS interface have to be separated in order to further improve the efficiencies of the related devices.

Résumé en Français

Contexte - Les cellules photovoltaïques basées sur une hétérojonction constituée d'un absorbeur de $Cu(In,Ga)Se_2$ (CIGS) co-évaporé et d'une couche tampon de CdS déposée par bain chimique (CBD) sont les dispositifs en couches minces permettant d'atteindre les plus hauts rendements de conversion photovoltaïque. Ces hauts rendements sont notamment rendus possibles par la présence d'espèces alcalines au sein de l'absorbeur. Jusqu'à très récemment, seul le sodium (Na) était utilisé. Ce Na peut être apporté par diffusion d'espèces sodées contenues dans le substrat de verre à travers le molybdène ou par évaporation délibérée d'un précurseur contenant du Na, tel que du NaF, avant, pendant ou après la croissance de l'absorbeur. La présence de Na pendant la croissance du CIGS impacte ses propriétés structurales et morphologiques. Que le Na soit apporté pendant ou après le dépôt de l'absorbeur, sa présence au sein du dispositif augmente significativement la densité effective de trous, et donc la tension de circuit ouvert. Récemment, l'équipe du Professeur Tiwari a introduit un traitement post-dépôt de l'absorbeur sous vapeur de KF et sous pression partielle séléniée (KF-PDT), permettant d'atteindre des rendements de conversion jusqu'à 21.7% à l'échelle du laboratoire. Ce traitement de la surface de l'absorbeur a pour effet d'augmenter significativement la tension de circuit ouvert (V_{oc}) et le facteur de forme (FF) des dispositifs. Il a également été montré que le temps de dépôt par CBD de la couche de CdS sur cette surface modifiée pouvait être réduit sans détériorer la V_{oc} et le FF, permettant ainsi d'augmenter la densité de courant de court-circuit (J_{sc}). En effet les photons absorbés au sein des couches de type n (ZnO, CdS) n'étant que très partiellement collectés, la réduction de l'épaisseur de la couche tampon permet de réduire l'absorption des photons de hautes énergies (λ<550 nm).

Les origines de l'augmentation des paramètres photovoltaïques (*i.e.* V_{oc}, FF et J_{sc}) par ce traitement sont néanmoins source de discussions. Il a été montré que le KF-PDT induisait une forte déplétion en cuivre (Cu) à la surface de l'absorbeur. De même, il semblerait que pendant le dépôt du CdS par CBD, le Cd diffuserait plus facilement à travers le CIGS ayant été traité avec le KF-PDT. Il a ainsi été proposé que la formation de défauts de type donneur Cd_{Cu} serait facilitée par le KF-PDT. La formation de ces défauts compensateurs participe à l'inversion de type (p→n) de la surface du CIGS et permet l'enterrement de la jonction pn. La séparation de la jonction électronique de la jonction physique (métallurgique) permet de limiter les recombinaisons d'interface. Il a ainsi été proposé que l'augmentation de la V_{oc} était vraisemblablement due à cette plus forte inversion de type de la surface de l'absorbeur. De même, la diffusion du Cd dans le CIGS pendant le bain chimique étant plus efficace dans les absorbeurs traités au KF, le temps nécessaire pour former ces défauts compensateurs serait réduit réduisant d'autant le temps de dépôt de la couche de CdS.

Problématiques de la thèse - Le premier objectif de la thèse a été d'atteindre l'état de l'art concernant l'obtention de hauts rendements de conversion photovoltaïque par l'utilisation d'un KF-PDT. Nous avons bien mis en évidence l'augmentation de la V_{oc} par l'utilisation de ce traitement, comme l'atteste les courbes courant-tension (J-V) et de rendement quantique externe (EQE) présentées Figure 5-11. Par rapport à la cellule non traitée (REF#1), la cellule traitée (K-PDT#1) présente une V_{oc} supérieure de 35.4 mV pour un FF et un J_{sc} équivalent. Cependant, l'efficacité du KF-PDT est restreinte à des conditions expérimentales souvent difficiles à déterminer, donc à maîtriser. La Figure 5-12 illustre le fait que le

traitement KF-PDT peut également conduire à une dégradation des performances photovoltaïque des cellules. Dans ce cas la cellule non traitée (REF#2) présente un rendement de conversion énergétique de 17.3%, équivalent à la cellule non traitée (REF#1) du cas précédent (pour lequel le KF-PDT avait un effet bénéfique) mais l'utilisation du KF-PDT (K-PDT#2) conduit à une forte dégradation de tous les paramètres photovoltaïques.

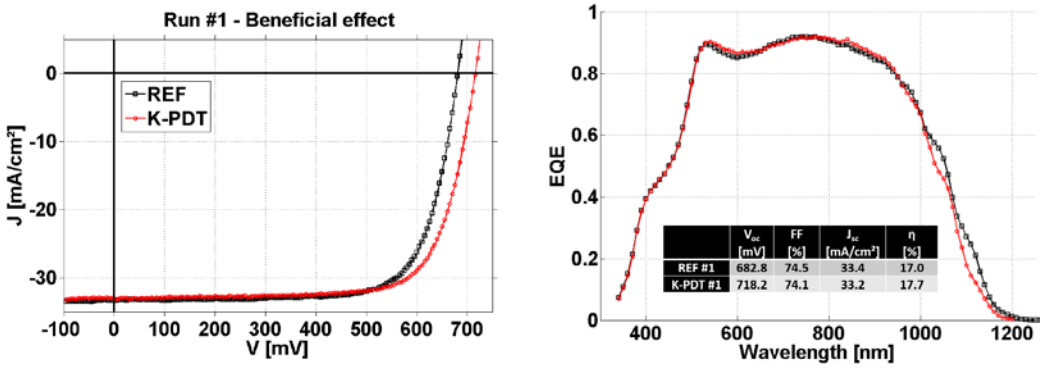

Figure 5-11 – Courbes courant-tension (gauche) et rendements quantiques externes (droite) de cellules photovoltaïques avec un absorbeur traité au KF (rouge) or non (noir) illustrant l'effet bénéfique du KF-PDT

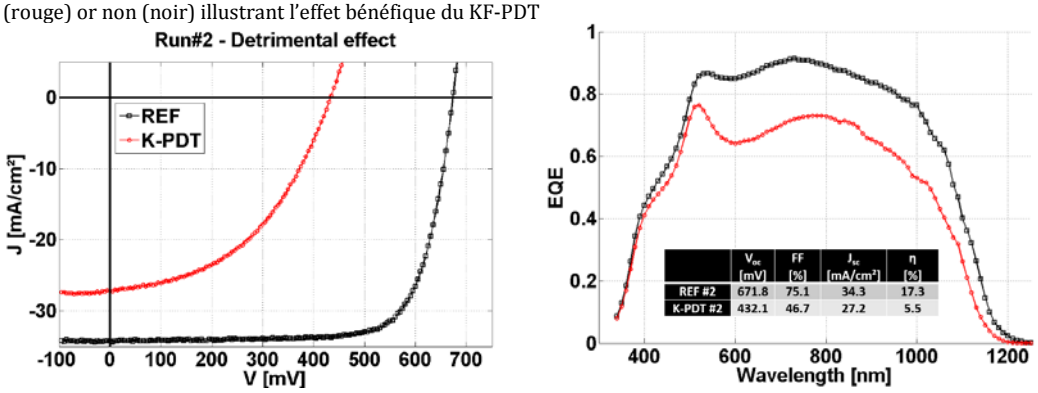

Figure 5-12 - Courbes courant-tension (gauche) et rendements quantiques externes (droite) de cellules photovoltaïques avec un absorbeur traité au KF (rouge) or non (noir) illustrant l'effet néfaste du KF-PDT

La reproducibilité des performances des dispositifs est cruciale pour une implémentation au niveau industriel. Considérant la complexité et le nombre d'étapes nécessaires à la préparation des cellules solaires, le processus doit montrer une grande tolérance aux variations des paramètres de synthèse. En l'absence de traitement KF, cette tolérance est généralement obtenue. L'utilisation du traitement KF réduit cette tolérance, ce qui tend à réduire considérablement son impact bénéfique. La première question qui se pose est donc de savoir (1) quelles sont les propriétés de l'absorbeur qui rendent l'impact du traitement KF bénéfique ou néfaste sur le rendement de conversion photovoltaïque ?

Un autre challenge concerne l'identification des méchanismes améliorant la qualité de la jonction lorsque le traitement KF est bénéfique. Un des objectifs de la thèse est de tester la validité des modèles proposés dans la littérature (forte et rapide inversion de type de la surface de l'absorbeur pendant le dépôt par bain chimique de la couche de CdS). Un second objectif de la thèse est de construire (I) un modèle de croissance pour la formation de l'hétérojonction. Ce modèle doit permettre de déterminer (2) pourquoi le temps de dépôt de la couche de CdS peut-être réduit et pourquoi une quantité minimum de KF doit être évaporée afin de tirer profit du KF-PDT ? Enfin, les modèles proposés dans la littérature ne prennent pas en compte la présence d'une couche de surface additionnelle induite par le traitement KF à la surface de l'absorbeur (non chalcopyrite). Le but de cette thèse est donc dans un second temps de (II) proposer un nouveau modèle électrique expliquant l'amélioration de la qualité de la jonction.

Modification de la surface du CIGS pendant le KF-PDT - Le premier objectif de ce travail a donc été de montrer que la présence d'une phase chalcopyrite déficitaire en cuivre (OVC) à la surface de l'absorbeur avant le KF-PDT est nécessaire pour éviter la ségrégation de Cu_xSe, très néfaste pour la qualité de la jonction. Cette nouvelle phase a été mise en évidence par spectroscopie de photoélectrons induits par rayons X (XPS), spectroscopie Raman et diffraction X en incidence rasante (GIXRD). Lorsque l'absorbeur présente un OVC avant le traitement, cette phase déficitaire en cuivre (Cu) disparait (expliquant la déplétion en Cu induite par le traitement et déjà reportée dans la littérature) au profit d'une phase superficielle (~5 nm) de $KInSe_2$. Cette phase a été mise en évidence par XPS et ce matériau est compatible avec les résultats d'une étude d'absorption X réalisée au synchrotron Soleil. La structure adamentane de cette phase est différente de la structure chalcopyrite et peu expliquer l'élargissement du gap de surface de l'absorbeur également reporté dans la littérature.

Que l'absorbeur présente un OVC ou non avant le traitement KF, nous avons mis en évidence la forte déplétion de gallium (Ga) induite par le traitement à la surface du CIGS et déjà rapportée dans la littérature. Nous avons montré que cette déplétion était due à la formation de GaF_3 qui se solubilise dans le bain de CdS. De même, dans les deux cas le traitement s'accompagne de ségrégation de Se métallique, également néfaste pour la qualité de la jonction. La quantité de Se élémentaire ségrégé est cependant plus importante dans le cas où l'absorbeur ne présente pas d'OVC.

Les équations (5.2) et (5.3) résument l'effet du traitement KF sur la surface de l'absorbeur lorsque ce dernier présente un OVC (cas bénéfique, équation 5.2) ou non (cas néfaste, équation 5.3) avant le traitement :

$$\frac{3}{2}CuIn_2GaSe_5 + 3\,KF \xrightarrow{Flux\ de\ Se} GaF_3 + 2\,KInSe_2 + \frac{1}{2}Cu_3In_2GaSe_6 + \frac{1}{2}Se^0 + \frac{1}{2}K_2Se \qquad (5.2)$$

$$Cu_3In_2GaSe_6 + 3\,KF \xrightarrow{Flux\ de\ Se} GaF_3 + 2\,CuInSe_2 + \frac{1}{2}Cu_2Se + \frac{3}{2}Se^0 + \frac{3}{2}K_2Se \qquad (5.3)$$

Modification de l'interface absorbeur/couche tampon pendant le dépôt de CdS - Nous avons montré que la présence de la couche superficielle de $KInSe_2$ modifie la croissance du CdS par bain chimique (CBD). La croissance du CdS sur $KInSe_2$ est beaucoup plus homogène que sur CIGS, comme l'atteste les clichés de la Figure 5-13 (obtenus dans un microscope électronique à balayage) de la surface d'absorbeurs traités ou non au KF et plongés pendant 3min30s dans le bain chimique de CdS. Le dépôt de CdS ne se fait plus, comme sur CIGS, uniquement sur certains plans, mais bien sur toute la surface du $KInSe_2$.

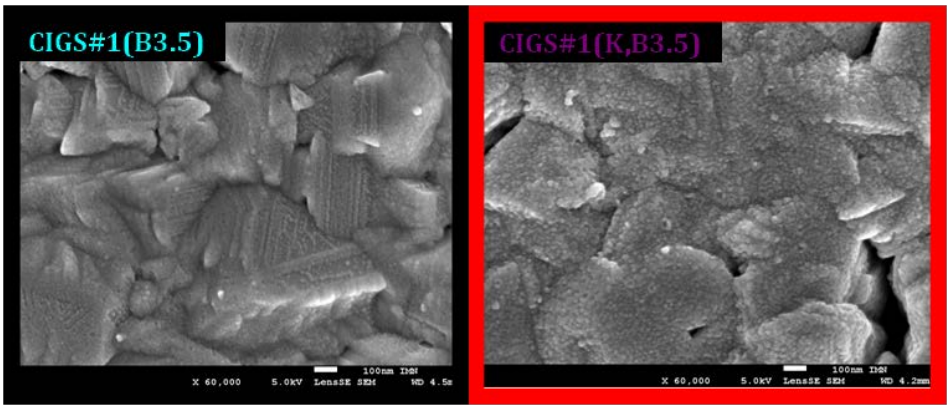

Figure 5-13 – Clichés obtenus dans un microscope électronique à balayage de la surface de l'absorbeur traité au KF (à droite) ou non (à gauche) après 3min30s dans le bain de CdS

Un nouveau matériau $CdIn_2(S,Se,OH)_4$ dérivant de la phase de $KInSe_2$ est formé à l'hétéro-interface CIGS/CdS. Cette couche d'interface est visible (i) sur le cliché de la Figure 5-14 (obtenu dans un microscope électronique à transmission) d'une couche transverse de cellule complète présentant un absorbeur ayant été traité au KF (cliché de droite). La composition de ce matériau a été obtenue par analyse chimique à fort grossissement. Cette couche résulte de la substitution du K par le Cd et du Se par le S lors du dépôt par bain chimique du CdS. Nous mettons également en évidence la ségrégation de CdSe ((ii), Figure 5-14). Nous avons également montré que le CdS au dessus de la couche de $CdIn_2(S,Se,OH)_4$ était similaire (composition, structure) au CdS présent dans les cellules non traitées.

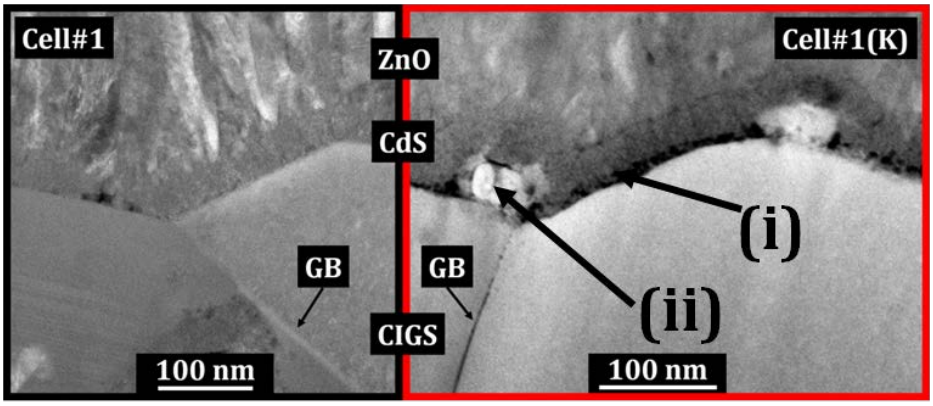

Figure 5-14 – Clichés obtenus dans un microscope électronique à transmission de coupes transverses de cellules complètes présentant un absorbeur traité au KF (à droite) ou non (à gauche)

L'équation (5.4) résume les réactions chimiques ayant lieu dans le bain chimique avant le dépôt effectif de CdS (en assumant une substitution totale de K par Cd et Se par S, ce qui est peu probable) :

$$2\,KInSe_2 + 4\,S^{2-} + 5Cd^{2+} + 2OH^- \rightarrow CdIn_2S_4 + 2\,KOH + 4\,CdSe \qquad (5.4)$$

Modification des joints de grains – Nous avons montré à l'aide de cartographie EDS que les joints de grains proche de l'interface avec le CdS présentaient une forte déplétion en Cu et en Ga, une présence de Cd et de S et une absence de ségrégation de K, laissant supposer la formation de la même phase de $CdIn_2(S,Se,OH)_4$. Plus profondément dans l'absorbeur, une analyse par sonde atomique tomographique a révélé que le potassium ségrégeait bien au niveau des joints de grains. De même, ces joints de grains ne présentent pas l'enrichissement en indium habituellement détecté au niveau des joints de grains des cellules à haut rendement. La Figure 5-15 représente les profiles de concentration (extrait de cette méthode) au niveau d'un joint de grain de CIGS traité au KF.

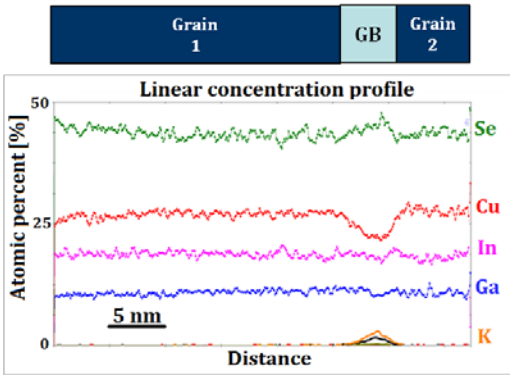

Figure 5-15 – Profils de concentrations linéaires extraits de mesures par sonde atomique tomographique au niveau d'un joint de grain dans un abasorbeur traité au KF

Modèle électrique – Des mesures de capacitance effectuées à basse température sur des cellules complètes préalablement excitées (10 min à P=P_{max} et sous une illumination AM1.5 avant de descendre en température) ont révélés que la densité de trous libres au sein des absorbeurs traités au KF était supérieure d'au moins un ordre de grandeur par rapport à celle des absorbeurs non traités. Nous suggérons que cette augmentation de la concentration de trous libres provient des changements matériaux au niveau des joints de grains ainsi que de la modification très probable de la position du niveau de Fermi[28] induit par la présence de la couche d'interface de $CdIn_2(S,Se,OH)_4$ dopée n^+. Des mesures courant-tension à basse température (I(V,T)) ont montré que les cellules traitées au KF étaient peu sujettes aux recombinaisons d'interface. Le chemin de recombinaison dominant reste dans la zone de charge d'espace (ZCE), malgré la forte diminution de la largeur de la ZCE accompagnant naturellement l'augmentation de la concentration de trous.

L'augmentation de la tension de circuit ouvert dans les cellules traitées au KF s'explique donc par :

(i) *L'augmentation de la concentration effective de trous* - Les performances des dispositifs à base d'absorbeur présentant un fort gradient de composition en gallium en surface sont particulièrement sensibles à la réduction de la largeur de la ZCE. Dans ces absorbeurs, le gap moyen dans la ZCE augmente à mesure que la ZCE s'amincie, résultant en une augmentation de l'énergie d'activation du courant de recombinaison (déterminée par I(V,T)), et donc une diminution des recombinaisons.

(ii) *Une jonction électronique enterrée* - La présence de la couche de $CdIn_2(S,Se,OH)_4$ crée une hétérojonction de type n^+p. Elle induit une position du niveau de Fermi proche de la bande de conduction à l'interface avec le CIGS, ce qui a pour effet d'enterrer la jonction électrique. Cela limite les recombinaisons d'interface, qui pourraient être renforcées par effet tunnel dû au champ électrique élevé proche de l'interface métallurgique.

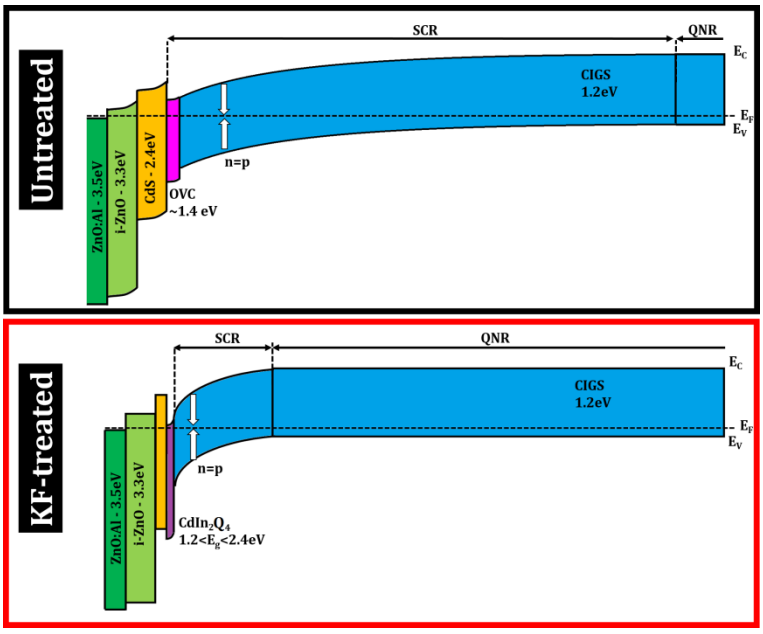

Figure 5-16 – Structures de bande suggérées pour une cellule standard (non traitée au KF, en noir) et une cellule traitée (en rouge). Les cellules sont dans un état excité et sous 0V. Les absorbeurs ne présentent aucun gradient de composition.

[28] La position du niveau de Fermi influence la conversion de défauts amphotères de la configation donneur à accepteur au sein du CIGS, et donc la concentration effective de trous.

L'augmentation de la densité de courant de court-circuit s'explique par :

(i) *La possibilité de réduire l'épaisseur de la couche de CdS* – La couche d'interface étant fortement dopée, la jonction électronique est assurée par le couple CIGS/$CdIn_2(S,Se,OH)_4$. Le bain de CdS sert donc à former la couche d'interface et le dépôt de CdS une fois la couche de $CdIn_2(S,Se,OH)_4$ formée semble donc inutile, voire néfaste. Cela explique pourquoi le temps dans le bain de CdS peut être réduit.

(ii) *L'augmentation de la longueur de diffusion* – Puisque la largeur de la ZCE est considérablement réduite par le traitement KF, la collection des porteurs photogénérés loin de la jonction devrait être diminuée. Toutefois, cette collection dans les dispositifs traités au KF est plus élevée que celle dans les cellules non traitées, comme le montre l'évolution du rendement quantique externe, aux grandes longueurs d'ondes, entre une cellule non traitée et une cellule traité au KF (Figure 5-17, à droite). Nous suggérons que cette amélioration de la collecte provient d'une amélioration de la longueur de diffusion des électrons dans le CIGS en raison des changements matériaux induits par le KF-PDT au niveau des joints de grains.

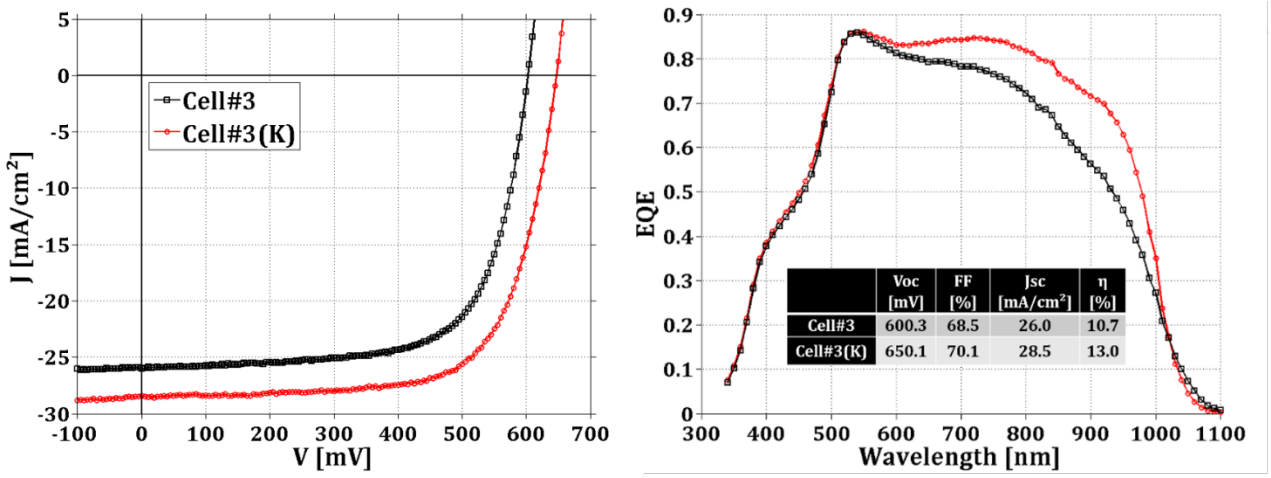

Figure 5-17 – Courbes J(V) et rendements quantiques externs de cellules sans gradient de composition, traitée (rouge) ou non (noir) au KF

A – Technical details - XPS

Setup - XPS measurements have been performed on a Kratos Nova spectrometer using a monochromatic Al Kα X-ray source with a 20 eV pass energy. XPS analyses have been performed on sample from Run#1 (grown in Na-free conditions or not) and from Run#2. The samples have been investigated either "as deposited" or rinced one minute in diluted ammonia solution.

Spectra analysis – The position of the In $3d_{5/2}$ core level at 444.7 eV corresponding to In in CIGS [143] is used as energy reference for all spectra.

Ga $2p_{3/2}$, Na 1s, Cu $2p_{3/2}$, O 1s, In $3d_{5/2}$ K 2p and Se 3d XPS peaks have been fitted by Gaussian-Lorentzian function and linear background (adjustable for SeLMM-K 2p region) in several samples. For reference samples, fits have been realized with the minimum of contributions considering reasonable (in the range given in literature for the selected element) Full Width at Half Maximum (FWHM) and an acceptable normalized residual standard deviation. For treated samples we started the fit from the result in reference samples by constraining the fit; contributions were removed or added and constraints slowly removed in order to reach an unconstrained result in good agreement with experimental data satisfying our criterion.

Se 3d peaks branching ratio 5/2:3/2 was fixed to 1.5, the spin-orbit coupling of the 3d peaks to 0.86 eV, and the FWHM limited to 1.1 eV. We tolerated a variation of 10% of the FWHM between the $3d_{5/2}$ and $3d_{3/2}$ peaks.

For the In $3d_{5/2}$ peaks, FWHM below 0.9 eV was considered for the contribution corresponding to In in CIGS, as can be found in literature [143], whereas FWHM below 1.3 eV were considered for other contributions (indium oxides or fluorides).

As FWHM are generally high for the O1s XPS peaks in CIGS, the fit of the oxygen contributions was not straightforward. However at least 4 contributions have been identified, with binding energies (BE) ranging from 529.8 to 531.9 eV. Different fits were possible, in particular for the O1s XPS peak in CIGS#2(K) that can be fitted with only 2 contributions and a residual satisfying our criterion. However in that case FWHM are too high. We then decided to start the fit from the fit result of the non rinced corresponding sample (CIGS#2(K,AG)) and added a contribution.

For the K 2p doublet the branching ratio 3/2:1/2 was fixed to 2 and the spin-orbit coupling to 2.8 eV.

XPS fits in chapter 4

Table 5.3 lists all the contributions found in the core-shells samples investigated in chapter 4; BE, FWHM and the suggested corresponding compounds are indicated.

Table 5.3 – Binding energies, suggested associated compound and FWHM of fitted XPS contributions

Core shell	Contribution			FWHM [eV]						
	Label	Binding Energy [eV]	Suggested corresponding compound	CIGS#1(SiN)	CIGS#1	CIGS#2	CIGS#1(SiN,K)	CIGS#1(K)	CIGS#2(K)	CIGS#2(K,AG)
Se $3d_{5/2}$	Se-1	54.2 ± 0.1	CIGS	0.83	0.82	0.83	0.95	0.91	0.74	0.79
	Se-2	54.9 ± 0.1	CIGS	0.92	0.86	0.90	-	-	-	-
	Se-3	55.2 ± 0.2	Se^0	-	-	-	0.86	0.93	0.94	1.11
	Se-4	53.5 ± 0.1	Indium selenide based compound	-	-	-	0.71	0.90	-	-
	Se-5	54.7 ± 0.1	$Cu_{2-x}Se$	-	-	-	-	-	0.8	0.81
K 2p	K-1	293.2 ± 0.1	indium selenide based compound	-	-	-	0.97	1.06	-	-
	K-2	293.7 ± 0.1	-	-	-	-	-	-	-	1.38
In $3d_{5/2}$	In-1	444.7 ± 0.1	CIGS	0.78	0.77	0.80	0.88	0.88	0.80	0.76
	In-2	445.3 ± 0.1	Indium oxides	0.76	0.66	0.99	0.92	0.90	1.20	1.29
	In-3	446.2 ± 0.1	InF_3	-	-	-	-	-	-	1.19
O 1s	O-1	531.7 ± 0.1	Indium oxides	1.99	2.3	1.65	2.28	2.4	2.18	1.85
	O-2	531.3 ± 0.1	Gallium oxides	-	-	-	1.55	1.75	1.35	1.38
	O-3	530.3 ± 0.1	Indium oxides	-	-	1.26	-	-	1.01	-
	O-4	529.9 ± 0.1	Alkali-related compound	-	-	-	1.06	0.99	-	-
F 1s	F-1	685.5 ± 0.1	GaF_3	-	-	-	-	-	-	1.35
Cu $2p_{3/2}$	Cu-1	932.2 ± 0.1	CIGS	0.92	0.95	1.02	0.94	0.96	0.98	1.01
	Cu-2	932.9 ± 0.1	Cu_2Se	-	-	-	-	-	1.45	1.47
Ga $2p_{3/2}$	Ga-1	1117.7±0.2	CIGS	1.14	1.12	1.23	1.15	1.24	1.11	1.16
	Ga-2	1118.6±0.2	Gallium oxides	-	-	1.40	-	-	1.42	-
	Ga-3	1119.3±0.2	GaF_3	-	-	-	-	-	-	1.53
Na 1s	Na-1	1071.4±0.1	Na “non reacted”	-	1.01	1.25	-	-	-	1.38
	Na-2	1071.9±0.1	Na “reacted”	-	1.19	1.3	-	1.09	-	-

B – Additional informations – TEM

The following figure shows the EDS mapping of Cu, In, Ga, Se, Cd, S, Zn, O and K in the near CIGS/CdS interface region of Cell#1 and Cell#1(K). The mapping of K in Cell#1 is missing due to a problem during the record of the data. Contrary to Cell#1(K), Cell#1 shows no depletion or enrichement neither at the CIGS/CdS interface nor at the GB. The EDS mapping in Cell#1(K) has been discussed in the PhD thesis.

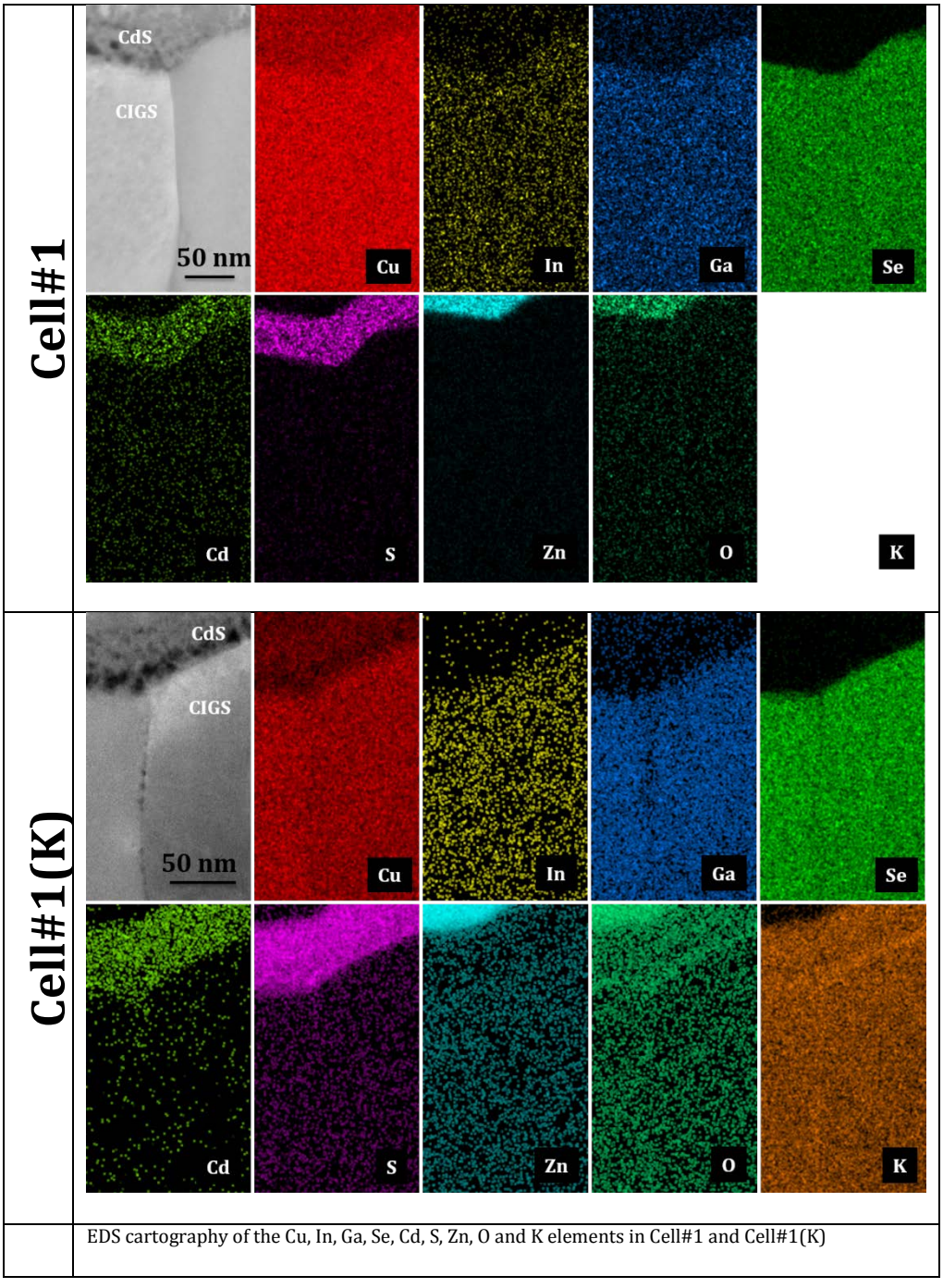

EDS cartography of the Cu, In, Ga, Se, Cd, S, Zn, O and K elements in Cell#1 and Cell#1(K)

C – Synthesis method – (CBD)CdS

Configuration – The important specificity of the (CBD)CdS deposition at the IMN is the fact that tha bath is "opened". In particular the ammonia can evaporate during the deposition. The stirrer is not in the chemical bath as it would induce preferential depositions of the CdS. The samples are agitated ramdomly by the grower.

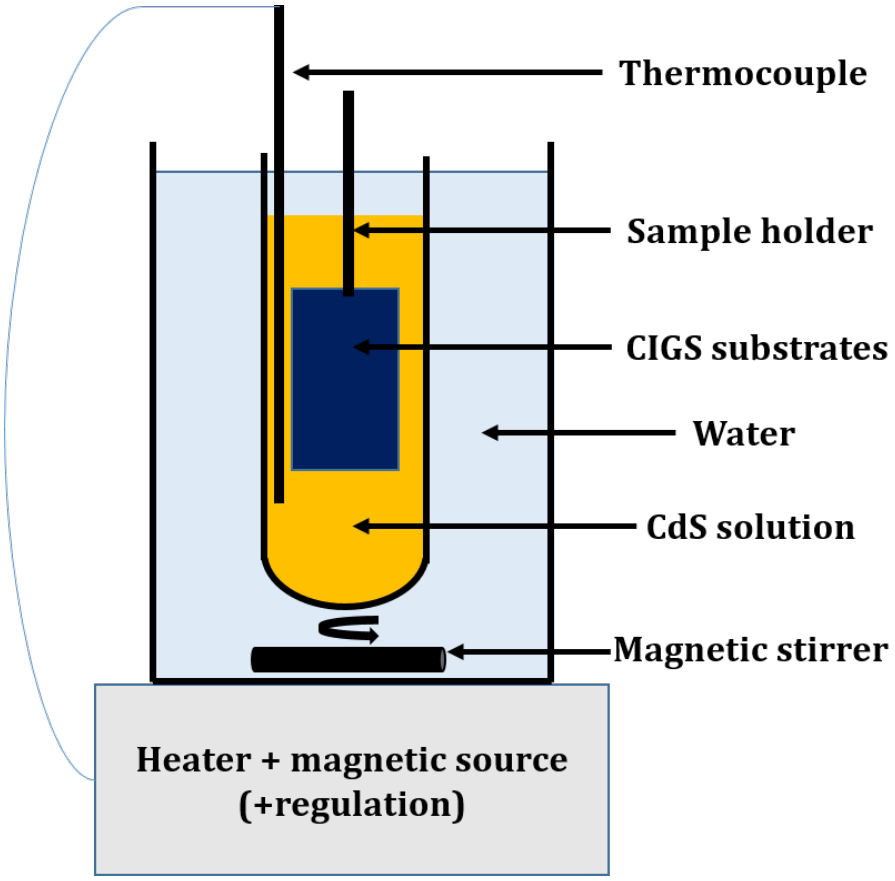

Configuration of the (CBD)CdS at the IMN

Composition of the bath - For a standard deposition we use 20 mL of NH3 (1 mol/L), 12 mL of Cd acetate dihydrate $(CH_3COO)_2Cd*H_2O$ (2.6 10^{-3} mol/L) and 12 mL of thiourea H_2NCSNH_2 (9.5 10^{-2} mol/L).

Duration – Standard duration is 7 minutes. The CdS starts to form at 2,5 min.

References

[1] C. Zheng and D. M. Kammen, "An innovation-focused roadmap for a sustainable global photovoltaic industry," *Energy Policy*, vol. 67, pp. 159–169, Apr. 2014.

[2] N. Naghavi, D. Abou-Ras, N. Allsop, N. Barreau, S. Bücheler, A. Ennaoui, C.-H. Fischer, C. Guillen, D. Hariskos, J. Herrero, R. Klenk, K. Kushiya, D. Lincot, R. Menner, T. Nakada, C. Platzer-Björkman, S. Spiering, A. n. Tiwari, and T. Törndahl, "Buffer layers and transparent conducting oxides for chalcopyrite Cu(In,Ga)(S,Se)2 based thin film photovoltaics: present status and current developments," *Prog. Photovolt. Res. Appl.*, vol. 18, no. 6, pp. 411–433, Sep. 2010.

[3] P. Jackson, D. Hariskos, R. Wuerz, O. Kiowski, A. Bauer, T. M. Friedlmeier, and M. Powalla, "Properties of Cu(In,Ga)Se2 solar cells with new record efficiencies up to 21.7%," *Phys. Status Solidi RRL – Rapid Res. Lett.*, vol. 9, no. 1, pp. 28–31, Jan. 2015.

[4] W. Shafarman, Stolt L., *Handbook of photovoltaic science and engineering*, vol. Chapter 13, p567–616. John Wiley & Sons, 2011.

[5] L. L. Kazmerski, F. R. White, and G. K. Morgan, "Thin-film CuInSe2/CdS heterojunction solar cells," *Appl. Phys. Lett.*, vol. 29, no. 4, pp. 268–270, Aug. 1976.

[6] T. Lepetit, L. Arzel, and N. Barreau, "Impact of maximum copper content during the 3-stage process on CdS thickness tolerance in Cu(In,Ga)Se2-based solar cell," *MRS Online Proc. Libr.*, vol. 1538, pp. 33–38, 2013.

[7] R. Wuerz, A. Eicke, F. Kessler, S. Paetel, S. Efimenko, and C. Schlegel, "CIGS thin-film solar cells and modules on enamelled steel substrates," *Sol. Energy Mater. Sol. Cells*, vol. 100, pp. 132–137, May 2012.

[8] A. Chirilă, S. Buecheler, F. Pianezzi, P. Bloesch, C. Gretener, A. R. Uhl, C. Fella, L. Kranz, J. Perrenoud, S. Seyrling, R. Verma, S. Nishiwaki, Y. E. Romanyuk, G. Bilger, and A. N. Tiwari, "Highly efficient Cu(In,Ga)Se2 solar cells grown on flexible polymer films," *Nat. Mater.*, vol. 10, no. 11, pp. 857–861, Nov. 2011.

[9] M. A. Green, K. Emery, Y. Hishikawa, W. Warta, and E. D. Dunlop, "Solar cell efficiency tables (Version 45)," *Prog. Photovolt. Res. Appl.*, vol. 23, no. 1, pp. 1–9, Jan. 2015.

[10] N. Kohara, S. Nishiwaki, Y. Hashimoto, T. Negami, and T. Wada, "Electrical properties of the Cu(In,Ga)Se2/ MoSe2/Mo structure," *Sol. Energy Mater. Sol. Cells*, vol. 67, no. 1–4, pp. 209–215, Mar. 2001.

[11] J.-H. Yoon, J.-H. Kim, W. M. Kim, J.-K. Park, Y.-J. Baik, T.-Y. Seong, and J. Jeong, "Electrical properties of CIGS/Mo junctions as a function of MoSe2 orientation and Na doping," *Prog. Photovolt. Res. Appl.*, vol. 22, no. 1, pp. 90–96, Jan. 2014.

[12] R. Caballero, M. Nichterwitz, A. Steigert, A. Eicke, I. Lauermann, H. W. Schock, and C. A. Kaufmann, "Impact of Na on MoSe2 formation at the CIGSe/Mo interface in thin-film solar cells on polyimide foil at low process temperatures," *Acta Mater.*, vol. 63, pp. 54–62, Jan. 2014.

[13] S. Niki, M. Contreras, I. Repins, M. Powalla, K. Kushiya, S. Ishizuka, and K. Matsubara, "CIGS absorbers and processes," *Prog. Photovolt. Res. Appl.*, vol. 18, no. 6, pp. 453–466, 2010.

[14] A. J. McEvoy and T. Markvart, *Practical Handbook of Photovoltaics: Fundamentals and Applications*. Academic Press, 2012.

[15] S. Siebentritt, M. Igalson, C. Persson, and S. Lany, "The electronic structure of chalcopyrites—bands, point defects and grain boundaries," *Prog. Photovolt. Res. Appl.*, vol. 18, no. 6, pp. 390–410, Sep. 2010.

[16] J. Malmström, "On Generation and Recombination in Cu(In,Ga)Se2 Thin-Film Solar Cells," Uppsala University, 2005.

[17] M. Gloeckler, "Device physics of Cu (In, Ga) Se2 thin-film solar cells," Colorado state University, 2005.
[18] S. S. Hegedus and W. N. Shafarman, "Thin-film solar cells: device measurements and analysis," *Prog. Photovolt. Res. Appl.*, vol. 12, no. 2–3, pp. 155–176, Mar. 2004.
[19] C.-T. Sah, R. N. Noyce, and W. Shockley, "Carrier Generation and Recombination in P-N Junctions and P-N Junction Characteristics," *Proc. IRE*, vol. 45, no. 9, pp. 1228–1243, Sep. 1957.
[20] P. Zabierowski, U. Rau, and M. Igalson, "Classification of metastabilities in the electrical characteristics of ZnO/CdS/Cu(In,Ga)Se2 solar cells," *Thin Solid Films*, vol. 387, no. 1–2, pp. 147–150, May 2001.
[21] U. Rau and H.-W. Schock, "Electronic properties of Cu (In, Ga) Se2 heterojunction solar cells–recent achievements, current understanding, and future challenges," *Appl. Phys. A*, vol. 69, no. 2, pp. 131–147, 1999.
[22] V. Nadenau, U. Rau, A. Jasenek, and H. W. Schock, "Electronic properties of CuGaSe2-based heterojunction solar cells. Part I. Transport analysis," *J. Appl. Phys.*, vol. 87, no. 1, pp. 584–593, Jan. 2000.
[23] M. Rusu, A. Rumberg, S. Schuler, S. Nishiwaki, R. Würz, S. M. Babu, M. Dziedzina, C. Kelch, S. Siebentritt, R. Klenk, T. Schedel-Niedrig, and M. C. Lux-Steiner, "Optimisation of the CBD CdS deposition parameters for ZnO/CdS/CuGaSe2/Mo solar cells," *J. Phys. Chem. Solids*, vol. 64, no. 9–10, pp. 1849–1853, Sep. 2003.
[24] M. Turcu and U. Rau, "Compositional trends of defect energies, band alignments, and recombination mechanisms in the Cu(In,Ga)(Se,S)2 alloy system," *Thin Solid Films*, vol. 431–432, pp. 158–162, mai 2003.
[25] T. Godecke, T. Haalboom, and F. Ernst, "Phase equilibria of Cu-In-Se. I. Stable states and nonequilibrium states of the In2Se3-Cu2Se subsystem," *Z. Für Met.*, vol. 91, no. 8, pp. 622–634, 2000.
[26] B. J. Stanbery, "Copper Indium Selenides and Related Materials for Photovoltaic Devices," *Crit. Rev. Solid State Mater. Sci.*, vol. 27, no. 2, pp. 73–117, Apr. 2002.
[27] U. Rau and H. W. Schock, *Cu(In,Ga)Se2 SOLAR CELLS (chap7) in Clean electricity from photovoltaics*, London Imperial College Press. 2001.
[28] S. Wei, S. B. Zhang, and A. Zunger, "Effects of Ga Addition to Cuinse{sub 2} on Its Electronic, Structural, and Defect Properties," *Appl. Phys. Lett.*, vol. 72, no. 24, Jun. 1998.
[29] R. Herberholz, U. Rau, H. W. Schock, T. Haalboom, T. Gödecke, F. Ernst, C. Beilharz, K. W. Benz, and D. Cahen, "Phase segregation, Cu migration and junction formation in Cu(In, Ga)Se $_2$," *Eur. Phys. J. Appl. Phys.*, vol. 6, no. 2, pp. 131–139, May 1999.
[30] S. B. Zhang, S.-H. Wei, A. Zunger, and H. Katayama-Yoshida, "Defect physics of the CuInSe2 chalcopyrite semiconductor," *Phys. Rev. B*, vol. 57, no. 16, pp. 9642–9656, avril 1998.
[31] S.-H. Wei, S. B. Zhang, and A. Zunger, "Effects of Na on the electrical and structural properties of CuInSe2," *J. Appl. Phys.*, vol. 85, no. 10, pp. 7214–7218, May 1999.
[32] J. E. Jaffe and A. Zunger, "Defect-induced nonpolar-to-polar transition at the surface of chalcopyrite semiconductors," *Phys. Rev. B*, vol. 64, no. 24, p. 241304, Nov. 2001.
[33] C. Heske, D. Eich, R. Fink, E. Umbach, T. van Buuren, C. Bostedt, L. J. Terminello, S. Kakar, M. M. Grush, T. A. Callcott, F. J. Himpsel, D. L. Ederer, R. C. C. Perera, W. Riedl, and F. Karg, "Observation of intermixing at the buried CdS/Cu(In, Ga)Se2 thin film solar cell heterojunction," *Appl. Phys. Lett.*, vol. 74, no. 10, pp. 1451–1453, Mar. 1999.
[34] T. Nakada and A. Kunioka, "Direct evidence of Cd diffusion into Cu(In, Ga)Se2 thin films during chemical-bath deposition process of CdS films," *Appl. Phys. Lett.*, vol. 74, no. 17, pp. 2444–2446, Apr. 1999.
[35] D. Liao and A. Rockett, "Cd doping at the CuInSe2/CdS heterojunction," *J. Appl. Phys.*, vol. 93, no. 11, pp. 9380–9382, Jun. 2003.
[36] K. Hiepko, J. Bastek, R. Schlesiger, G. Schmitz, R. Wuerz, and N. A. Stolwijk, "Diffusion and incorporation of Cd in solar-grade Cu(In,Ga)Se2 layers," *Appl. Phys. Lett.*, vol. 99, no. 23, p. 234101, Dec. 2011.

[37] J. B. Varley and V. Lordi, "Intermixing at the absorber-buffer layer interface in thin-film solar cells: The electronic effects of point defects in Cu(In,Ga)(Se,S)2 and Cu2ZnSn(Se,S)4 devices," *J. Appl. Phys.*, vol. 116, no. 6, p. 063505, Aug. 2014.
[38] A. Z. Stephan Lany, "Light and bias-induced metastabilities in Cu(In,Ga)Se2 based solar cells caused by the (VSe-VCu) vacancy complex," *J. Appl. Phys. - J APPL PHYS*, vol. 100, no. 11, 2006.
[39] J.-F. Guillemoles, L. Kronik, D. Cahen, U. Rau, A. Jasenek, and H.-W. Schock, "Stability Issues of Cu(In,Ga)Se2-Based Solar Cells," *J. Phys. Chem. B*, vol. 104, no. 20, pp. 4849–4862, May 2000.
[40] C. Persson, Y.-J. Zhao, S. Lany, and A. Zunger, "n-type doping of CuInSe2 and CuGaSe2," *Phys. Rev. B*, vol. 72, no. 3, p. 035211, Jul. 2005.
[41] A. Niemegeers, M. Burgelman, R. Herberholz, U. Rau, D. Hariskos, and H.-W. Schock, "Model for electronic transport in Cu(In,Ga)Se2 solar cells," *Prog. Photovolt. Res. Appl.*, vol. 6, no. 6, pp. 407–421, Nov. 1998.
[42] M. Gloeckler and J. R. Sites, "Efficiency limitations for wide-band-gap chalcopyrite solar cells," *Thin Solid Films*, vol. 480–481, pp. 241–245, Jun. 2005.
[43] R. Herberholz, V. Nadenau, U. Rühle, C. Köble, H. W. Schock, and B. Dimmler, "Prospects of wide-gap chalcopyrites for thin film photovoltaic modules," *Sol. Energy Mater. Sol. Cells*, vol. 49, no. 1–4, pp. 227–237, Dec. 1997.
[44] J. Heath, J. Cohen, W. Shafarman, D. Liao, and A. Rockett, "Effect of Ga Content on Defect States in $CuIn_{1-x}Ga_xSe_2$ Photovoltaic Devices," *Fac. Publ.*, Jan. 2002.
[45] W. Wang, S.-Y. Han, S.-J. Sung, D.-H. Kim, and C.-H. Chang, "8.01% CuInGaSe2 solar cells fabricated by air-stable low-cost inks," *Phys. Chem. Chem. Phys.*, vol. 14, no. 31, pp. 11154–11159, Jul. 2012.
[46] D. Lincot, J. F. Guillemoles, S. Taunier, D. Guimard, J. Sicx-Kurdi, A. Chaumont, O. Roussel, O. Ramdani, C. Hubert, J. P. Fauvarque, N. Bodereau, L. Parissi, P. Panheleux, P. Fanouillere, N. Naghavi, P. P. Grand, M. Benfarah, P. Mogensen, and O. Kerrec, "Chalcopyrite thin film solar cells by electrodeposition," *Sol. Energy*, vol. 77, no. 6, pp. 725–737, Dec. 2004.
[47] V. S. Saji, I.-H. Choi, and C.-W. Lee, "Progress in electrodeposited absorber layer for CuIn(1−x)GaxSe2 (CIGS) solar cells," *Sol. Energy*, vol. 85, no. 11, pp. 2666–2678, Nov. 2011.
[48] K. Kushiya, "CIS-based thin-film PV technology in solar frontier K.K.," *Sol. Energy Mater. Sol. Cells*, vol. 122, pp. 309–313, Mar. 2014.
[49] W. N. Shafarman and J. Zhu, "Effect of substrate temperature and depostion profile on evaporated Cu(InGa)Se2 films and devices," *Thin Solid Films*, vol. 361–362, pp. 473–477, Feb. 2000.
[50] M. A. Contreras, J. Tuttle, A. Gabor, A. Tennant, K. Ramanathan, S. Asher, A. Franz, J. Keane, L. Wang, J. Scofield, and R. Noufi, "High efficiency Cu(In,Ga)Se2-based solar cells: processing of novel absorber structures," in *IEEE Photovoltaic Specialists Conference - 1994, 1994 IEEE First World Conference on Photovoltaic Energy Conversion, 1994., Conference Record of the Twenty Fourth*, 1994, vol. 1, pp. 68–75 vol.1.
[51] N. Barreau, T. Painchaud, F. Couzinié-Devy, L. Arzel, and J. Kessler, "Recrystallization of CIGSe layers grown by three-step processes: A model based on grain boundary migration," *Acta Mater.*, vol. 58, no. 17, pp. 5572–5577, Oct. 2010.
[52] J. Kessler, J. Scholdstrom, and L. Stolt, "Rapid Cu(In,Ga)Se2 growth using end point detection," in *Conference Record of the Twenty-Eighth IEEE Photovoltaic Specialists Conference, 2000*, 2000, pp. 509–512.
[53] O. Lundberg, J. Lu, A. Rockett, M. Edoff, and L. Stolt, "Diffusion of indium and gallium in Cu(In,Ga)Se2 thin film solar cells," *J. Phys. Chem. Solids*, vol. 64, no. 9–10, pp. 1499–1504, Sep. 2003.
[54] A. M. Gabor, J. R. Tuttle, D. S. Albin, M. A. Contreras, R. Noufi, and A. M. Hermann, "High-efficiency CuInxGa1−xSe2 solar cells made from (Inx,Ga1−x)2Se3 precursor films," *Appl. Phys. Lett.*, vol. 65, no. 2, pp. 198–200, Jul. 1994.
[55] T. Lepetit, D. Mangin, E. Gautron, M. Tomassini, S. Harel, L. Arzel, and N. Barreau, "Impact of DC-power during Mo back contact sputtering on the alkali distribution in Cu(In,Ga)Se2-based thin film solar cells," *Thin Solid Films*, vol. 582, pp. 304–307, mai 2015.
[56] O. Lundberg, M. Edoff, and L. Stolt, "The effect of Ga-grading in CIGS thin film solar cells," *Thin Solid Films*, vol. 480–481, pp. 520–525, Jun. 2005.

[57] M. Pawłowski, P. Zabierowski, R. Bacewicz, and N. Barreau, "Influence of Ga-notch position on recombination processes in Cu(In,Ga)Se2-based solar cells investigated by means of photoluminescence," *Thin Solid Films*, vol. 535, pp. 336–339, mai 2013.
[58] T. Dullweber, G. Hanna, W. Shams-Kolahi, A. Schwartzlander, M. A. Contreras, R. Noufi, and H. W. Schock, "Study of the effect of gallium grading in Cu(In,Ga)Se2," *Thin Solid Films*, vol. 361–362, pp. 478–481, Feb. 2000.
[59] M. Gloeckler and J. R. Sites, "Band-gap grading in Cu(In,Ga)Se2 solar cells," *J. Phys. Chem. Solids*, vol. 66, no. 11, pp. 1891–1894, Nov. 2005.
[60] O. Lundberg, M. Bodegård, J. Malmström, and L. Stolt, "Influence of the Cu(In,Ga)Se2 thickness and Ga grading on solar cell performance," *Prog. Photovolt. Res. Appl.*, vol. 11, no. 2, pp. 77–88, Mar. 2003.
[61] Nishiwaki, S., et al., "Preparation of Cu (In, Ga) Se 2 thin films from In–Ga–Se precursors for high-efficiency solar cells.," *J. Mater. Res.*, vol. 14, no. 12, pp. 4514–4520, 1999.
[62] J. Kessler, C. Chityuttakan, J. Lu, J. Schöldström, and L. Stolt, "Cu(In,Ga)Se2 thin films grown with a Cu-poor/rich/poor sequence: growth model and structural considerations," *Prog. Photovolt. Res. Appl.*, vol. 11, no. 5, pp. 319–331, Aug. 2003.
[63] R. Klenk, T. Walter, H.-W. Schock, and D. Cahen, "A model for the successful growth of polycrystalline films of CuInSe2 by multisource physical vacuum evaporation," *Adv. Mater.*, vol. 5, no. 2, pp. 114–119, Feb. 1993.
[64] S. Niki, P. J. Fons, A. Yamada, Y. Lacroix, H. Shibata, H. Oyanagi, M. Nishitani, T. Negami, and T. Wada, "Effects of the surface Cu2-xSe phase on the growth and properties of CuInSe2 films," *Appl. Phys. Lett.*, vol. 74, p. 1630, Mar. 1999.
[65] R. D. Doherty, D. A. Hughes, F. J. Humphreys, J. J. Jonas, D. J. Jensen, M. E. Kassner, W. E. King, T. R. McNelley, H. J. McQueen, and A. D. Rollett, "Current issues in recrystallization: a review," *Mater. Sci. Eng. A*, vol. 238, no. 2, pp. 219–274, Nov. 1997.
[66] A. Luque and S. Hegedus, *Handbook of Photovoltaic Science and Engineering*. John Wiley & Sons, 2011.
[67] A. J. Nelson, S. Gebhard, A. Rockett, E. Colavita, M. Engelhardt, and H. Höchst, "Synchrotron-radiation photoemission study of CdS/CuInSe2 heterojunction formation," *Phys. Rev. B*, vol. 42, no. 12, pp. 7518–7523, Oct. 1990.
[68] D. Schmid, M. Ruckh, F. Grunwald, and H. W. Schock, "Chalcopyrite/defect chalcopyrite heterojunctions on the basis of CuInSe2," *J. Appl. Phys.*, vol. 73, no. 6, pp. 2902–2909, Mar. 1993.
[69] T. Löher, W. Jaegermann, and C. Pettenkofer, "Formation and electronic properties of the CdS/CuInSe2 (011) heterointerface studied by synchrotron-induced photoemission," *J. Appl. Phys.*, vol. 77, no. 2, pp. 731–738, Jan. 1995.
[70] L. Kronik, L. Burstein, M. Leibovitch, Y. Shapira, D. Gal, E. Moons, J. Beier, G. Hodes, D. Cahen, D. Hariskos, R. Klenk, and H.-W. Schock, "Band diagram of the polycrystalline CdS/Cu(In,Ga)Se2 heterojunction," *Appl. Phys. Lett.*, vol. 67, no. 10, pp. 1405–1407, Sep. 1995.
[71] J. Kessler, K. O. Velthaus, M. Ruckh, R. Laichinger, H. W. Schock, D. Lincot, R. Ortega, and J. Vedel, "Chemical bath deposition of CdS on CuInSe2, etching effects and growth kinetics," *Proccedings Sixth Int PVSEC*, pp. 1005–1010, 1992.
[72] C. Heske, D. Eich, R. Fink, E. Umbach, S. Kakar, T. van Buuren, C. Bostedt, L. J. Terminello, M. M. Grush, T. A. Callcott, F. J. Himpsel, D. L. Ederer, R. C. C. Perera, W. Riedl, and F. Karg, "Localization of Na impurities at the buried CdS/Cu(In, Ga)Se2 heterojunction," *Appl. Phys. Lett.*, vol. 75, no. 14, pp. 2082–2084, Oct. 1999.
[73] W. Li, S. R. Cohen, and D. Cahen, "Effect of chemical treatments on nm-scale electrical characteristics of polycrystalline thin film Cu(In,Ga)Se2 surfaces," *Sol. Energy Mater. Sol. Cells*, vol. 120, Part B, pp. 500–505, Jan. 2014.
[74] D. Liao and A. Rockett, "Epitaxial growth of Cu(In, Ga)Se2 on GaAs(110)," *J. Appl. Phys.*, vol. 91, no. 4, pp. 1978–1983, Feb. 2002.
[75] S. Kashida, W. Shimosaka, M. Mori, and D. Yoshimura, "Valence band photoemission study of the copper chalcogenide compounds, Cu2S, Cu2Se and Cu2Te," *J. Phys. Chem. Solids*, vol. 64, no. 12, pp. 2357–2363, Dec. 2003.

[76] H. Mönig, C.-H. Fischer, A. Grimm, B. Johnson, C. A. Kaufmann, R. Caballero, I. Lauermann, and M. C. Lux-Steiner, "Surface Cu-depletion of Cu(In,Ga)Se2 thin films: Further experimental evidence for a defect-induced surface reconstruction," *J. Appl. Phys.*, vol. 107, no. 11, p. 113540, Jun. 2010.
[77] H. Z. Xiao, L.-C. Yang, and A. Rockett, "Structural, optical, and electrical properties of epitaxial chalcopyrite CuIn3Se5 films," *J. Appl. Phys.*, vol. 76, no. 3, pp. 1503–1510, Aug. 1994.
[78] S. B. Zhang, S.-H. Wei, and A. Zunger, "Intrinsic n-type versus p-type doping asymmetry and the defect physics of ZnO," *Phys. Rev. B*, vol. 63, no. 7, p. 075205, Jan. 2001.
[79] M. A. Contreras and R. Noufi, "Chalcopyrite Cu(In,Ga)Se2 and defect-chalcopyrite Cu(In,Ga)3Se5 materials in photovoltaic P *J. Cryst. Growth*, vol. 174, no. 1–4, pp. 283–288, Apr. 1997.
[80] P. Migliorato, J. L. Shay, H. M. Kasper, and S. Wagner, "Analysis of the electrical and luminescent properties of CuInSe2," *J. Appl. Phys.*, vol. 46, no. 4, pp. 1777–1782, Apr. 1975.
[81] M. Rusu, M. Bär, S. Lehmann, S. Sadewasser, L. Weinhardt, C. A. Kaufmann, E. Strub, J. Röhrich, W. Bohne, I. Lauermann, C. Jung, C. Heske, and M. C. Lux-Steiner, "Three-dimensional structure of the buffer/absorber interface in CdS/CuGaSe2 based thin film solar cells," *Appl. Phys. Lett.*, vol. 95, no. 17, p. 173502, Oct. 2009.
[82] T. Nakada, "Nano-structural investigations on Cd-doping into Cu(In,Ga)Se2 thin films by chemical bath deposition process," *Thin Solid Films*, vol. 361–362, pp. 346–352, février 2000.
[83] U. Rau, K. Taretto, and S. Siebentritt, "Grain boundaries in Cu(In, Ga)(Se, S)2 thin-film solar cells," *Appl. Phys. A*, vol. 96, no. 1, pp. 221–234, Dec. 2008.
[84] Y. Yan, C.-S. Jiang, R. Noufi, S.-H. Wei, H. R. Moutinho, and M. M. Al-Jassim, "Electrically Benign Behavior of Grain Boundaries in Polycrystalline ${\mathrm{CuInSe}}_{2}$ Films," *Phys. Rev. Lett.*, vol. 99, no. 23, p. 235504, Dec. 2007.
[85] D. Cahen and R. Noufi, "Defect chemical explanation for the effect of air anneal on CdS/CuInSe2 solar cell performance," *Appl. Phys. Lett.*, vol. 54, no. 6, pp. 558–560, Feb. 1989.
[86] L. Kronik, U. Rau, J.-F. Guillemoles, D. Braunger, H.-W. Schock, and D. Cahen, "Interface redox engineering of Cu(In,Ga)Se2 – based solar cells: oxygen, sodium, and chemical bath effects," *Thin Solid Films*, vol. 361–362, pp. 353–359, février 2000.
[87] M. Raghuwanshi, E. Cadel, P. Pareige, S. Duguay, F. Couzinie-Devy, L. Arzel, and N. Barreau, "Influence of grain boundary modification on limited performance of wide bandgap Cu(In,Ga)Se2 solar cells," *Appl. Phys. Lett.*, vol. 105, no. 1, p. 013902, Jul. 2014.
[88] M. J. Hetzer, Y. M. Strzhemechny, M. Gao, M. A. Contreras, A. Zunger, and L. J. Brillson, "Direct observation of copper depletion and potential changes at copper indium gallium diselenide grain boundaries," *Appl. Phys. Lett.*, vol. 86, no. 16, p. 162105, Apr. 2005.
[89] J. Hedstrom, H. Ohlsen, M. Bodegard, A. Kylner, L. Stolt, D. Hariskos, M. Ruckh, and H. Schock, "ZnO/CdS/Cu(In,Ga)Se2 thin film solar cells with improved performance," in *, Conference Record of the Twenty Third IEEE Photovoltaic Specialists Conference, 1993*, 1993, pp. 364–371.
[90] J. H. Scofield, S. Asher, D. Albin, J. Tuttle, M. Contreras, D. Niles, R. Reedy, A. Tennant, and R. Noufi, "Sodium diffusion, selenization, and microstructural effects associated with various molybdenum back contact layers for CIS-based solar cells," in *IEEE Photovoltaic Specialists Conference - 1994, 1994 IEEE First World Conference on Photovoltaic Energy Conversion, 1994., Conference Record of the Twenty Fourth*, 1994, vol. 1, pp. 164–167 vol.1.
[91] M. Ruckh, D. Schmid, M. Kaiser, R. Schaffler, T. Walter, and H. W. Schock, "Influence of substrates on the electrical properties of Cu(In,Ga)Se 2 thin films," in *IEEE Photovoltaic Specialists Conference - 1994, 1994 IEEE First World Conference on Photovoltaic Energy Conversion, 1994., Conference Record of the Twenty Fourth*, 1994, vol. 1, pp. 156–159 vol.1.
[92] M. Bodegård, K. Granath, L. Stolt, and A. Rockett, "The behaviour of Na implanted into Mo thin films during annealing," *Sol. Energy Mater. Sol. Cells*, vol. 58, no. 2, pp. 199–208, juin 1999.
[93] E. Gautron, M. Tomassini, L. Arzel, and N. Barreau, "Investigation of intergrain compounds in sputtered Mo films applied in CuIn1 – xGaxSe2-based solar cell," *Surf. Coat. Technol.*, vol. 211, pp. 29–32, Oct. 2012.
[94] P. Bommersbach, L. Arzel, M. Tomassini, E. Gautron, C. Leyder, M. Urien, D. Dupuy, and N. Barreau, "Influence of Mo back contact porosity on co-evaporated Cu(In,Ga)Se2 thin film properties and related solar cell," *Prog. Photovolt. Res. Appl.*, vol. 21, no. 3, pp. 332–343, mai 2013.

[95] C. Roger, G. Altamura, F. Emieux, O. Sicardy, F. Roux, R. Fillon, P. Faucherand, N. Karst, H. Fournier, L. Grenet, F. Ducroquet, A. Brioude, and S. Perraud, "Sodium-doped Mo back contacts for Cu(In,Ga)Se2 solar cells on Ti foils: Growth, morphology, and sodium diffusion," *J. Renew. Sustain. Energy*, vol. 6, no. 1, p. 011405, Feb. 2014.

[96] P. Blösch, S. Nishiwaki, L. Kranz, C. M. Fella, F. Pianezzi, T. Jäger, C. Adelhelm, E. Franzke, S. Buecheler, and A. N. Tiwari, "Sodium-doped molybdenum back contact designs for Cu(In,Ga)Se2 solar cells," *Sol. Energy Mater. Sol. Cells*, vol. 124, pp. 10–16, mai 2014.

[97] M. A. Contreras, B. Egaas, P. Dippo, J. Webb, J. Granata, K. Ramanathan, S. Asher, A. Swartzlander, and R. Noufi, "On the role of Na and modifications to Cu(In,Ga)Se2 absorber materials using thin-MF (M=Na, K, Cs) precursor layers [solar cells]," in *, Conference Record of the Twenty-Sixth IEEE Photovoltaic Specialists Conference, 1997*, 1997, pp. 359–362.

[98] D. Rudmann, A. F. da Cunha, M. Kaelin, F. Kurdesau, H. Zogg, A. N. Tiwari, and G. Bilger, "Efficiency enhancement of Cu(In,Ga)Se2 solar cells due to post-deposition Na incorporation," *Appl. Phys. Lett.*, vol. 84, no. 7, pp. 1129–1131, Feb. 2004.

[99] V. Probst, J. Rimmasch, W. Riedl, W. Stetter, J. Holz, H. Harms, F. Karg, and H. W. Schock, "The impact of controlled sodium incorporation on rapid thermal processed Cu(InGa)Se2-thin films and devices," in *IEEE Photovoltaic Specialists Conference - 1994, 1994 IEEE First World Conference on Photovoltaic Energy Conversion, 1994., Conference Record of the Twenty Fourth*, 1994, vol. 1, pp. 144–147 vol.1.

[100] J. E. Granata, J. R. Sites, S. Asher, and R. J. Matson, "Quantitative incorporation of sodium in CuInSe2 and Cu(In,Ga)Se2 photovoltaic devices," in *, Conference Record of the Twenty-Sixth IEEE Photovoltaic Specialists Conference, 1997*, 1997, pp. 387–390.

[101] B. M. Keyes, F. Hasoon, P. Dippo, A. Balcioglu, and F. Abulfotuh, "Influence of Na on the electro-optical properties of Cu(In,Ga)Se 2," in *, Conference Record of the Twenty-Sixth IEEE Photovoltaic Specialists Conference, 1997*, 1997, pp. 479–482.

[102] L. Kronik, D. Cahen, and H. W. Schock, "Effects of Sodium on Polycrystalline Cu(In,Ga)Se2 and Its Solar Cell Performance," *Adv. Mater.*, vol. 10, no. 1, pp. 31–36, Jan. 1998.

[103] A. Urbaniak, M. Igalson, F. Pianezzi, S. Bücheler, A. Chirilă, P. Reinhard, and A. N. Tiwari, "Effects of Na incorporation on electrical properties of Cu(In,Ga)Se2-based photovoltaic devices on polyimide substrates," *Sol. Energy Mater. Sol. Cells*, vol. 128, pp. 52–56, Sep. 2014.

[104] K. Granath, M. Bodegård, and L. Stolt, "The effect of NaF on Cu(In, Ga)Se2 thin film solar cells," *Sol. Energy Mater. Sol. Cells*, vol. 60, no. 3, pp. 279–293, Jan. 2000.

[105] A. Laemmle, R. Wuerz, T. Schwarz, O. Cojocaru-Mirédin, P.-P. Choi, and M. Powalla, "Investigation of the diffusion behavior of sodium in Cu(In,Ga)Se2 layers," *J. Appl. Phys.*, vol. 115, no. 15, p. 154501, Apr. 2014.

[106] E. Cadel, N. Barreau, J. Kessler, and P. Pareige, "Atom probe study of sodium distribution in polycrystalline Cu(In,Ga)Se2 thin film," *Acta Mater.*, vol. 58, no. 7, pp. 2634–2637, avril 2010.

[107] O. Cojocaru-Mirédin, P.-P. Choi, D. Abou-Ras, S. S. Schmidt, R. Caballero, and D. Raabe, "Characterization of Grain Boundaries in Cu(In,Ga)Se Films Using Atom-Probe Tomography," *IEEE J. Photovolt.*, vol. 1, no. 2, pp. 207–212, Oct. 2011.

[108] C. Heske, D. Eich, U. Groh, R. Fink, E. Umbach, T. van Buuren, C. Bostedt, N. Franco, L. J. Terminello, M. M. Grush, T. A. Callcott, F. J. Himpsel, D. L. Ederer, R. C. C. Perera, W. Riedl, and F. Karg, "Self-limitation of Na content at the CdS/Cu(In,Ga)Se2 solar cell heterojunction," *Thin Solid Films*, vol. 361–362, pp. 360–363, février 2000.

[109] D. Rudmann, G. Bilger, M. Kaelin, F.-J. Haug, H. Zogg, and A. N. Tiwari, "Effects of NaF coevaporation on structural properties of Cu(In,Ga)Se2 thin films," *Thin Solid Films*, vol. 431–432, pp. 37–40, mai 2003.

[110] M. A. Contreras, B. Egaas, D. King, A. Swartzlander, and T. Dullweber, "Texture manipulation of CuInSe2 thin films," *Thin Solid Films*, vol. 361–362, pp. 167–171, Feb. 2000.

[111] B. J. Stanbery, A. Davydov, C. H. Chang, and T. J. Anderson, "NREL/SNL Photovoltaics Program Review.," *Proceedings of the 14th Conference*, pp. 579–588, 1996.

[112] B. J. Stanbery, E. S. Lambers, and T. J. Anderson, "XPS studies of sodium compound formation and surface segregation in CIGS thin films [solar cells]," in *, Conference Record of the Twenty-Sixth IEEE Photovoltaic Specialists Conference, 1997*, 1997, pp. 499–502.

[113] S. Seyrling, A. Chirila, D. Güttler, P. Blösch, F. Pianezzi, R. Verma, S. Bücheler, S. Nishiwaki, Y. E. Romanyuk, P. Rossbach, and A. N. Tiwari, "CuIn1−xGaxSe2 growth process modifications: Influences on microstructure, Na distribution, and device properties," *Sol. Energy Mater. Sol. Cells*, vol. 95, no. 6, pp. 1477–1481, Jun. 2011.

[114] P. Villars, *Pearson's handbook: crystallographic data for intermetallic phases*. ASM international, 1997.

[115] H. Rodriguez-Alvarez, R. Mainz, R. Caballero, D. Abou-Ras, M. Klaus, S. Gledhill, A. Weber, C. A. Kaufmann, and H.-W. Schock, "Real-time study of Ga diffusion processes during the formation of Cu(In,Ga)Se2: The role of Cu and Na content," *Sol. Energy Mater. Sol. Cells*, vol. 116, pp. 102–109, Sep. 2013.

[116] F. Couzinie-Devy, E. Cadel, N. Barreau, L. Arzel, and P. Pareige, "Atom probe study of Cu-poor to Cu-rich transition during Cu(In,Ga)Se2 growth," *Appl. Phys. Lett.*, vol. 99, no. 23, p. 232108, Dec. 2011.

[117] F. Couzinié-Devy, N. Barreau, and J. Kessler, "Re-investigation of preferential orientation of Cu(In,Ga)Se2 thin films grown by the three-stage process," *Prog. Photovolt. Res. Appl.*, vol. 19, no. 5, pp. 527–536, Aug. 2011.

[118] C. Heske, R. Fink, E. Umbach, W. Riedl, and F. Karg, "Na-induced effects on the electronic structure and composition of Cu(In,Ga)Se2 thin-film surfaces," *Appl. Phys. Lett.*, vol. 68, no. 24, pp. 3431–3433, Jun. 1996.

[119] S. Seyrling, A. Chirila, D. Güttler, F. Pianezzi, P. Rossbach, and A. N. Tiwari, "Modification of the three-stage evaporation process for CuIn1−xGaxSe2 absorber deposition," *Thin Solid Films*, vol. 519, no. 21, pp. 7232–7236, Aug. 2011.

[120] D. Braunger, D. Hariskos, G. Bilger, U. Rau, and H. W. Schock, "Influence of sodium on the growth of polycrystalline Cu(In,Ga)Se2 thin films," *Thin Solid Films*, vol. 361–362, pp. 161–166, février 2000.

[121] U. Rau, M. Schmitt, F. Engelhardt, O. Seifert, J. Parisi, W. Riedl, J. Rimmasch, and F. Karg, "Impact of Na and S incorporation on the electronic transport mechanisms of Cu(In, Ga)Se2 solar cells," *Solid State Commun.*, vol. 107, no. 2, pp. 59–63, mai 1998.

[122] D. W. Niles, K. Ramanathan, F. Hasoon, R. Noufi, B. J. Tielsch, and J. E. Fulghum, "Na impurity chemistry in photovoltaic CIGS thin films: Investigation with x-ray photoelectron spectroscopy," *J. Vac. Sci. Technol. A*, vol. 15, no. 6, pp. 3044–3049, Nov. 1997.

[123] A. Virtuani, E. Lotter, M. Powalla, U. Rau, J. H. Werner, and M. Acciarri, "Influence of Cu content on electronic transport and shunting behavior of Cu(In,Ga)Se2 solar cells," *J. Appl. Phys.*, vol. 99, no. 1, p. 014906, Jan. 2006.

[124] B. J. Stanbery, S. Kincal, W. K. Kim, T. J. Anderson, O. D. Crisalle, S. P. Ahrenkiel, and G. Lippold, "Role of sodium in the control of defect structures in CIS [solar cells]," in *Conference Record of the Twenty-Eighth IEEE Photovoltaic Specialists Conference, 2000*, 2000, pp. 440–445.

[125] M. Bodeg Ård, K. Granath, and L. Stolt, "Growth of Cu(In,Ga)Se2 thin films by coevaporation using alkaline precursors," *Thin Solid Films*, vol. 361–362, pp. 9–16, Feb. 2000.

[126] A. Chirilă, P. Reinhard, F. Pianezzi, P. Bloesch, A. R. Uhl, C. Fella, L. Kranz, D. Keller, C. Gretener, H. Hagendorfer, D. Jaeger, R. Erni, S. Nishiwaki, S. Buecheler, and A. N. Tiwari, "Potassium-induced surface modification of Cu(In,Ga)Se2 thin films for high-efficiency solar cells," *Nat. Mater.*, vol. 12, no. 12, pp. 1107–1111, Nov. 2013.

[127] A. Laemmle, R. Wuerz, and M. Powalla, "Efficiency enhancement of Cu(In,Ga)Se2 thin-film solar cells by a post-deposition treatment with potassium fluoride," *Phys. Status Solidi RRL – Rapid Res. Lett.*, vol. 7, no. 9, pp. 631–634, Sep. 2013.

[128] P. Jackson, D. Hariskos, R. Wuerz, W. Wischmann, and M. Powalla, "Compositional investigation of potassium doped Cu(In,Ga)Se2 solar cells with efficiencies up to 20.8%," *Phys. Status Solidi RRL – Rapid Res. Lett.*, vol. 8, no. 3, pp. 219–222, Mar. 2014.

[129] A. Laemmle, R. Wuerz, and M. Powalla, "Investigation of the effect of potassium on Cu(In,Ga)Se2 layers and solar cells," *Thin Solid Films*.
[130] P. Pistor, D. Greiner, C. A. Kaufmann, S. Brunken, M. Gorgoi, A. Steigert, W. Calvet, I. Lauermann, R. Klenk, T. Unold, and M.-C. Lux-Steiner, "Experimental indication for band gap widening of chalcopyrite solar cell absorbers after potassium fluoride treatment," *Appl. Phys. Lett.*, vol. 105, no. 6, p. 063901, Aug. 2014.
[131] M. A. Contreras, M. J. Romero, B. To, F. Hasoon, R. Noufi, S. Ward, and K. Ramanathan, "Optimization of CBD CdS process in high-efficiency Cu(In,Ga)Se2-based solar cells," *Thin Solid Films*, vol. 403–404, pp. 204–211, février 2002.
[132] W. Shockley and H. J. Queisser, "Detailed Balance Limit of Efficiency of p-n Junction Solar Cells," *J. Appl. Phys.*, vol. 32, no. 3, pp. 510–519, Mar. 1961.
[133] J. Eid, H. Liang, I. Gereige, S. Lee, and J. V. Duren, "Combinatorial study of NaF addition in CIGSe films for high efficiency solar cells," *Prog. Photovolt. Res. Appl.*, 2013.
[134] P. Reinhard, B. Bissig, F. Pianezzi, H. Hagendorfer, G. Sozzi, R. Menozzi, C. Gretener, S. Nishiwaki, S. Buecheler, and A. N. Tiwari, "Alkali-Templated Surface Nanopatterning of Chalcogenide Thin Films: A Novel Approach Toward Solar Cells with Enhanced Efficiency," *Nano Lett.*, vol. 15, no. 5, pp. 3334–3340, mai 2015.
[135] R. Miranda, "The mechanisms of the alkali-enhanced oxidation of semiconductors," in *Materials science monographs*, 1989, vol. 57, pp. 425–447.
[136] F. Pianezzi, P. Reinhard, A. Chirilă, B. Bissig, S. Nishiwaki, S. Buecheler, and A. N. Tiwari, "Unveiling the effects of post-deposition treatment with different alkaline elements on the electronic properties of CIGS thin film solar cells," *Phys. Chem. Chem. Phys.*, vol. 16, no. 19, p. 8843, 2014.
[137] F. Pianezzi, P. Reinhard, A. Chirilă, S. Nishiwaki, B. Bissig, S. Buecheler, and A. N. Tiwari, "Defect formation in Cu(In,Ga)Se2 thin films due to the presence of potassium during growth by low temperature co-evaporation process," *J. Appl. Phys.*, vol. 114, no. 19, p. 194508, Nov. 2013.
[138] F. Pianezzi, P. Reinhard, A. Chirilă, B. Bissig, S. Nishiwaki, S. Buecheler, and A. N. Tiwari, "Unveiling the effects of post-deposition treatment with different alkaline elements on the electronic properties of CIGS thin film solar cells," *Phys. Chem. Chem. Phys.*, vol. 16, no. 19, p. 8843, 2014.
[139] M. A. Contreras, J. Tuttle, A. Gabor, A. Tennant, K. Ramanathan, S. Asher, A. Franz, J. Keane, L. Wang, and R. Noufi, "High efficiency graded bandgap thin-film polycrystalline Cu(In,Ga) Se2-based solar cells," *Sol. Energy Mater. Sol. Cells*, vol. 41–42, pp. 231–246, juin 1996.
[140] M. Tomassini, "Synthèse de couches minces de Molybdène et application au sein des cellules solaires à base de Cu(In,Ga)Se2 co-évaporé," Nantes, 2013.
[141] D. F. Marrón, A. Meeder, S. Sadewasser, R. Würz, C. A. Kaufmann, T. Glatzel, T. Schedel-Niedrig, and M. C. Lux-Steiner, "Lift-off process and rear-side characterization of CuGaSe2 chalcopyrite thin films and solar cells," *J. Appl. Phys.*, vol. 97, no. 9, p. 094915, May 2005.
[142] M. Bär, L. Weinhardt, C. Heske, S. Nishiwaki, and W. N. Shafarman, "Chemical structures of the Cu(In,Ga)Se2/Mo and Cu(In,Ga)(S,Se)2/Mo interfaces," *Phys. Rev. B*, vol. 78, no. 7, p. 075404, août 2008.
[143] D. Schmid, M. Ruckh, and H. W. Schock, "Photoemission studies on Cu(In, Ga)Se2 thin films and related binary selenides," *Appl. Surf. Sci.*, vol. 103, no. 4, pp. 409–429, décembre 1996.
[144] W. K. Liu, W. T. Yuen, and R. A. Stradling, "Preparation of InSb substrates for molecular beam epitaxy," *J. Vac. Sci. Technol. B*, vol. 13, no. 4, pp. 1539–1545, Jul. 1995.
[145] B. Canava, J. Vigneron, A. Etcheberry, J. F. Guillemoles, and D. Lincot, "High resolution XPS studies of Se chemistry of a Cu(In, Ga)Se2 surface," *Appl. Surf. Sci.*, vol. 202, no. 1–2, pp. 8–14, décembre 2002.
[146] C. Platzer-Björkman, P. Zabierowski, J. Pettersson, T. Törndahl, and M. Edoff, "Improved fill factor and open circuit voltage by crystalline selenium at the Cu(In,Ga)Se2/buffer layer interface in thin film solar cells," *Prog. Photovolt. Res. Appl.*, vol. 18, no. 4, pp. 249–256, Jun. 2010.
[147] I. Miyake, T. Tanpo, and C. Tatsuyama, "XPS Study on the Oxidation of InSe," *Jpn. J. Appl. Phys.*, vol. 23, no. 2R, p. 172, Feb. 1984.

[148] E. P. Domashevskaya, V. V. Gorbachev, V. A. Terekhov, V. M. Kashkarov, E. V. Panfilova, and A. V. Shchukarev, "XPS and XES emission investigations of d–p resonance in some copper chalcogenides," *J. Electron Spectrosc. Relat. Phenom.*, vol. 114–116, pp. 901–908, Mar. 2001.
[149] V. Lyahovitskaya, Y. Feldman, K. Gartsman, H. Cohen, C. Cytermann, and D. Cahen, "Na effects on CuInSe2: Distinguishing bulk from surface phenomena," *J. Appl. Phys.*, vol. 91, no. 7, pp. 4205–4212, Apr. 2002.
[150] NIST, *electron-inelastic-mean-free-path code (imfpwin)*. .
[151] M. Faur, M. Faur, D. T. Jayne, M. Goradia, and C. Goradia, "XPS investigation of anodic oxides grown on p-type InP," *Surf. Interface Anal.*, vol. 15, no. 11, pp. 641–650, Nov. 1990.
[152] G. Hollinger, R. Skheyta-Kabbani, and M. Gendry, "Oxides on GaAs and InAs surfaces: An x-ray-photoelectron-spectroscopy study of reference compounds and thin oxide layers," *Phys. Rev. B*, vol. 49, no. 16, pp. 11159–11167, Apr. 1994.
[153] M. Tabbal, A. Lecours, R. Izquierdo, M. Meunier, and A. Yelon, "Surface Studies of Laser Processing of W on GaAs from WF6," in *Symposium B – Photons and Low Energy Particles in Surface Processing*, 1991, vol. 236.
[154] K. L. Seaward, N. J. Moll, and W. F. Stickle, "Surface contamination and damage from CF4 and SF6 reactive ion etching of silicon oxide on gallium arsenide," *J. Electron. Mater.*, vol. 19, no. 4, pp. 385–391, Apr. 1990.
[155] T. K. Paul and D. N. Bose, "Improved surface properties of InP through chemical treatments," *J. Appl. Phys.*, vol. 70, no. 12, pp. 7387–7391, Dec. 1991.
[156] Y. Kawamoto, K. Ogura, M. Shojiya, M. Takahashi, and K. Kadono, "F1s XPS of fluoride glasses and related fluoride crystals," *J. Fluor. Chem.*, vol. 96, no. 2, pp. 135–139, Jul. 1999.
[157] P. R. Varekamp, W. C. Simpson, D. K. Shuh, T. D. Durbin, V. Chakarian, and J. A. Yarmoff, "Electronic structure of GaF3 films grown on GaAs via exposure to XeF2," *Phys. Rev. B*, vol. 50, no. 19, pp. 14267–14276, Nov. 1994.
[158] W. Witte, R. Kniese, and M. Powalla, "Raman investigations of Cu(In,Ga)Se2 thin films with various copper contents," *Thin Solid Films*, vol. 517, no. 2, pp. 867–869, Nov. 2008.
[159] V. Izquierdo-Roca, R. Caballero, X. Fontané, C. A. Kaufmann, J. Álvarez-García, L. Calvo-Barrio, E. Saucedo, A. Pérez-Rodríguez, J. R. Morante, and H. W. Schock, "Raman scattering analysis of Cu-poor Cu(In,Ga)Se2 cells fabricated on polyimide substrates: Effect of Na content on microstructure and phase structure," *Thin Solid Films*, vol. 519, no. 21, pp. 7300–7303, Aug. 2011.
[160] X. Chuan-Ming, S. Yun, L. Feng-Yan, Z. Li, X. Yu-Ming, H. Qing, and L. Hong-Tu, "Nonlinear Shift of the Raman A1 Mode in Ga-Incorporated CuInSe2 Thin Films," *Chin. Phys. Lett.*, vol. 23, no. 4, p. 1002, Apr. 2006.
[161] K. Feng, D. Mei, L. Bai, Z. Lin, J. Yao, and Y. Wu, "Synthesis, structure, physical properties, and electronic structure of KGaSe2," *Solid State Sci.*, vol. 14, no. 8, pp. 1152–1156, Aug. 2012.
[162] P. Wang, X. Huang, Y. Liu, Y. Wei, J. Li, and H. Guo, "Solid state synthesis at intermediate temperature and structural characterization of KInSe2," *Acta Chim Sin.*, vol. 58, no. 8, pp. 1005–1008, 2000.
[163] C. K. Lowe-Ma, D. O. Kipp, and T. A. Vanderah, "On the crystal structure of KInS2-I," *J. Solid State Chem.*, vol. 92, no. 2, pp. 520–530, Jun. 1991.
[164] P. Lemoine, D. Carré, and M. Guittard, "Structure du sulfure de gallium et de potassium, KGaS2," *Acta Crystallogr. C*, vol. 40, no. 6, pp. 910–912, Jun. 1984.
[165] Z. Z. Kish, V. B. Lazarev, E. Y. Peresh, and E. E. Semrad, "Compounds in In_2Se_3 - K_2Se," 1988.
[166] F. Q. Huang, B. Deng, D. E. Ellis, and J. A. Ibers, "Preparation, structures, and band gaps of RbInS2 and RbInSe2," *J. Solid State Chem.*, vol. 178, no. 6, pp. 2128–2132, Jun. 2005.
[167] D. W. Lee, S. B. Kim, and K. M. Ok, "Cation Size Effect on the Framework Structures in a Series of New Alkali-Metal Indium Selenites, AIn(SeO3)2 (A = Na, K, Rb, and Cs)," *Inorg. Chem.*, vol. 51, no. 15, pp. 8530–8537, Aug. 2012.
[168] D. Abou-Ras, B. Marsen, T. Rissom, F. Frost, H. Schulz, F. Bauer, V. Efimova, V. Hoffmann, and A. Eicke, "Enhancements in specimen preparation of Cu(In,Ga)(S,Se)2 thin films," *Micron*, vol. 43, no. 2–3, pp. 470–474, Feb. 2012.

[169] S. K. Srivastava, M. Pramanik, D. Palit, B. K. Mathur, A. K. Kar, B. K. S. Ray, H. Haeuseler, and W. Cordes, "Electrical, Optical, and Scanning Tunneling Microscopic Studies on Layer Type CdIn2S4-xSex (1.75 ≤ x ≤ 2.75)," *Chem. Mater.*, vol. 13, no. 11, pp. 4342–4347, Nov. 2001.

[170] S. Endo, T. Irie, and H. Nakanishi, "Preparation and some properties of CuInSe2 single crystals," *Sol. Cells*, vol. 16, pp. 1–15, Jan. 1986.

[171] I. Kaur, D. K. Pandya, and K. L. Chopra, "Growth kinetics and polymorphism of chemically deposited CdS films," *J. Electrochem. Soc.*, 1980.

[172] R. Hunger, T. Schulmeyer, A. Klein, W. Jaegermann, M. V. Lebedev, K. Sakurai, and S. Niki, "SXPS investigation of the Cd partial electrolyte treatment of CuInSe2 absorbers," *Thin Solid Films*, vol. 480–481, pp. 218–223, Jun. 2005.

[173] W. Witte, D. Abou-Ras, and D. Hariskos, "Chemical bath deposition of Zn(O,S) and CdS buffers: Influence of Cu(In,Ga)Se2 grain orientation," *Appl. Phys. Lett.*, vol. 102, no. 5, p. 051607, Feb. 2013.

[174] D. R. Acosta, C. R. Magaña, A. I. Martínez, and A. Maldonado, "Structural evolution and optical characterization of indium doped cadmium sulfide thin films obtained by spray pyrolysis for different substrate temperatures," *Sol. Energy Mater. Sol. Cells*, vol. 82, no. 1–2, pp. 11–20, May 2004.

[175] T. H. Weng, "Flash Evaporated Films of Indium-Doped CdS and CdS x Se1 − x," *J. Electrochem. Soc.*, vol. 126, no. 10, pp. 1820–1822, Oct. 1979.

[176] E. Bertran, A. Lousa, M. Varela, M. V. García-Cuenca, and J. L. Morenza, "Optical properties of indium doped CdS thin films," *Sol. Energy Mater.*, vol. 17, no. 1, pp. 55–64, Jan. 1988.

[177] P. J. George, A. Sánchez, P. K. Nair, and M. T. S. Nair, "Doping of chemically deposited intrinsic CdS thin films to n type by thermal diffusion of indium," *Appl. Phys. Lett.*, vol. 66, no. 26, pp. 3624–3626, Jun. 1995.

[178] L. D. Partain, G. J. Sullivan, and C. E. Birchenall, "Effects of indium on the electrical properties of n-type CdS," *J. Appl. Phys.*, vol. 50, no. 1, pp. 551–554, Jan. 1979.

[179] G. Perna, V. Capozzi, A. Minafra, M. Pallara, and M. Ambrico, "Effects of the indium doping on structural and optical properties of CdSe thin films deposited by laser ablation technique," *Eur. Phys. J. B - Condens. Matter Complex Syst.*, vol. 32, no. 3, pp. 339–344, Apr. 2003.

[180] G. Perna, V. Capozzi, M. Ambrico, V. Augelli, T. Ligonzo, A. Minafra, L. Schiavulli, and M. Pallara, "Structural and optical characterization of undoped and indium-doped CdS films grown by pulsed laser deposition," *Thin Solid Films*, vol. 453–454, pp. 187–194, Apr. 2004.

[181] G. S. Shahane, K. M. Garadkar, and L. P. Deshmukh, "Structural, optical and electrical properties of indium doped CdS0.9Se0.1 thin films," *Mater. Chem. Phys.*, vol. 51, no. 3, pp. 246–251, décembre 1997.

[182] G. S. Shahane and L. P. Deshmukh, "Structural and electrical transport properties of CdS0.9Se0.1:In thin films: effect of film thickness," *Mater. Chem. Phys.*, vol. 70, no. 1, pp. 112–116, avril 2001.

[183] L. Peraldo Bicelli, S. Maffi, P. Tagliavini, and L. Zanotti, "Lithium insertion into layered quaternary chalcogenides: CdIn2S2Se2," *Solid State Ion.*, vol. 24, no. 4, pp. 297–304, Sep. 1987.

[184] C. Paracchini, A. Parisini, and L. Tarricone, "CdIn2S2Se2: A new semiconducting compound," *J. Solid State Chem.*, vol. 65, no. 1, pp. 40–44, Nov. 1986.

[185] A. A. Lavrent'ev, N. Y. Safontseva, V. A. Dubeiko, B. V. Gabrel'yan, and I. Y. Nikiforov, "Electronic band structure of In2S3 and CdIn2S4 semiconductor spinels from the data of x-ray spectroscopy and theoretical calculations," *Phys. Solid State*, vol. 42, no. 11, pp. 2047–2053, Nov. 2000.

[186] A. Anedda, L. Garbato, F. Raga, and A. Serpi, "Photoconductivity and trap distribution in CdIn2S4," *Phys. Status Solidi A*, vol. 50, no. 2, pp. 643–650, décembre 1978.

[187] P. Reyes-Figueroa, T. Painchaud, T. Lepetit, S. Harel, L. Arzel, J. Yi, N. Barreau, and S. Velumani, "Structural properties of In2Se3 precursor layers deposited by spray pyrolysis and physical vapor deposition for CuInSe2 thin-film solar cell applications," *Thin Solid Films*.

[188] W. E. Vargas, D. E. Azofeifa, and N. Clark, "Retrieved optical properties of thin films on absorbing substrates from transmittance measurements by application of a spectral projected gradient method," *Thin Solid Films*, vol. 425, no. 1–2, pp. 1–8, février 2003.

[189] R. S. Mane and C. D. Lokhande, "Studies on chemically deposited cadmium sulphoselenide (CdSSe) films," *Thin Solid Films*, vol. 304, no. 1–2, pp. 56–60, Jul. 1997.
[190] T. M. Friedlmeier, D. Braunger, D. Hariskos, M. Kaiser, H. N. Wanka, and H. W. Schock, "Nucleation and growth of the CdS buffer layer on Cu(In,Ga)Se2 thin films," in *, Conference Record of the Twenty Fifth IEEE Photovoltaic Specialists Conference, 1996*, 1996, pp. 845–848.
[191] D. Lincot and R. O. Borges, "Chemical Bath Deposition of Cadmium Sulfide Thin Films. In Situ Growth and Structural Studies by Combined Quartz Crystal Microbalance and Electrochemical Impedance Techniques," *J. Electrochem. Soc.*, vol. 139, no. 7, pp. 1880–1889, Jul. 1992.
[192] M. K. Miller, K. F. Russell, and G. B. Thompson, "Strategies for fabricating atom probe specimens with a dual beam FIB," *Ultramicroscopy*, vol. 102, no. 4, pp. 287–298, Mar. 2005.
[193] F. Couzinie-Devy, E. Cadel, N. Barreau, L. Arzel, and P. Pareige, "Na distribution in Cu(In,Ga)Se2 thin films: Investigation by atom probe tomography," *Scr. Mater.*, vol. 104, pp. 83–86, juillet 2015.
[194] J. Heath and P. Zabierowski, "Capacitance Spectroscopy of Thin-Film Solar Cells," in *Advanced Characterization Techniques for Thin Film Solar Cells*, D. Abou-Ras, T. Kirchartz, and U. Rau, Eds. Wiley-VCH Verlag GmbH & Co. KGaA, 2011, pp. 81–105.
[195] R. Klenk, "Characterisation and modelling of chalcopyrite solar cells," *Thin Solid Films*, vol. 387, no. 1–2, pp. 135–140, mai 2001.
[196] J. F. Guillemoles, "The puzzle of Cu(In,Ga)Se2 (CIGS) solar cells stability," *Thin Solid Films*, vol. 403–404, pp. 405–409, Feb. 2002.
[197] T. Drobiazg, L. Arzel, A. Dönmez, P. Zabierowski, and N. Barreau, "Influence of indium/gallium gradients on the Cu(In,Ga)Se2 devices deposited by the co-evaporation without recrystallisation," *Thin Solid Films*, vol. 582, pp. 47–50, May 2015.
[198] C. Platzer Björkman, "Band Alignment Between ZnO-Based and Cu(In,Ga)Se2 Thin Films for High Efficiency Solar Cells," Uppsala Universitet, 2006.
[199] L. C. Olsen, W. Lei, F. W. Addis, W. N. Shafarman, M. A. Contreras, and K. Ramanathan, "High efficiency CIGS and CIS cells with CVD ZnO buffer layers," in *, Conference Record of the Twenty-Sixth IEEE Photovoltaic Specialists Conference, 1997*, 1997, pp. 363–366.
[200] S. Wiedeman, J. Kessler, L. Russell, J. Fogleboch, S. Skibo, and R. Arya, "Progress in thin film CIGS modules," 1997, vol. 394, pp. 133–142.
[201] G. H. Bauer, R. Brüggemann, S. Tardon, S. Vignoli, and R. Kniese, "Quasi-Fermi level splitting and identification of recombination losses from room temperature luminescence in Cu(In1−xGax)Se2 thin films versus optical band gap," *Thin Solid Films*, vol. 480–481, pp. 410–414, Jun. 2005.

l'université nantes angers le mans
PÔLE DE RECHERCHE ET D'ENSEIGNEMENT SUPÉRIEUR

UNIVERSITÉ DE NANTES

Thèse de Doctorat

Thomas LEPETIT

Influence of KF post deposition treatment on the polycrystalline Cu(In,Ga)Se_2/CdS heterojunction formation for photovoltaic application

Influence du procédé de dépôt à base de KF sur la formation de l'hétérojonction polycristalline Cu(In,Ga)Se_2/CdS pour application photovoltaïque

Résumé

La mise en place d'un traitement post-dépôt de l'absorbeur de Cu(In,Ga)Se_2(CIGS) sous vapeur de KF sous pression partielle séléniée (KF-PDT) au sein des dispositifs photovoltaïques à base d'hétérojonctions de type CIGS/CdS permet l'obtention de rendements de conversion supérieurs à 20 % à l'échelle du laboratoire. Les origines de l'augmentation des paramètres photovoltaïques (*i.e.* V_{oc}, FF, J_{sc}) par ce traitement sont néanmoins source de discussions, d'autant que son efficacité est restreinte à des conditions expérimentales souvent difficiles à déterminer, donc à maîtriser. Le premier objectif de ce travail a donc été de montrer que la présence d'une phase chalcopyrite déficitaire en cuivre à la surface de l'absorbeur avant le KF-PDT est nécessaire pour éviter la ségrégation de Cu_xSe et ainsi obtenir les effets bénéfiques du traitement. Dans ce cas nous montrons que le KF-PDT implique la formation d'une nouvelle phase superficielle (~5 nm) qui modifie la croissance du CdS par bain chimique (CBD). Un nouveau matériau $CdIn_2S_4$ dérivant de cette phase est formé à l'hétéro-interface CIGS/CdS, dont les propriétés opto-électroniques sont remarquablement pertinentes pour les performances de l'hétérojonction. La modification des propriétés des homo-interfaces de CIGS (*i.e*. joints de grains) induite par le traitement est également étudiée. Enfin nous discutons des propriétés opto-électroniques particulières de ces cellules solaires et proposons un modèle électrique, en lien avec le modèle chimique de la modification simultanée des homo- et hétéro-interfaces par le KF-PDT et lors du dépôt du CdS par CBD, permettant d'expliquer l'amélioration des performances liées à ce traitement.

Mots clés

Cellule solaire, Cu(In,Ga)Se_2, CdS, hétérojonction, couches minces, alcalins, co-évaporation

Abstract

Among photovoltaic technologies, Mo/Cu(In,Ga)Se_2 (CIGS)/CdS/ZnO/ZnO:Al solar cell is the only thin film based structure demonstrating record energy conversion efficiency of 21.7 %. This outstanding level of performance for such polycrystalline and hetero-junction based devices has been made possible by the use of a so-called potassium fluoride post deposition treatment (KF-PDT) after the absorber synthesis. Such treatment indeed improves all photovoltaic parameters of the solar cell (i.e. V_{oc}, FF, J_{sc}). Nevertheless, this paradigm appears closely dependent to specific CIGS-surface characteristics which, if not fully satisfied, can yield hindered device performance. In the present work, CIGS absorbers leading to either beneficial or detrimental impact of KF-PDT have been firstly finely investigated. From this study it appeared conclusive that the presence of an ordered vacancy compound (OVC) on top of the CIGS is requested to avoid –detrimental- Cu_xSe segregation and to take advantage of the KF-PDT. It is herein proposed that this superficial Cu-poor chalcopyrite results in a new phase that turns during the chemical bath deposition of CdS into a ~5 nm-thick $CdIn_2S_4$ layer. This mechanism can in particular explain the much more homogeneous CBD-growth of the buffer layer. Moreover, it is shown that cubic $CdIn_2S_4$ material, which has n+-type conductivity, forms a defect-free interface with the CIGS. The final part of this work aims at discussing the impact of KF-PDT on the electro-optical properties of CIGS/CdS solar cell, based on the modifications it implies on both heterojunction and grain boundary characteristics.

Key Words

Solar cell, Cu(In,Ga)Se_2, CdS, heterojunction, thin film, alkali, co-evaporation